Probing the biocompatibility of biomedical interfaces using the Quartz Crystal Microbalance with Dissipation

A thesis submitted in fulfilment of the requirements for the degree

in

Masters of Science

at

Rhodes University

by

Mary Cromhout

Supervisor: Prof. J.L. Limson

Co-Supervisor: Dr. A. Edkins

February 2011

ABSTRACT

The biomedical application of nanotechnology has come into the spotlight, with the promise of 'personalised' therapeutics that couple early diagnosis with targeted therapeutic activity. Due to the rapid growth of the biomedical applications of nanoparticles, along with the lack of understanding concerning their interactions with biomolecules, there is a pressing need for the development of standard methods directed at investigating the effect of introducing these unique particles into the human body. The central aim of this research is to establish a platform directed at assessing the biological fate of pioneering therapeutic particulate agents, such as metallophthalocyanines (MPcs) and multi-walled carbon nanotubes (*F*MWCNTs). In particular, we proposed, that Quartz Crystal Microbalance with Dissipation (QCM-D) technology may be employed to assess the composition of blood protein corona deposited on the therapeutic surface, and subsequently assess the biocompatibility of such particles.

The proposed method of protein detection utilises the nanogram sensitivity of QCM-D technology to monitor highly specific antibody-antigen interactions. In particular those interactions which occur when probe antibodies are used to detect adsorbed blood proteins deposited on target particle-modified sensor surfaces. Protein detection analysis was directed toward identification of surface bound human serum albumin, complement factor C3c, and human plasma fibrinogen.

Preliminary analysis of generic biomedical surfaces indicated human serum albumin demonstrates a higher binding affinity towards positively charged surfaces (i.e. cysteamine self-assembled monolayer), followed by hydrophobic surfaces. Detection of complement C3c, corresponded with literature, where lower levels were detected on negatively charged surfaces (i.e. mercapto undecanoic acid self-assembled monolayer), and higher levels of more hydrophobic surfaces (i.e. 11-amino undecane thiol self-assembled monolayer). Human plasma fibrinogen was observed to favour hydrophilic over hydrophobic self-assembled monolayer surfaces, which was in accordance with literature.

Application of the proposed protein detection method for biocompatibility analysis of target therapeutic molecules, namely metallophthalocyanines and acid functionalised multi-walled carbon nanotubes, demonstrated a dependence on modified-surface film characteristics, such as surface charge and topography with regards to human serum albumin and human plasma fibrinogen analysis representing new insights into their potential biomolecular interactions The highest levels of detected human serum albumin and complement C3c were detected on the $GePcS_{mix}$-modified surfaces. $AlPcS_{mix}$-modified surfaces analysis suggested the highest levels of human plasma fibrinogen. Two methods of acid functionalisation were employed, using both nitric and sulphuric acid, and pure nitric acid. A general increase in detected human serum albumin, corresponding with an increase in functionalisation time, was observed. Complement C3c detection suggested an increase in deposited complement C3c, with increasing functionalisation time, when assessing nitric acid functionalised multi-walled carbon nanotubes, and a decrease, with increasing functionalisation time, when assessing nitric and sulphuric acid functionalised multi-walled carbon nanotubes. Analysis of human plasma fibrinogen was inconclusive, as were cytotoxicity experiments utilising MCF-7 cells in the presence of metallophthalocyanine complexes, raising simultaneously important considerations for their application and study.

In the first such detailed examination of its kind it was concluded that the proposed method of protein detection, using QCM-D, allows for the rudimentary but rapid means of analysis of select protein corona deposited on particulate biomedical surfaces.

ACKNOWLEDGMENTS

I extend my sincere thanks to my supervisor, Prof. J. Limson, and co-supervisor, Dr. A. Edkins, for their guidance and encouragement. Prof. T. Nyokong for donating the MPc samples. DST/Mintek NIC for financial support. To the members of BioSENs, for their continuous support and assistance. A very special mention to Dr. R. Fogel for his endless patience, time and willingness to help. Finally, I would like to thank my family and friends, in particular my father, Mr. P. Cromhout, who has remained my inspiration.

PAGE OF CONTENTS

Title		Page Number
Abstract		I
Acknowledgments		III
Page of Contents		IV
List of Tables		VII
List of Figures		IX
List of Abbreviations		XIII
CHAPTER 1:		
OVERALL INTRODUCTION		
1.1	Overview	1
1.2	Quartz Crystal Microbalance with Dissipation Technology	3
1.2.1	QCM-D Principal	3
1.3	Target Proteins	5
1.3.1	Human Serum Albumin	6
1.3.2	Human Complement C3c	7
1.3.3	Human Plasma Fibrinogen	8
1.4	Target Therapeutic Particles	9
1.4.1	Metallophthalocyanines	9
1.4.2	Carbon Nanotubes	12
1.5	Research Aims and Objectives	14
CHAPTER 2:		
BIOMOLECULAR INTERACTIONS WITH METAL SURFACES AND MODIFIED GOLD SURFACES		
2.1	**Introduction**	**16**
2.1.1	Preliminary Studies	16
2.1.2	QCM-D Sensor Surface Modification	16
2.1.2.1	Self-Assembled Monolayer Modification	17
2.1.2.2	Antibody Modification	18
2.1.3	Chapter Aims and Objectives	19
2.2	**Instrumentation and Methodology**	**20**
2.2.1	Instrumentation	20
2.2.2	Reagents	21
2.2.3	Methodology	21
2.2.3.1	Preparation of QCM-D System	21
2.2.3.2	Sensor Surface Modification	22
2.2.3.2.1	Self-Assembled Monolayer	22
2.2.3.2.2	Antibody Controls	22
2.2.4	QCM-D Monitoring and Quantification	23
2.3	**Results and Discussion**	**24**
2.3.1	Introduction to QCM-D Analysis	24
2.3.2	QCM-D Monitoring and Quantification of Surface Modification: Antibody Controls	32
2.3.3	QCM-D Monitoring and Quantification of Biomolecular Interactions with Surfaces: Modified and Unmodified	43
2.3.3.1	QCM-D Monitoring and Quantification of Blood Protein Adsorption on Unmodified and Modified Surfaces	43
2.3.3.2	QCM-D Monitoring and Quantification of Probe Antibody Binding to Unmodified and Modified Surfaces	48
2.4	**Conclusion**	**56**

CHAPTER 3:
BIOMOLECULAR INTERACTIONS WITH METALLOPHTHALOCYANINES

3.1	**Introduction**	**59**
3.1.1	Overview of MPcs	59
3.1.2	Chapter Aims and Objectives	59
3.2	**Instrumentation and Methodology**	**60**
3.2.1	Instrumentation	60
3.2.2	Additional Reagents	60
3.2.3	Methodology	61
3.2.3.1	Characterisation of Sulphonated MPcs	61
3.2.3.1.1	Degree of Sulphonation Analysis via HPLC	61
3.2.3.1.2	Spectrophotometric Analysis of MPc Aggregation	61
3.2.3.2	Surface Modification with MPcs	61
3.2.3.3	QCM-D Monitoring and Quantification	62
3.3	**Results and Discussion**	**62**
3.3.1	Characterisation of Sulphonated MPcs	62
3.3.1.1	Degree of Sulphonation Analysis via HPLC	62
3.3.1.2	Spectrophotometric Analysis of MPc Aggregation	65
3.3.2	Surface Modification with MPcs	67
3.3.2.1	Theoretical Determination of Expected MPc Monolayer Mass	68
3.3.2.2	QCM-D Monitoring and Quantification of Surface Modification: MPcs	70
3.3.3	QCM-D Analysis of Biomolecular Interactions with MPc-Modified Surfaces	86
3.3.3.1	QCM-D Monitoring and Quantification of Blood Protein Adsorption on MPc-Modified Surfaces	86
3.3.3.2	QCM-D Monitoring and Quantification of Probe Antibody Binding to MPc-Modified Surfaces	92
3.4	**Conclusion**	**100**

CHAPTER 4:
IMPORTANCE OF NANOSTRUCTURES IN BIOMEDICAL APPLICATION: CARBON NANOTUBES

4.1	**Introduction**	**104**
4.1.1	Multi-Walled Carbon Nanotubes	104
4.1.2	Chapter Aims and Objectives	105
4.2	**Instrumentation and Methodology**	**106**
4.2.1	Instrumentation	106
4.2.2	Additional Reagents	106
4.2.3	Methodology	106
4.2.3.1	Acid Functionalisation of Multi-Walled Carbon Nanotubes	106
4.2.3.2	Characterisation of Acid Functionalised Multi-Walled Carbon Nanotubes	107
4.2.3.3	Surface Modification with *F*MWCNTs	107
4.2.3.4	QCM-D Monitoring and Quantification	108
4.3	**Results and Discussion**	**109**
4.3.1	Characterisation of Acid Functionalised Multi-Walled Carbon Nanotubes	109
4.3.2	QCM-D Analysis of Biomolecular Interactions with *F*MWCNT-modified Surfaces	116
4.3.2.1	QCM-D Monitoring and Quantification of Blood Protein Adsorption on *F*MWCNT-Modified Surfaces	116
4.3.2.2	QCM-D Monitoring and Quantification of Probe Antibody Binding to *F*MWCNT-Modified Surfaces	122
4.4	**Conclusion**	**129**

CHAPTER 5:
METALLOPHTHALOCYANINE –INDUCED CYTOTOXICITY IN MCF-7 CELL LINE

5.1	**Introduction**	**131**
5.1.1	Metallophthalocyanine Application in Photodynamic Therapy	131
5.1.2	Cytotoxicity of Metallophthalocyanine Molecules	132
5.1.3	Chapter Aims and Objectives	132
5.2	**Instrumentation and Methodology**	**133**
5.2.1	Instrumentation and Additional Reagents	133
5.2.2	Methodology	133
5.2.2.1	MPc Preparation	133
5.2.2.2	Identification of MPc Interference with Cytotoxicity Analysis	134
5.2.2.2.1	Spectrophotometric Analysis of MPc Preparations	134
5.2.2.2.2	Spectrophotometric Analysis of MTT and WST-1 Cell Proliferation Assay	134
5.2.2.3	MCF-7 Culture Preparation	134
5.2.2.4	WST-1 Cell Proliferation Assay	135
5.2.2.4.1	Validation of WST-1 Cell Proliferation Assay	135
5.2.2.4.2	Cytotoxicity Analysis of MPc Preparations	135
5.3	**Results and Discussion**	**136**
5.3.1	Identification of MPc Interference with Cytotoxicity Analysis	136
5.3.1.1	Spectrophotometric Analysis of MPc Preparations	136
5.3.1.2	Spectrophotometric Analysis of MTT and WST-1 Cell Proliferation Assays	137
5.3.2	Validation of WST-1 Cell Proliferation Assay	139
5.3.3	MPc-Induced MCF-7 Cytotoxicity	141
5.3.4	Comparison Between MPc Protein Binding Analysis and Cytotoxicity Studies	147
5.4	**Conclusion**	**149**

CHAPTER 6: OVERALL CONCLUSIONS	**150**
Appendix	**153**
Reference	**158**

LIST OF TABLES

Table Title		Page Number
Table 2.1	Voigt-determined film parameters following the adsorption of human serum to 11-amino undecane thiol SAM, and the subsequent binding of anti-human C3c.	29
Table 2.2	Assessing the effect of modelling parameters in the Voigt-determination of serum protein film parameters adsorbed to an 11-amino undecane thiol SAM-modified gold sensor surfaces.	30
Table 2.3	QCM-D Frequency and Dissipation Shifts Following Gold Surface Modification with Anti-Human Serum Albumin, Human IgG, and Anti-Human Plasma Fibrinogen, for control experiments.	34
Table 2.4	Sauerbrey and Voigt Modelled Analysis of Gold Surface Modification with Human IgG, Anti-Human Serum Albumin, and Anti-Human Plasma Fibrinogen, for control experiments.	38
Table 2.5	Sauerbrey and Voigt Modelled Analysis of Blood Protein Adsorption on Unmodified and Modified Surfaces.	45
Table 2.6	Sauerbrey and Voigt Modelled Analysis of Probe Antibody Binding to Unmodified and Modified Surfaces.	50
Table 3.1	HPLC Analysis of the Degree of Metallophthalocyanine Sulphonation.	64
Table 3.2	Theoretical MPc Immobilised Mass ($ng.cm^{-2}$) for Edge-On and Planar Conformations.	70
Table 3.3	QCM-D Frequency and Dissipation Shifts Following Metallophthalocyanine Immobilisation to 11-Amino Undecane Thiol Self-Assembled Monolayer.	71
Table 3.4	QCM-D Analysis of Metallophthalocyanine Immobilisation on 11-Amino Undecane Thiol Self-Assembled Monolayer.	77
Table 3.5	Summary of Conclusions Derived on the Immobilised Metallophthalocyanine Films.	85
Table 3.6	QCM-D Shifts in Frequency and Dissipation Shifts Due to Human Serum/Human Plasma Adsorption on MPc-Modified Surfaces.	88

Table 3.7 QCM-D Analysis of Human Serum and Human Plasma Adsorption on MPc-Modified Surfaces. 90

Table 3.8 QCM-D Analysis Antibody Binding to Adsorbed Human Serum and Plasma Proteins on the MPc-Modified Surfaces. 94

Table 4.1 Sauerbrey and Voigt Modelled Analysis of Blood Protein Adsorption on *F*MWCNT-Modified 11-Amino Undecane Thiol SAM Surfaces. 117

Table 4.2 Sauerbrey and Voigt Modelled Analysis Probe Antibody Binding to Blood Protein Coated *F*MWCNT-modified surfaces. 123

Table A.1 QCM-D Frequency and Dissipation Shifts Monitoring the Adsorption of Blood Proteins to the Target Surfaces 153

Table A.2 QCM-D Frequency and Dissipation Shifts Monitoring Probe Antibody Binding to Blood Protein Coated Target Surfaces 154

Table B.1 QCM-D Change in Frequency and Dissipation Shifts due to Target Antibody Binding to Blood Protein Coated MPc-Modified Surfaces 155

Table C.1 QCM-D Frequency and Dissipation Responses Monitoring Blood Protein Adsorption to the *F*MWCNT-Modified 11-Amino Undecane Thiol SAM Surfaces 156

Table C.2 QCM-D Frequency and Dissipation Responses Monitoring Probe Antibody Binding to Blood Protein Coated *F*MWCNT-Modified Surfaces 157

LIST OF FIGURES

Figure	Title	Page Number
Figure 1.1 (A)	Schematic representation of film deformation under shear strain illustrating film viscosity.	5
Figure 1.1 (B)	Schematic representation of film deformation under shear strain illustrating film shear modulus.	5
Figure 1.2	Rasmol images of human serum albumin (PDB: 1E78).	7
Figure 1.3	Rasmol images of complement factor C3c (PBD: 2A74).	8
Figure 1.4	Rasmol images of human plasma fibrinogen (PDB: 3GHF).	9
Figure 1.5	Modified Jablonski diagram illustrating the photosensitising process of MPc molecules.	9
Figure 1.6	Schematic representation of a tetra-substituted metallophthalocyanine molecule.	11
Figure 1.7	Schematic representation of single-walled (I) and multi-walled (II) carbon nanotubes.	13
Figure 1.8	Main objectives for the analysis of QCM-D application in biocompatibility analysis of metallophthalocyanines and acid functionalised multi-walled	15
Figure 2.1 (A)	Schematic representation of target surfaces probed for blood protein adsorption.	19
Figure 2.1 (B)	Schematic representation of adsorbed target protein detection protocol monitored using QCM-D.	19
Figure 2.2	QCM-D frequency (Blue) and dissipation (Red) shifts illustrating human serum adsorption to the 11-amino undecane thiol self-assembled monolayer-modified gold sensor surface (I) and subsequent anti-human C3c binding (II).	25
Figure 2.3	Dissipation versus frequency plot of human serum adsorption, and the subsequent anti-human C3c binding, to the gold QCM-D sensor surface modified with an 11-amino undecane thiol SAM.	26
Figure 2.4	Schematic representation of adsorbed target protein detection and the corresponding QCM-D response.	31
Figure 2.5	Rasmol generated illustration of human immunoglobulin G (PDB: 1IGY).	33
Figure 2.6	Schematic illustration of the adsorbed IgG orientations within a monolayer deposited on gold.	34

Figure 2.7	Frequency versus dissipation plots of anti-human albumin (A), IgG (B), and anti-human fibrinogen (C) adsorption to gold.	36
Figure 2.8	Sauerbrey-(Blue) and Voigt-(Red) determined adsorbed antibody mass to the gold sensor surface.	42
Figure 2.9	Sauerbrey (Blue) and Voigt (Red) determined adsorbed blood protein mass to unmodified, antibody-modified, and SAM modified surfaces.	48
Figure 3.1	HPLC trace for MPcs indicating the degree of sulphonation of the MPc species present in the MPc preparations.	63
Figure 3.2	Absorbance spectrophotometric analysis of MPc aggregation.	66
Figure 3.3	Schematic representation of immobilised metallophthalocyanine orientation.	68
Figure 3.4	Rasmol determined MPc molecular diameter.	69
Figure 3.5	Representative dissipation versus frequency plot of the metallophthalocyanine immobilisation processes.	74
Figure 3.6	Schematic representation of the experimental process utilised in assessing the biomolecular interactions which occur with metallophthalocyanines.	86
Figure 3.7	Sauerbrey (Blue) and Voigt (Red) determined human serum (S) and human plasma (P) mass adsorbed to previously immobilised metallophthalocyanines films.	91
Figure 3.8	Sauerbrey- (I) and Voigt- (II) determined adsorbed human serum mass versus immobilised MPc film interface property.	92
Figure 3.9	Sauerbrey- (I) and Voigt- (II) determined adsorbed anti-human albumin mass, as a proportion of total blood protein mass, versus immobilised MPc film interface property.	96
Figure 3.10	Sauerbrey (I) and Voigt (II) determined adsorbed anti-human C3c mass, as a proportion of total blood protein mass, versus immobilised MPc film interface property.	98
Figure 3.11	Sauerbrey (I) and Voigt (II) determined adsorbed anti-human fibrinogen mass, as a proportion of total blood protein mass, versus immobilised MPc film interface property.	99
Figure 4.1	Schematic representation of the chemical oxidation functionalisation of CNTs.	105
Figure 4.2	Schematic representation of the EDC/NHS activity in immobilisation of *F*MWCNTs to 11-AUT SAM-modified surface.	108
Figure 4.3	Transmission Electron Microscope imaging of non-functionalised MWCNTs.	110
Figure 4.4	Transmission Electron Microscopy images of nitric acid and sulphuric functionalised MWCNTs (a:*F*MWCNTs).	111

Figure 4.5 Transmission Electron Microscopy images of nitric acid functionalised MWCNTs (b:*F*MWCNTs). 114

Figure 4.6 Sauerbrey- (I), and Voigt- (II) determined adsorbed human serum (Red) and human plasma (Blue) protein mass to the nitric and sulphuric acid functionalised MWCNT-modified surfaces. 118

Figure 4.7 Sauerbrey- (I), and Voigt- (II) determined adsorbed human serum (Red) and human plasma (Blue) protein mass to the nitric acid functionalised MWCNT-modified surfaces. 121

Figure 4.8 Sauerbrey- (I), and Voigt- (II) determined adsorbed human serum (Red) and human plasma (Blue) protein mass to the a:*F*MWCNT-modified surfaces as a function of the blood protein film interface. 121

Figure 4.9 (A) Sauerbrey- (Red) and Voigt- (Blue) determined adsorbed anti-human albumin mass to the human serum coated a: *F*MWCNT modified surfaces 124

Figure 4.9 (B) Sauerbrey- (Red) and Voigt- (Blue) determined adsorbed anti-human albumin mass to the human serum coated b:*F*MWCNT modified surfaces 124

Figure 4.10 Sauerbrey- (Blue) and Voigt- (Red) Determined Anti-Human Albumin Adsorbed Mass to a: *F*MWCNT- (▲) and b: *F*MWCNT- (■) modified surfaces as a Proportion of the Total Human Serum Adsorbed Mass 125

Figure 4.11 Sauerbrey- (Blue) and Voigt- (Red) Determined Anti-Human C3c Adsorbed Mass to a: *F*MWCNT- (▲) and b: *F*MWCNT- (■) modified surfaces as a Proportion of the Total Human Serum Adsorbed Mass 126

Figure 4.12 Sauerbrey- (Blue) and Voigt- (Red) Determined Anti-Human Fibrinogen Adsorbed Mass to a:*F*MWCNT- (▲) and b:*F*MWCNT- (■) modified surfaces as a Proportion of the Total Human Serum Adsorbed Mass 127

Figure 4.13 Schematic illustration of surface topography on human plasma fibrinogen binding. 129

Figure 5.1 Absorbance spectral scans of MPc preparations prepared in $PBS_{Mg/Ca}$-DMEM. 137

Figure 5.2 Absorbance spectrophotometric analysis of the tetrazolium salts, and the respective cleavage products, employed in the WST-1 and MTT cell proliferation assays. 138

Figure 5.3 MCF-7 cell proliferation studies using Cell Proliferation Reagent WST-1. 139

Figure 5.4 Analysis of MPc interference with WST-1 cell proliferation assay efficiency. 140

Figure 5.5 Analysis of the effect of DMSO on cell viability as measured by WST-1 cell proliferation assay efficiency. 141

Figure 5.6 $AlPcS_{mix}$-induced cytotoxicity in MCF-7 cell line. 142

Figure 5.7 Cytotoxicity of modified and unmodified CoPc's in MCF-7 cell line. 144

Figure 5.8 CuTSPc-induced cytotoxicity in MCF-7 cell line. 145

Figure 5.9 $GePcS_{mix}$-induced cytotoxicity in MCF-7 cell line. 146

Figure 5.10 $ZnPcS_{mix}$-induced cytotoxicity in MCF-7 cell line. 147

Figure 5.11 Comparison between Sauerbrey-determined adsorbed antibody mass and the percentage cell survival of MCF-7 cells following the administration of MPc preparations. 148

Figure 5.12 Comparison between Voigt-determined adsorbed antibody mass and the percentage cell survival of MCF-7 cells following the administration of MPc preparations. 148

LIST OF ABBREVIATIONS

Abbreviation	Definition
μ_f	Elastic Shear Modulus
η_f	Shear Viscosity
δ_f	Film Thickness
ρ_f	Film Density
% CV	Percentage Coefficient of Variation
11-AUT	11-Amino Undecane Thiol
2D-PAGE	Two Dimensional Polyacrylamide Gel Electrophoresis
Ab_{C3c}	Anti-Human Complement C3c Antibody
Ab_{C3c-}	Anti-Human Complement C3c Antibody (in PBS)
Ab_{C3c+}	Anti-Human Complement C3c Antibody (in PBSMg/Ca)
Ab_{HPF}	Anti-Human Plasma Fibrinogen Antibody
Ab_{HSA}	Anti-Human Serum Albumin Antibody
Ab_{IgG}	Immunoglobulin IgG Antibody
Ab_{IgG-}	Immunoglobulin IgG Antibody (in PBS)
Ab_{IgG+}	Immunoglobulin IgG Antibody (in PBSMg/Ca)
Ab_m	Antibody Mass
AFM	Atomic Force Microscopy
a:*F*MWCNTs	Nitric and Sulphuric Acid Functionalised Multi-Walled Carbon Nanotubes
Al	Aluminum
Al^{3+}	Aluminum Ion
$AlPcS_4$	Tetra-Sulphonated Aluminum Phthalocyanine
$AlPcS_{mix}$	Sulphonated Aluminum Phthalocyanine Mixture
ATCC	American Type Culture Collection
b:*F*MWCNTs	Nitric Acid Functionalised Multi-Walled Carbon Nanotubes
BP_m	Blood Protein Mass
CNTs	Carbon Nanotubes
CO_2	Carbon Dioxide
Co^{2+}	Cobalt Ion
CoPc	Cobalt Phthalocyanine
$CoPcS_{mix}$	Sulphonated Cobalt Phthalocyanine Mixture
CoTCPc	Tetra-Carboxylated Cobalt Phthalocyanine
Cu^{2+}	Copper Ion
CuTSPc	Tetra-Sulphonated Copper Phthalocyanine
Cyst.	Cysteamine
D	Dissipation (1E-06)
D_7	Dissipation (overtone 7)
DMEM	Dulbecco's Modified Eagle Medium
DMSO	Dimethyl Sulphoxide
EDC	Ethyl(Dimethylaminopropyl) Carbodiimide
ELISA	Enzyme Linked Immunoassay
f	Frequency (Hz)
f_7	Frequency (overtone 7)
*F*MWCNTs	Acid Functionalised Multi-Walled Carbon Nanotubes
Ge	Germanium
$GePcS_{mix}$	Sulphonated Germanium Phthalocyanine Mix
H_2SO_4	Sulphuric Acid
HCl	Hydrochloric Acid
HNO_3	Nitric Acid
HP	Human Plasma
HPF	Human Plasma Fibrinogen

HPLC	High Pressure Liquid Chromatography
HS	Human Serum
HSA	Human Serum Albumin
IC_{50}	Half the Maximal Inhibitory Concentration
IgG	Immunoglobulin G
ISC	Intersystem Crossing
MCF-7	Mammalian Breast Cancer Cell Line
MES	2-(N-Morpholino)Ethanesulfonic Acid
MPc	Metallophthalocyanines
MPS	Mononuclear Phagocyte System
MUA	Mercapto Undecanoic Acid
MWCNTs	Multi-Walled Carbon Nanotubes
NHS	N-Hydroxysuccinimide
PBS	Phosphate Buffered Saline
$PBS_{Mg/Ca}$	Phosphate Buffered Saline (containing Mg2+ and Ca2+ ions)
PS	Photosensitiser
Pc	Phthalocyanine
PDB	Protein Data Bank
QCM-D	Quartz Crystal Microbalance with Dissipation
SAM	Self-Assembled Monolayer
SDS	Sodium Dodecyl Sulphate
SEM	Scanning Electron Microscopy
SPR	Surface Plasmon Resonance
SWCNTs	Single-Walled Carbon Nanotubes
TEM	Transmission Electron Microscopy
Zn^{2+}	Zinc Ion
$ZnPcS_{mix}$	Sulphonated Zinc Phthalocyanine Mixture

CHAPTER 1: OVERALL INTRODUCTION

1.1. Overview

Medical treatments involving the introduction of foreign surfaces to human blood components, such as implantations and the systemic administration of therapeutic drugs, is required to undergo rigorous biocompatibility testing to determine the haematocompatibility of the product before considering commercialization [1]. The ultimate objective of any therapeutic is the rapid and accurate diagnosis and treatment of a disease or illness, resulting in minimal secondary side effects [2]. Research into the adsorption of blood proteins to therapeutic surfaces has been highlighted as an important factor in the field of biocompatibility and biomaterials. The adsorbed protein corona substantially influences the biodistribution and clearance of the drug molecule in biological systems, which would in turn potentially disrupt the delivery to the target site for its intended application and reduce the drugs efficiency. In addition, the composition of the adsorbed protein coat may potentially trigger defence mechanisms, such as the coagulation and complement system cascades [3-5]. In particular, once introduced to the circulatory system, biomedical surfaces instantaneously encounter blood plasma proteins, such as opsonins (i.e. complement factor proteins and human plasma fibrinogen), which when bound, may result in the rapid uptake of the particle by the mononuclear phagocyte system (MPS) [6-8]. Conversely, the binding of dysopsonins (human serum albumin) to the surface results in an extended circulation lifetime of the particle within the blood system [9]. Numerous efforts have been directed towards the preferential binding of 'inactive' serum proteins to the biomaterial surface, such as human serum albumin (HSA), within the biological system. The design and development of such surfaces requires an in-depth understanding of adsorption that occurs at the biomaterial interface within the complex biological media, in terms of protein composition, and conformation [5].

To date, methods aimed at identification of the adsorbed protein coat composition, deposited on particulate therapeutics, predominantly involve gel electrophoresis analysis. In particular, two dimensional polyacrylamide gel electrophoresis (2D-PAGE), sodium dodecyl sulphate (SDS) PAGE, and Western blot analysis [10-17]. These particular techniques require extensive preparation of the sample, where centrifugation is utilised in the separation of the protein coated particle from non-adsorbed proteins in solution. This separation step introduces the

possibility of false protein identification, as protein aggregates, and larger protein molecules, may be unexpectedly incorporated in the purified sample preparation. In addition to the increase in possible experimental error, the above mentioned techniques require the active removal of the absorbed serum protein from the therapeutic surfaces, using solubilising agents. This active removal of serum proteins restricts the identification analysis to total level of protein present, omitting analysis of protein surface exposure, which is an influential factor. The detection and quantification of the adsorbed proteins is determined through comparative studies with control samples, therefore limiting the detection range [10-15].

Alternative methods utilised for the identification of adsorbed protein include, enzyme-liked immunosorbent assays (ELISA) and Surface Plasmon Resonance (SPR) [12, 14, 18]. Both the ELISA- and SPR-based methods require the immobilisation of the therapeutic to the relevant substrate. The utilisation of SPR for protein detection and identification provides real-time analysis of the protein-substrate adsorption process, in comparison to the analysis of the end-point product employed in ELISA studies. Similarly, Quartz Crystal Microbalance with Dissipation (QCM-D) has been employed for the analysis of blood protein adsorption, identification, and quantification. The latter method demonstrates reproducible, real-time measurements with the possibility of equal sensitivity, through optimisation, in comparison to ELISA methods, in a fraction of the time, consequently providing the 'rapid' aspect of the protocol to be designed [19, 20]. A comparison between SPR and QCM-D revealed no considerable differences, with respect to limit of detection, cost, sensitivity, etc. QCM-D does, however, allow for the analysis of structural changes, namely due to protein-substrate, and protein-protein interactions, which are essential aspects to consider when assessing protein adsorption, and therefore biocompatibility [20-22].

QCM-D technology has demonstrated application in a variety of fields, including, the development of biosensors, monitoring of biofouling and surface functionalisation, analysis of surfactants-based studies, and in particular, analysis of biomaterials and drug development [23-28]. According to Sellborn *et al.* (2002) [21], QCM-D may be utilised to assess the complement activating ability of model biomaterial surfaces, prepared on the QCM-D sensor crystal. This was reported to be achieved through the monitoring and quantification of anti-human C3c binding to the target surfaces, following treatment with human serum [21]. It

was on this basis that the utilisation of QCM-D, in this thesis, was proposed for the identification of adsorbed serum proteins on target surfaces. In particular, through the monitoring and quantification of subsequent target antibody binding, namely antibodies directed against human serum albumin, complement factor C3, and human plasma fibrinogen. Furthermore, the proposed method was assessed in terms of its application for protein detection on surfaces modified with therapeutic agents (i.e. metallophthalocyanines) and nanomaterials (i.e. multi-walled carbon nanotubes), and therefore potentially providing insight into their biocompatibility. To my knowledge, the utilisation of QCM-D for the identification and quantification of protein binding to therapeutic particle-modified sensor surfaces has not yet been assessed.

1.2. Quartz Crystal Microbalance with Dissipation Technology

Quartz Crystal Microbalance with Dissipation (QCM-D) technology stems from the classical QCM technique which is described as a surface sensitive piezoelectric based method for the monitoring and quantification of adsorbed mass [29, 30]. The QCM-D system demonstrates applications in the characterization of the formation of thin films, due to its nanogram sensitive mass measurements, provided by frequency (*f*) changes, and its insight into structural properties, provided by the dissipation (D) changes [30].

1.2.1. QCM-D Principal

QCM-D involves the administration of an alternating current applied to a thin, disc-shaped quartz crystal, sandwiched between a pair of metal electrode films (i.e. Au), to generate a fundamental, or overtone, resonance frequency [29, 30]. In response to the adsorption of mass onto the electrodes, a decrease in resonance *f* is observed which, in the case of the adsorption of a thin, rigid film with negligible internal friction, is proportional to the mass added [22]. This relationship is demonstrated by the Sauerbrey equation:

$$\Delta f = -\Delta m/\mathrm{nC} \qquad \textit{Eq. 1}$$

Where 'f' is the resonance frequency of the oscillating crystal, 'm' is the adsorbed mass, 'n' is the overtone number (1, 3, 5, 6…), and 'C' is the mass sensitivity constant (17.7 ng.Hz^{-1}.cm^{-2} for a 5 MHz quartz crystal) [31].

With regards to the adsorption of thick, and/or, loosely-structured viscoelastic films, the Sauerbrey equation does not hold true and leads to the underestimation of the adsorbed mass [22]. The 'failure' of the Sauerbrey equation in accurately determining adsorbed mass is due to the behaviour of the adsorbed viscoelastic film and its dampening influence on the propagation of the shear acoustic wave [32]. An additional factor contributing to the underestimation of the Sauerbrey adsorbed mass is due to the Sauerbrey model omitting coupled water/solvent molecules on or in the film. Coupled water has been reported to result in mass-uptake between 1.5 and 4 times greater than that of the adsorbed film dry mass [32].

The monitoring of an additional parameter, namely, dissipation, D, in combination with the *f* response, aids in overcoming the short-comings of the Sauerbrey-based determination of adsorbed mass, and allows for the concomitant characterisation of structural variations [25]. The D factor may be described as the dissipative energy loss of the oscillating crystal due to the internal friction of the adsorbed film [22, 29-30].

Shifts in the *f* and D responses have been related, through derivations by Voinova *et al.* (1999) [34], to the film density, thickness, and viscoelastic parameters, namely, viscosity and shear modulus [33]. In the event of the film-surface system behaving in accordance with a spring and dashpot mechanical element analogy for the system, where the spring corresponds with the shear rigidity of the film, and the dashpot with the viscosity, Voigt-based modelling of the film parameters is achievable [33]. The Voigt-based viscoelastic film model utilises both the *f* and D shifts to express the oscillatory motion of the shear acoustic wave propagating through a single homogeneous adsorbed layer, under non-slip conditions, when the film is in contact with a semi-infinite Newtonian liquid [32]. The mathematical model represents the adsorbed viscoelastic film via employing four unknown parameters, namely; elastic shear modulus (μ_f), shear viscosity (η_f), film thickness (δ_f), and film density (ρ_f), by the use of *f* and D shifts of 2 or more harmonics. The coupled water in or on the adsorbed film is taken into account when using this model [32, 34]. Shear modulus is described as the ratio of shear stress applied to a body to the shear strain produced, in particular, the tangential forces to angular deformation. Viscosity is the measure of the resistance to flow presented by a fluid when subjected to shear stress [Internet Reference 1]. Figure 1.1 schematically illustrates the

viscoelastic film parameters, namely shear modulus (A) and viscosity (B), in terms of film deformation under shear stress.

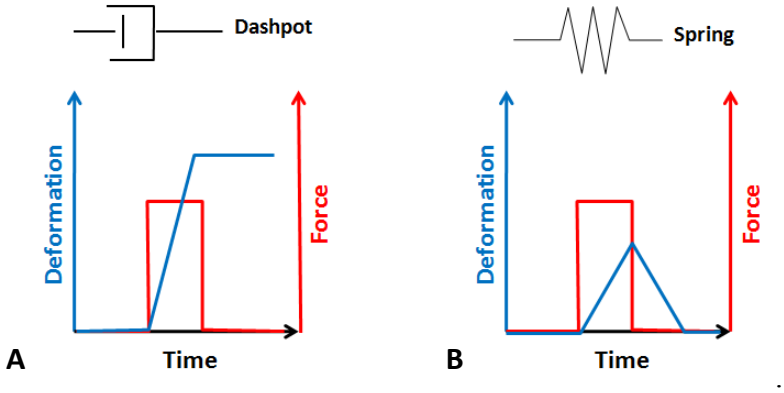

Figure 1.1. Schematic representation of film deformation under shear strain illustrating film viscosity (A), and shear modulus (B). Adaption of q-sense ® [Internet Reference 1].

The Voigt model has, however, set requirements of the film for the accurate prediction of the *f* and D response (at any overtone) to *n* viscoelastic layers, namely [Alternative Reference 1];

- Total coverage of the sensor surface, of each layer, must be achieved
- The deposited films are required to be of uniform thickness and homogeneous in nature
- The viscoelastic properties of the deposited films are required to comply with either the Voigt, or Maxwell, viscoelastic representations
- The film is required to demonstrate overtone-independent viscoelastic properties
- All layers are free of internal stress
- The film is required to be in contact with a bulk Newtonian fluid

1.3. Target Proteins

An ideal biomedical therapeutic is one which demonstrates an extended serum half-life, therefore increasing target site delivery, one which is non-toxic to biological components, one which evades the immune system, and one which maintains its integrity while within the biological system [3, 17]. The blood proteins of interest for this research are proteins which have been reported to be influential in biocompatibility, namely; human serum albumin

(Figure 1.2), a dysopsonin involved in particle blood circulation, human complement C3c (Figure 1.3), an opsonin involved in surface induced complement activation via the alternative pathway, and human plasma fibrinogen (Figure 1.4) an opsonin involved in the coagulation cascade.

1.3.1. Human Serum Albumin

The globular protein, human serum albumin (HSA), is an abundant protein in human plasma (45mg/ml), which has been reported to demonstrate a high binding affinity towards negatively charged surfaces, as well as a greater affinity towards hydrophobic surfaces in comparison to hydrophilic surfaces [35, 36]. However, the protein retention time on the hydrophobic surface is reported to be shorter, in addition to demonstrating a greater surface coverage of the HSA molecules [36]. This increase in surface coverage is due to HSA exhibiting an isoelectric point (*pI*) value of 4.7, and therefore rendering it highly charged in physiological conditions, which subsequently results in the protein molecule demonstrating a decrease in stability with increase in pH shift from the *pI* value [36]. X-ray crystallographic analysis of the protein indicates equilateral triangular dimensions of 8 nm (sides) × 3 nm (depth) (Figure 1.2) [5]. Rasmol generated images were based on the relevant Protein Data Bank (PDB) files obtained from Research Collaboratory for Structural Bioinformatics (RCSB).

Its relatively small size, and high serum concentration, results in HSA being a dominant protein identified on biomedical surfaces. Its presence on the surface greatly influences the circulation half-life of biomaterial, prolonging circulation and inhibiting phagocytosis [18]. In addition, it has been documented that the presence of a HSA coating on biomedical surfaces reduces negative side effects, such as coagulation and inflammation [37]. This feature of evading the immune, and the coagulation system, and subsequently increasing particle circulation time, is attributed to the adsorption of HSA on the biomedical surface, providing the surface with a hydrophilic nature, therefore reducing further blood protein binding [38]. As a result of these qualities, albumin has been reported to be utilised as a drug carrier molecule [39].

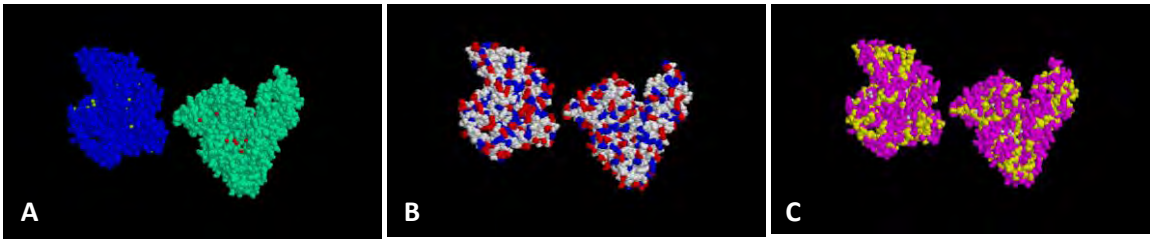

Figure 1.2. Rasmol images of human serum albumin (PDB: 1E78). A, indicates the chains of the protein; B, indicates the basic (blue) and acidic (red) moieties; and C, indicates the hydrophobic (yellow) and hydrophilic (magenta) moieties.

1.3.2. Human Complement C3c

In the event of immune complement activation by therapeutic drugs and medical devices, not only alterations in the biodistribution and clearance of the drug are observed, but life-threatening conditions may arise, such as hypersensitivity and anaphylaxis [9]. Numerous methods aimed at determining the immune complement activation potential of a novel surface have been reported. Such as the detection of the C5a and C3a soluble complement components using radioimmunoassay and ELISA techniques, or detecting the presence of surface-bound complement factors such as C3 and C3b using methods such as surface plasmon resonance (SPR) and quartz crystal microbalance with dissipation (QCM-D) [9]. The detection of surface bound C3c has been reported as an arbitrary measure of bound complement factor C3, an indicator of surface induced complement activation [29].

Each activation pathway of the complement system results in the cleavage, and therefore activation, of the 185 kDa complement component 3 (C3) into 9 kDa C3a and 180 kDa C3b peptide fragments via the action of the C3 convertase generated by each pathway [18, 40, 41]. The resultant C3a fragment is released into the fluid medium, while C3b undergoes conformational change and is bound to the surface of the activating substance [40, 41]. Examples of complement activating surfaces are surfaces which display nucleophiles, such as hydroxyl and amino groups, while non-activating surfaces display negatively charged groups, e.g. carboxyl group [40]. The presence of negatively charged groups results in the increase in the affinity of the C3b complement for the complement regulation protein, Factor H [40].

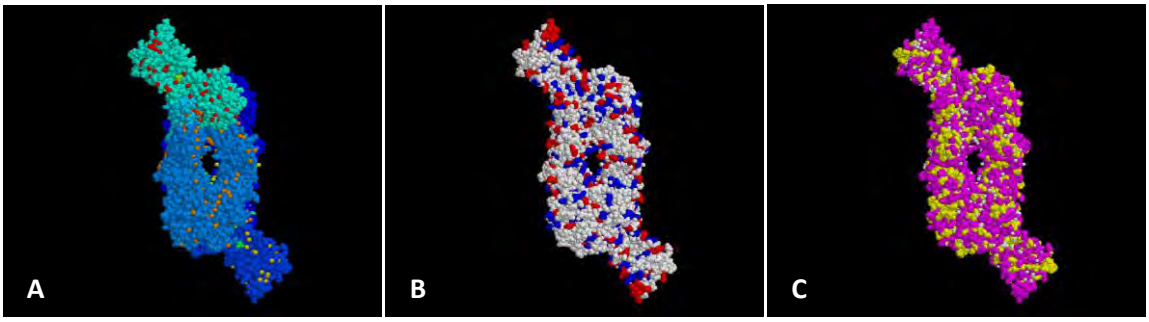

Figure 1.3. Rasmol images of complement factor C3c (PBD: 2A74). A, indicates the chains of the protein; B, indicates the basic (blue) and acidic (red) moieties; and C, indicates the hydrophobic (yellow) and hydrophilic (magenta) moieties.

1.3.3. Human Plasma Fibrinogen

Human plasma fibrinogen (HPF), a key protein in the coagulation cascade, and platelet adhesion and aggregation, is a highly elongated protein with a molecular weight of 340 kDa and dimensions of approximately 47 x 4.5 x 4.5 nm^3, which is abundantly found in human plasma (3mg/ml) [5, 28, 42-44]. Structurally, HPF is composed of 6 polypeptides and demonstrates a *pI* of approximately 5.5, and therefore a net negative charge at physiological pH (Figure 1.4) [28, 44]. Functionally, HPF plays a role in blood coagulation, aggregation and adhesion processes of platelets, and is therefore an influential protein in biomaterial biocompatibility [42-44]. A high affinity towards hydrophobic surfaces has been reported, however, hydrophobic terminating self-assembled monolayers (SAMs) (e.g. CH_3) have also been reported to deposit significantly lower amounts of fibrinogen in comparison to hydrophilic terminating SAMs (e.g. OH) [27].

It has been postulated that the adsorption of fibrinogen to hydrophobic surfaces results in conformational change of the protein [45]. According to literature, Gessner *et.al.* (2002) [46], fibrinogen deposition on polymeric nanoparticles, demonstrating various surface charge densities, was the dominant protein when assessing human plasma deposition, along with immunoglobulin G (IgG) [46]. The D- and αC-domains of the protein are reported to be the surface active domains, where initial binding occurs through weak interactions with the αC-domain (Figure 1.4). It has been documented that HPF adsorbs in a concentration-dependent manner, where, under low concentrations, rearrangement of the molecule may occur, to allow surface adsorption between both the αC- and D-domains. This concentration

dependent adsorption of the HPF molecules to surfaces attributes to the variability in the structure of the film [28].

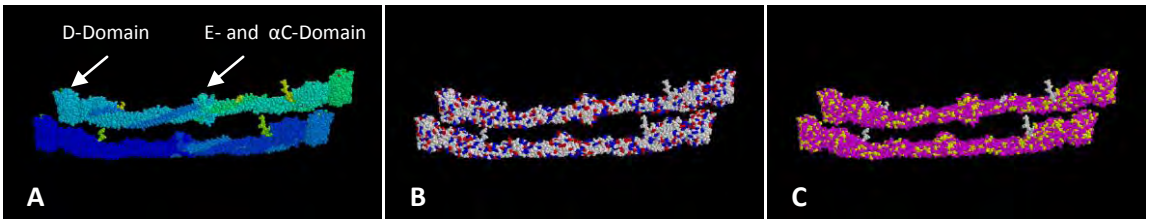

Figure 1.4. Rasmol images of human plasma fibrinogen (PDB: 3GHF). A, indicates the chains of the protein; B, indicates the basic (blue) and acidic (red) moieties; and C, indicates the hydrophobic (yellow) and hydrophilic (magenta) moieties.

1.4. Target Therapeutic Particles

1.4.1. Metallophthalocyanines

Photodynamic Therapy

Photodynamic Therapy (PDT) is a promising treatment of malignant (cancer of the lungs, stomach, bladder, etc.) and non-malignant conditions (macular degeneration) [47, 48]. Selective cell death is induced in the presence of photosensitiser (PS), such as metallophthalocyanines (MPcs), visible light, and oxygen [47, 48]. The mechanism through which the PS molecules, such as MPcs, are activated, and subsequently induces cell death, is illustrated in Figure 1.5.

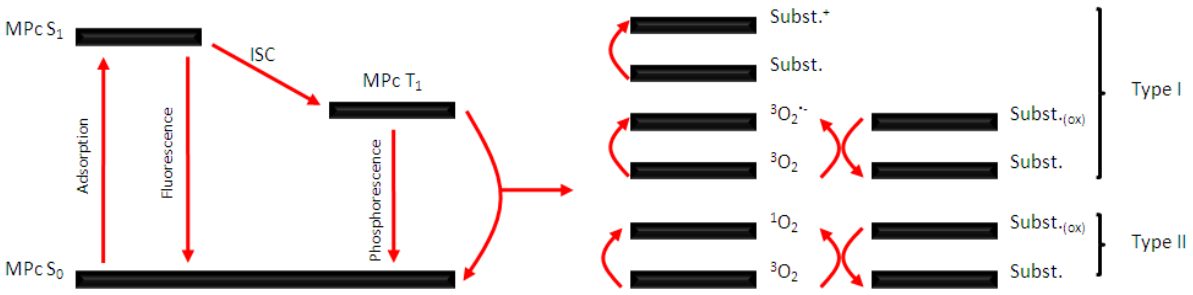

Figure 1.5. Modified Jablonski diagram illustrating the photosensitising process of MPc molecules.

As Figure 1.5 displays, on absorption of visible light, the MPc molecule is excited to a short-lived singlet state (MPc S_0 → MPc S_1), where through intersystem crossing (ISC), a

radiationless relaxation process, excites the MPc triplet state (MPc T_1). It is this excited triplet state which undergoes either Type I or Type II mechanism reactions where it reacts with the surrounding environment.

In the Type I mechanism, the triplet state energy of the MPc molecule is transferred to surrounding substrate molecules (Subst.) or ground state oxygen ($^3O_2$), resulting in the oxidation of the substrate ($Subst._{(ox)}$) through the production of superoxide radicals ($^3O_2^{\bullet-}$), hydrogen peroxide, and hydroxyl radicals. Type II mechanism involves the transfer of energy from the excited triplet state MPc to ground state oxygen, to generate cytotoxic excited singlet state oxygen ($^1O_2$) [47, 49-51]. Cell death results due to damage of the cellular membranes, organelle structures and genetic material from radicals and singlet state oxygen [50, 51]. Additionally to the direct cytotoxic action of PDT (outlined in Type I and II mechanisms in Figure 1.5), triggered release of complement proteins, inflammatory mediators, and growth factors occurs, as well as damage to the vasculature associated with the tumour [50].

Attributes required from a viable PS molecule include selective tumour localising ability, absorption of light in the red or near infra-red region of the spectrum, as greater tissue penetration is achieved at longer wavelengths, in addition to being non-toxic. Through modification of the Pc molecule, such as ring substitution and strategic selection of central metals, MPcs may be designed to bear these desired traits [52]. The ease of substitution of the MPc aromatic rings, and incorporation of the metal centres, allows for the modulation of physicochemical properties to increase the activation wavelength, triplet state quantum yield, solubility, and triplet lifetimes [49, 53-55].

Chemical and Structural Properties

Metallophthalocyanines (MPcs) are aromatic metal complexes composed of N_4 - ligands which resemble naturally occurring biological molecules, such as vitamin B_{12} (cyanocobalamine) [56, 57]. Essentially, phthalocyanines adopt a planar conformation, however, distortion of the macrocycle geometry may occur when large central metal ions are

employed (e.g. lead), as well as through conformational stress experienced due to the presence of ring substituents [49]. Figure 1.6 schematically illustrates the MPc structure.

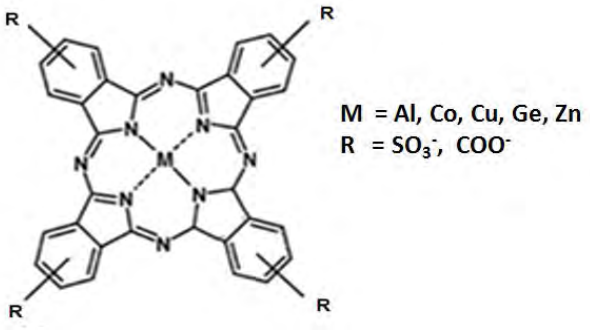

Figure 1.6. Schematic representation of a tetra-substituted metallophthalocyanine molecule. Metal centres and substituents present in scheme form the basis for research reported on in this chapter.

Metallophthalocyanine Applications

MPc compounds have been reported to catalyse an array of chemical reactions, both homogeneous and heterogeneous [56]. The distinct physical and chemical properties of MPc compounds allow them to be utilized in a variety of applications, such as sensors, electrocatalysts, and photosensitisers. [57]. Pertinent to the purposes of this research, MPc are utilized photosensitizers in the photodynamic treatment of cancer, such as skin, breast, oesophageal, and lung cancer [53, 58]. MPc molecules utilised in the latter contain non-transition metal ions (i.e. Al, and Ge) as the central metal, as they promote high triplet state quantum yields, as well as extended triplet lifetimes [49].

Metallophthalocyanine Aggregation

An additional requirement of the MPc molecule intended for use as a PS agent is the exhibition of a hydrophilic nature to aid particle solubility, as administration of the therapeutic is through intravenous injection [50]. Ring substitution of the macrocycle MPc, with sulphonic acid and carboxylic acid, has proved to be an effective modality in promoting MPc solubility [59]. However, water-soluble MPcs display a tendency to aggregate when in aqueous solution. This aggregation of MPc molecules is the result of the formation of π-π interactions, which are permitted by the planar geometry of the macrocycle [60]. MPc

aggregation has a negative effect on the production of the singlet oxygen quantum yield as it results in the dissipation of the excited singlet state energy [49]. Aggregation has been reported for MPc molecules demonstrating a low degree of sulphonation, such as $CuPcS_2$ and ZnPcS [60, 61].

Surfactant dissociation of the MPc aggregates has been demonstrated, however, the use of such a method is not applicable in the current experimental procedure, as interference with MPc immobilisation to the SAM surface, and with blood protein binding may occur [49]. Mechanical means of dispersion, namely, extended ultra-sonication of the MPc solutions, was therefore favoured.

Currently, derivatives of sulphonated aluminum phthalocyanines have been utilized in the photodynamic treatment of cancer, while non-transition metal sulphonated phthalocyanines, Zn and Mg phthalocyanines, and thiol-derivatized MPc's are under investigation [56]. The biocompatibility of MPc molecules was the subject of Chapter 3, and 5.

1.4.2. Carbon Nanotubes

Structurally, carbon nanotubes (CNTs) are hollow cylinders composed of hexagonal arrangements of carbon atoms that demonstrate significant electrical, electrochemical and mechanical characteristics [62]. Two forms of synthesised CNTs exist, namely, single-walled carbon nanotubes (SWCNTs), which consist of one single-walled tube, and multi-walled carbon nanotubes (MWCNTs), which consist of layers of carbon tubes (Figure 1.7) [63].

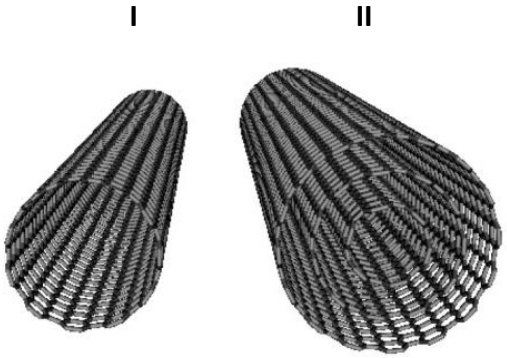

Figure 1.7. Schematic representation of single-walled (I) and multi-walled (II) carbon nanotubes.

Carbon Nanotube Application

To date, the use of CNTs for the encapsulation of therapeutic drugs has been investigated, as well as their application in gene therapy, tissue engineering and as scaffolds for cellular growth [63-65]. Numerous studies have been conducted, aimed at assessing the biocompatibility of such materials, however, results obtained have generally been inconclusive and often contradictory [66-69]. Several *in vitro* studies report little, or no CNT-induced cytotoxicity [69, 70], while some indicate adverse effects, such as decrease in cell viability, activation of inflammatory responses [71], apoptosis [72], and oxidative stress [73]. One of the key concerns, in terms of CNT nanotoxicity, is the presence of contaminants, generated through CNT synthesis, as well as the tendency of CNTs to aggregate [62, 68].

Carbon Nanotube Functionalisation

There are several proposed methods currently researched to address the aspects of CNT purity and aggregation, in particular, surface oxidation of nanotubes. This can proceed via chemical oxidation, photo-oxidation, gas phase treatment, and exposure of CNTs to oxygen plasma [74]. Of particular interest is that of chemical oxidation, as it is a well established, simple and efficient means of functionalising CNT surfaces with oxygen containing groups [75].

In addition to increasing purity and decreasing aggregates, oxidation of CNTs adds further substituents, such as hydroxyls and carboxyl groups, which allows for further functionalisation of the CNT surface, as the substituents provide sites for covalent and non-covalent attachment of other particles to the sidewalls of the CNTs [63, 76]. Functionalisation, through chemical oxidation, therefore provides a means to alter surface properties of the CNTs, towards improving biocompatibility [76].

The biocompatibility of CNTs, both non-functionalised and functionalised is of immediate research interest given their rapid incorporation into several technologies (e.g. drug delivery) [64]. This was the subject of Chapter 4.

1.5. Research Aims and Objectives

The central aim of this research is to establish a platform directed at assessing the biological fate of pioneering therapeutic particulate agents, such as metallophthalocyanines (MPcs) and multi-walled carbon nanotubes (MWCNTs). In particular, we proposed, in this thesis, that QCM-D technology may be utilised to assess the composition of blood protein coats deposited on the therapeutic surface, and subsequently assess the biocompatibility of such particles. Figure 1.8 illustrates the main objectives addressed, in the relevant chapters, to asses QCM-D applicability in as a screening method for target particle biocompatibility.

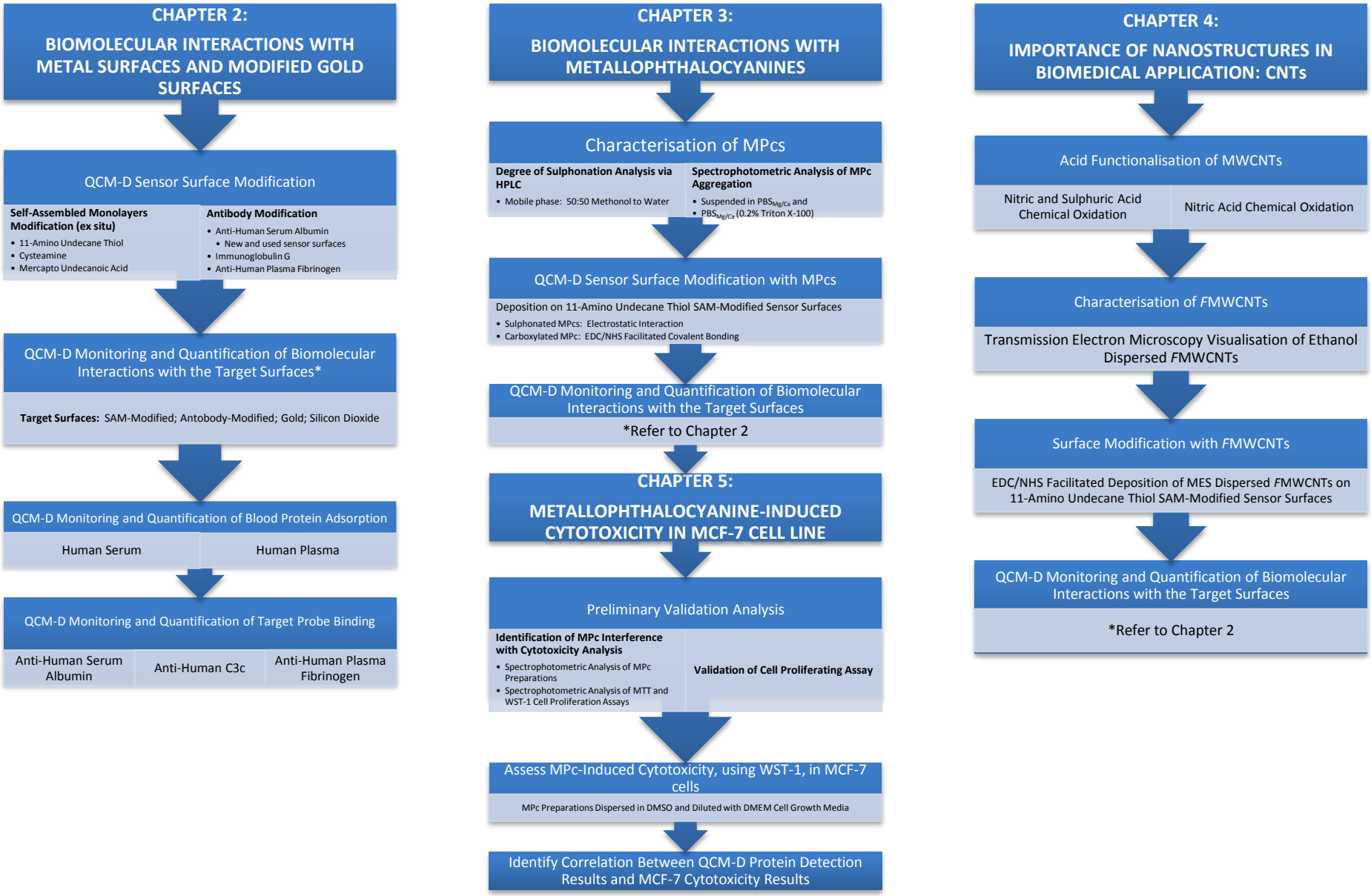

Figure 1.8 Main objectives addressed for the analysis of QCM-D applicability in biocompatibility analysis of metallophthalocyanines and acid functionalised multi-walled carbon nanotubes.

CHAPTER 2:

BIOMOLECULAR INTERACTIONS WITH METAL SURFACES AND MODIFIED GOLD SURFACES

2.1. INTRODUCTION

2.1.1. Preliminary Studies

Prior to investigations assessing the composition of the blood protein films which coat the target therapeutics, namely acid functionalised multi-walled carbon nanotubes (*F*MWCNTs) and MPc molecules, preliminary studies were necessary to assess both the accuracy, and reproducibility of the proposed detection method, as well as establishing the uppermost levels of target protein detection, via the design of control experiments.

2.1.2. QCM-D Sensor Surface Modification

In order to examine the biocompatibility of a wide range of biomedical surfaces, techniques such as Surface Plasmon Resonance (SPR), Atomic Force Microscopy (AFM), ellipsometry, and recently, QCM-D, have been relied on the use of generic surface modification techniques [21, 27, 42, 77-81]. In particular, surface modification through the formation of self-assembled monolayers (SAMs) has proven to be a highly reproducible and stable method [21, 27, 77, 82].

The metal electrode surface (i.e. gold) of the quartz crystal sensor, utilised in QCM-D, exhibits favourable surface properties which facilitate simple electrode surface modifications. In addition to diversifying the range of the QCM-D sensor surface characteristics, with respect to surface charge, surface moieties, etc., these electrode modifications prove to be beneficial in the immobilization of target molecules via the introduction of required chemical properties on the surface, and therefore the construction of a desired interface [83].

2.1.2.1. Self-Assembled Monolayer Modification

The use of a self-assembled monolayer (SAM) deposition is a simple and effective means of modifying an electrode as it provides reproducibility and stability. This spontaneous organization of a single layer of SAM molecules is the result of the high affinity of the molecules terminal functional group for the target surface [56]. In the case of gold surface modification, *n*-alkyl thiols are reported to assemble in a monolayer fashion, where strong interactions between the thiol sulphur and the gold surface results in an approximately 30° near polar covalent interaction. Studies reveal distinct differences in monolayer structure when assessing long- and short-chain alkyl thiols: more densely-packed, reproducible films are deposited when the chain length exceeds $n = 9$ [84-86]. The selection criteria for the SAM molecules is based on what is to be immobilized (i.e. target molecule) onto the Au substrates and to what it is being immobilized to (i.e. electrode surface), as well as the desired monolayer thickness.

A wide range of thiolated molecules are available for gold surface modification. Through monolayer coverage of surfaces, SAM surface modification provides for the study of the biocompatibility of a range of different exposed functional groups, of differing charges and differing physical properties. It also provides a platform for the immobilisation of the different target molecules, and the study of the biocompatibility thereof (as described in Chapters 3 and 4, for MPc- and CNT- modified surfaces, respectively).

For the purpose of this study protein adsorption to gold and silicon dioxide coated sensor surfaces, and both positively and negatively charged SAM interfaces formed on Au substrates, were assessed. The utilisation of gold and silicon dioxide sensor surfaces (whereby protein interactions at the surface is examined directly) provides information on the interaction between the blood proteins and hydrophobic, and negatively charged hydrophilic solid surfaces, respectively. Furthermore, utilisation of differently charged SAM surfaces allows the influence of surface charge on protein binding to be assessed. Varying length *n*-alky thiols were utilised for the generation of positively charged surfaces, also permitting the examination of the influence of film density on biocompatibility with the target proteins.

Cysteamine is frequently utilised for SAM surface modification yielding a positively charged surface with exposed NH_3^+ groups, with a chain length of $n = 2$. Likewise, 11-amino

undecane thiol exposes a NH_3^+ charge, but has a longer chain length of $n = 11$[83]. Mercapto undecanoic acid yields a negatively charged surface with exposed COO^- groups at physiological pH [87].

2.1.2.2. Antibody Modification

The deposition of antibody molecules on the gold sensor surface (Figure 2.1; A), directed against the target proteins, and the subsequent blood protein adsorption, served as a means of assessing the uppermost level of probe antibody binding, due to the specificity of the antibody-antigen interaction. In particular, anti-human albumin (Ab_{HSA}), human immunoglobulin G (IgG), and anti-human fibrinogen (Ab_{HPF}) were utilised in the surface modification of the gold sensor surface for the detection of adsorbed human serum albumin (HSA), complement factor C3c, and human plasma fibrinogen (HPF), respectively. IgG was employed for complement C3c detection as it is reported to be an activator of the complement system, through classical pathway activation [88]. The adsorption of IgG molecules to gold surfaces has been well documented, as well as its applicability in the detection of surface induced complement activation studies utilising anti-human C3c probe molecules [21, 89]. Figure 2.1 schematically illustrates the target surfaces evaluated in this chapter.

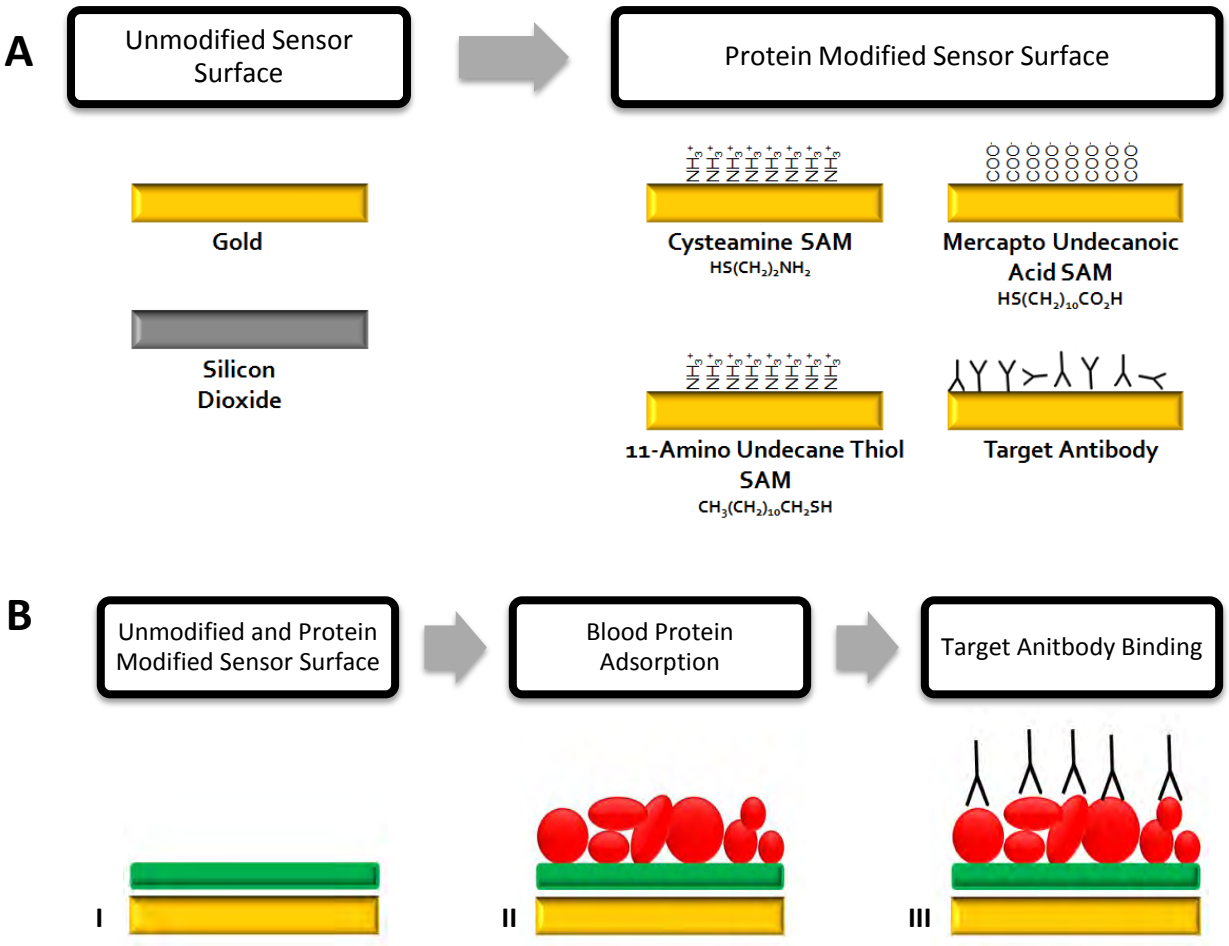

Figure 2.1. Schematic representation of (A) target surfaces probed for blood protein adsorption; (B) adsorbed target protein detection protocol monitored using QCM-D. I (B) illustrates the target surfaces, both modified and unmodified; II, the adsorption of blood proteins; and III, the detection of target proteins via antibody binding. Antibodies utilised were directed against human serum albumin, complement factor C3c, and human plasma fibrinogen.

2.1.3. Chapter Aims and Objectives

The principle aims of this chapter were to assess the efficiency of QCM-D in examining protein adsorption on surfaces which demonstrate known characteristics, secondly to establish control experiments, and thirdly, to evaluate experimental reproducibility.

Objectives

1. Fabricate target surfaces, with known characteristics, *ex situ*, for subsequent binding analysis
    a. SAM modification of the gold sensor surface, to generate positively charged (11-AUT and Cyst.), and negatively charged (MUA) surfaces
2. Fabricate control surfaces for HSA, complement C3c and HPF protein analysis
    a. Target antibody adsorption (Ab_{HSA}, IgG, and Ab_{HPF}) to the gold sensor surface, monitored and quantified using QCM-D
    b. Fabrication of the HSA control surface on both new, and used gold sensor surfaces, to assess experimental reproducibility dependence on the quality of the gold sensor surface
3. Monitor and quantify blood protein adsorption to the prepared modified, and unmodified surfaces, using QCM-D
4. Monitor and quantify probe antibody binding to the previously prepared blood protein coated surfaces, using QCM-D

2.2. INSTRUMENTATION AND METHODOLOGY

2.2.1. Instrumentation

Frequency and dissipation measurements were recorded in a Quartz Crystal Microbalance with Dissipation E-4 system (Q-Sense AB, Goteborg, Sweden), using QSoft Acquisition Software. The QCM-D sensors used were AT-cut quartz crystals, 14 mm in diameter, sandwiched between 100 nm thick polycrystalline gold electrodes, with fundamental resonance frequency of 5 MHz (Q-Sense AB, Goteborg, Sweden). Data analysis was performed using the QTools Analysing Software provided by Q-Sense. Ultrasonication of samples, for the purpose of degassing, was carried out using an S10H Elmasonic sonicator. Ultraviolet/ozonation, UV.TC.EU.003 (Bioforce Nanosciences), was utilised in the preparation of the quartz sensor surfaces.

2.2.2. Reagents

Protein adsorption analysis was performed in a 1 X PBS buffer solution, containing NaCl (Merck), KCl (Sigma), Na_2HPO_4 (Sigma), KH_2PO_4 (Merck), $MgCl_2$ (Merck) and $CaCl_2$ (Merck), referred to as $PBS_{Mg/Ca}$. For PBS buffer utilised in negative controls, referred to as PBS, both $MgCl_2$ and $CaCl_2$ supplements were omitted. The pH of the buffer was adjusted, using 0.2 mM NaOH (Merck), to the physiological pH of 7.4. PBS was utilised as the solvent in the preparation of 5% human serum solutions, obtained from 3 donors (Reagent A+; SANBS), and 5% human plasma solutions (Reagent A+; SANBS), as well as in 2% dilutions of polyclonal rabbit anti-human C3c complement, anti- human albumin, and anti-human fibrinogen, supplied by DakoCytomation, according to Sellborn, A. *et al.* (2002) [21]. In the case of the negative control, for complement C3 detection, heat inactivated human serum (iHS) was utilised. iHS was prepared via heat denaturation of the blood proteins for a period of 30 min at 75°C. Prior to use, the buffers, as well as all the solutions prepared, were degassed via ultrasonication for a period of 10 min.

Surface modifications were prepared utilising Human IgG, Plasma (Calbiochem), anti- human albumin (DakoCytomation), anti-human fibrinogen (DakoCytomation), 11-amino undecane thiol, hydrochloride (Dojindo Laboratories), cysteaminium chloride (Merck), and 11-mercapto undecanoic acid (Merck), as per Figure 2.1.

Sodium dodecyl sulphate (90%), for cleaning purposes, was purchased from BDH Laboratory Supplies.

The above mentioned reagents were utilised throughout the experimental procedures outlined in chapters 3 to 5. Additional reagents required for analyses described in the latter chapters are listed in the relevant instrumentation and methodology sections.

2.2.3. Methodology

2.2.3.1. Preparation of QCM-D System

Prior to use, the gold coated, AT-cut, quartz crystal were thoroughly cleaned using an established protocol (Fogel, e*t al.* (2007)) [57]. The crystal is initially ultrasonicated in an

aqueous 2% solution of sodium dodecyl sulphate (SDS) to remove any loosely-bound proteins, followed by a rinse step with 95% absolute ethanol and MilliQ water, and a 5 min immersion in a 5:1:1 solution of MilliQ water, 30% hydrogen peroxide (Merck), and 25% ammonia (Merck) heated to 75°C, for the removal of lipids, thiols and proteins. The crystal was then thoroughly rinsed with 95% absolute ethanol and MilliQ water before drying with nitrogen gas (99.9%; Afrox) and exposure to ultraviolet/ozonation for approximately 2 min to remove organic contaminants.

Cleaning of the QCM-D chamber and tubing occurred before, and after each measurement, via flushing the system with 2% SDS, followed by MilliQ water, for a period of 15 min, respectively. The chamber was rinsed with absolute ethanol and MilliQ water, followed by 99.9% nitrogen gas (Afrox) drying.

2.2.3.2. Sensor Surface Modification

2.2.3.2.1. Self-Assembled Monolayer

The preparation of 11-amino undecane thiol (11-AUT), mercapto undecanoic acid (MUA), and cysteamine (Cyst.) SAMs was carried out to evaluate the surface induced human serum and plasma protein adsorption on homogenous carboxylic acid and amine terminating layers, in addition to aiding target particle immobilisation (Chapter 3 and 4). SAM surface modifications were achieved by immersing a newly cleaned crystal in either an ethanol solution of 11-amino undecane thiol, hydrochloride, or 11-mercapto undecanoic acid, or an aqueous solution of cysteaminium chloride, followed by incubation overnight at 4°C. Prior to addition of the SAM molecules, the ethanolic solvent, and aqueous solution were de-aerated via bubbling with nitrogen gas for a period of 10 min. Following the overnight incubation, the SAM-modified gold sensor crystals were thoroughly rinsed with ethanol and MilliQ water, several times, and dried with nitrogen gas prior to mounting in the QCM-D flow chamber.

2.2.3.2.2. Antibody Controls

Adsorption of the relevant antibodies to the gold sensor surface was monitored using QCM-D. For the positive detection of surface induced complement activation, i.e.

complement C3 adsorption, 0.01μg/ml of IgG in $PBS_{Mg/Ca}$ was introduced to the crystal surface. The negative control, for complement activation, involved the deposition of IgG, dispersed in PBS buffer at a concentration of 0.01μg/ml. Anti-human albumin- and anti-human fibrinogen-$PBS_{Mg/Ca}$ solutions were introduced to the sensor surface in a 0.14 mg/ml dilution. Theoretically determined IgG-monolayer mass was determined for two scenario's, namely, edge-on and planar orientation, with the aid of X-ray chrystillographic determined dimensions, using the following formulae:

Calculations

Edge-On: $Height_{IgG} \times Breadth_{IgG} = Surface\ Area(SA)_{IgG\ (1)}$ *Eq. 2*

Planar: $Length_{IgG} \times Breadth_{IgG} = Surface\ Area\ (SA)_{IgG\ (2)}$ *Eq. 3*

$SA_{Au\ Crystal} \div SA_{IgG} = Number\ of\ molecules\ on\ Au\ surface_{IgG}$ *Eq. 4*

$Number\ of\ molecules_{IgG} \times Atomic\ Mass\ Unit = Monolayer\ Mass_{IgG}$ *Eq. 5*

$Monolayer\ Mass_{IgG} \times 1/\ SA_{Au\ Crystal} = Monolayer\ Mass\ per\ cm^{-2}{}_{IgG}$ *Eq. 6*

2.2.4. QCM-D Monitoring and Quantification

The complement activation detection protocol for the analysis of macromolecular surface induced complement activation using QCM-D technology reported by Sellborn, *et al.* (2002) was followed, with modifications, for the detection of the surface bound proteins [21]. The procedure involved obtaining stable frequency and dissipation baselines in buffer solution, followed by the introduction of a 5% dilution of human serum/plasma in buffer, to allow serum protein binding to the quartz crystal surface, modified or unmodified. Following a buffer rinse, an antibody specific for the target protein was introduced, in a 2% dilution with buffer. This was followed by a buffer rinse. $PBS_{Mg/Ca}$ buffer solutions were used for all the complement activation analyses, with the exception of the negative control, where PBS buffer was utilised. The flow rate and temperature parameters of the QCM-D system were set at 100 $\mu l.min^{-1}$ and 32.0°C, respectively. Both the biomolecular interaction between the prepared surface and human serum proteins, as well as the interaction between the bound serum proteins and antibody was monitored, and quantified, using QCM-D technology.

2.3. RESULTS AND DISCUSSION

Section 2.3.1. provides an introduction to data analysis techniques employed when assessing QCM-D responses. Section 2.3.2. details gold surface modification through antibody adsorption obtained using QCM-D technology. Section 2.3.3. addresses the composition of the adsorbed blood protein coat generated on both the modified and unmodified surfaces, in particular, the detection of HSA, complement factor C3, and HPF, using probe antibodies binding, monitored using QCM-D.

2.3.1. Introduction to QCM-D Data Analysis

Quartz Crystal Microbalance with Dissipation (QCM-D) is a surface sensitive piezoelectric based method for the monitoring and quantification of adsorbed mass, in the nanogram scale. QCM-D technology simultaneously measures two parameters, namely, frequency (*f*), which is dependent on the oscillating adsorbed mass and the intrinsic properties of the film, and dissipation (D), which is dependent on the films viscoelastic properties [45, 90, 91]. Figure 2.2 illustrates the *f* and D outputs, at overtones of 7, 9, and 11, produced from the adsorption of human serum (HS) to the 11-AUT SAM-modified gold sensor surface, and the subsequent anti-human C3c binding (Ab_{C3c}). Crude analysis of the *f* and D responses recorded provides information on deposited film rigidity, film interface roughness, and subsequent structural changes of the deposited film due to the particle/protein adsorption [23, 30, 92].

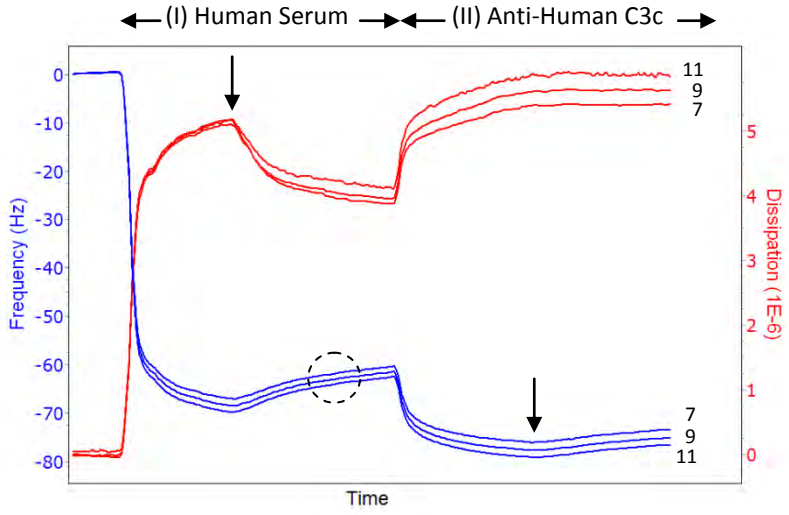

Figure 2.2. QCM-D frequency (Blue) and dissipation (Red) shifts illustrating human serum adsorption to the 11-amino undecane thiol self-assembled monolayer-modified gold sensor surface (I) and subsequent anti-human C3c binding (II). The frequency shifts represented are *f*/*n*, where *n* represents the overtone number. Introduction of $PBS_{Mg/Ca}$ buffer, for the removal of non-specifically bound protein, is illustrated by the vertical arrows. Separation of *f*, suggesting surface roughness, is indicated by the dashed circle. Overtones 7, 9 and 11 are illustrated.

QCM-D Response Analysis

An important film parameter, obtainable from frequency (Δf) and dissipation (ΔD) shifts generated from the deposition of a film, is that of ($\Delta f/\Delta D$). This parameter provides information on relative film rigidity: the higher the value of $\Delta f/\Delta D$, the more rigid the film, while low values are indicative of the adsorption of a fairly viscoelastic film [36]. The $\Delta f/\Delta D$ value of a film may also serve as an indication of the validity of the Sauerbrey determined film thickness and adsorbed mass. When this value is below 10 Hz/1E-6, there is no longer a linear relationship between the Δf and adsorbed mass (Δm), therefore resulting in the 'failure' of the Sauerbrey model [23].

Structural properties of the film interface are indicated by the dependence of the Δf, and therefore Δm, on the overtone number. An overtone-dependent mass shift suggests the deposition of a film which demonstrates a 'rough', or 'fuzzy' interface, while an overtone-independent mass shift suggests a 'sharp' interface [30]. A rough film interface is visible as a

separation of the ($\Delta f/n$) values, as observed in the HS adsorption to the gold sensor surface in Figure 2.2 (Phase I; dashed circle). For the purpose of this study, the nature of the film interface is represented in terms of the average ($\Delta f/n$) percentage coefficient of variation (% CV), where a high % CV corresponds with a 'rough' interface, and vice versa.

Analysis of structural changes due to the addition of molecules to the surface may be represented through plotting D versus *f* responses. The latter method of analysis illustrates the time-independent structural changes of the film due to the addition of individual mass units [92]. Figure 2.3 illustrates the D versus *f* plot (overtone $n = 7$) generated from the adsorption of HS on an 11-AUT SAM-modified surface, and the subsequent Ab_{C3c} binding. This plot serves as an example for the interpretation of D vs. *f* plots. D vs. *f* plots, in addition to providing information on film structural changes, schematically illustrate the time dependence of the adsorption process. This is observed in the separation of the data points: further separation is an indication of a higher rate of mass addition, and vice versa [30, 22].

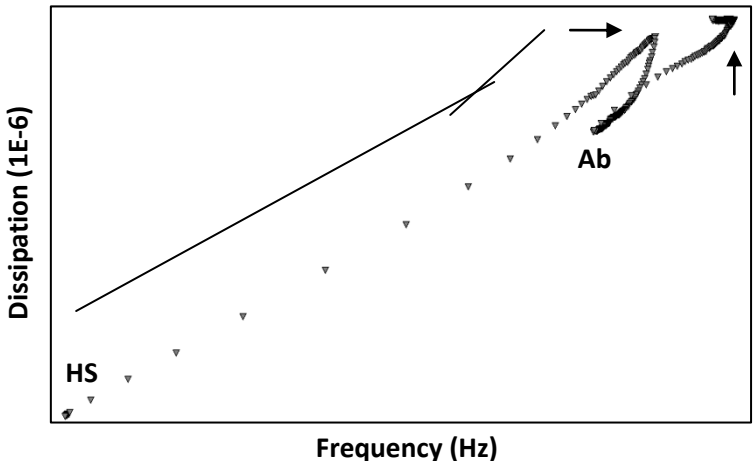

Figure 2.3. Dissipation versus frequency plot of human serum adsorption, and the subsequent anti-human C3c binding, to the gold QCM-D sensor surface modified with an 11-amino undecane thiol SAM. The gradient of the plot is schematically illustrated by the solid lines. Point of introduction of human serum, anti-human C3c, and $PBS_{Mg/Ca}$ buffer are indicated by HS, Ab, and arrows, respectively. Overtone 7 was utilised in the plot generating.

According to literature, a single-phase adsorption mechanism is expected to generate a straight line when plotting D vs. *f* [22]. The adsorption of HS (Figure 2.3) generated a slightly

upwards sloping curve in the D_7 vs. f_7 plot, indicating that each protein molecule attaching results in a greater increase in D, and therefore film viscoelasticity, in comparison to the underlying adsorbed protein film. In contrast, a downwards sloping D_7 vs. f_7 plot would be interpreted as an increase in film rigidity with the addition of new molecules, as there would be an increase in f without a linear increase in D. Nearing the end of the HS adsorption process (Figure 2.3), the gradient of the plot increased, suggesting a greater increase in film viscoelasticity [23]. This may be interpreted as the addition of loosely adsorbed proteins on the surface of the already deposited film. Following the introduction of $PBS_{Mg/Ca}$, as a rinsing step, a large decrease in both D_7 and f_7 are observed, indicating the removal of a large portion of the loosely bound serum proteins. The subsequent addition of Ab_{C3c} was observed as a downward sloping curve, suggesting an increase in film rigidity as each antibody molecules adsorbed. Possible explanations for this occurrence are, firstly, the 'filling-in' of the depressions found at the serum protein interface, or secondly, that antibody binding results in conformational changes in the target protein which renders them more rigid. Thirdly, antibody-antibody interactions may occur between the bound probe antibodies, which would subsequently increase the film rigidity [81].

In the event of the 'failure' of the Sauerbrey model in determining adsorbed mass, viscoelastic modelling of the film is required, which provides additional information on film parameters in comparison to the $\Delta f/\Delta D$ and mass shift values. QTools provides a mathematical model, developed by Voinova *et al.*, 1999 [34], which is able to predict f_n and D_n responses to n viscoelastic layers, under certain considerations [30, Alternative Reference 1]. In particular, the Voigt-based model takes into consideration both the viscoelastic nature of the film, and the influence of the bulk liquid. The latter model defines films in terms of thickness, density, and the viscoelastic properties, such as shear modulus, and viscosity [23].

Voigt-Based Modelling

Viscoelastic modelling of QCM-D involves setting parameters, such as film thickness, viscosity, and shear modulus, to generate fitted responses for the extraction of viscoelastic parameters. Initially, general parameter ranges are selected, which are later refined following fitting of the data as resultant viscoelastic parameters provide an indication of the accuracy of

the generated model. Detailed below is an example of the modelling process utilised in this study, using the modelling of HS adsorption to an 11-AUT SAM (Table 2.1), as an example.

In the following example, fitted data were generated from the QCM-D responses where the film parameters were limited to a particular range, namely film viscosity (0.005 – 0.1 $kg.ms^{-1}$), shear modulus (5000- 1E8 Pa), and thickness (1E-11 – 2E-8 m), to illustrate the effect of the various fitting options (Table 2.1; Table 2.2). Fitting of the data may be carried out in both descending or ascending increments, and may be either forced to fit within the selected parameters, or just guided by the set parameters. Table 2.1. illustrates the data plot of the original QCM-D responses (solid lines) and the fitted data obtained through Voigt modelling (symbols). The purpose of this particular plot is to provide a visual indication of the accuracy of the Voigt-model. An accurate model would be observed as the QCM-D responses and the fitted data overlapping, as observed for the descending fitted data, while devation of fitted data from the original data, as observed for the ascending fitted data, indicates failure of the model to accurately predict film parameters. Accuracy of the model system is indicated by a low χ^2 value.

Further analysis on the accuracy of the Voigt prediction is through examination of both the film viscosity and shear modulus trends in comparison to the film thickness. Prior knowledge of adsorption characteristics of the target molecule proves helpful in this aspect. For example, introduction of $PBS_{Mg/Ca}$ functions to remove loosely bound protein, and is therefore expected to result in a decrease in the total film viscoelasticity. The latter is predicted to be observed as an increase in both the film viscosity and shear modulus. This is apparent when utilising the descending fit analysis technique, in the chosen example, however, the ascending fit generates viscosity values well below that of water, and concommitantly produces shear modulus values unrealistically low (Table 2.2). Although these observations indicate the descending fit analysis as superior, that is not always the case. Alterations to set parameters may drastically change the output; it is therefore necessary to critically assess the accuracy of the generated model by varying the set parameter.

A comparison made between assessing two layers together or as individual layers (Table 2.1), revealed that analysis of each layer independently proved to be more accurate, as indicated by the lower χ^2 value. This means of analysis was therefore favoured for the current studies.

Table: 2.1. Voigt-determined film parameters following the adsorption of human serum to 11-amino undecane thiol SAM, and the subsequent binding of anti-human C3c.

Layer	Fitted Parameters			Voigt-Determined Parameter Values			
	Parameters	**Min Estimation**	**Max Estimation**	**Descending Fit**		**Ascending Fit**	
				Open Fit	**Force Fit**	**Open Fit**	**Force Fit**
1	L1 visc ($kg.ms^{-1}$)	0.0005	0.01	0.0047	0.0047	0.0006	0.0006
	L1 shear (Pa)	5000	1E8	9.3143E5	9.3143E5	4980	5124
	L1 thick (m)	1E-11	2E-8	1.3522E-8	1.3522E-8	1.4353E-11	1.4353E-11
	Total ChiSqr	---	---	54983	55013	3.9756E6	1.6486E5
1 and 2	L1 visc ($kg.ms^{-1}$)	0.0005	0.01	0.0044	0.0044	0.0040	0.0050
	L1 shear (Pa)	5000	1E8	3.2046E5	8.2069E5	5000	5144.5
	L1 thick (m)	1E-11	2E-8	1.7192E-8	1.7192E-8	1.001E-11	1.0225E-11
	Total ChiSqr	---	---	4.6309E5	4.6353E5	1.245E7	5.398E5
2	L1 visc ($kg.ms^{-1}$)	0.0005	0.01	0.0044	0.0044	0.0047	0.0047
	L1 shear (Pa)	5000	1E8	8.2046E5	8.2069E5	9.1031E5	9.1031E5
	L1 thick (m)	1E-11	2E-8	1.7192E-8	1.7191E-8	1.352E-8	1.352E-8
	Total ChiSqr	---	---	1.8874E5	1.8874E5	1.8871E5	1.8871E5

- *Overtones 7, 9 and 11 were utilised in the following studies*
- *Film properties listed represent the final parameter value following protein addition*

Table 2.2. Assessing the effect of modelling parameters in the Voigt-determination of serum protein film parameters adsorbed to an 11-amino undecane thiol SAM-modified gold sensor surfaces.

Plot	Decending Fit		Ascending Fit	
	Open Fit	Force Fit	Open Fit	Force Fit
Data Plot	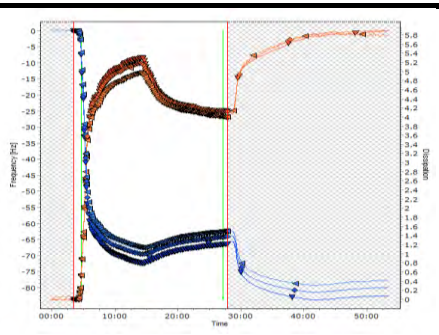	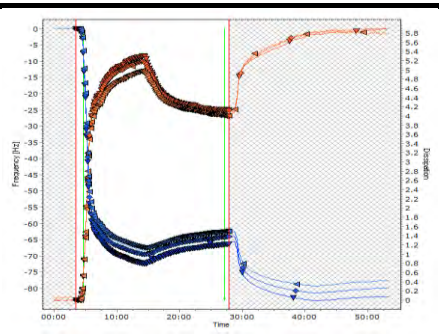	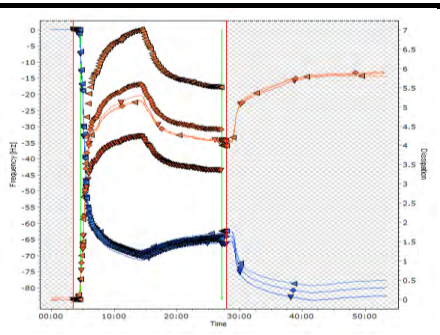	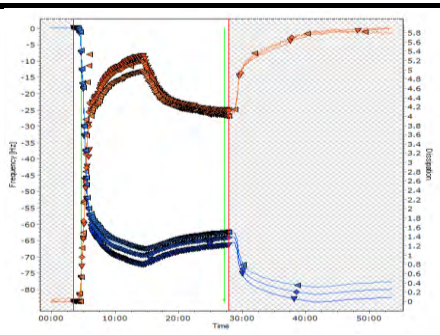
Thickness and Shear Modulus	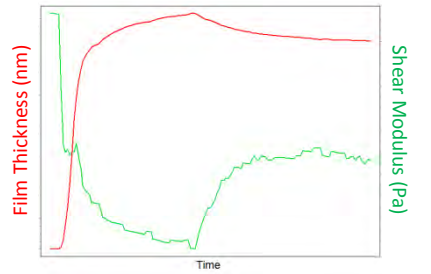	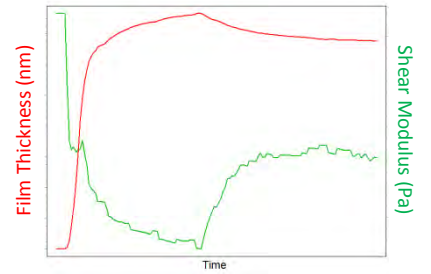	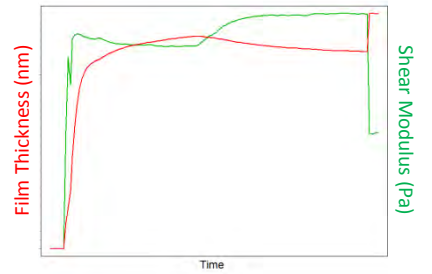	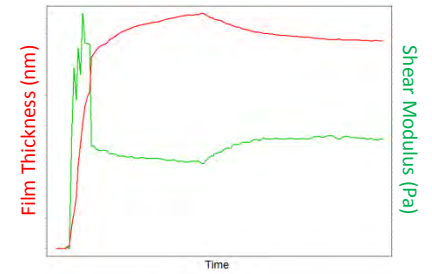
Thickness and Viscosity	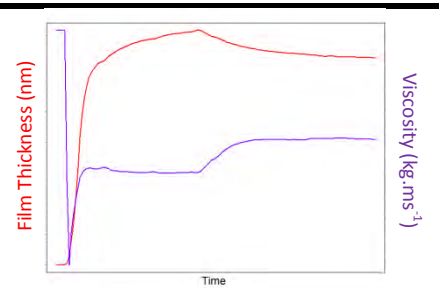	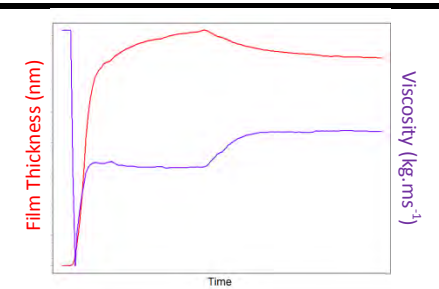	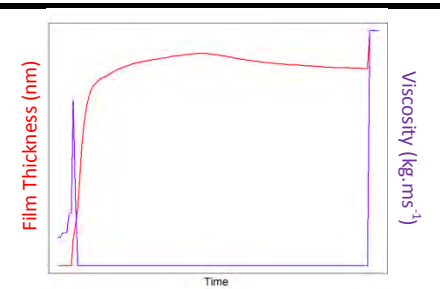	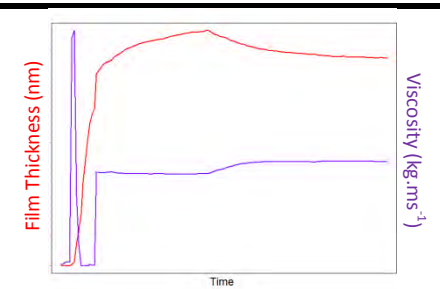

QCM-D Monitoring and Quantification of Adsorbed Mass

As previously mentioned, the aim of these studies was to develop a rapid technique designed at identifying the composition of the blood protein coat that may deposit following intravenous administration of therapeutic agents. Initial studies were thus directed toward protein identification on serum-coated planar surfaces, namely, gold, silicon dioxide, as well as SAM-modified gold, and antibody-modified surface controls, to identify relative target protein binding affinity trends. Figure 2.4. schematically illustrates the protein adsorption that takes place at the sensor surface, with the corresponding QCM-D *f* and D responses, for the detection of IgG-induced complement activation.

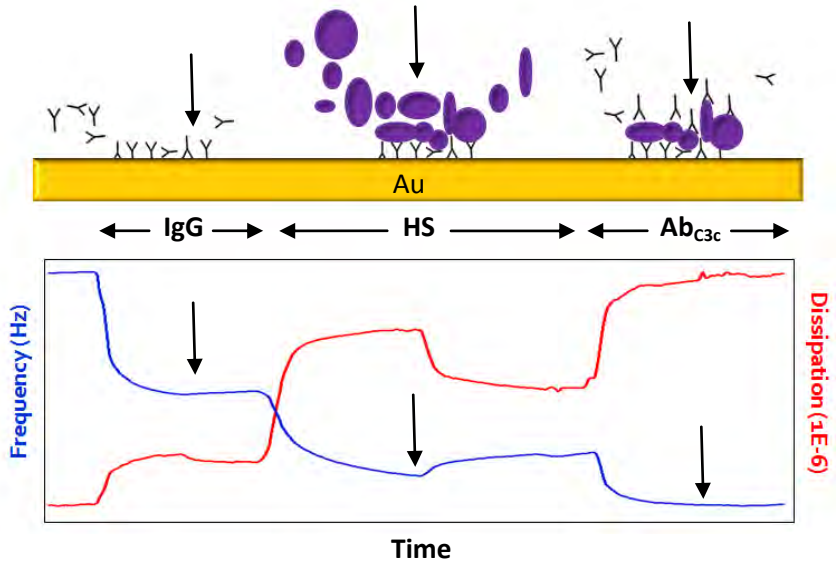

Figure 2.4. Schematic representation of adsorbed target protein detection and the corresponding QCM-D response. The detection of complement factor C3 on a human serum coated IgG-modified gold surface is illustrated. The point of introduction of $PBS_{Mg/Ca}$ buffer is indicated by vertical arrows. Overtone 7 was utilised.

As Figure 2.4 illustrates, the introduction of IgG, and the subsequent HS and Ab_{C3c}, resulted in a decrease in *f*, and an increase in D. This decrease in *f* and increase in D correlates with an increase in adsorbed mass an increase in the film viscoelasticity, respectively. The adsorption of IgG resulted in the deposition of a fairly rigid film, as observed by the low level of D increase and large decrease in *f* (i.e. high *f*/D). The adsorption of both HS and Ab_{C3c} resulted in the deposition of a fairly viscoelastic films, as indicated by the high shift in D, and low shift in *f* (i.e. low *f*/D).

Following the initial buffer rinse, a minor increase in *f* and decrease in D indicates the removal of loosely bound IgG molecules from the surface. The buffer rinse, following the addition of HS, resulted in the removal of non-specifically bound HS protein from the antibody-modified surface, rendering it less viscoelastic in nature, as observed by the large increase in *f* and decrease in D. The introduction of the buffer rinse, following the deposition of the probe antibody, Ab_{C3c}, did not influence the antibody film, in terms of non-specifically bound protein removal, due to the high specificity of the antibody-antigen interactions. This level of Ab_{C3c} recorded serves as an indication of the level of bound complement C3 molecules present in the HS film deposited on the IgG-modified surface.

2.3.2. QCM-D Monitoring and Quantification of Surface Modification: Antibody Controls

In order to assess the level of antibody attachment indicative of adsorption to a surface which promotes target protein binding, the binding of antibodies directed against the relevant serum/plasma proteins to the gold sensor surface were employed as controls. Ab_{HSA} control experiments were performed in triplicate, on both new and previously utilised gold coated crystals. The purpose of assessing protein binding to the two crystal types was to determine the effect of the chemical cleaning protocol employed on the gold surface, and therefore to assess an aspect of experimental reproducibility.

Surface modification, via the deposition of SAMs was not monitored using QCM-D due to chemical restraints of the QCM-D system precluding the use of ethanol, the solvent utilised in SAM protein deposition (Section 2.2.3.2). However, the generation of SAMs has been well documented in previous research, and is reported to be highly reproducible on gold surfaces [45].

Information regarding antibody structure and target epitopes is limited for the specific Ab_{HSA} and Ab_{HPF} molecules used as probes in these studies. However, immunoglobulin G (IgG) has been well characterised within literature [5, 89]. For the purpose of analysis, both the Ab_{HSA}

and Ab_{HPF} molecules were assumed to exhibit similar structural properties to that of the IgG molecule.

IgG is a flexible, heterogenous (160 kDa) protein which, according to X-ray crystallographic data, adopts the 'Y-model' conformation, demonstrating dimensions of 14.2 × 8.5 × 3.8 nm (Figure 2.5) [5]. IgG-surface interactions have been reported to be both time-dependent and binding site dependent [89]. In addition, adsorption of IgG aggregates have been reported on surfaces, such as gold, as well as adsorption-induced denaturation of the IgG molecule [89]. Due to the time-dependence of IgG adsorption and interaction with the substrate surface, antibody exposure to the gold sensor surface was limited to 30 min.

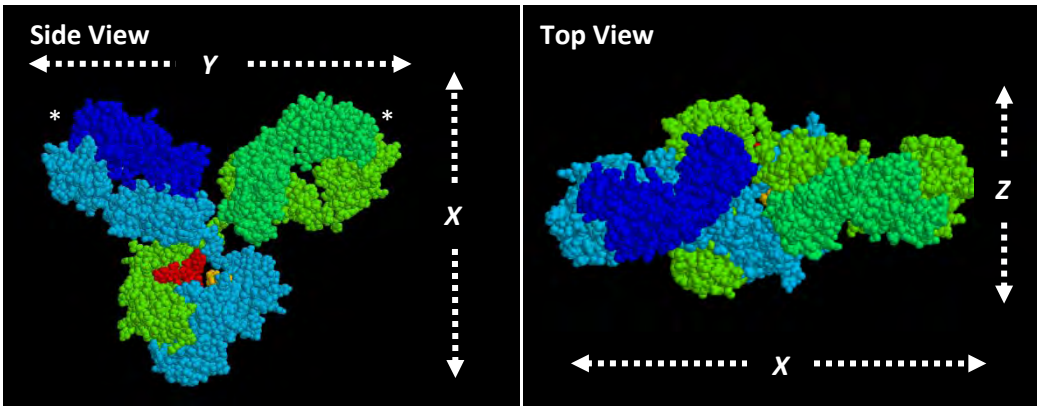

Figure 2.5. Rasmol generated illustration of human immunoglobulin G (PDB: 1IGY). The *x*-, *y*-, and *z*-axis correspond to the lengths 14.2 nm, 8.5 nm, and 3.8 nm, respectively. The polyclonal antibody active sites are indicated by the asterisk.

Theoretical Determination of IgG Monolayer

For the purpose of antibody adsorption analysis, predicted mass shift of IgG monolayer deposition were theoretically determined utilising reported IgG dimensions. These values served as a comparison for the Sauerbrey- and Voigt-determined mass shifts obtained experimentally. Figure 2.6. schematically illustrates IgG monolayers adsorbed to gold, emphasising the potential variations in protein orientation expected. Theoretical mass shifts for edge-on and planar orientated IgG monolayers were determined as 822.56 $ng.cm^{-2}$ and 492.38 $ng.cm^{-2}$, respectively.

Figure 2.6. Schematic illustration of the adsorbed IgG orientations within a monolayer deposited on gold. I-planar, II-edge-on, and III- mixed deposited orientation.

QCM-D Response Analysis

Crude analysis of the QCM-D response generated from the deposition of antibody molecules on the gold coated crystal surface suggested fairly rigid antibody films were adsorbed in all cases, as observed by the high $\Delta f/\Delta D$ values, which were greater than approximately 20 (Table 2.3). The latter also confirms the validity of the Sauerbrey determined film parameters. Furthermore, the low percentage coefficient of variation of the average *f* shift, in all cases, indicated the nature of the film interfaces as being sharp/uniform.

Table 2.3. QCM-D Frequency and Dissipation Shifts Following Gold Surface Modification with Anti-Human Serum Albumin, Human IgG, and Anti-Human Plasma Fibrinogen, for control experiments

Molecule [a]	f_7 D_7	f_9 D_9	f_{11} D_{11}	Ave. f [b]	Ave. f % CV	Ave. D [b]
Ab_{HSA} (new crystal)	24.22	24.26	34.84	-41.44 ±1.40	3.38	1.54 ±0.33
	26.98	24.97	24.75	-36.19 ±0.44	1.22	1.42 ±0.05
	34.13	34.71	32.83	-44.90 ±0.20	0.45	1.33 ±0.04
Ab_{HSA} (used crystal)	37.47	30.72	34.20	-46.54 ±0.32	0.69	1.37 ±0.14
	32.73	31.83	30.38	-45.19 ±0.24	0.53	1.43 ±0.05
	19.44	19.25	19.51	-50.79 ±0.84	1.65	2.62 ±0.05
Ab_{IgG+}	34.78	39.07	34.10	-47.15 ±0.44	0.93	1.31 ±0.09
Ab_{IgG-}	30.39	35.28	28.77	-50.61 ±0.62	1.23	1.62 ±0.16
Ab_{HPF}	32.56	33.11	33.58	-49.09 ±0.09	0.18	1.48 ±0.03

a: *Surface modification molecules utilised in the fabrication of the control surfaces*
b: *Average values determined using responses obtained from overtones 7 -11*

Examination of the antibody adsorption process was facilitated by generating D_7 versus f_7 plots (Figure 2.7). In each case, adsorption phases were identified according to shifts in the gradient of the linear portions of the each slope. The focus of this phase of research was to aid in the characterisation of the deposited film. In particular, to identify monolayer, or multilayer surface coverage, and to assist in the determination of adsorbed antibody orientation. In general, phase one indicates a uniform increase in both the *f* and D shifts,

whereas shifts to the slope gradient indicate changes in the film viscoelastic properties. An increase in the gradient of the slope (i.e. decrease in f/D) is interpreted as an increase in film viscoelasticity, while a decrease in the gradient (i.e. increase in f/D) indicates and increase in film rigidity. As the first phase in each adsorption process being fairly uniform in behaviour between antibodies, focus was rather directed towards the shifts in gradient, and their corresponding interpretations.

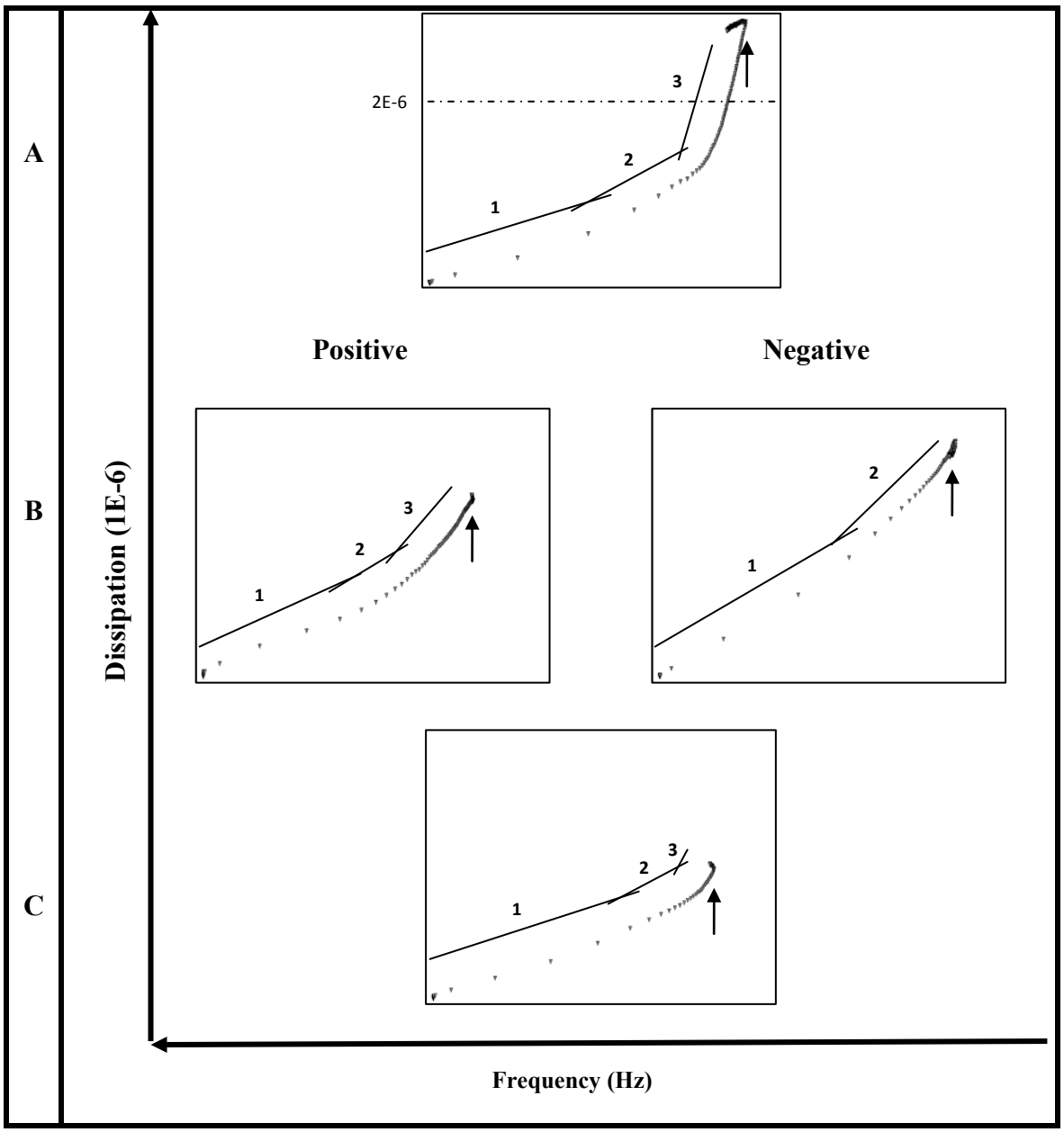

Figure 2.7. Frequency versus dissipation plots of anti-human albumin (A), IgG (B), and anti-human fibrinogen (C) adsorption to gold. Symbols indicate D (y-axis) responses plotted relative to the *f* (x-axis) responses. Solid lines schematically illustrate the gradient change, the first of which is indicated by 1. The scale for the D_7 and f_7 responses was maintained at 2E-6 and -60Hz, respectively, with the exception of Ab_{HSA} adsorption D_7 response, indicated by the dashed line. Point of introduction of the $PBS_{Mg/Ca}$ buffer rinse is indicated by the vertical arrows. Overtone 7 was utilised in generating the plots.

Analysis of Ab_{HSA} adsorption, via D_7 vs. f_7 plots indicated fairly constant adsorption mechanisms for both the new and used gold sensor surfaces. Figure 2.7 (A) illustrates a representative D_7 vs. f_7 plot of the Ab_{HSA} adsorption processes recorded. Adsorption of the antibody to the gold substrate was observed as a three phase process, as indicated by the solid

lines in Figure 2.7. The initial adsorption phase illustrated further separation of the $\Delta f/\Delta D$ data points, suggesting the initial rate of adsorption as being higher than the rate observed in phase two and three. The second phase demonstrated a slight increase in the positive slope gradient of phase one, suggesting a greater increase in the D_7 shifts, and therefore film viscoelasticity, with the subsequent addition of antibody molecules. This increase in the viscoelasticity of the film may be interpreted as either protein denaturation or protein reorientation on the gold surface. Phase three demonstrated a considerable increase in the slope gradient, and therefore D_7 shifts, which corresponded with a minor increase in f_7 shifts. This large increase in the slope gradient suggests the incoming antibody molecules are loosely bound to the previously deposited antibody surface, therefore contributing to the high viscoelastic nature of the adsorbed film.

The introduction of the buffer rinse, indicated by the vertical arrows in Figure 2.7, resulted in a small decrease in both the f_7 and D_7 shifts, suggesting removal of the loosely bound proteins. Furthermore, f_7 shifts, and therefore adsorbed mass, resorted back to the approximate value recorded prior to the addition of the loosely bound proteins, in phase three. However, the same D_7 value was not restored. The f_7 and D_7 shifts observed during phase three of the adsorption process correspond with the initial deposition of a second layer of antibodies. The adsorption of the multilayer to the previously adsorbed antibody layer arises from protein-protein interactions. These interactions may produce conformation distortion of the underlying protein layer, therefore accounting for the large increase in film viscoelastic properties, observed during the addition of the loosely adsorbed molecules, and following their removal [89].

D_7 vs. f_7 plots monitoring IgG adsorption (Figure 2.7; B) indicated both two and three phase processes in the absence (negative control) and presence of Mg^{2+} and Ca^{2+} ions (positive control), respectively. Similarly, a three phase adsorption mechanism was observed for Ab_{HPF}-modification of the gold sensor surface (Figure 2.7; C). In the case of the three phase process, when assessing Ab_{IgG+} and Ab_{HPF} adsorption, both phase two and three indicate slight increases in the slope gradient, suggesting an increase in the viscoelasticity of the film, potentially the result of protein denaturation or antibody reorientation. The two phase process observed in the absence of the supplemented ions (negative control), indicates an

increase in the slope gradient, suggesting an increase in the viscoelastic nature of the film, similar to that observed in the presence of the Mg^{2+} and Ca^{2+} ions. Noteworthy change in the film properties were not apparent following the introduction of buffer rinse.

It was concluded, from the D vs. *f* plot analysis (Figure 2.7), that deposited monolayer films remain following the buffer rinse, however, it is unknown whether these films are mono-dispersed, or in fact, deposited aggregates. This knowledge proved helpful when analysing the Sauerbrey and Voigt-determined film parameters, as it provided a basis on which to assess the recorded adsorbed film mass, in terms of it being a representation of a monolayer, or multilayer.

Sauerbrey and Voigt-Based Analysis

Table 2.4 summarises the Sauerbrey- and Voigt-determined film parameters of the surface modification, with target antibodies, for the control experiments.

Table 2.4. Sauerbrey and Voigt Modelled Analysis of Gold Surface Modification with Human IgG, Anti-Human Serum Albumin, and Anti-Human Plasma Fibrinogen, for control experiments

Molecule [a]	Sauerbrey Model			Voigt Model					$\frac{\text{Sauerbrey}_m}{\text{Voigt}_m}$ [d]
	Film Thickness (nm)	Mass (ng/cm^2) [b]	Ave. Mass (ng/cm^2)	Viscosity (kg/m.sec) [c]	Shear Modulus (Pa) [c]	Film Thickness (nm)	Mass (ng/cm^2)	Ave. Mass (ng/cm^2)	
Ab_{HSA} (new crystal)	6.74 ±0.23	741.61 ±25.07	740.66 ±92.61 (12.5% CV)	6.26E-03	1.22E+06	8.33	832.55	802.47 ±88.20 (11.0% CV)	0.89
	5.89 ±0.07	647.58 ±7.85		6.38E-03	1.79E+06	7.03	703.16		0.92
	7.57 ±0.05	832.80 ±5.74		8.06E-03	3.09E+06	8.72	871.70		0.96
Ab_{HSA} (used crystal)	7.30 ±0.03	803.52 ±3.59	840.36 ±59.47 (7.1% CV)	3.07E-03	3.57E+04	12.49	1249.45	1239.26 ±108.02 (8.7% CV)	0.64
	7.35 ±0.04	808.59 ±4.28		2.77E-03	2.22E+04	13.42	1341.82		0.60
	6.07 ±5.26	908.96 ±15.07		4.85E-03	5.06E+05	11.27	1126.50		0.81
Ab_{IgG+}	8.44 ±0.08	843.67 ±7.80	---	7.56E-03	4.18E+06	8.65	865.13	---	0.98
Ab_{IgG-}	9.06 ±0.12	905.70 ±11.13	---	7.78E-03	1.87E+06	9.79	978.89	---	0.93
Ab_{HPF}	8.78 ±0.02	878.18 ±2.00	---	6.16E-03	4.32E+05	10.53	1052.54	---	0.83

a: *Surface modification molecules utilised in the fabrication of the control surfaces*
b: *Sauerbrey-determined adsorbed mass. Standard deviation is obtained from 3 overtone responses.*
c: *Viscoelastic film parameters indicating film rigidity levels*
d: *Indicates level of film hydration*

Analysis of Ab_{HSA} adsorption to the gold surface revealed the deposition of films with Sauerbrey determined thickness ranging from 5.89 to 7.57 nm, on new crystals, and 6.07 to 7.35 nm, on used crystals (Table 2.4). According to the IgG dimensions, these thickness values correlate with the planar orientation of the antibody molecules, which is expected to demonstrate a film thickness of approximately 8.5 nm (Figure 2.6, I). Although experimentally determined film thickness values were recorded to be below the predicted thickness of 8.5 nm, the planar orientation is still permissible, as IgG is reported to undergo conformational change once adsorbed to gold, therefore altering its dimensions [16]. Similarly, the planar orientation was suggested by the Sauerbrey determined film thickness values for the IgG deposited film intended for the positive detection of adsorbed complement factor C3. A film thickness greater than 8.5 nm, as seen for IgG adsorption of the complement factor C3 negative control (9.06 nm), and Ab_{HPF} (8.78 nm), may rule out the possibility of the deposition of a monolayer of planar orientated antibody molecules. The latter film thickness values suggest the deposition of either edge-on orientated molecules, or both edge-on and planar orientated antibody molecules.

The Voigt-determined film thickness values, on the other hand, indicate the deposition of notably thicker films in comparison to the Sauerbrey model, suggesting the formation of either multilayer films, or edge-on orientated monolayers, with the exception of IgG adsorption. The analysis of adsorbed antibody orientation is an important parameter of the deposited film, as the degree of antibody active site exposure would demonstrate a great influence over the subsequent blood protein adsorption phase (Figure 2.6, II), in terms of mass bound and film viscoelastic parameters. Film thickness alone is not sufficient to derive conclusions on the nature of the adsorbed film, due to the possibility of protein conformational change and/or denaturation. It is necessary to make a comparison between theoretical and experimental adsorbed mass, together with viscoelastic parameters, namely, film viscosity and shear modulus (Table 2.4).

Adsorption of Ab_{HSA} on new crystal surfaces resulted in the deposition of highly rigid films, as indicated by the high film viscosity and shear modulus, whose Voigt-determined mass was recorded to be somewhat greater than that determined through Sauerbrey analysis. The Sauerbrey-determined adsorbed mass values suggest the possibility of films being composed

of mixed orientated molecules (741.61 ng.cm^{-2} and 647.58 ng.cm^{-2}), and purely edge-on orientation (832.80 ng.cm^{-2}), while edge-on orientated molecules (832.55 ng.cm^{-2} and 871.70 ng.cm^{-2}), and mixed orientated molecules (703.16 ng.cm^{-2}) were suggested by the Voigt-based mass values (Figure 2.6). Ab_{HSA} deposited films demonstrated high $Sauerbrey_{mass}/Voigt_{mass}$ values, suggesting a low portion of the adsorbed Voigt-mass is due to the entrapment of water molecules within the film [30]. The nature of the film interface, high film viscosity, high shear modulus, and low water content of the films leads one to conclude that densely-packed antibody films are deposited on the new gold surfaces, composed of both planar and edge-on orientated molecules.

The adsorption of IgG on gold occurs at surface defects and impurities on the substrate [90]. With regards to the new crystal surface, these surface defects and impurities are predicted to be at a minimum, therefore limiting the level of binding sites available for antibody adsorption [Internet Reference 1]. In this event, antibody molecules are reported to bind to the isolated binding sites, followed by deposition of antibody molecules adjacent to the already deposited antibodies [89]. For this reason, one may expect the deposition of densely-packed films on the new crystal surface, which correlates with experimental data.

Contrary to this, adsorption of Ab_{HSA} on used crystals indicated the deposition of more viscoelastic films, suggested by the lower viscosity and shear modulus values. These adsorbed films demonstrate considerably greater Voigt-mass (1126.50 ng.cm^{-2} – 1341.82 ng.cm^{-2}) in comparison to the Sauerbrey determined mass values (803.52 ng.cm^{-2} – 908.96 ng.cm^{-2}), and therefore low $Sauerbrey_{mass}/Voigt_{mass}$ values, indicating high levels of trapped water within the films. Based on literature, if the degree of surface binding sites (i.e. defect sites on Au substrate) is high, as in the case of the used crystal surface, antibody aggregates are expected to adsorb, interacting with each other to extend across the surface until a smoother layer is generated [89]. The adsorption of such aggregates may explain the lower film viscosity and shear moduli observed for antibody binding on used crystal surface, as well as the high level of water present.

Reproducibility analysis, in terms of new versus used crystal surfaces, suggested a higher level of reproducibility for the modification of the used crystal surface (Table 2.4). However, the reproducibility of antibody immobilisation step, may only be assessed by the final step in the protein detection protocol, namely, the probe antibody binding, as the orientation of the surface modification antibody molecules plays a crucial role in the control experiment design. However, it is important to note differences in the film parameters between the modified new and used crystal surfaces (Table 2.4). The occurrence of these deviations emphasises the influence of crystal quality on protein adsorption.

Deposition of IgG molecules on the new gold sensor surface (Table 2.4), for the selective binding of complement factor C3c, was determined to result in the formation of highly rigid films, as indicated by the high viscosity and shear moduli, which demonstrate low level of water entrapment, indicated by the high $Sauerbrey_{mass}/Voigt_{mass}$ values. Both the Sauerbrey and Voigt-determined adsorbed mass indicate the deposition of either edge-on orientated monolayers, or planar multilayers. The D_7 vs. f_7 plot analysis indicated monolayer deposition, however, the analysis was inconclusive, in terms of the nature of the monolayer, whether it is composed of mono-dispersed antibody molecules, or aggregates. Irrespectively, the high film viscosity and shear moduli, together with the significantly low water content prediction, suggest the adsorption of densely-packed layers. This high density of the film may lead to steric hindrance of the antibody molecule by surrounding antibody molecules, therefore one may predict, in the case of edge-on orientated molecules, an increase in both the film thickness. The lower degree of entrapped water reported within the IgG film deposited for the positive detection of complement factor C3 may be explained by the composition of the solution buffer. $PBS_{Mg/Ca}$ contains both Mg^{2+} and Ca^{2+} ions, included to aid in protein-protein interactions, in this case, antibody-antibody interactions, while these supplements are omitted in PBS [93].

Adsorption of Ab_{HPF}, on the other hand, resulted in the formation of a rigid film, demonstrating high viscosity and shear modulus, which contained higher levels of trapped water, in comparison to IgG. Both the Sauerbrey and Voigt calculated adsorbed mass values for the adsorption of Ab_{HPF} suggested multilayer formation, as they were greater than the expected value for an edge-on monolayer, 822.56 $ng.cm^{-2}$. However, the high rigidity of the

film, and therefore high density, as previously discussed, leads one to consider a densely-packed edge-on monolayer as a possible occurrence. Figure 2.8. graphically displays the Sauerbrey and Voigt-determined adsorbed mass values observed when modifying the gold QCM-D sensor surface with the target antibodies described.

The replicant studies indicate a variance of at least ± 50 ng.cm^{-2} between the surfaces for antibody adsorption. These levels of variation are considered to indicate that reasonable, if not acceptable, reproducibility was achieved, in terms of total mass adsorbed.

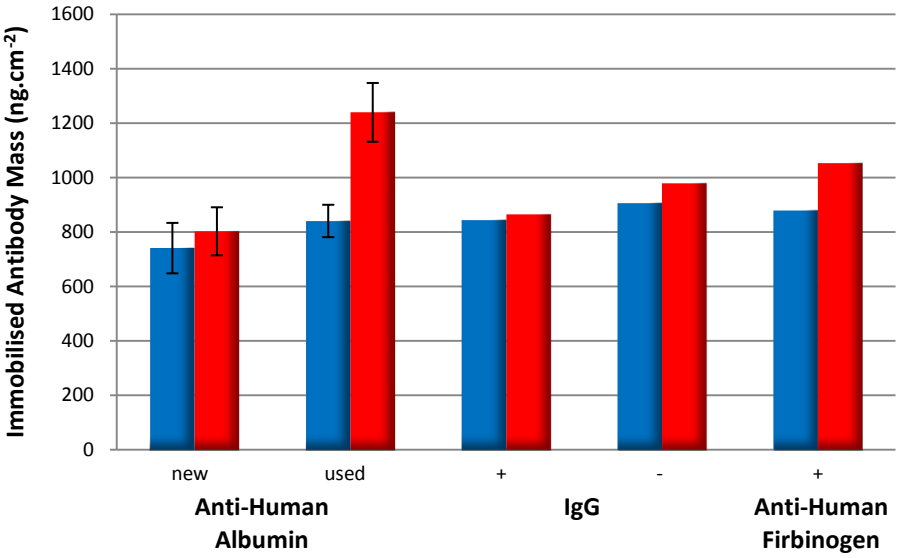

Figure 2.8. Sauerbrey-(Blue) and Voigt-(Red) determined adsorbed antibody mass to the gold sensor surface. Error bars indicate standard deviation where n = 3.

The function of the antibody surface modification was to provide an indication of the level of probe antibody binding to a surface which primarily binds the target protein of interest. In particular, analysis of the blood protein adsorption, and subsequent target antibody binding to the antibody films prepared was predicted to provide a positive control, to which the results of protein detection analysis on test surfaces may be compared.

2.3.3. QCM-D Monitoring and Quantification of Biomolecular Interactions with the Surfaces: Modified and Unmodified

Following surface modifications of the gold sensor surface using either SAM molecules or antibody molecules, target surfaces were introduced to either human blood plasma (HP) or human serum (HS). Subsequently, target probe antibody (Ab_{HSA}, Ab_{C3c}, and Ab_{HPF}) binding was assessed for the detection of target proteins, namely HSA, complement C3c, and HPF.

2.3.3.1. QCM-D Monitoring and Quantification of Blood Protein Adsorption to Unmodified and Modified Surfaces

The adsorption of blood proteins to the target surfaces was assessed, using QCM-D, to provide information on characteristic blood protein adsorption behaviour, namely level of adsorbed protein on surfaces with known charge, and to provide a basis for the protein detection analysis. HS is derived from HP through the removal of both the clotting factors, such as fibrinogen, and small molecules [94]. HS does not contain blood cells and clotting factors. It was for this reason that human fibrinogen binding analysis was assessed utilising HP coated surfaces.

Due to the complexity of proteins present in human blood samples, in-depth analysis of the binding process that occurs between the target surfaces and the serum/plasma was not explored other than antibody-antigen profiling of the surface. Rather, analysis was focused on examining the reproducibility of the adsorption step, and the subsequent effect on protein detection reproducibility. Analysis of the propagation of error from surface modification to blood protein binding and subsequently target protein detection, from a sensor perspective, provides an assessment of the robustness of the proposed protein detection method, and therefore its applicability as a biocompatibility screening technique. Reproducibility analysis was limited to assessing HS adsorption on the unmodified and protein modified surfaces, and HP adsorption to the unmodified gold surface, due to the financial cost of performing these studies, in terms of the probe antibodies, and quartz crystal sensors.

QCM-D Response Analysis

The key function of the preliminary analysis of the *f* and D shifts generated during the blood protein adsorption step, on unmodified and modified surfaces, was to assess the validity of the Sauerbrey model as a means of monitoring blood protein attachment (Table A.1). Little deduction could be made concerning reproducibility from surface interface analysis (% Coefficient of Variation) and film rigidity (*f*/D) values due to the heterogenous nature of the blood samples. Inter-phase shifts in film parameter, namely, film thickness, adsorbed mass, film viscosity and shear modulus, are represented for blood protein adsorption to the antibody modified surfaces, in comparison to the final film parameters being reported, as in the case of the bare and SAM modified surfaces. This means of representation was selected to present the analysis of the blood protein deposition stages independently, rather than as an addition to the already deposited antibody layer.

Sauerbrey and Voigt Analysis

Controls

The attachment of blood proteins in HS on the Ab_{HSA}-modified surfaces was observed to be a highly variable process, when assessing either the new and used antibody-modified surfaces (Table 2.5.). This high degree of variability is assumed to be the result of variations in the underlying antibody film, namely, antibody conformation, orientation, and packing density (Section 2.3.2.1; Table 2.4). In general, HS adsorption to deposited antibody films adsorbed on new crystal surfaces, display lower levels of trapped water in comparison to the procedures where used crystals were employed. The higher level of trapped water suggests conformational change of the target protein as a result of the antibody-protein interaction. Table 2.5 summarises the Sauerbrey- and Voigt-determined parameters of the blood protein films deposited on the modified and unmodified surfaces.

Table 2.5. Sauerbrey and Voigt Modelled Analysis of Blood Protein Adsorption on Unmodified and Modified Surfaces

Surface	BP [a]	Sauerbrey Model		Voigt Model				$\frac{\text{Sauerbrey}_m}{\text{Voigt}_m}$ [d]
		Mass (ng/cm^2) [b]	Ave. Mass (ng/cm^2)	Viscosity (kg/m.sec) [c]	Shear Modulus (Pa) [c]	Mass (ng/cm^2)	Ave. Mass (ng/cm^2)	
Ab_{HSA} (new crystal)	HS	772.02 ±24.44	610.46 ±158.78 (26.00 % CV)	Decrease	Decrease	801.43	668.68 ±133.51 (19.97 % CV)	0.96
		454.61 ±11.53		Decrease	Decrease	534.43		0.85
		604.75 ±16.84		Decrease	Decrease	670.19		0.90
Ab_{HSA} (used crystal)		548.86 ±23.29	563.26 ±144.10 (25.58 % CV)	Decrease	Increase	1044.61	1216.10 ±647.97 (53.28 % CV)	0.53
		426.90 ±6.41		Increase	Increase	671.12		0.64
		714.02 ±25.49		Decrease	Decrease	1932.56		0.37
Ab_{IgG}	HS	613.17 ±28.08	---	Decrease	Decrease	645.12	---	0.95
	iHS	281.34 ±17.65	---	Decrease	Decrease	394.59	---	0.71
Ab_{HPF}	HP	1045.25 ±22.32	---	Decrease	Decrease	1575.16	---	0.66
Gold	HS	1157.41 ±20.66	1212.35 47.56 (3.92 % CV)	Increase	Increase	2106.18	1510.19±303.93 (20.13 % CV)	0.55
		1258.70 ±112.81		Increase	Increase	1388.52		0.91
		1191.46 ±17.62		Increase	Increase	1423.20		0.84
		1192.18 ±27.50		Increase	Increase	1305.11		0.91
		1192.06 ±27.96		Increase	Increase	1305.90		0.91
		1282.28 ±25.73		Increase	Increase	1532.22		0.84
	HP	998.77 ±17.47	802.13 ±343.94 (42.88 % CV)	Increase	Increase	1100.87	914.86 ±367.82 (40.21 % CV)	0.91
		404.98 ±14.92		Increase	Increase	491.19		0.82
		1002.63 ±40.41		Increase	Increase	1152.53		0.87
Silicon Dioxide	HS	1125.52 ±14.14	1071.66 ±86.08 (8.03 % CV)	Increase	Increase	1256.84	1240.06 ±80.02 (6.45 % CV)	0.90
		1117.08 ±19.78		Increase	Increase	1310.35		0.85
		972.39 ±17.01		Increase	Increase	1152.98		0.84
	HP	935.54 ±21.11	---	Increase	Increase	1128.98	---	0.83
11-AUT SAM	HS	977.35 ±25.20	1012.21 ±124.06 (12.26 % CV)	Increase	Increase	1147.53	1242.27 ±103.39 (8.32 % CV)	0.85
		1149.97 ±27.78		Increase	Increase	1352.55		0.85
		909.32 ±17.97		Increase	Increase	1226.72		0.74
	HP	866.74 ±18.81	---	Increase	Increase	1000.00	---	0.87
Cyst. SAM	HS	804.65 ±23.29	781.18 ±45.23 (5.79 % CV)	Increase	Increase	835.10	946.88 ±142.92 (15.09 % CV)	0.96
		729.04 ±5.05		Increase	Increase	1107.91		0.66
		809.84 ±12.07		Increase	Increase	897.64		0.90
	HP	1070.27 ±16.49	---	Increase	Increase	1129.59	---	0.95
MUA SAM	HS	593.46 ±13.06	666.36 ±65.74 (9.87 % CV)	Increase	Increase	697.98	786.99 ±77.19 (9.81 % CV)	0.85
		721.15 ±10.87		Increase	Increase	835.54		0.86
		684.46 ±13.75		Increase	Increase	827.44		0.83
	HP	892.12 ±25.09	---	Increase	Increase	1175.28	---	0.76

a: *Blood protein (BP) sample adsorbed to the test surface*
b: *Sauerbrey-determined adsorbed mass. Standard deviation is obtained from 3 overtone responses.*
c: *Viscoelastic film parameters indicating film rigidity levels*
d: *Indicates level of film hydration*

In terms of reproducibility, the process of HS binding to Ab_{HSA} modified surfaces exhibits similar coefficients of variation, for both new (26.00 %) and used (25.58%) modified crystals, when utilising the Sauerbrey model for mass detection (Table 2.5). However, Voigt analysis suggested the adsorption of the serum coat on the new antibody-modified crystals (19.97 %) as being far more reproducible in comparison to the experiments assessing the

used crystal surfaces (53.28 %). Although low reproducibility was reported, this is not however an indication of the irreproducibility of the proposed method. Adsorption of the final probe antibody, for the detection of target protein, is the crucial step. Acceptable reproducibility, assumed as less than 10% variability, of the latter step, in the presence of irreproducible antibody surface modification and blood protein binding, would highlight the robust nature of the proposed methods, as the propagation of error would be eliminated.

The adsorption of HS on the IgG coated gold surface generated a greater mass shift in comparison to the adsorption of heat inactivated human serum (iHS) (Table 2.5). This occurrence is predicted, as well as the high level of trapped water within the iHS film, due to the denatured state of the heat inactivated blood sample, and the inactivation of C3c, resulting in lower mass binding. HP adsorption to the Ab_{HPF} (fibrinogen control in Figure 2.9) coated surface resulted in the deposition of a fairly thick film, as observed by both the Sauerbrey and Voigt-determined parameters. The low $Sauerbrey_{mass}/Voigt_{mass}$ value indicates a high level of hydration.

Unmodified Crystal Surfaces

The adsorption of HS on the hydrophobic gold coated crystal surfaces was observed as the deposition of protein films which demonstrate varying degrees of hydration, as indicated by the $Sauerbrey_{mass}/Voigt_{mass}$ values (Table 2.5). High reproducibility, in terms of the Sauerbrey determined adsorbed mass (3.92 % CV), was reported for HS adsorption on gold, however, the reproducibility decreases when assessing protein adsorption using the Voigt model (20.13 % CV). The latter occurrence suggests varying degrees of protein denaturation occurred during the adsorption process, possibly due to the variations in the topography of the gold surface as a result of the chemical cleaning process. In addition, low, comparable reproducibility was recorded for both the Sauerbrey and Voigt analysis of HP adsorption. The high variability in the adsorption process of HP may be the result of the composition of the blood sample, or variability in fibrinogen deposition, as it is a time-dependent process.

Acceptable reproducibility, where the coefficient of variation percentage is below 10 %, was reported for HS adsorption to the negatively charged SiO_2 surface, with respect to both the Sauerbrey and Voigt determined adsorbed mass (Table 2.5). An overall decrease in HS adsorption mass was recorded in comparison to that adsorbed to the gold surface. This occurrence is predicted as HS proteins demonstrate a higher affinity towards hydrophobic surfaces over hydrophilic [95].

SAM-Modified Surfaces

Analysis of HS adsorption to the amine terminating SAM surfaces (Table 2.5), namely 11-AUT SAM and Cyst. SAM surfaces, indicated higher mass adsorption occurred on the 11-AUT SAM modified surfaces, suggesting the surface is more hydrophobic in nature, and therefore less protenated [95]. HS adsorption to the Cyst. SAM modified surfaces demonstrated higher Sauerbrey mass reproducibility in comparison to 11-AUT SAM surfaces, however, the Voigt-determined adsorbed mass suggested HS adsorption was more reproducible when assessing the 11-AUT SAM surfaces. In addition, protein films deposited on the Cyst. SAM surfaces were reported to be less hydrated, suggesting a higher level of protein conformational change occurred. Adsorption analysis of HS on the negatively charged MUA SAM-modified surfaces, reported lower levels of HS were deposited, and similar, acceptable reproducibility of the process was observed using both the Sauerbrey and Voigt-determined mass values.

The levels of bound blood proteins recorded to adsorb to the test surfaces, both unmodified, and SAM modified, are predicted to be substantially greater than the blood protein levels deposited on the control surfaces (i.e. antibody-modified surfaces), due to the specificity of the antibody-antigen interactions.

Overall Trends

In general, HS protein exhibited a higher binding mass towards hydrophobic solid surfaces in comparison to hydrophilic surfaces, and hydrophobic SAM surfaces over hydrophilic SAM surfaces. According to the both the Sauerbrey and Voigt-determined HP film parameters, HP

favours hydrophilic over hydrophobic surfaces. Figure 2.9. summarised the adsorbed blood protein mass parameters and their adsorption reproducibility.

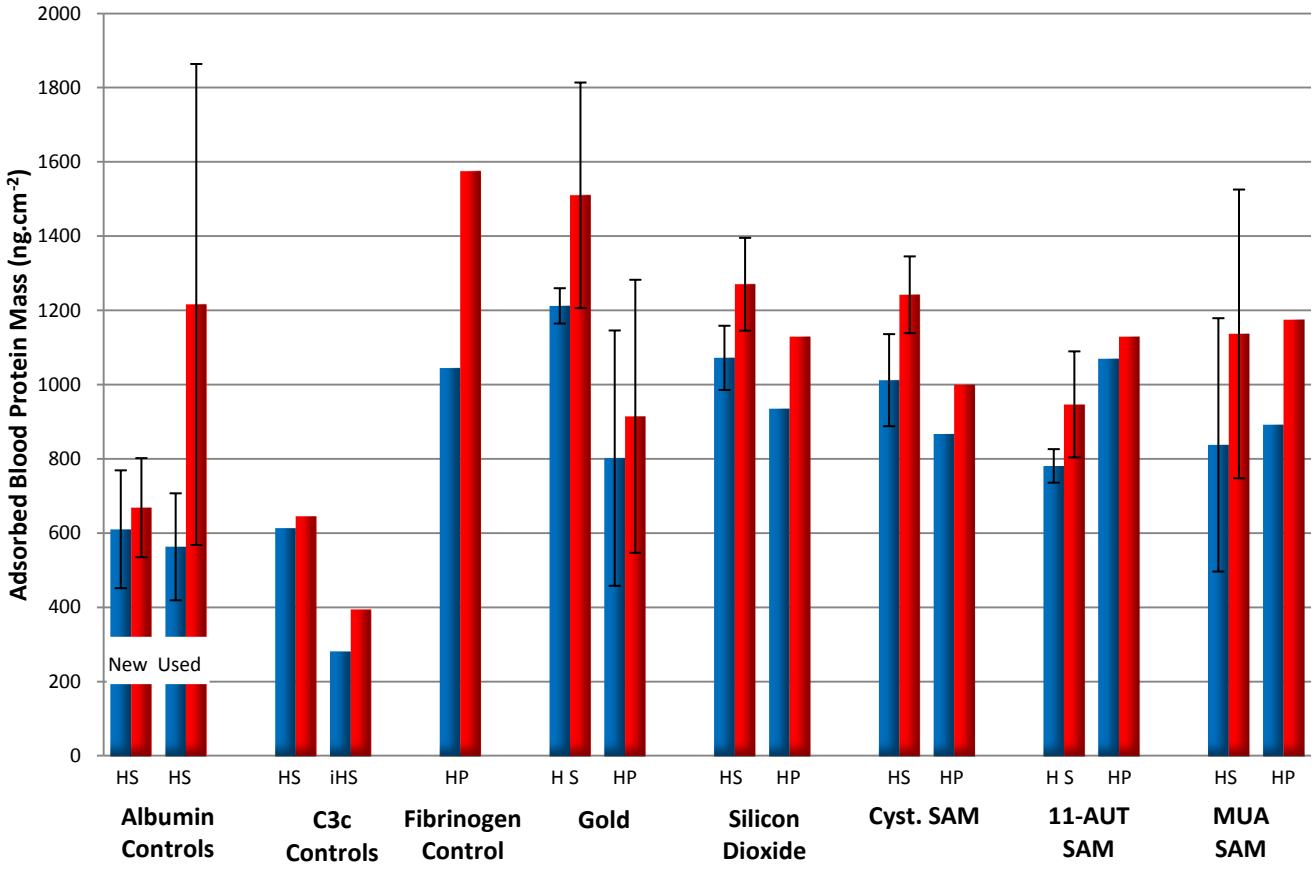

Figure 2.9. Sauerbrey (Blue) and Voigt (Red) determined adsorbed blood protein mass to unmodified, antibody-modified, and SAM modified surfaces. iHS refers to the heat inactivated HS utilised for the negative C3c control. Error bars indicate standard deviation where n =3, with the exception of gold HS binding where n = 6.

2.3.3.2. QCM-D Monitoring and Quantification of Probe Antibody Adsorption to Unmodified and Modified Surfaces

The detection of adsorbed target blood proteins was executed using the specificity of the antibody-antigen interaction. The subsequent binding of probe antibodies, to the previously deposited blood protein coat, was monitored using QCM-D (Figure 2.1; B-III).

When assessing the QCM-D responses obtained from Ab_{HSA} adsorption to the controls surfaces, the effect observed in terms of film interface properties were varying (Table A.2).

In cases where film interface roughness was reported to decrease, 'filling-in of the depressions in the adsorbed HS layer was assumed to take place during the probe antibody adsorption process. Contrary to this, possible explanations for the increase in surface roughness as a result of antibody deposition, include, the patterning of the probe antibody on the surface, and conformational change generated by the adsorbed target protein as a result of antibody binding. In general, increases in film interface roughness, due to antibody binding, were recorded for the remainder of the surfaces, with the exception of the Ab_{HPF}, which demonstrated a decrease in the film interface roughness.

Table 2.6 summarises the Sauerbrey and Voigt film parameters of the of the probe antibody films. Of particular interest, is the adsorbed mass parameter, which serves as an indication of the level of exposed target protein present of the test surface.

Table 2.6. Sauerbrey and Voigt Modelled Analysis of Probe Antibody Binding to Modified and Unmodified Surfaces

Surface	Probe [a]	Sauerbrey Model			Voigt Model					Sauerbrey$_m$ [e] / Voigt$_m$
		Δ Mass (ng/cm^2) [b]	Ave. Δ Mass (ng/cm^2)	$\frac{\Delta Ab_m}{\Delta Bb_m}$ [c]	Δ Viscosity (kg/m.sec) [d]	Δ Shear Modulus (Pa) [d]	Δ Mass (ng/cm^2)	Ave. Δ Mass (ng/cm^2)	$\frac{\Delta Ab_m}{\Delta Bb_m}$ [c]	
Ab_{HSA} (new crystal)	Ab_{HSA}	2612.84 ±101.38	2510.97 ±195.42 (7.78% CV)	3.38	Decrease	Decrease	4916.09	3520.18 ±1289.50 (36.63% CV)	6.13	0.53
		2634.4 ±88.78		5.79	Increase	Decrease	3270.96		6.12	0.81
		2285.66 ±46.88		3.78	Increase	Increase	2373.48		3.54	0.96
Ab_{HSA} Albumin (used crystal)		2171.53 ±28.34	2055.43 ±193.52 (9.42% CV)	3.96	Increase	Increase	2521.15	2350.57 ±404.51 (17.21% CV)	2.41	0.86
		2162.72 ±39.27		5.07	Increase	Increase	2641.84		3.94	0.82
		1832.03 ±30.77		2.57	Increase	Increase	1888.71		0.98	0.97
Ab_{IgG}	Ab_{C3c+}	677.94 ±46.53	---	1.11	Decrease	Decrease	789.75	---	1.22	0.86
	Ab_{C3c-}	-19.07 ±6.96	---	-0.07	Increase	Increase	-81.03	---	-0.21	0.24
Ab_{HPF}	Ab_{HPF}	1796.9 ±1.09	---	1.72	Increase	Increase	1714.99	---	1.09	1.05
Gold	Ab_{HSA}	112.87 ±9.67	109.68 ±13.56 (12.36% CV)	0.10	Decrease	Increase	356.49	241.73 ±104.39 (43.18% CV)	0.17	0.32
		94.81 ±64.21		0.08	Decrease	Decrease	152.4		0.11	0.62
		121.36 ±12.39		0.10	Decrease	Decrease	216.3		0.15	0.56
	Ab_{C3c}	291.08 ±29.47	276.53 ±25.30 (9.15% CV)	0.24	Increase	Increase	312.93	303.69 ±15.33 (5.05% CV)	0.24	0.93
		291.20 ±28.94		0.24	Increase	Increase	312.15		0.24	0.93
		247.32 ±9.34		0.19	Increase	Increase	285.99		0.19	0.86
	Ab_{HPF}	1041.70 ±14.08	1016.38 ±181.31 (17.84% CV)	1.04	Increase	Increase	1058.90	1033.00 ±178.07 (17.24% CV)	0.96	0.98
		1183.70 ±8.30		2.92	Increase	Increase	1196.70		2.44	0.99
		823.74 ±42.64		0.82	Increase	Increase	843.39		0.73	0.98
Silicon Dioxide	Ab_{HSA}	100.61 ±12.32	---	0.09	Decrease	Decrease	211.65	---	0.17	0.48
	Ab_{C3c}	41.26 ±7.79	---	0.04	Increase	Increase	34.49	---	0.03	1.20
	Ab_{HPF}	114.12 ±10.50	---	0.12	Increase	Increase	116.44	---	0.10	0.98
11-AUT SAM	Ab_{HSA}	213.66 ±14.85	---	0.22	Decrease	Decrease	319.91	---	0.28	0.67
	Ab_{C3c}	282.12 ±16.38	---	0.25	Decrease	Decrease	362.37	---	0.27	0.78
	Ab_{HPF}	204.67 ±20.46	---	0.24	Decrease	Decrease	277.05	---	0.28	0.74
Cyst. SAM	$A_{b(A)}$	313.68 ±22.74	---	0.39	Decrease	Decrease	365.23	---	0.44	0.86
	Ab_{C3c}	47.24 ±3.15	---	0.06	Decrease	Decrease	212.82	---	0.19	0.22
	Ab_{HPF}	1461.24 ±3.70	---	1.37	Increase	Increase	1424.73	---	1.26	1.03
MUA SAM	Ab_{HSA}	76.10 ±16.93	---	0.13	Decrease	Decrease	198.68	---	0.28	0.38
	Ab_{C3c}	18.42 ±1.05	---	0.03	Decrease	Increase	14.92	---	0.02	1.23
	Ab_{HPF}	210.73 ±7.79	---	0.24	Increase	Decrease	290.73	---	0.25	0.72

a: *Probe antibody for the detection of adsorbed HSA (Ab_{HSA}), complement factor C3 (Ab_{C3c}), and HPF(Ab_{HPF})*
b: *Sauerbrey-determined adsorbed mass. Standard deviation is obtained from 3 overtone responses.*
c: *Antibody probe mass as a proportion of total blood protein mass*
d: *Viscoelastic film parameters indicating film rigidity levels*
e: *Indicates level of film hydration*

Sauerbrey and Voigt Analysis

Controls Analysis

On average, the adsorption of Ab_{HSA} on the control surfaces (resulted in large increases in film thickness (data not shown), deposited mass, film viscosity and shear modulus, and varying levels of film hydration (Table 2.6). The occurrence of film thickness increases, greater than that predicted for an edge-on monolayer of antibody (Figure 2.5; 14.2 nm), suggests the possibility of antibody binding-induced conformational change of the target protein takes place. Acceptable levels of reproducibility were reported for the Sauerbrey determined film mass parameters (new: 7.78 %; used: 9.42 %), while a decrease in

reproducibility was observed for the Voigt-based analysis (new: 36.63 %; used: 17.21 %). This decrease in reproducibility, as a result of taking into account trapped water, places emphasis on the target protein structural changes induced by antibody binding.

A promising aspect concerning experimental reproducibility is the fact that the reproducibility of probe antibody detection is not dependent on the reproducibility of the blood protein adsorption step (Tables 2.4, 2.5, and 2.6). This is observable in the case of the positive Ab_{HSA} control, where a used crystal surface was employed: surface modification of the sensor surface with the target Ab_{HSA} antibody demonstrated 7.1 % CV, and 8.7 % CV. experimental reproducibility of the Sauerbrey- and Voigt-determined mass, respectively (Table 2.4). The experimental reproducibility reported for the subsequent blood protein adsorption process, summarised in Table 2.5, indicated considerably lower reproducibility, of 25.9 % CV (Sauerbrey), and 53.3 % CV (Voigt). However, an increase in the reproducibility of the protein detection method was observed in the final, probe antibody step, where the Sauerbrey- and Voigt-determined mass demonstrated 9.4 % CV and 17.2 % CV, respectively (Table 2.6). This lack of the propagation of error, from the initial, surface modification step, to the final, probe antibody binding step, highlights the robustness of the proposed protocol.

According to the reproducibility analysis of the utilisation of new, and used, crystal sensor surfaces, the new crystal surface demonstrated more reproducible protein detection results, in terms of the Sauerbrey model, while the used crystal sensor surface demonstrate more reproducible Voigt model results (Table 2.6). However, with respect to the aim of this particular control experiment, it is important of assess the reproducibility of the antibody modified surface in the selective adsorption of the target protein, namely HSA. This may be assessed in terms of the total probe antibody mass as a proportion of the blood protein adsorbed mass (Table 2.6; Ab_m/BP_m). The Ab_m/BP_m value indicates the selectivity of the test surface in binding the target protein, where the higher the value, the more selective the blood protein adsorption process. On average, the utilisation of the new crystal sensor surface generated higher Ab_m/BP_m values (Sauerbery: 4.3; Voigt: 5.3) in comparison to the results obtained using the used crystal surface (Sauerbery: 3.9; Voigt: 2.4), suggesting the new crystal surface was more effective in generating a positive control surface. Reproducibility of the control experiments, in terms of the blood protein film, and probe antibody film

(i.e. Ab_m/BP_m) indicated the new crystal demonstrated more reproducible results (Sauerbrey: 0.3 % CV; Voigt: 0.3 % CV, data not shown), in comparison to the used crystal surface (Sauerbrey: 0.3 % CV; Voigt: 0.6 % CV, data not shown). It was therefore concluded, that the chemical cleaning process, and the utilisation of the crystal surfaces, negatively influence the reproducibility of experimental QCM-D procedures. To my knowledge, this is the first documentation of QCM-D sensor crystal reproducibility analysis, in terms of the influence of chemical cleaning and reuse.

Analysis of Ab_{C3c+} binding to the already deposited HS coated IgG film, for the positive detection of complement C3, indicated a decrease in the viscoelastic properties, with respect to viscosity and shear modulus (Table 2.6). This increase in viscoelasticity was coupled with a slight increase in interface roughness, and increase in film hydration (Table 2.6; Table A.2). Furthermore, both the Sauerbrey and Voigt-determined film thickness values of the deposited film were recorded to be substantially lower than the predicted edge-on monolayer thickness of 14.5 nm, suggesting monolayer coverage of the HS surface was not achieved (Data not shown). Taking these factors into consideration, antibody binding-induced target protein conformational change was considered to be unlikely. In the case of HS protein adsorption to the IgG coated gold sensor surface, high levels of complement factor C3c are anticipated as IgG is a known activator of the complement system, and therefore high levels of probe Ab_{C3c+} are predicted to bind [21]. High levels of Ab_{C3c+}, in terms of total antibody mass, and Ab_m/BP_m, were reported to bind to the IgG-modified surface, therefore correlating with the predicted results (Table 2.6).

A negative mass response was reported for Ab_{C3c-} binding to the iHS coat adsorbed to the IgG-modified surface, generated for the negative control (Table 2.6). This negative mass suggests the removal of adsorbed heat inactivated blood proteins from the IgG surface, by the Ab_{C3c-} molecules.

Ab_{HPF} binding to the previously deposited HP coated Ab_{HPF} film resulted in the generation of a highly rigid film, whose Sauerbrey-determined mass value was an overestimation, and loss of trapped water was observed (Table 2.6). This occurrence has been recorded in literature,

where it was attributed to antibody-antibody interactions which result in the 'stiffening' of the fibrinogen film. The possibility of antibody-antibody interactions occurring of the fibrinogen-rich surface are greatly increased due to the fact that approximately 35 antibody molecules may potentially bind to one fibrinogen molecule [81]. High levels of HPF were predicted to adsorb to the adsorbed Ab_{HPF}-modified surface, due to the specificity of the antibody-antigen interaction. High levels of probe Ab_{HPF} were therefore expected to bind to the HP coated Ab_{HPF}-modified surface. The experimentally determined results concur with the theoretically predicted results (Table 2.6).

Reproducibility Analysis: Unmodified Gold Surface

Adsorption of probe antibodies on blood protein coated gold surfaces resulted in a decrease in film viscosity, in comparison to the film HS film parameters (Table 2.5) when assessing HSA, while an increase in film viscosity was observed when assessing complement C3c and HPF (Table 2.6). As previously discussed, Ab_{HSA} binding is predicted to result in conformational changes of the HSA molecule, while both Ab_{C3c} and Ab_{HPF} binding have little effect on the conformation of their respective target antigens. Both analysis of HSA and HPF adsorption on gold demonstrated low levels of reproducibility, however, acceptable levels were reported for complement C3 detection (Sauerbrey 9.2% CV; Voigt: 5.1 % CV). These higher standard deviations observed for HSA and HPF may be attributed to by the number of antibody epitopes present on the target molecules, therefore emphasising the importance of protein conformation for detection purposes. Both HSA and HPF proteins are reported to undergo some degree of conformational change when adsorbing to gold, therefore resulting in the exposure, or concealment of the target epitomes [81].

Ab_{HSA} Binding Trends

When assessing probe antibody binding, as a proportion of the blood protein bound (Ab_m/BP_m), the Sauerbrey- and Voigt-determined adsorbed mass values indicated identical binding trends. For simplicity, only the Voigt-based parameter will be referenced when discussing probe antibody binding. Voigt-determined film parameters were predicted as a more accurate representation of the adsorbed protein films, as the mathematical model takes into account coupled water [34].

The highest level of Ab_{HSA} (Ab_m/BP_m) adsorbed on the unmodified and SAM-modified surfaces (Table 2.6) was observed on the Cyst. SAM surface (0.44), followed by the 11-AUT SAM surface (0.28), MUA SAM surface (0.28), unmodified SiO_2 (0.17), unmodified gold (0.11-0.17). Although HSA is reported to demonstrates a high binding affinity towards negatively charged surfaces, as well as hydrophobic surfaces, under physiological conditions, HSA carries a net negative charge, at physiological pH, as the molecule demonstrates an isoelectric point (p*I*) of approximately 4.7 [17, 95, 96]. The presence of this negative charge is predicted to influence the binding affinity of the target protein to the positively charged surfaces, via electrostatic interactions. This prediction corresponds with the experimentally determined occurrences, where higher levels of HSA were detected on the positively charged SAM surfaces (Cyst. and 11-AUT), in comparison to the negatively charges SAM (MUA). The similar HSA levels detected on the hydrophobic gold surface and the negatively charged SiO_2 is in accordance with literature, as HSA is reported bind to both negatively charged and hydrophobic surfaces with a high affinity [35, 36].

An alternative explanation for the deviation of the experimentally determined adsorbed HSA levels with literature reported binding affinity, may be the level of surface-induced conformational change of the protein. High levels of HSA conformational change, upon adsorption to the test surfaces, may either increase or decrease the subsequent binding of the probe antibody, depending on the position of the antibody epitopes on the target protein following conformational change. It has been reported that protein adsorption to both rigid, and hydrophobic surfaces, results in conformational changes of the protein on the surface [27,35].

A comparison between the level of Ab_{HSA} binding to the positive control surfaces (Ab_{HSA}-modified gold), generated on both the new (3.51) and used (0.98) crystal surfaces, and the results obtained for the test surfaces, indicated substantially lower levels of HSA were deposited on the test surfaces, in comparison to the control surfaces.

Ab_{C3c} Binding Trends

The levels of complement factor C3 (Table 2.6; Ab_m/BP_m), via the detection of complement C3c, observed on the surfaces were: 11-AUT SAM (0.27) > gold surface (0.24 and 0.19) ≥ Cyst. SAM (0.19) > SiO_2 (0.03) ≥ MUA SAM (0.02). According to literature, complement activating surfaces display nucleophiles, such as hydroxyls and amino groups, while the presence of negatively charge groups, such as carboxyls, is reported on non-activating surfaces [9]. The experimentally determined binding trends observed for the complement factor C3 therefore correspond with literature findings, as higher levels of complement C3 were reported on the positively charged SAMs (11-AUT and Cyst.) in comparison to the negatively charged SAM (MUA). The 11-AUT SAM-modified surfaces were reported to demonstrate a more hydrophobic nature, determined via HS adsorption analysis, in comparison to the Cyst. SAM-modified surfaces. This occurrence corresponds with a decrease in 11-AUT SAM surface protenation, therefore resulting in the generation of a surface composed of nucleophiles, which are complement activating [9]. Lower levels of adsorbed complement factor C3 were detected on the negatively charged surfaces silicon dioxide surface (Table 2.6). The levels of Ab_{C3c} adsorption (Ab_m/BP_m) on the test surfaces, fell within the range on the positive (1.22) and negative (-0.21) control surfaces.

Ab_{HPF} Binding Trends

The level of detected adsorbed HPF (Table 2.6; Ab_m/BP_m) decreased as follows: Cyst. SAM surface (12.6), 11-AUT SAM surface (0.28), MUA SAM surface (0.25), and unmodified SiO_2 (0.10). Varying levels of HPF were detected on the gold, hydrophobic surface, however, the levels were similar to that observed of the Cyst. SAM surface (0.73 to 2.44). HPF has been reported to demonstrate a high affinity towards hydrophobic surfaces, as well as favouring hydrophilic over hydrophobic SAM-modified surfaces [97, 98]. The experimentally determined HPF binding trend corresponded with literature, as the hydrophilic SAM-modified surfaces (Cyst.) demonstrated higher levels of HPF adsorbed to the surface, while the more hydrophobic SAM-modified surface (11-AUT) demonstrated a lower level of HPF. However, similar levels of HPF were detected on the 11-AUT and the MUA SAM-modified surfaces. The low level observed on the negatively charged SAM surface are predicted, as HPF demonstrates a p*I* of approximately 5.5, therefore rendering the molecule negatively charged at physiological pH [44]. A higher binding affinity towards the

hydrophobic gold surface was demonstrated in comparison to the unmodified negatively charged SiO_2 surface.

On average, the levels of HPF detected, via probe antibody binding, on the test surfaces did not exceed that observed on the control surface (1.09), with the exception of Ab_{HPF} binding on one unmodified gold surface (2.44), and the Cyst. SAM-modified surface (1.26). These high levels of detected HPF highlight HPF adsorbed protein orientation as a potentially influential factor when detecting protein levels using probe Ab_{HPF}.

2.4. CONCLUSIONS

In conclusion, HSA detection, utilising the proposed method of probe antibody detection in conjunction with QCM-D technology, indicated high target protein levels on the positively charged Cyst. SAM-modified sensor surface, followed by 11-AUT SAM, MUA SAM, unmodified SiO_2, and unmodified gold sensor surfaces (Table 2.6). The levels of detected HSA on the test surfaces are supported by literature, therefore emphasising the accuracy of the proposed method of detection. However, protein conformation change of the large, globular HSA, as a result of adsorption with the target surface, was suggested as a possible influential factor when detecting protein levels using probe antibody binding. Assessment of the influence of conformational change may be carried out in studies where the target surfaces are incubated with pure HSA, instead of HS, followed by protein detection, using Ab_{HSA}. The assessment of the HSA adsorption on the surface, using Sauerbrey- and Voigt-determined film parameters, is expected to aid in identification of protein conformational change, via film hydration, and film viscoelasticity analysis.

Detection of the complement system activation potential of the target surfaces, via complement C3 detection using Ab_{C3c} binding, indicated the following binding trend: 11-AUT SAM > unmodified gold surface ≥ Cyst. SAM > unmodified SiO_2 ≥ MUA SAM. The experimentally determined Ab_{C3c}, and therefore complement C3, binding trend corresponds with literature, as the nucleophiles bearing surface, 11-AUT, (i.e. complement activating) demonstrated higher levels of protein detection in comparison to that observed on

the carboxyl bearing surface, MUA SAM (i.e. non-activating) [9]. This correlation between the theoretical predictions and the experimentally determined results indicates the accuracy of the protein detection method.

Ab_{HPF} probe antibody binding results indicated the following binding trend: unmodified gold > Cyst. SAM surface> unmodified gold > 11-AUT SAM > MUA SAM > unmodified SiO_2 (Table 2.6). High levels of variability were observed for HPF binding to the hydrophobic gold. The orientation of adsorbed HPF was highlighted as an influential factor when detecting the levels of adsorbed protein using Ab_{HPF} antibody probes.

With regards to experimental reproducibility, Ab_{C3c} detection of adsorbed complement C3 proteins demonstrated the highest level of reproducibility (Sauerbrey: 9.15 % CV, Voigt: 5.05 % CV) in comparison to the detection of HSA and HPF (Table 2.6). This high level of reproducibility may be attributed to by the small size of the target protein (i.e. complement C3c), and therefore lower predicted antibody : antigen (Ab:Ag) ratio [35]. The small size of the protein, and low Ab:Ag ratio, suggests the effects of conformational change of the target protein, on protein detection, would be minimum. An additional factor to consider, is that the target protein, complement C3c, is tightly associated with other complement proteins on the target surface [35, 40, 41]. This tight association is predicted to limit the level of conformational change of the target C3c protein, therefore attributing to the reproducibility of the protein detection method.

Ab_{HSA} detection of HSA demonstrated reasonably experimental reproducibility (12.36 % CV) when assessing the binding using the Sauerbrey model, however, the Voigt model indicated considerably low reproducibility (43.18 % CV). This variability in reproducibility, between the two modelling systems, emphasises target protein conformational change as an influential factor. The detection of HPF, using Ab_{HPF} probe antibody, indicated the lowest level of reproducibility (Sauerbrey: 17.84 % CV, Voigt: 17.24 % CV), which was proposed to be the result of adsorbed HPF orientation.

It is important to note the lack of error propagation from the surface modification, to the blood protein adsorption, and subsequent probe antibody binding steps (Table 2.4, 2.5, and 2.6). This is a favourable aspect when considering sensor design.

CHAPTER 3:

BIOMOLECULAR INTERACTION WITH METALLOPHTHALOCYANINES

3.1. INTRODUCTION

3.1.1. Overview of MPcs

To date, information regarding the interaction of MPc molecules with subcellular biological components, such as blood proteins, is limited, and chiefly directed towards the effect of protein adsorption on MPc dispersion and therapeutic effectiveness. Investigations into the interaction of human and bovine serum albumin have, however, been conducted as serum albumin plays a significant role in the biodistribution of therapeutics through the circulatory system. The dominating analytical method utilised in such studies were that of spectrophotometry and circular dichroism [64, 95, 99]. Although both methods of analysis provide useful information of protein interactions, they demonstrate a key limitation, namely, that proteins may only be assessed as independent molecules, rather than a component of a complex matrix, such as human blood. The proposed method of utilising QCM-D technology, may provide a means of overcoming these limitations as biomolecular interactions between MPc molecules and human blood proteins, as a complex medium, were to be examined in terms of the protein coat composition when introduced to the circulatory system.

3.1.2. Chapter Aims and Objectives

The central aim this set of experimental procedures was to analyse the blood protein coat that adsorbs to MPc surfaces following introduction of human serum and human plasma, and subsequently assess the applicability of the proposed method of protein identification, using QCM-D, for analysis of particulate therapeutics.

Objectives

1. Particle characterisation of prepared MPc molecules
    a. HPLC analysis of the degree of sulphonation of the MPc preparations
    b. Absorbance spectrophotometric analysis of the MPc preparations to assess particle aggregation
2. Designing of strategies for the immobilisation of the MPc molecules to the QCM-D sensor surface using SAM-modification
3. Monitoring and quantification of the sensor surface modification with the MPc molecules, using QCM-D
4. Monitoring and quantification of human serum/plasma protein adsorption on the MPc-modified surfaces, using QCM-D
5. Identification of surface bound serum/plasma proteins through QCM-D monitoring and quantification of the adsorption of antibodies directed against:
    a. Opsonins: Complement component C3c and human plasma fibrinogen (HPF)
    b. Dysopsonin: Human serum albumin (HSA)

3.2. INSTRUMENTATION AND METHODOLOGY

3.2.1. Instrumentation

High Pressure Liquid Chromatography analysis of the MPc preparations was performed using Programmable Solvent Module 116 (Beckman System Gold); fitted with a C_{18} analytical column (Waters Symmetry; 3.9 × 260 mm), connected to UV detection unit (Beckman System Gold) The mobile phase, 50:50 dilution of methanol to water, was degassed through a filtration process. Absorbance spectral scans were performed using PowerWave X (Bio-Tek Instruments, Inc.), for the analysis of MPc aggregation.

3.2.2. Additional Reagents

Sulphonated MPc samples in this study, containing a mixture of species with varying degrees of sulphonation, namely, sulphonated aluminum phthalocyanine mixture ($AlPcS_{mix}$), sulphonated cobalt phthalocyanine mixture ($CoPcS_{mix}$), sulphonated germainium phthalocyanine mixture ($GePcS_{mix}$), sulphonated zinc phthalocyanine mixture ($ZnPcS_{mix}$),

and the tetra-carboxylated cobalt phthalocyanine (CoTCPc), were provided by Prof. T. Nyokong of the Department of Chemistry, Rhodes University. Tetra-sulphonated copper phthalocyanine (CuTSPc) was purchased from Sigma.

3.2.3. Methodology

3.2.3.1. Characterisation of Sulphonated Metallophthalocyanines

3.2.3.1.1. Degree of Sulphonation Analysis via HPLC

The HPLC analysis protocol was carried out, as explained by Ogunsipe and Nyokong (2005) [101], to determine the degree of MPc sulphonation. 0.1 mg/ml concentrations of each MPc mixture were prepared using the mobile phase, followed by an ultrasonication period of 15 min [95]. The flow rate was set at 1 ml/min and injection volumes of 20 µl were analysed. CuTSPc, obtained from Sigma, provided an indication of the retention time expected for tetra-sulphonated species.

3.2.3.1.2. Spectrophotometric Analysis of MPc Aggregation

Absorbance spectrophotometric analysis of MPc dilutions prepared in $PBS_{Mg/Ca}$ buffer and $PBS_{Mg/Ca}$ buffer containing a 0.2% concentration of Triton X-100, a know surfactant, was carried out to assess MPc aggregation in the chosen buffer intended for QCM-D analysis.

3.2.3.2. Surface Modification with MPcs

The protocol for the immobilisation of the sulphonated MPc samples, to previously prepared 11-AUT SAM surfaces, involved the suspension of 0.1 mg/ml MPc in $PBS_{Mg/Ca}$ buffer (pH 7.4), followed by ultrasonication for a period of 15 min using 'degas' setting. The QCM-D analysis of the immobilisation firstly involved obtaining stable *f* and D baselines using the $PBS_{Mg/Ca}$ buffer, followed by the introduction of the suspended $MPcS_n$ sample, and subsequent $PBS_{Mg/Ca}$ rinse. Immobilisation of the tetra-carboxylated MPc sample, CoTCPc, was achieved through EDC/NHS facilitated binding. 0.1 mg/ml CoTCPc samples were prepared in MES buffer (pH 4.7), and ultrasonicated for a period of 15 min. 15 mM EDC and 15 mM NHS were then introduced, followed by a further sonication for 20 min, in the

dark. QCM-D analysis of the immobilisation process involved introducing PBS $_{Mg/Ca}$ buffer, then MES buffer, MPc-EDC/NHS preparation, MES buffer, and a final rinse with $PBS_{Mg/Ca}$ buffer.

3.2.3.3. QCM-D Monitoring and Quantification

Monitoring of protein binding, both blood protein and antibody binding, to the immobilised MPc samples was performed using a similar approach described in Chapter 2 Section 2.2.4.

3.3. RESULTS AND DISCUSSION

Section 3.3.1 reports on MPc characterisation, in terms of sulphonation and particle aggregation in $PBS_{Mg/Ca}$, while Section 3.3.2 examines the MPc immobilisation process in terms of theoretically determined parameters (3.3.2.1), and experimentally determined parameters, of the deposited MPc film. Section 3.3.3 details protein adsorption to the deposited MPc film, both the blood protein adsorption (3.3.3.1), and antibody probe binding (3.3.3.2).

3.3.1. Characterisation of Sulphonated MPcs

3.3.1.1. Degree of Sulphonation Analysis via HPLC

HPLC analysis of the sulphonated MPc samples was performed to evaluate the degree of sulphonation of the species present in the independently synthesised mixtures. The response exhibited by CuTSPc provided a standard to which the HPLC retention times reported for the remainder of the MPc preparations could be compared, as CuTSPc sourced and purified to homogeneity by the commercial supplier. Figure 3.1 illustrates examples of the HPLC retention times demonstrated by each MPc mixture. No retention time peak was recorded for the CoTCPc sample. Due to the negative charge carried by the analytical column, one assumes the initial peak recorded to be the more sulphonated species, followed by the second highest sulphonated species, and so on [101].

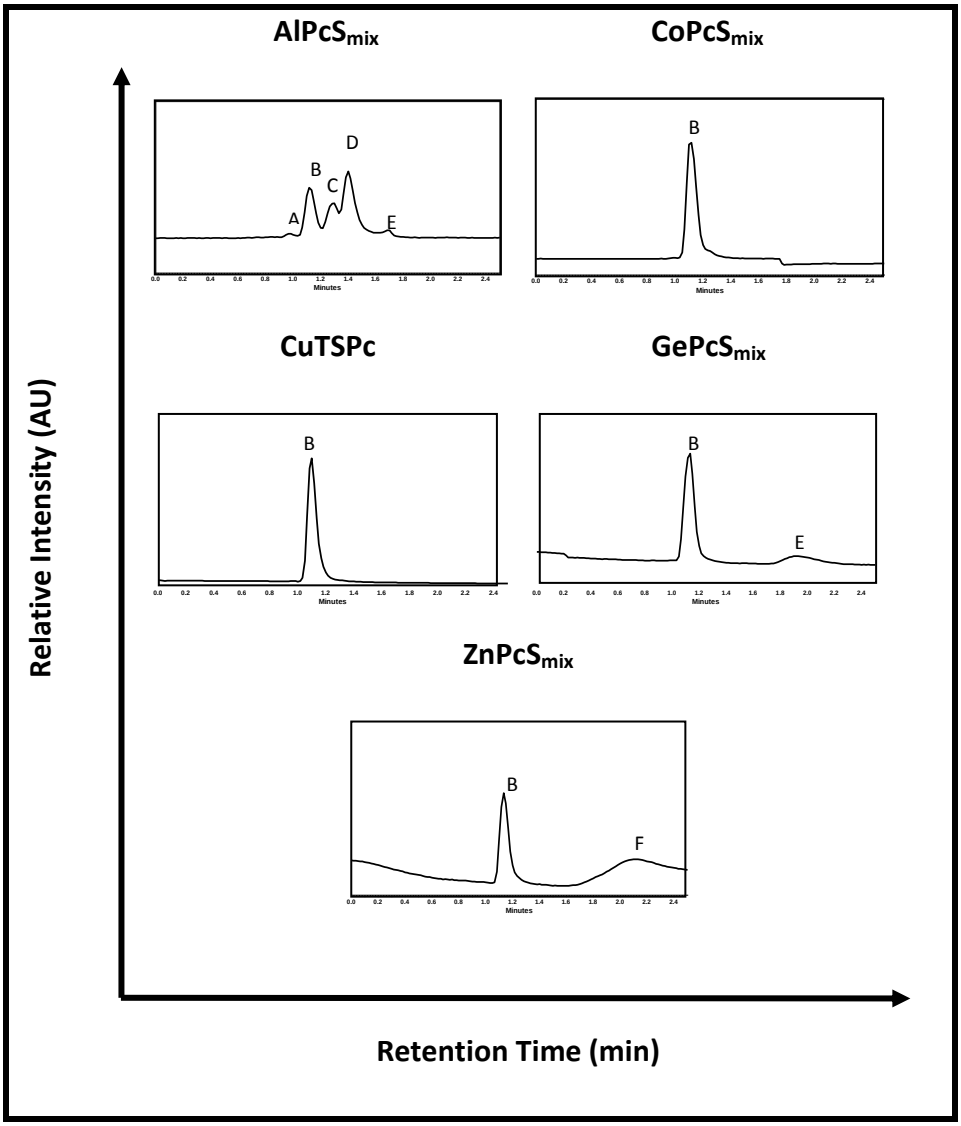

Figure 3.1. HPLC trace for MPcs indicating the degree of sulphonation of the MPc species present in the MPc preparations. The MPc preparations analysed were $AlPcS_{mix}$, $CoPcS_{mix}$, CuTSPc, $GePcS_{mix}$ and $ZnPcS_{mix}$. HPCL traces are illustrated for retention time 0 to 2.5 min. Peak retention times are summarised in Table 3.1.

As Figure 3.1 indicates, five peaks were recorded for $AlPcS_{mix}$, two for $GePcS_{mix}$ and $ZnPcS_{mix}$, and one for the $CoPcS_{mix}$, and CuTSPc. Table 3.1 summarises the average peak retention times recorded for the peaks observed in Figure 3.1, and the subsequent conclusions drawn from the study. The single peak observed for the purchased CuTSPc was assumed to be indicative of a tetra-sulphonated species, therefore suggesting peaks possessing a retention time of 1.10 min arise from the presence of a tetra-sulphonated species in MPc_{mix}. A single dominant peak was recorded when examining $CoPcS_{mix}$, demonstrated a similar retention time to that of CuTSPc. It was therefore concluded that the $CoPcS_{mix}$ contained tetra-

sulphonated species (Table 3.1). Similarly, tetra-sulphonated species were assumed to be present in the $AlPcS_{mix}$, $GePcS_{mix}$, and $ZnPcS_{mix}$ samples, (Figure 3.1 and Table 3.1). HPLC analysis of $AlPcS_{mix}$ indicated the presence of five variants of the sulphonated MPc, observed as five peaks (Figure 3.1). The initial peak (A), demonstrated a retention time substantially less than that of the predicted tetra-sulphonated species. This lower retention time suggests the presence of species which demonstrate a greater negative charge in comparison to that of the tetra-sulphonated species, and therefore a higher degree of sulphonation. From the assumed tetra-sulphonated AlPc retention time, the responses obtained for the remainder of the peaks, namely, C, D, and E, were utilised as an indication of the retention times expected for tri-, di-, and mono- sulphonated species, respectively. It was therefore concluded that $GePcS_{mix}$, contained both tetra- and mono-sulphonated species. The HPLC response for $ZnPcS_{mix}$, indicated a broad band demonstrating a high retention time (F). The high retention time of the species suggests the presence of MPc aggregates, possibly consisting of low charged ZnPc molecules (i.e. mono-sulphonated). According to literature, the degree of aggregation is dependent on the lipophilicity of the MPc molecules, therefore suggesting an increase in particle aggregation as the level of sulphonation decreases. [101].

Table 3.1. HPLC Analysis of the Degree of Metallophthalocyanine Sulphonation

MPc	Ave. Retention Time (min)						Degree of Sulphonation[a]
	Peak A	Peak B	Peak C	Peak D	Peak E	Peak F	
$AlPcS_{mix}$	0.98	1.13 ± 0.01	1.29	1.38 ±0.02	1.68		Penta-; Tetra-; Tri-; Di-; Mono-
$CoPcS_{mix}$		1.11 ± 0.01					Tetra-
CuTSPc		1.10 ±0.00					Tetra-
$GePcS_{mix}$		1.12 ±0.01			1.74 ±0.11		Tetra-; Mono-
$ZnPcS_{mix}$		1.13 ±01.00				2.12 ±0.03	Tetra-; Aggregates

a : Determined by retention time
Number of replicants was 3. Uncertainty was standard deviation from the mean.
In the case of standard deviation being omitted, peaks were not apparent in all three replicants

In conclusion, HPLC analysis indicated; $AlPcS_{mix}$ contained penta-, tetra, tri-, di-, and mono-sulphonated species; both $CoPcS_{mix}$ and CuTSPc contained tetra-sulphonated species; $GePcS_{mix}$ contained tetra- and mono-sulphonated species; and $ZnPcS_{mix}$ contained tetra-sulphonated species and aggregates.

3.3.1.2. Spectrophotometric Analysis of MPc Aggregation

Phthalocyanine absorption spectra are characterised by two absorption bands, namely, the Soret/B-band (~350 nm), and the Q-band (~680 nm) [95, 99]. According to literature, aggregation of Pc molecules may be evaluated through observing the Q-band. Splitting or broadening of the latter band has been reported to correspond with the presence of particle aggregates [49, 51, 95, 102]. Therefore, the focus of the spectrophotometric analysis of MPc aggregation was on the Q-band.

Absorbance spectrophotometric analysis of the MPc preparations was performed to crudely assess particle aggregation in the chosen buffer utilised for MPc immobilisation analysis via QCM-D, namely, $PBS_{Mg/Ca}$ (pH 7.4). Comparisons were made between the absorbance spectra (Q-band) of the MPc preparations in $PBS_{Mg/Ca}$ buffer, with that of the spectra obtained where the surfactant, Triton X-100, was utilised as a dispersing agent (Figure 3.2). Similar means of investigating MPc aggregation were reported by Ogunsipe and Nyokong (2005) [101].

Figure 3.2 illustrates the absorbance spectra obtained for the MPc preparations, both in $PBS_{Mg/Ca}$ buffer, and when dispersed in $PBS_{Mg/Ca}$ using 0.2% Triton X-100. Q-band splitting was observed in all MPc preparations. In the case of MPcs dispersed in $PBS_{Mg/Ca}$, the Q-band splitting may suggest one of two occurrences. Firstly, that aggregated species are present, and/or secondly, the presence of species bearing varying degrees of sulphonation, which would therefore suggest individual Q-bands were observed, in comparison to Q-band splitting [95]. The addition of the surfactant, Triton X-100, was expected to result in monomerization of any MPc aggregates present in solution. This was predicted to be observed as peak sharpening and and/or an increase in peak intensity [95].

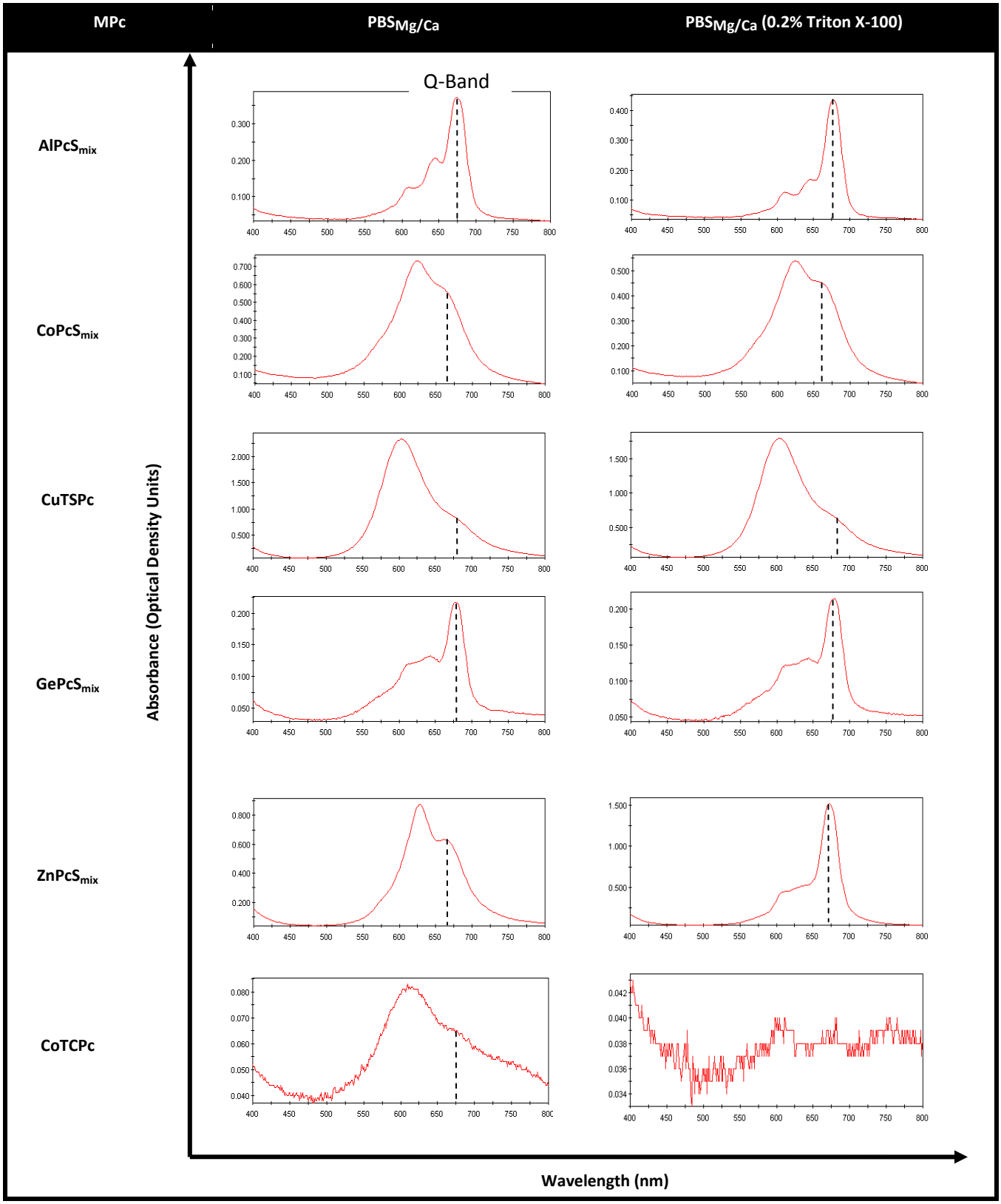

Figure 3.2. Absorbance spectrophotometric analysis of MPc aggregation. Absorbance spectral scans of MPc preparations in $PBS_{Mg/Ca}$ buffer (pH 7.4) and $PBS_{Mg/Ca}$ (0.2% Triton X-100). Dashed lines indicate the MPc monomer Q-band.

Similar to the findings in literature, the addition of Triton X-100 resulted in an increase in peak intensity, when assessing $AlPcS_{mix}$ (Figure 3.2). The latter implies monomerisation of the MPc aggregates. However, the factor responsible for the splitting of the Q-band was concluded to be the degree of sulphonation within the mixture rather than particle aggregation [95]. Spectrophotometic analysis of $AlPcS_{mix}$ (Figure 3.2) corresponds with HPLC analysis (Table 3.1), which suggests the presence of mono-, di-, tri-, tetra-, and penta-sulphonated MPc species, as MPc molecules demonstrating lower levels of sulphonation have been suggested to aggregate in aqueous solution [95, 101].

The addition of Triton X-100 to both the $CoPcS_{mix}$, CuTSPc and CoTCPc preparations resulted in a decrease in peak intensity. According to literature, a decrease in Q-band intensity is indicative of photodegradation of the MPc molecule as a result of exposure to light [101]. The proposed photodegradation of CoTCPc, resulted in a decrease in absorbance levels, which generated the Q-band almost unidentifiable. The presence of surfactant resulted in slight peak sharpening when assessing $GePcS_{mix}$ preparations, therefore suggesting that majority of the MPc species were in monomer form while in aqueous solution, with a small portion are present in aggregate form. These results correspond with the HPLC analysis of the MPc preparation, which suggested high levels of tetra-sulphonated species and low levels of mono-sulphonated species. The inclusion of Triton X-100 to the $ZnPcS_{mix}$ preparation resulted in a considerable change in peak intensities, suggesting a large portion of the MPc molecules are in aggregated form when in aqueous solution, as suggested by HPLC analysis indicating possible aggregation (Table 3.1).

3.3.2. Surface Modification with MPcs

According to literature, MPc molecules may adopt two conformations when immobilised to a target surface, namely, edge-on and/or planar conformations [49]. For the purpose of this research, immobilisation of both sulphonated and carboxylated MPcs were carried out using the amine terminating SAM, 11-AUT. A positively charged SAM surface was utilised as it is predicted to promote MPc immobilisation through electrostatic interactions with the sulfonic acid groups present on sulphonated MPc molecules (Figure 1.6), and form a basis for covalent bonding with the carboxylic acid group of CoTCPc molecules. 11-AUT SAM

modification was favoured over Cyst. modification, due to the longer chain length, which has been reported to aid in the ordering of the self assembly process [84-86]. Figure 3.3 provides a schematic illustration of the anticipated orientations of MPc molecules immobilised on an 11-AUT SAM.

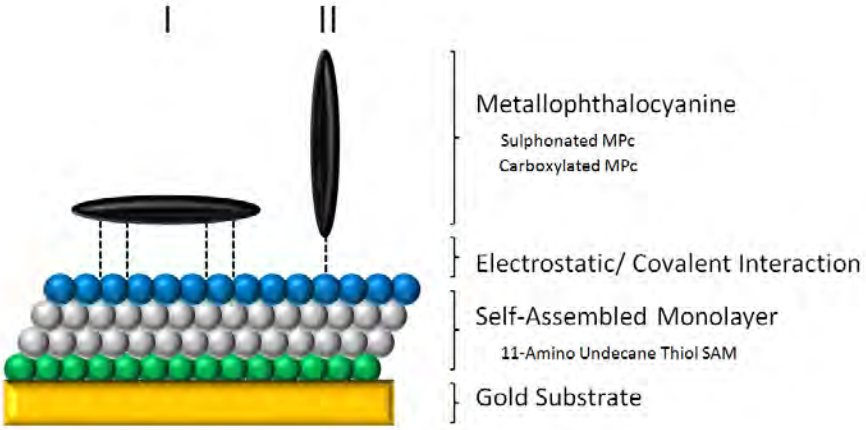

Figure 3.3. Schematic representation of immobilised metallophthalocyanine orientation. Planar and edge-on MPc conformations are illustrated by I and II, respectively.

3.3.2.1. Theoretical Determination of Expected MPc Monolayer Mass

When calculating the theoretical mass shifts expected during the immobilisation of MPc molecules on the 11-AUT SAM surface, four scenarios were considered where two aspects of the occurrence varied. Firstly, the diameter of the MPc molecule was determined, where the ring substitutions were both included and excluded (Figure 3.4). Secondly, the expected adsorbed mass was calculated for two conformations of the MPc molecule on the surface, namely side-on and planar conformation (Figure 3.3). Possible distortion of the macrocylic geometry, due to the central metal, was omitted.

Calculations

- MPc surface area was calculated, using the two scenarios illustrated in Figure 3.3, for the edge-on and planar conformations using the following formulae:

Edge-On:

$$\text{Atomic radius}_{\text{MPc central metal}} \times \text{Molecular Diameter}_{\text{MPc}} = \text{Surface Area}_{\text{MPc}} \qquad \textit{Eq. 7}$$

Planar:

$$\pi \times (\text{Molecular Radius}_{\text{MPc}})^2 = \text{Surface Area}_{\text{MPc}} \qquad \textit{Eq. 8}$$

- The reciprocal of which indicates MPc occupancy on the sensor surface (i.e. MPc molecules.cm^{-2})
- From this, coverage of the MPc molecules was determined, followed by the number of mol's of MPc per cm^2, and finally the total mass per cm^2

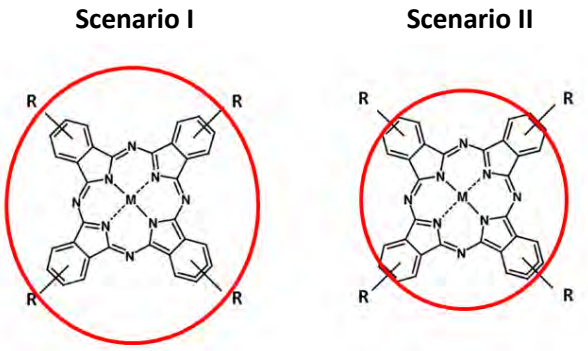

Figure 3.4. Rasmol determined MPc molecular diameter. MPc diameters of 1.375 nm and 0.769 nm were recorded for scenario I and II, respectively. (PDB: 691745)

The theoretical expected adsorbed mass for an MPc monolayer which adopts the edge-on and planar conformation, are summarised in Table 3.2. These values were utilised in the assessment of MPc immobilisation, monitored using QCM-D.

Table 3.2. Theoretical MPc Immobilised Mass (ng.cm^{-2}) for Edge-On and Planar Conformations

Edge-On Conformation											
Substituents		**Tetra-SO_4^-**		**Tri- SO_4^-**		**Di- SO_4^-**		**Mono- SO_4^-**		**Tetra-COO^-**	
Scenario		**I**	**II**	**I**	**II**	**I**	**II**	**I**	**II**	**I**	**II**
MPc	**Al**	285.24	510.03	258.68	462.53	232.12	415.04	205.56	367.55	---	---
	Co	322.42	576.49	---	---	---	---	---	---	271.95	486.25
	Cu	344.73	616.39	---	---	---	---	---	---	---	---
	Ge	359.66	643.09	---	---	---	---	264.25	472.48	---	---
	Zn	356.80	637.97	---	---	---	---	---	---	---	---
Planar Conformation											
Substituents		**Tetra-SO_4^-**		**Tri- SO_4^-**		**Di- SO_4^-**		**Mono- SO_4^-**		**Tetra-COO^-**	
Scenario		**I**	**II**	**I**	**II**	**I**	**II**	**I**	**II**	**I**	**II**
MPc	**Al**	96.14	307.38	87.19	278.76	78.24	250.13	69.29	221.51	---	---
	Co	99.72	318.80	---	---	---	---	---	---	84.11	268.90
	Cu	100.23	320.46	---	---	---	---	---	---	---	---
	Ge	101.25	323.69	---	---	---	---	74.39	237.82	---	---
	Zn	100.44	321.11	---	---	---	---	---	---	---	---

Scenario I: MPc dimensions including the ring substituents (Figure 3.4)
Scenario II: MPc dimensions excluding ring substituents

3.3.2.2. QCM-D Monitoring and Quantification of Surface Modification: MPcs

The process for immobilisation of the MPc molecules to the 11-AUT SAM surface was monitored using QCM-D. A brief examination of the *f* and D shifts, summarised in Table 3.4, provided information on the rigidity of the immobilised MPc film. For the purpose of assessing immobilised film properties, final frequency (*f*) and dissipation (D) values, after immobilisation, are reported, instead of changes in both Δf and ΔD. This means of data depiction was favoured due to more realistic results being obtained from the Voigt-based modelling, in comparison to utilising the changes in shifts from initial (prior immobilisation) and final (post immobilisation) data. In all cases, immobilisation was recorded in quadruplicate (surfaces 0 – 3), with the exception of $ZnPcS_{mix}$ immobilisation, which was carried out to generate 9 replicates.

QCM-D Response Analysis

Table 3.3 summarises the *f* and D responses recorded for the immobilisation of the MPc molecules to the 11-AUT SAM surface. *f*/D values higher than 10 Hz/1E-6 were recorded for

overtones 7 to 11 for the immobilisation procedures, suggesting fairly rigid MPc films were deposited, with the exception of $AlPcS_{mix}$ (2, 4), $GePcS_{mix}$ (0, 3) $ZnPcS_{mix}$ (1B, 1C, 2C, 3A, 3B) and CoTCPc (1, 3) (Table 3.3). Rigidity may also serve as an indication of the validity of Sauerbrey determined film thickness and adsorbed mass (Chapter 2; Section 2.3.1). One may therefore conclude, from the crude assessment of the raw data, the Sauerbrey determined adsorbed film thickness (δ_f) and mass are valid for all the immobilised surfaces, with the exception of the above listed films where the *f*/D values were below 10.

Table 3.3. QCM-D Frequency and Dissipation Shifts Following Metallophthalocyanine Immobilisation to 11-Amino Undecane Thiol Self-Assembled Monolayer

Metallophthalocyanine		f_7 / D_7	f_9 / D_9	f_{11} / D_{11}	Ave. F [a]	Ave. f % CV	Ave. D [a]
AlPcSmix	0	11.40	12.24	11.39	-17.24 ±0.94	5.45	1.48 ±0.10
	1	11.48	10.95	11.96	-26.91 ±1.10	4.09	2.35 ±0.18
	2	7.63	7.15	7.82	-22.79 ±0.65	2.85	3.03 ±0.20
	3	8.57	9.64	8.82	-20.58 ±0.61	2.96	2.29 ±0.16
CoPcSmix	0	203.52	194.15	55.55	-4.52 ±0.30	6.64	-0.03 ±0.05
	1	13.05	13.96	11.71	-10.70 ±0.23	2.15	0.83 ±0.07
	2	200.14	128.6	143.46	-5.27 ±0.09	1.71	-0.04 ±0.01
	3	227.00	78.50	78.33	-4.65 ±0.09	1.94	-0.05 ±0.02
CuTSPc	0	596.91	1462.66	228.11	-3.75 ±0.09	2.40	0.01 ±0.01
	1	80.01	61.53	345.82	-9.49 ±0.41	4.32	0.00 ±0.14
	2	34.54	33.11	22.17	-12.23 ±0.68	5.56	0.42 ±0.09
	3	40.75	38.00	34.00	-11.34 ±0.1	0.88	0.3 ±0.02
GePcSmix	0	5.68	5.89	5.65	-10.77 ±0.67	6.22	1.88 ±0.12
	1	11.36	11.55	14.45	-9.57 ±0.60	6.27	0.78 ±0.14
	2	18.94	17.56	17.94	-7.58 ±0.43	5.67	0.42 ±0.02
	3	2.44	6.66	10.79	-9.05 ±1.45	16.02	1.87 ±1.34
ZnPcSmix	1A	22.83	17.71	18.90	-7.23 ±0.39	5.39	0.37 ±0.04
	1B	6.38	6.03	6.31	-18.96 ±0.95	5.01	3.04 ±0.17
	1C	7.64	7.59	7.13	-17.54 ±0.77	4.39	2.35 ±0.05
	2A	13.85	18.17	16.67	-7.27 ±0.15	2.06	0.45 ±0.06
	2B	14.23	16.44	19.6	-6.91 ±0.13	1.88	0.42 ±0.07
	2C	5.33	5.16	5.09	-27.25 ±1.86	6.83	5.25 ±0.24
	3A	5.55	5.40	3.51	-14.57 ±2.06	14.14	3.08 ±0.37
	3B	8.47	7.92	8.43	-6.54 ±0.3	4.59	0.79 ±0.04
	3C	33.06	20.78	25.24	-5.47 ±0.18	3.29	0.22 ±0.05
CoTCPc	0	16.42	25.68	59.60	-5.57 ±0.44	7.90	-0.21 ±0.1
	1	5.25	7.22	10.99	-15.62 ±1.97	12.61	2.14 ±0.57
	2	13.54	11.57	16.17	-14.16 ±0.51	3.60	1.04 ±0.14
	3	10.65	9.39	6.58	-13.59 ±1.60	11.77	1.56 ±0.23

a: Average values determined using responses obtained from overtones 7 -11

An additional parameter which may provide information on the nature of film deposited is that of the average *f* percentage coefficient of variation (ave. *f* % CV) from a range of overtones. In this case, overtones 7-11 were utilised as higher overtones generate more stable responses [Internet Reference 1]. High standard deviations are indicative of a rough film interface, while low standard deviations suggest a fairly uniform/sharp interface (Chapter 2; Section 2.3.1) [30]. The monitoring of MPc immobilisation, via QCM-D, to my knowledge, has not yet been reported in literature, and therefore the degree of variation in the percentage coefficient of variation has not yet been assessed. There are therefore no absolute values which may be considered to be indicative of highly varied surface interfaces. For the purpose of comparison, an ave. *f* % CV of below 10 % was considered to be an indication of a uniform/sharp interface. High ave. *f* % CV values were reported for the $CoPcS_{mix}$ (0), $GePcS_{mix}$ (3), $ZnPcS_{mix}$ (3A), and CoTCPc (1, 3) surfaces. This 'rough' interface is proposed to be the result of either the MPc molecules immobilising in mixed orientations, the patterning of the MPc molecules on the SAM surface, or the accumulation of MPc aggregates on the surface.

Assessment of film formation process in terms of changes in film rigidity with the addition of MPc molecules was evaluated using D vs. *f* plots. D vs. *f* plots (Figure 3.5) eliminates time as a parameter, and provides information on the changes in film structure, namely, the changes in dissipative energy per unit mass adsorbed (Chapter 2; Section 2.3.1). Figure 3.7 illustrates representative examples of the D vs. *f* plots of the MPc immobilisation processes.

The immobilisation of $AlPcS_{mix}$ to the SAM surface was observed as a two phase process, according to the generated D_7 vs. f_7 plot (Figure 3.5). The initial, more rapid phase, was followed by a phase with a more positive gradient, suggesting an increase in film viscoelasticity with the addition of in-coming MPc molecules, and therefore multilayer formation. The point at which the gradient increases occurs at approximately 0.8 E-6/-8.0 Hz. This *f* shift corresponds to approximately 140 $ng.cm^{-2}$, when applying the Sauerbrey equation, which falls with in the range of theoretically determined planar monolayer mass (Table 3.2). It was therefore concluded that $AlPcS_{mix}$ immobilisation results in the deposition of multilayers on the SAM surfaces. Similarly, two phase immobilisation processes were recorded for CuTSPc, $GePcS_{mix}$, and $ZnPcS_{mix}$, suggesting multilayer

deposition (Figure 3.5). However, in the case of CuTSPc immobilisation, the initial phase indicated highly rigid deposition of the MPc molecules to the surface, observed as an increase in *f* and minimal or no change in D, which demonstrated an approximate mass of 100 ng.cm^{-2} (0.2 E-6/ -5.6 Hz), and therefore corresponding with the theoretical prediction of a planar monolayer (Table 3.2). In addition, the buffer rinse step suggests the removal of the loosely bound MPc molecules adsorbed in phase two, rendering the final film as a monolayer, likely to be in the planar orientation, due to the high rigidity of the deposition (Figure 3.5).

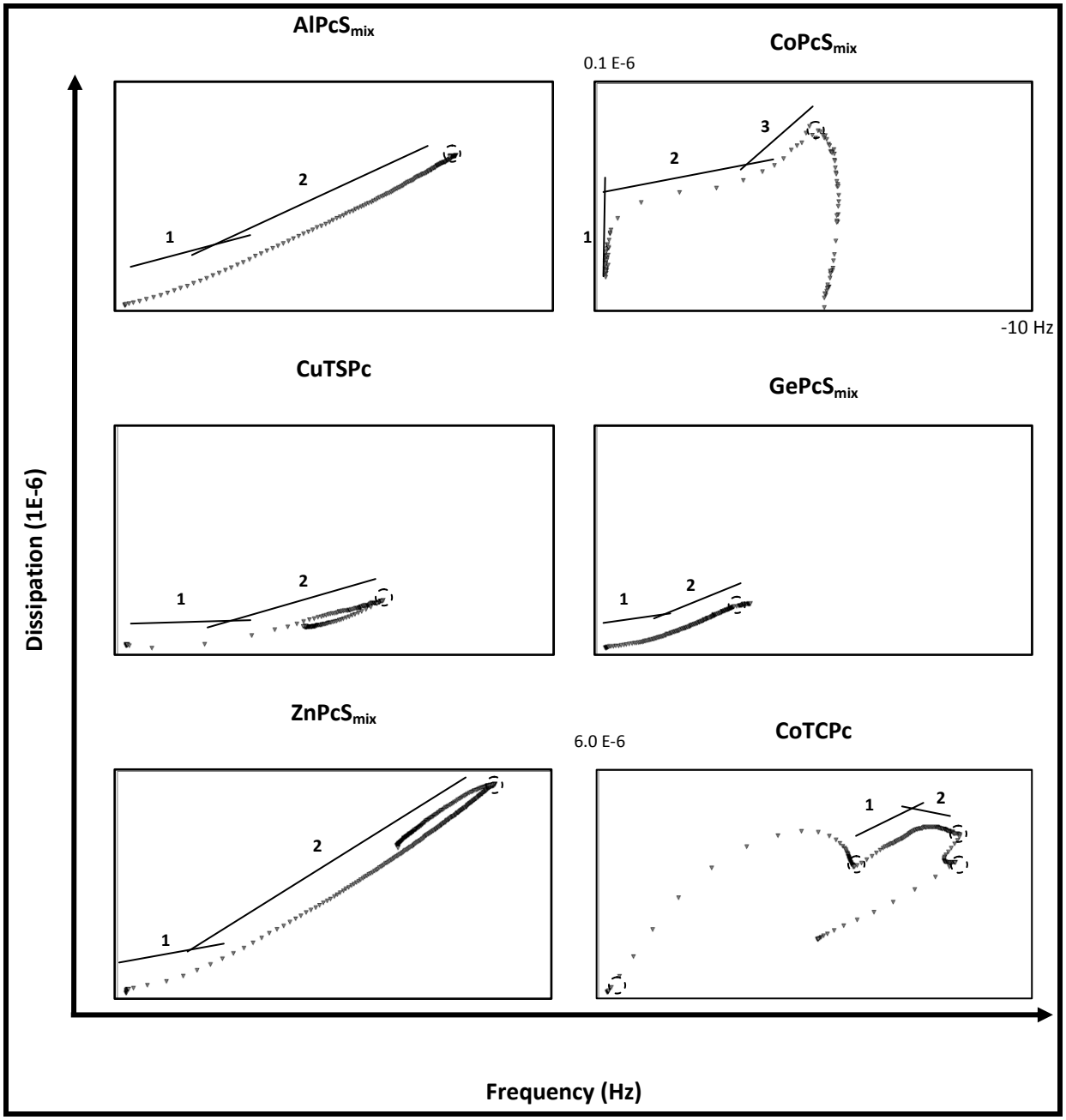

Figure 3.5. Representative dissipation versus frequency plot of the metallophthalocyanine immobilisation processes. f (x-axis) and D (y-axis) shifts for overtone 7 were utilised. The solid lines indicate the gradient shifts of the mass addition. The point of introducing the 'rinse stage' is highlighted using dashed circles. Scale employed was -30 Hz (f) and 4.5E-6 (D), unless stated.

Similarly, rigid deposition of $GePcS_{mix}$ and $ZnPcS_{mix}$ sub-monolayer (0.1 E-6/ -3.0 Hz and 0.3 E-6/ -4.0 Hz, respectively) were recorded, however, the buffer rinse did not indicate the removal of the loosely bound MPc molecules, suggesting the deposition of a multilayer.

Adsorption of $CoPcS_{mix}$ to SAM surface occurred in a three-phase process, observable by the three distinct slopes in the D_7 vs. f_7 plot (Figure 3.5). The initial phase indicates low levels of adsorbed mass, which corresponded to high D shifts. A distinct decrease in the slope gradient was observed in phase two. This decrease suggests an increase in film viscosity as subsequent MPc molecules bound, suggesting the 'filling in' of the already deposited MPc film, deposited in phase one. Phase three demonstrated an increase in the gradient of the slope in phase two, suggesting an increase in the film viscoelasticity as MPc molecules bind, and therefore the formation of a multilayer. The point at which the gradient of the slope in phase two increase, to give rise to phase three, is approximately 0.4 E-6/ 3.0 Hz. This increase indicates approximately 55 $ng.cm^{-2}$ had adsorbed, using the Sauerbrey equation. According to the theoretically determined monolayer mass values (Table 3.2), this corresponded with the deposition of a planar orientated monolayer, or sub-monolayer. A large decrease in the D shifts was recorded during the buffer rinse step, which corresponded with a small decrease in the *f,* and therefore mass, suggesting the removal of loosely associated MPc molecules (Figure 3.5), The $CoPcS_{mix}$ film was concluded to be a highly rigid film composed of a low mass, demonstrating a planar orientated monolayer, or sub-monolayer.

Examination of D versus *f* plot for the immobilisation of CoTCPc proved to be more challenging due to the utilisation of two different buffer solutions, namely $PBS_{Mg/Ca}$, and MES (Figure 3.5). The primary focus was the introduction of MPc molecules, and not the effect of buffer alterations. The portion of the plot that was of interest lies between the first and third dashed circles in Figure 3.5. The data points that lie between the first and second dashed circle represent the introduction of the MPc/MES and EDC/NHS solution, while the data points between the second and third circle represent the buffer rinse. CoTCPc immobilisation to the SAM surface was observed as a two phase process. The initial phase was observed as an increase in D with the addition of in coming MPc molecules (Figure 3.5). The second phase indicated a decrease in slope gradient, suggesting the 'filling-in' of the already deposited film. This conclusion corresponds with the deposition of an edge-on film.

Sauerbrey and Voigt Based Analysis

With the aid of Sauerbrey and Voigt-based modelling, film parameters such as thickness (δ_f), mass, viscosity (η_f) and shear modulus (μ_f) were determined for the immobilised MPc films (Table 3.4). A comparison between the modelled film thickness (δ_f) and mass, with the theoretical-based predicted thickness obtained from the MPc dimensions (Figure 3.5) and theoretically calculated monolayer mass values (Table 3.2), allowed for conclusions to be drawn regarding the nature of the immobilised MPc film. Table 3.4. illustrates the Sauerbrey- and Voigt-determined immobilised MPc film parameters.

Table 3.4. QCM-D Analysis of Metallophthalocyanine Immobilisation on 11-Amino Undecane Thiol Self-Assembled Monolayer.

Metallophthalocyanine [a]		Sauerbrey Model			Voigt Model					$\frac{\text{Sauerbrey}_m}{\text{Voigt}_m}$ [d]
		Film Thickness (nm) [b]	Mass (ng/cm^2) [b]	Ave. Mass (ng/cm^2)	Viscosity (kg/m.sec) [c]	Shear Modulus (Pa) [c]	Film Thickness (nm)	Mass (ng/cm^2)	Ave. Mass (ng/cm^2)	
AlPcS$_{mix}$	0	3.09 ±0.17	308.52 ±16.93	391.42 ±72.52 (18.53 % CV)	2.04E-03	2.47E+05	3.01	301.25	565.57 ±177.51 (31.39 % CV)	0.69
	1	4.09 ±0.65	481.52 ±19.81		3.17E-03	5.63E+05	6.25	624.52		
	2	4.07 ±0.12	407.36 ±12.03		2.48E-03	1.79E+05	6.75	675.27		
	3	3.68 ±0.11	368.29 ±11.00		2.18E-03	1.69E+05	6.61	661.23		
CoPcS$_{mix}$	0	0.80 ±0.05	80.41 ±5.24	104.04 ±59.13 (56.83 % CV)	7.98E-03	4.45E+04	0.94	94.24	129.41 ±65.13 (50.33 % CV)	0.80
	1	1.92 ±0.04	191.48 ±4.13		3.41E-03	8.68E+05	2.27	226.86		
	2	0.93 ±0.02	61.01 ±52.84		1.00E-02	1.00E+03	1.03	103.38		
	3	0.83 ±0.02	83.25 ±1.69		8.65E-03	1.00E+03	0.93	93.15		
CuTSPc	0	0.67 ±0.02	67.14 ±1.58	165.48 ±68.37 (41.32 % CV)	5.41E-03	9.99E+03	0.83	82.56	198.13 ±79.46 (40.10 % CV)	0.84
	1	1.72 ±0.05	172.49 ±4.36		3.08E-03	2.68E+04	2.60	260.07		
	2	2.19 ±0.12	219.29 ±11.92		6.67E-03	2.13E+06	2.37	237.46		
	3	2.03 ±0.02	202.99 ±1.87		8.12E-03	2.75E+06	2.12	212.42		
GePcS$_{mix}$	0	1.75 ±0.11	192.8 ±12.00	165.93 ±21.29 (12.83 % CV)	1.81E-03	3.45E+05	3.09	309.34	246.17 ±59.91 (24.34 % CV)	0.67
	1	1.71 ±0.10	170.99 ±10.55		2.66E-03	3.02E+05	2.48	248.16		
	2	1.43 ±0.09	142.82 ±8.56		4.06E-03	1.02E+06	1.65	165.37		
	3	1.57±0.26	157.09 ±0.22		1.83E-03	2.07E+05	2.62	261.82		
ZnPcS$_{mix}$	1A	1.29 ±0.08	129.14 ±7.11	222.19 ±135.37 (60.93 % CV)	4.49E-03	1.45E+06	1.43	142.93	355.21 ±226.74 (63.83 % CV)	0.63
	1B	3.39 ±0.17	338.38 ±16.96		1.92E-03	2.74E+05	5.84	583.81		
	1C	3.14 ±0.14	313.81 ±13.86		2.17E-03	5.17E+05	4.3	429.95		
	2A	1.30 ±0.03	130.17 ±2.72		2.75E-03	2.29E+05	1.97	196.90		
	2B	1.26 ±0.06	126.1 ±6.36		1.43E-03	1.89E+04	4.25	424.71		
	2C	4.88 ±0.33	487.64 ±33.27		1.80E-03	3.64E+05	7.82	782.49		
	3A	2.60 ±0.36	259.50 ±36.38		1.19E-03	4.98E+05	3.56	355.71		
	3B	1.17 ±0.05	117.04 ±5.4		2.21E-03	3.21E+05	1.82	181.76		
	3C	0.98 ±0.03	97.96 ±3.26		5.73E-04	3.01E+06	0.99	98.61		
CoTCPc	0	1.00 ±0.08	99.62 ±7.85	218.82 ±80.95 (36.99 % CV)	1.88E-03	2.32E+07	0.95	94.85	311.18 ±167.07 (53.69 % CV)	0.70
	1	2.53 ±0.09	253.31 ±9.15		2.82E-03	2.89E+05	3.70	346.16		
	2	2.43 ±0.29	242.85 ±28.87		2.14E-03	7.40E+05	3.06	303.68		
	3	2.70 ±0.35	279.5 ±35.30		2.39E-03	2.22E+05	5.00	500.01		

a: Surface modification molecules
b: Sauerbrey-determined film parameter. Standard deviation is obtained from 3 overtone responses.
c: Viscoelastic film parameters indicating film rigidity levels
d: Indicates level of film hydration

Immobilisation of $AlPcS_{mix}$

From the MPc dimensions and theoretical monolayer mass, one would predict an edge-on monolayer of $AlPcS_{mix}$ to demonstrate a rigid film with a thickness of approximately 1.375 nm to 0.769 nm and immobilised mass ranging between 205.56 03 $ng.cm^{-2}$ and 510.03 $ng.cm^{-2}$ (Table 3.2). If the MPc molecule adopted a planar conformation, a film thickness of approximately 0.364 nm (according to the atomic radius of Al), and film mass between 69.29 $ng.cm^{-2}$ and 307.38 $ng.cm^{-2}$, would be expected (Table 3.2). Sauerbrey modelling of the immobilisation of $AlPcS_{mix}$ revealed film thicknesses ranging between 3.09 nm and 4.09 nm, and immobilised mass between ~308 $ng.cm^{-2}$ and ~481 $ng.cm^{-2}$. The *f*/D values for surfaces 2 and 3 suggested the deposition of viscoelastic MPc films, in addition to the underestimation of the Sauerbrey equation, therefore required analysis using the Voigt-based modelling system. Voigt modelling for the $AlPcS_{mix}$ film deposition indicated film thicknesses between 3.01 nm and 6.75 nm, and immobilised mass values between ~301 $ng.cm^{-2}$ and ~675 $ng.cm^{-2}$.

Although the Sauerbrey and Voigt values differ significantly for the surface modification with $AlPcS_{mix}$, both modelled film thickness values rule out the possibility of the MPc immobilising in a monolayer if adopting a planar conformation. This is not to say that planar conformations of the MPcs molecules are not present, rather that a monolayer is not achieved. This conclusion corresponded with those of the D vs. *f* plot, suggesting multilayer deposition. HPLC analysis of the $AlPcS_{mix}$ sample revealed the presence of tetra-, tri-, di-, and mono-sulphonated species within the preparation (Table 3.1). This presence of di- and mono-sulphonated MPc molecules permits the possibility of MPc aggregate formation. Due to the fact that the determined Sauerbrey film thickness, which may be an underestimation, ranged from approximately double, and even three times larger than that of the expected edge-on monolayer maximum thickness versus the planar monolayer thickness (Table 3.2), one may conclude that aggregated MPc column structures are present on the surface. This occurrence, taken into consideration with the, what is assumed to be, low ave. *f* % CV (Table 3.3) of the MPc film, suggests that the immobilised film was either a composed of a multilayer of edge-on orientated molecules, or, more likely, aggregated planar columns with similar height dimensions. The likelihood of complete monolayer formation in the edge-on orientation occurring in this case, in the presence of di- and mono- sulphonated species, was

improbable. The immobilisation of the $AlPcS_{mix}$ molecules resulted in film which demonstrates a viscosity higher than that of water (η_{water} = 0.765 $\times 10^{-3}$ kg/m.sec; at T°C 20 [Internet Reference 2]) and high shear modulus, confirming high film rigidity.

Assessing the correlation between the Sauerbrey- and Voigt-determined mass, and the subsequent film hydration level, was achieved through calculating the Sauerbrey mass over Voigt mass value. For the immobilisation of $AlPcS_{mix}$ this value was determined on average to be 0.69, for the four surfaces, suggesting that 31% of the Voigt mass was the result of the immobilised films interaction with water molecules. The deposited $AlPcS_{mix}$ film on the 11-AUT SAM surface were therefore concluded to demonstrate high levels of hydration, and possible multilayer edge-on orientation, or aggregate formation. Similarly, the *f* and D shifts, and modelled Sauerbrey and Voigt film parameters, were utilised to assess the remainder of the immobilised MPc films.

Immobilisation of $CoPcS_{mix}$

Immobilisation of the $CoPcS_{mix}$ sample resulted in the deposition of a film with a reasonably high *f* versus D ratios (Table 3.3), suggesting that the Sauerbrey determine film thickness and mass were valid, in addition to the immobilised films being rigid in nature. Low % CV values calculated from the averaged *f* shifts for overtones 7 – 11, implied a fairly uniform/sharp film interface with the buffer solution.

Sauerbrey and Voigt analysis of the film parameters indicated the deposition of MPc mass (Table 3.4), which correlated with the immobilisation of a monolayer of planar orientated MPc molecules (Table 3.2). This was observed as the deposition of mass which did not exceed the maximum theoretically determined value for the immobilisation of a planar orientated monolayer (318.80 ng.cm^{-2}). However, adsorbed mass values were recorded which were lower than that of the minimum theoretically determined value for a planar monolayer, therefore suggesting the possibility of sub-monolayer deposition (99.72 ng.cm^{-2}). Both the Sauerbrey- and Voigt-determined film thickness of the $CoPcS_{mix}$ immobilised films suggested the deposition of either a monolayer of edge-on orientated MPc molecules, or a

multilayer, as the recorded thickness values were greater than the minimum theoretically determined film thickness (0.763 nm) for an edge-on monolayer (Table 3.4). HPLC analysis of $CoPcS_{mix}$ suggested the presence of only tetra-sulphonated species (Table 3.1). Due to the high degree of sulphonation of a high portion of the MPc molecules, one may omit the possibility of MPc aggregation occurring. This conclusion was supported by the spectrophotometric analysis of $CoPcS_{mix}$ aggregation, which indicated no signs of MPc aggregation (Figure 3.4). The high degree of sulphonation may furthermore promote planar orientation of the molecules on the SAM surface. In addition, low standard % CV (Table 3.3) of the average *f* shifts, suggested a fairly uniform film interface, therefore leading one to accept the proposed planar orientation. This was supported by the significantly high film viscosity values. The use of the film thickness parameter in assessing the MPc immobilised films was therefore concluded as unreliable, in comparison to the adsorbed mass values.

The Sauerbrey mass over Voigt mass value of 0.80 indicated approximately 20% of the immobilised film was due to the interaction with water molecules. The latter percentage of water is substantially lower than that observed with $AlPcS_{mix}$ immobilisation (31%). This, together with the % CV of the average *f* shifts being, on average, lower than that recorded for $AlPcS_{mix}$ films, supports the assumption that a more ordered layer is deposited, possibly planar monolayer in nature. The assumption of $CoPcS_{mix}$ monolayer corresponded with the deductions made from the D vs. *f* plot analyses.

Immobilisation of CuTSPc

Similarly to $CoPcS_{mix}$ immobilisation, monitoring of CuTSPc immobilisation on 11-AUT SAM coated surfaces resulted in high *f* over D values with low shift in D (Table 3.3), suggesting the deposition of a highly rigid film whose film parameters may be accurately determined through the Sauerbrey equation. The low % CV calculated for the average *f* shifts, for overtone 7-11, suggests a uniform interface between the immobilised film and buffer solution.

Comparison between the Sauerbrey and Voigt-determined film mass parameters (Table 3.4), with the theoretically determined mass values for planar and edge-on monolayer deposition (Table 3.2), indicated that monolayer, or sub-monolayer CuTSPc films were immobilised. The latter was concluded as the modelled parameters did not exceed that of the maximum theoretically determined planar monolayer mass (320.46 $ng.cm^{-2}$), however, the adsorbed mass levels were reported to be below that of the theoretical minimum planar orientated monolayer mass (100.23 $ng.cm^{-2}$). The possibility of a monolayer depositing is supported by HPLC analysis, which indicated CuTSPc contains only tetra-sulphonated molecules, implying that the molecules take on monomer form when in aqueous solution (Table 3.1). Both the Voigt determined viscosity and shear modulus values were, on average, high for the immobilisation of the CuTSPc molecules, confirming their rigid immobilisation. The Sauerbrey mass over Voigt mass value suggests approximately 16% of the Voigt-determined film mass was due to the presence of water molecules in the film. In conclusion, CuTSPc films were determined to be highly rigid monolayers composed of planar orientated MPc molecules, corresponding to the D vs. *f* plots deductions.

Immobilisation of $GePcS_{mix}$

On observation of the *f* and D shifts recorded for the immobilisation of the $GePcS_{mix}$ (Table 3.3), the process of immobilisation appears to vary significantly for the four experiments performed. HPLC analysis of the sample suggests the presence of both tetra- and mono-sulphonated MPc molecules (Table 3.1). The low degree of sulphonation of the mono-sulphonated molecules is assumed to permit MPc aggregation, which may have contributed to that irreproducibility of the MPc immobilisation. $\Delta f/\Delta D$ values determined for surfaces 1 and 2 indicated the deposition of a fairly rigid film (>10 Hz/1E-06), while surfaces 0 and 3 suggest the deposition of a fairly viscoelastic film (<10 Hz/1E-06), whose adsorbed mass may have been underestimated when being assessed using the Sauerbrey equation. The low % CV reported for the average *f* shift, when assessing surfaces 0, 1 and 2, may be assumed to be indicative of a uniform film interface. Conversely, a high ave. *f* % CV was calculated for the MPc utilised for surface 3, possibly suggesting either varied MPc orientation, or aggregation of the MPc molecules on the SAM surface.

The Sauerbrey-determined adsorbed $GePcS_{mix}$ mass on the 11-AUT SAM surfaces (Table 3.4) indicated the deposition of planar orientated MPc monolayers, as the maximum level of adsorbed mass fell within the theoretically determined mass range (Table 3.2) for a planar monolayer (74.39 $ng.cm^{-2}$ to 323.69 $ng.cm^{-2}$), and was well below the minimum adsorbed theoretical mass value for an edge-on orientated monolayer (264.25 $ng.cm^{-2}$). The Voigt-determined film mass parameter indicated the possibility of planar orientated immobilisation of MPc monolayers on surfaces. However, the results also suggest the possible deposition of edge-on orientated monolayers, as surfaces 0, 1, and 3 indicated the deposition of MPc mass of ~309 $ng.cm^{-2}$, ~248 $ng.cm^{-2}$, ~262 $ng.cm^{-2}$, respectively (Table 3.4). The high film rigidity of the $GePcS_{mix}$ film on surface 2 demonstrated the highest level of rigidity, when comparing to surfaces 0, 1, and 3, as observed by the higher *f*/D values (Table 3.3), and higher viscoelastic properties determined through Voigt analysis (Table 3.4), in addition to the lowest level of surface roughness (Table 3.3) and film hydration (Table 3.4). These film characteristics, in combination with the HPLC analysis indicating tetra- and mono-sulphonated species were present, and the spectrophotometric analysis indicating possible minor aggregation in $PBS_{Mg/Ca}$, suggest a planar orientated monolayer was deposited on surface 2, while surfaces 0, 1, and 3, may demonstrate mixed MPc orientation, and/or deposited aggregates. The deposition of a multilayer corresponds to the conclusions drawn from the D vs. *f* plots.

Immobilisation of $ZnPcS_{mix}$

Monitoring of $ZnPcS_{mix}$ immobilisation revealed the process demonstrated low reproducibility (Table 3.3). Highly variable results, between the replicants, were determined for the immobilisation of $ZnPcS_{mix}$ films, in terms of film rigidity (*f*/D), and film interface properties (ave. *f* % CV). Furthermore, analysis of the $ZnPcS_{mix}$ film deposition, using the Sauerbrey and Voigt models, indicated highly variable results, in terms of film thickness, adsorbed mass, film hydration ($Sauerbrey_{mass}$/$Voigt_{mass}$), and viscoelastic parameters, namely film viscosity and shear modulus (Table 3.4). HPLC analysis of the MPc sample indicated the presence of tetra-sulphonated species, as well as an unidentifiable broad band (Table 3.1), which was confirmed to be MPc aggregates, via spectrophotometric analysis (Figure 3.4). This low reproducibility of film deposition was therefore attributed to the deposition of MPc

aggregates on the 11-AUT SAM surface. The deposition of $ZnPcS_{mix}$ multilayers on the SAM surface are in accordance with the D vs. *f* plot conclusions.

Immobilisation of CoTCPc

Immobilisation of the CoTCPc sample was carried out using the zero-length linker, EDC, in the presence of NHS (Section 3.2.3.2). The ordered method of MPc deposition resulted in fairly consistent average *f* and D shifts when monitoring the deposition of CoTCPc films, with the exception of surface 0 (Table 3.4). However, the deposited films demonstrated variability in film rigidity (*f*/D), and film interface roughness (ave. *f* % CV) (Table 3.3).

Sauerbrey analysis of the film parameters indicated the possibility of planar orientated monolayers being deposited on all surfaces, as the experimentally determined adsorbed mass values (Table 3.4) were similar to the theoretically determined mass values for a planar monolayer (~84 $ng.cm^{-2}$ to ~269 $ng.cm^{-2}$; Table 3.2). However, the Sauerbrey adsorbed mass values determined for surfaces 1, 2, and 3, may also be interpreted to indicate the deposition of edge-on monolayers (~272 $ng.cm^{-2}$ to ~486 $ng.cm^{-2}$; Table 3.2). The Voigt determined mass parameters, suggested edge-on orientated monolayer deposition of the CoTCPc molecules on surfaces 1, 2, and 3, while surface 0 was indicated to consist of a planar orientated monolayer. The latter film was reported to demonstrate a fairly sharp interface (i.e. low ave. *f* % CV; Table 3.3), rigid nature (*f*/D and shear modulus), and low film thickness, which contributed to the assumption that a planar orientated monolayer was deposited. Furthermore, the high film thickness (Table 3.4), adsorbed MPc mass, and viscoelastic parameters recorded for the deposition of CoTCPc on surfaces 1, 2, and 3, suggest the deposition of either edge-on monolayers or multilayer deposition.

Experimental Reproducibility

High variations in *f* and D shifts, and therefore Sauerbrey- and Voigt-based parameters, were recorded for each immobilisation of the individual MPc molecules, when comparing the immobilisation data generated from the separate experiments between the replicants (Table 3.3 and Table 3.4). Both the Sauerbrey- and Voigt-determined parameters

demonstrated similar reproducibility trends, where $GePcS_{mix}$ indicated the highest level of immobilisation reproducibility, followed by $AlPcS_{mix}$, (CoTCPc, CuTSPc), $CoPcS_{mix}$, and $ZnPcS_{mix}$ (Table 3.4). This occurrence highlights the irreproducibility of the immobilisation processes, which may prove to be of concern when analysing antibody binding. However, in order for accurate comparisons to be achieved, identical immobilised MPc films, for the entire set of MPc molecules, would be required. Due to the varying chemical nature of each MPc sample, and therefore varying intermolecular interactions, this would be an unrealistic goal when designing a rapid means of assessment. Optimisation of the immobilisation step may be achieved through further modification of the MPc molecule itself, however, this would alter the chemical structure of the MPc molecule and therefore jeopardise the accuracy of protein binding analysis, as well as increasing the sample preparation time.

For ease of comparison, concluding remarks on the above discussed immobilised MPc films were summarised in Table 3.5.

Table 3.5. Summary of Conclusions Derived on the Immobilised Metallophthalocyanine Films

Surface		Degree of Ring Substitution [a]	MPc Aggregation [b]	Film Rigidity (ΔF/ΔD) [c]	Assembly Mechanism [c]	Film Interface (Ave. F % STDev) [c]	Proposed MPc Orientation [d]	Surface Coverage [e]
$AlPcS_{mix}$	0	Tetra-, Tri-, Di- and Mono-	Aggregates present	Rigid (>10)	Multilayer	Sharp (5.45%)	Edge-On	Multilayer
	1			Rigid (>10)	Multilayer	Sharp (4.07%)	Edge-On	Multilayer
	2			Viscoelastic (<10)	Multilayer	Sharp (2.85%)	Edge-On	Multilayer
	3			Viscoelastic (<10)	Multilayer	Sharp (2.96%)	Edge-On	Multilayer
$CoPcS_{mix}$	0	Tetra-; Tri-	Inconclusive: Possible photodegradation	Rigid (>10)	Monolayer	Sharp (6.64%)	Planar	Monolayer; or Sub-Monolayer
	1			Rigid (>10)	Monolayer	Sharp (2.15%)	Planar	Monolayer
	2			Rigid (>10)	Monolayer	Sharp (1.71%)	Planar	Monolayer; or Sub-Monolayer
	3			Rigid (>10)	Monolayer	Sharp (1.94%)	Planar	Monolayer, or Sub-Monolayer
CuTSPc	0	Tetra-	Inconclusive: Possible photodegradation	Rigid (>10)	Monolayer	Sharp (2.40%)	Planar	Monolayer; or Sub-Monolayer
	1			Rigid (>10)	Monolayer	Sharp (4.32%)	Planar	Monolayer
	2			Rigid (>10)	Monolayer	Sharp (5.56%)	Planar	Monolayer
	3			Rigid (>10)	Monolayer	Sharp (0.88%)	Planar	Monolayer
$GePcS_{mix}$	0	Tetra- and Mono-	Aggregates present	Viscoelastic (<10)	Multilayer	Sharp (6.22%)	Planar/Edge-On	Monolayer, or Multilayer
	1			Rigid (>10)	Multilayer	Sharp (6.27%)	Planar	Monolayer
	2			Rigid (>10)	Multilayer	Sharp (5.67%)	Planar	Monolayer
	3			Viscoelastic (<10)	Multilayer	Rough (16.02%)	Planar/Edge-On	Monolayer; or Multilayer
$ZnPcS_{mix}$	1A	Tetra- and Aggregates	Aggregates present	Rigid (>10)	Multilayer	Sharp (5.39%)	Planar	Multilayer
	1B			Viscoelastic (<10)	Multilayer	Sharp (5.01%)	Planar/Edge-On	Multilayer
	1C			Viscoelastic (<10)	Multilayer	Sharp (4.39%)	Planar/Edge-On	Multilayer
	2A			Rigid (>10)	Multilayer	Sharp (2.06%)	Planar	Multilayer
	2B			Rigid (>10)	Multilayer	Sharp (1.88%)	Planar/Edge-On	Multilayer
	2C			Viscoelastic (<10)	Multilayer	Sharp (6.83%)	Edge-On	Multilayer
	3A			Viscoelastic (<10)	Multilayer	Rough (14.14%)	Planar/Edge-On	Multilayer
	3B			Viscoelastic (<10)	Multilayer	Sharp (4.59%)	Planar	Multilayer
	3C			Rigid (>10)	Multilayer	Sharp (3.29%)	Planar	Multilayer
CoTCPc	0	Tetra-	Inconclusive: Possible photodegradation	Rigid (>10)	Monolayer	Sharp (7.90%)	Planar	Monolayer
	1			Viscoelastic (<10)	Monolayer	Rough (12.61%)	Planar/Edge-On	Monolayer
	2			Rigid (>10)	Monolayer	Sharp (3.60%)	Planar/Edge-On	Monolayer
	3			Rigid (>10)	Monolayer	Rough (11.77%)	Edge-On	Monolayer

a and b: *based on MPc characterisation studies using HPLC and spectrophotometric analysis*
c: *based on the QCM-D D vs. f plots*
d: *derived from a comparison of the experimentally determined adsorbed mass and theoretically determine monolayer mass values*
e: *assumptions drawn from a – d results*

3.3.3. QCM-D Analysis of Biomolecular Interactions with MPc-Modified Surfaces

Directly following each immobilisation procedure, analysis of blood protein adsorption on the newly modified surface was conducted using QCM-D. The latter studies were carried out as previously stated, where human serum (HS) or plasma (HP) was introduced to the surface, followed by the desired probe, namely, anti-human albumin (Ab_{HSA}), anti-human C3c (Ab_{C3c}), and anti-human fibrinogen proteins (Ab_{HPF}) (Figure 3.6).

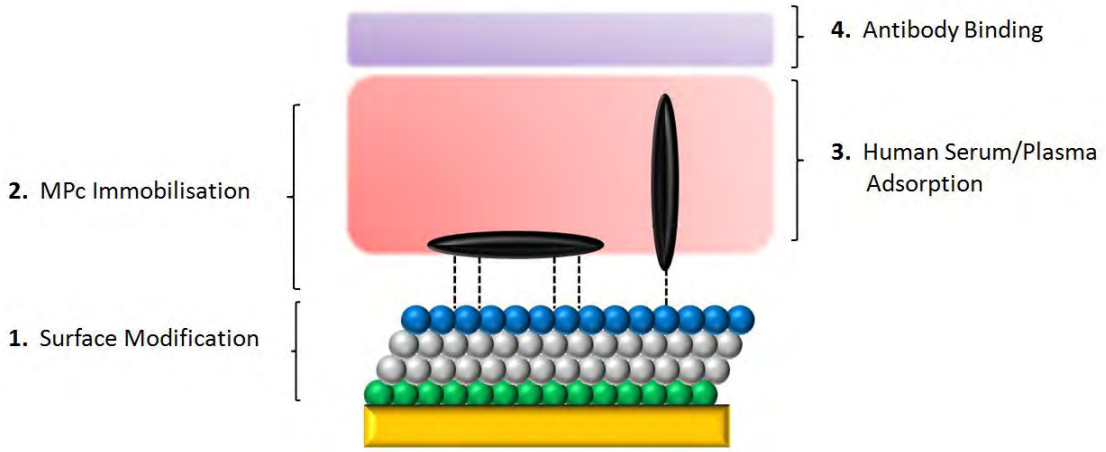

Figure 3.6. Schematic representation of the experimental process utilised in assessing the biomolecular interactions which occur with Metallophthalocyanines. Antibodies utilised were anti-human albumin, anti-human C3c, or anti-human fibrinogen.

Each subsequent layer, following MPc immobilisation, was assessed as though being an independent layer, in contrast to being a second, or third, layer. Simplistically, film properties generated from the underlying layer, namely film thickness (δ_f), film viscosity (η_f) and shear modulus (μ_f), were utilised as a basis for predicting the unknown Voigt model parameters. From this point forward, *f* shifts, D shifts, and film parameters discussed refer to the shifts generated by the addition of the particular layer rather than the absolute value.

3.3.3.1. QCM-D Monitoring and Quantification of Blood Protein Adsorption to MPc-Modified Surfaces

Analysis of the human blood protein coat adsorbed to the MPc-modified sensor surfaces served as a means to assess experimental reproducibility and general MPc interactions with

blood proteins, rather than the biomolecular interactions that take place at the MPc interface. Precise, selective examination of these biomolecular interactions, via QCM-D, is impractical due to the complex, heterogeneous nature of the blood samples.

QCM-D Response Analysis

A brief overview of the QCM-D shifts in *f* and D (Table 3.6) in response to blood protein adsorption, indicated $\Delta f/\Delta D$ values greater than 10 in all cases, with the exception of the following surfaces: $GePcS_{mix}$ (3); and $ZnPcS_{mix}$ (2B, 3C), for one or more of the selected onvertones. The majority of the $\Delta f/\Delta D$ values confirmed the deposition of fairly rigid protein films (i.e. $\Delta f/\Delta D > 10$), as well as validating the Sauerbrey determined adsorbed mass. The deposited blood protein coat appears to demonstrate a fairly uniform/sharp film interface, as indicated by the low average *f* percentage coefficient of variation (Table 3.6). This occurrence is predicted as the blood protein molecules are expected to 'fill in' the MPc film interface, and undergo conformational changes due to adsorption to the surface [18].

Table 3.6. QCM-D Shifts in Frequency and Dissipation Shifts Due to Human Serum/Human Plasma Adsorption on MPc-Modified Surfaces

Metallophthalocyanine [a]			Δf_7 / ΔD_7	Δf_9 / ΔD_9	Δf_{11} / ΔD_{11}	Ave. Δf [b]	Ave. f % CV	Ave. ΔD [b]
$AlPcS_{mix}$	0	HS	15.76	15.43	14.26	-42.75 ±0.84	1.96	2.83 ±0.10
	1		14.88	13.94	13.87	-67.95 ±2.32	3.41	4.78 ±0.09
	2		13.85	13.75	12.93	-62.66 ±0.99	1.58	4.64 ±0.10
	3	HP	17.70	17.58	16.96	-54.98 ±1.36	2.47	3.16 ±0.03
$CoPcS_{mix}$	0	HS	13.72	13.28	13.36	-55.09 ±1.27	2.31	4.10 ±0.06
	1		15.46	15.80	14.36	-45.47 ±0.87	1.91	2.99 ±0.12
	2		28.14	24.02	27.01	-46.26 ±1.51	3.26	1.76 ±0.14
	3	HP	15.35	13.95	13.57	-72.12 ±1.79	2.48	5.06 ±0.21
CuTSPc	0	HS	18.33	18.42	18.27	-50.36 ±0.89	1.77	2.75 ±0.05
	1		17.10	20.84	19.76	-53.36 ±0.85	1.59	2.80 ±0.34
	2		24.24	22.57	21.47	-41.77 ±1.76	4.21	1.84 ±0.04
	3	HP	17.08	17.21	19.19	-36.08 ±0.64	1.77	2.03 ±0.14
$GePcS_{mix}$	0	HS	11.98	11.64	11.36	-53.64 ±1.44	2.61	4.6 ±0.01
	1		13.73	14.18	15.36	-46.22 ±1.17	2.53	3.21 ±0.24
	2		17.59	16.79	16.13	-56.71 ±1.52	2.68	3.37 ±0.06
	3	HP	8.83	13.09	13.38	-44.01 ±0.71	1.61	3.87 ±0.92
$ZnPcS_{mix}$	1A	HS	14.82	14.82	14.47	-45.51 ±0.98	2.15	3.10 ±0.03
	1B		21.80	20.98	19.51	-38.10 ±1.23	3.23	1.84 ±0.06
	1C		15.91	14.71	13.79	-43.97 ±1.06	2.41	2.98 ±0.14
	2A		14.63	14.66	14.34	-40.56 ±0.76	1.87	2.79 ±0.03
	2B		10.49	9.76	9.86	-25.87 ±1.04	4.02	2.58 ±0.06
	2C		11.18	10.93	10.52	-29.84 ±0.82	2.75	2.74 ±0.01
	3A	HP	16.03	15.56	11.09	-36.98 ±1.64	4.43	2.66 ±0.44
	3B		16.95	15.56	14.77	-45.30 ±0.58	1.28	2.88 ±0.16
	3C		9.86	9.51	9.35	-25.34 ±0.69	2.72	2.65 ±0.02
CoTCPc	0	HS	13.68	13.17	12.79	-67.32 ±1.70	2.53	5.10 ±0.04
	1		12.84	11.65	12.21	-96.16 ±2.15	2.24	7.87 ±0.27
	2		14.58	14.97	13.34	-65.70 ±1.87	2.85	4.60 ±0.21
	3	HP	11.28	11.10	11.79	-67.28 ±1.00	1.49	5.91 ±0.27

a: *Surface modification molecules*
b: *Average values determined using responses obtained from overtones 7 -11*

Sauerbrey and Voigt Based Analysis

The focus of the modelled data for blood protein analysis (Table 3.7) was that of the adsorbed mass, in terms of its dependence on the underlying film interface, and reproducibility. Figure 3.7 summaries the Sauerbrey- and Voigt-determined adsorbed blood protein mass values observed when assessing each MPc-modified surface.

According to the modelled mass shifts, both Sauerbrey and Voigt, recorded for HS adsorption to the MPc films (Table 3.7), similar levels of adsorbed protein were observed to deposit on

the films previously proposed to be planar orientated monolayers, namely $CoPcS_{mix}$, CuTSPc, and $GePcS_{mix}$ (Table 3.5). In addition, higher levels of HS adsorption occurred on the $AlPcS_{mix}$, proposed multilayers, in comparison to the $ZnPcS_{mix}$ multilayers. This variation in HS binding may be attributed to the topography (i.e. MPc orientation, and monolayer or multilayer) and/or chemical composition (the net charge, and metal core) of the immobilised films. However, similar, sharp MPc film interface properties were determined for both the $AlPcS_{mix}$ and $ZnPcS_{mix}$ immobilised multilayer films (Table 3.3), therefore suggesting the chemical properties of the MPc film are the influential factors governing the HS adsorption.

Sauerbrey-based data modelling of blood protein adsorption to the modified surfaces indicated protein binding to the $GePcS_{mix}$-modified surface to be the most reproducible, followed by $CoPcS_{mix}$, CuTSPc, $ZnPcS_{mix}$, CoTCPc, and $AlPcS_{mix}$ (Table 3.7). These occurrences may be explained by the nature of the MPc film, namely, the orientation which the MPc molecule is assumed to adopt when deposited on the underlying SAM.

Table 3.7. QCM-D Analysis of Human Serum and Human Plasma Adsorption on MPc-Modified Surfaces

MPc [a]		BP [b]	Sauerbrey Model		Voigt Model				$\frac{\text{Sauerbrey}_m}{\text{Voigt}_m}$ [e]
			Δ Mass (ng/cm^2) [c]	Ave. Δ Mass (ng/cm^2)	Δ Viscosity ($kg/m.sec$) [d]	Δ Shear Modulus (Pa) [d]	Δ Mass (ng/cm^2)	Ave. Δ Mass (ng/cm^2)	
$AlPcS_{mix}$	0	HS	765.05 ±14.95	1034.12 ±237.78 (22.99 % CV)	Decrease	Decrease	870.70	1233.86 ±314.90 (22.52 % CV)	0.88
	1		1215.99 ±41.39		Increase	Increase	1431.18		0.85
	2		1121.32 ±17.67		Increase	Increase	1399.7		0.80
	3	HP	983.84 ±24.24	---	Increase	Increase	913.45	---	1.08
$CoPcS_{mix}$	0	HS	985.81 ±20.41	875.82 ±95.51 (10.91 % CV)	Decrease	Increase	1178.84	1010.97 ±150.21 (14.86 % CV)	0.84
	1		813.81 ±15.39		Increase	Decrease	964.81		0.84
	2		827.83 ±26.89		Decrease	Increase	889.26		0.93
	3	HP	1290.65 ±31.74	---	Decrease	Increase	1484.70		0.87
CuTSPc	0	HS	901.27 ±15.51	867.90 ±107.59 (12.40 % CV)	Decrease	Decrease	1029.59	1093.89 ±302.82 (27.68 % CV)	0.88
	1		954.86 ±14.65		Decrease	Decrease	1423.7		0.67
	2		747.58 ±31.45		Increase	Decrease	828.38		0.90
	3	HP	645.69 ±11.33	---	Decrease	Increase	761.26	---	0.85
$GePcS_{mix}$	0	HS	959.85 ±25.74	933.99 ±96.45 (10.33 % CV)	Increase	Increase	1171.38	1138.59 ±46.08 (4.05 % CV)	0.82
	1		827.25 ±20.42		Increase	Increase	1085.91		0.76
	2		1014.87 ±27.24		Increase	Increase	1158.48		0.88
	3	HP	787.61 ±12.62	---	Increase	Decrease	1337.13	---	0.59
$ZnPcS_{mix}$	1A	HS	814.44 ±15.74	670.51 ±142.38 (21.23 % CV)	Increase	Increase	935.45	860.79 ±272.89 (31.70 % CV)	0.87
	1B		681.77 ±22.03		Increase	Increase	756.6		0.90
	1C		786.80 ±18.89		Increase	Increase	881.66		0.89
	2A		743.12 ±34.2		Increase	Increase	1348.62		0.55
	2B		462.99 ±18.58		Increase	Increase	584.47		0.79
	2C		533.91 ±14.71		Increase	Increase	657.93		0.81
	3A	HP	661.77 ±29.39	641.95 ±179.40 (27.95 % CV)	Increase	Increase	720.8	739.34 ±162.16 (21.93 % CV)	0.92
	3B		810.62 ±10.4		Increase	Decrease	909.97		0.89
	3C		453.46 ±12.34		Increase	Increase	587.25		0.77
CoTCPc	0	HS	1204.61 ±14.79	1367.04 ±306.76 (22.44 % CV)	Increase	Decrease	1305.76	1649.55 ±562.05 (34.07 % CV)	0.92
	1		1720.87 ±34.15		Increase	Increase	2298.16		0.75
	2		1175.65 ±33.51		Increase	Increase	1344.72		0.87
	3	HP	1204.05 ±2.23	---	Increase	Increase	1650.15	---	0.73

a: *Surface modification molecules*
b: *Blood protein sample adsorbed to the test surface*
c: *Sauerbrey-determined film parameter. Standard deviation is obtained from 3 overtone responses.*
d: *Viscoelastic film parameters indicating film rigidity levels*
e: *Indicates level of film hydration*

In the case of $CoPcS_{mix}$, CuTSPc and $GePcS_{mix}$ surfaces, a monolayer of planar orientated MPc molecules was concluded to be a possibility (Table 3.5). This planar orientation of the MPc molecules on the SAM surface are predicted to result in a more uniform HS deposited film. $ZnPcS_{mix}$- and $AlPcS_{mix}$-modified surfaces, however, are predicted to be composed of MPc multilayers, and/or aggregates. The presence of MPc multilayer or aggregates on the SAM surface decreases the reproducibility of the MPc film topography, and therefore

decreases the reproducibility of protein binding to the already variable MPc-modified surface. Both the MPc orientation, as well as the MPc film surface charge may explain the high variability of protein binding to the CoTCPc surfaces. CoTCPc films were determined to be monolayers composed of edge-on MPc molecules, therefore suggesting the protein interaction is not due to the metal core. Protein binding to the latter monolayers is expected to differ greatly, similarly, to planar monolayers due varying surface charge densities. The adsorption of blood proteins has been reported to be dependent on the surface characteristics, such as charge, morphology as well as material composition [103].

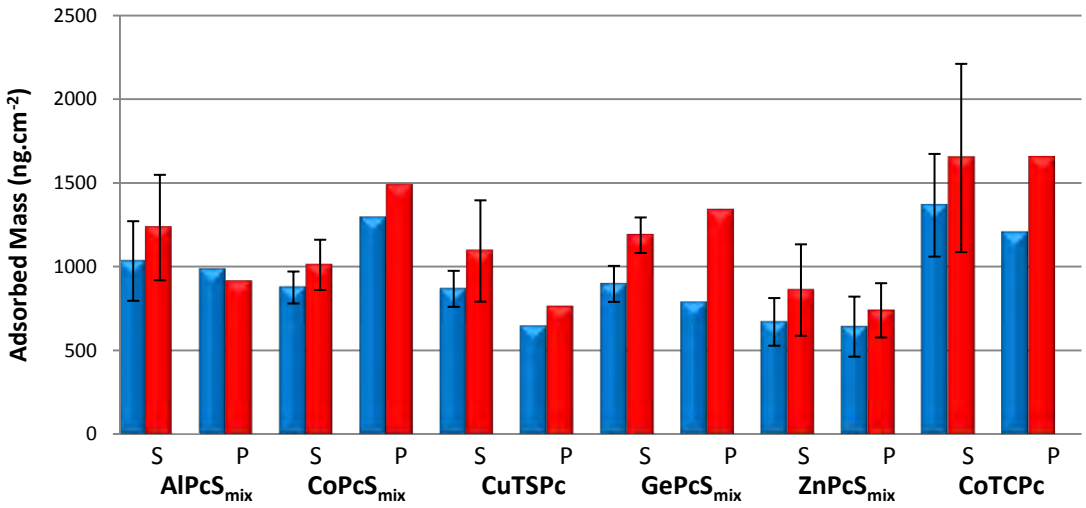

Figure 3.7. Sauerbrey (Blue) and Voigt (Red) determined human serum (S) and human plasma (P) mass adsorbed to previously immobilised metallophthalocyanines films. Error bars indicate standard deviation (n = 3), with the exception of $ZnPcS_{mix}$ where (n = 6).

A comparison between the amount of adsorbed HS mass and the MPc film interface roughness (ave. *f* % CV of MPc immobilisation process) revealed little correlation between the two (Figure 3.8). This fact highlights the dependence of serum protein binding on the surface charge, and/or chemical composition.

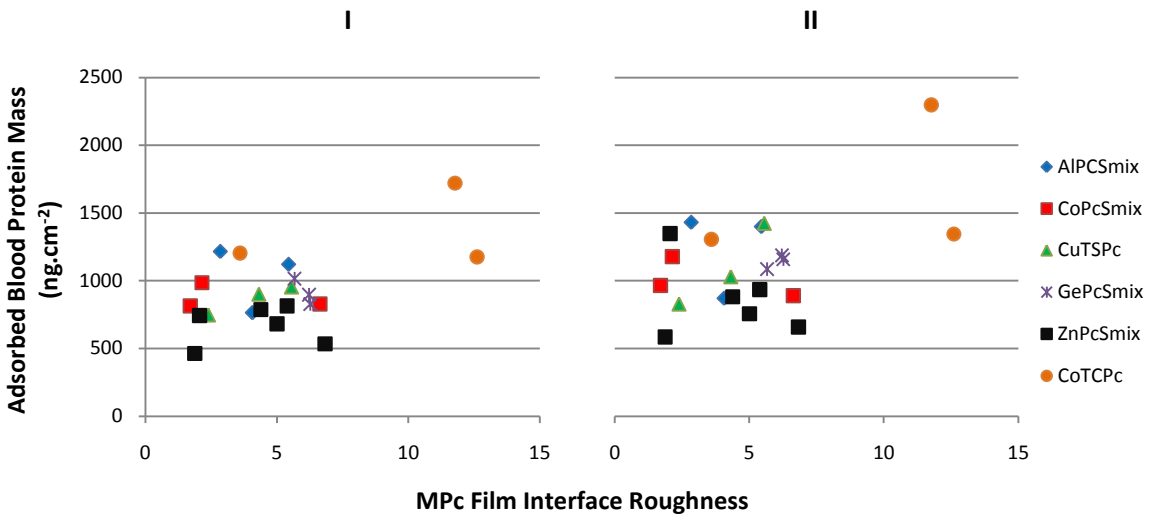

Figure 3.8. Sauerbrey- (I) and Voigt- (II) determined adsorbed human serum mass versus immobilised MPc film interface property. The MPc film interface property illustrated is the average *f* percentage coefficient of variation, which is an indication of surface roughness.

According to HP adsorption analysis to the $ZnPcS_{mix}$-modified surfaces, the process demonstrated a similar level of reproducibility to that of HS adsorption (Table 3.8). Little deduction could be made concerning HP adsorption to the MPc-modified surfaces, as film parameters were recorded to be highly variable, between each MPc surface, in terms of adsorbed mass and, topography, and hydration (Table 3.6 and 3.7).

3.3.3.2. QCM-D Monitoring and Quantification of Probe Antibody Binding to MPc-Modified Surfaces

When assessing target antibody binding to blood protein coated MPc-modified surfaces the proposed MPc surface topography, determined previously, was taken into consideration. Reproducibility of adsorbed blood protein detection, using target antibodies, was assessed using $ZnPcS_{mix}$-modified surfaces, as this MPc preparation demonstrated the highest level of cytotoxicity in MCF-7 cell lines (Chapter 5). Analysis of the experimental reproducibility using the total set of MPc surfaces was not feasible due to the constrained availability of the probe antibodies.

Crude analysis of the *f* and D shifts recorded for the antibody probe binding, to the blood protein surfaces, provided limited information on the properties of the deposited antibody films (Table B.1). Focus was therefore directed towards adsorbed antibody mass. Due to the varying MPc film interface characteristics, it was necessary to assess probe antibody binding mass as a proportion of the total adsorbed blood protein, mass, therefore eliminating the level of film interface roughness, in terms of exposed surface area, as an influencing factor. This was achieved via assessing the $Antibody_{mass}$/$Blood\ Protein_{mass}$ (Ab_m/BP_m). Table 3.8 summarises the Sauerbrey- and Voigt-determined film parameters of the bound probe antibody film.

Table 3.8. QCM-D Analysis Antibody Binding to Adsorbed Human Serum and Plasma Proteins on the MPc-Modified Surfaces

MPc	Probe [a]	Sauerbrey Model			Voigt Model					Sauerbrey$_m$ / Voigt$_m$ [e]
		Δ Mass (ng/cm^2) [b]	Ave. Δ Mass (ng/cm^2)	ΔAb$_m$ / ΔBb$_m$ [c]	Δ Viscosity (kg/m.sec) [d]	Δ Shear Modulus (Pa) [d]	Δ Mass (ng/cm^2)	Ave. Δ Mass (ng/cm^2)	ΔAb$_m$ / ΔBb$_m$ [c]	
AlPcS$_{mix}$	Ab$_{HSA}$	71.05 ±4.84	---	0.06	Increase	Increase	82.33	---	0.06	0.86
	Ab$_{C3c}$	127.27 ±2.00	---	0.11	Increase	Increase	94.53	---	0.07	1.35
	Ab$_{HPF}$	2185.43 ±58.65	---	2.22	Increase	Increase	2220.05	---	2.43	0.98
CoPcS$_{mix}$	Ab$_{HSA}$	443.27 ±24.51	---	0.54	Decrease	Decrease	635.70	---	0.66	0.70
	Ab$_{C3c}$	105.03 ±7.17	---	0.13	Increase	Increase	101.19	---	0.11	1.04
	Ab$_{HPF}$	2056.81 ±19.92	---	1.59	Increase	Increase	2118.46	---	1.43	0.97
CuTSPc	Ab$_{HSA}$	309.16 ±26.31	---	0.32	Decrease	Decrease	675.65	---	0.47	0.46
	Ab$_{C3c}$	53.8 ±7.10	---	0.07	Decrease	Decrease	69.20	---	0.08	0.78
	Ab$_{HPF}$	1049.52 ±44.37	---	1.63	Decrease	Increase	1120.18	---	1.47	0.94
GePcS$_{mix}$	Ab$_{HSA}$	651.25 ±124.97	---	0.79	Decrease	Decrease	2655.25	---	2.45	0.25
	Ab$_{C3c}$	669.09 ±56.63	---	0.66	Decrease	Decrease	996.25	---	0.86	0.67
	Ab$_{HPF}$	982.77 ±30.42	---	1.25	Increase	Increase	337.27	---	0.25	2.91
ZnPcS$_{mix}$	Ab$_{HSA}$	79.12 ±7.25	363.48 ±503.42	0.10	Decrease	Decrease	97.10	434.50 ±569.58	0.10	0.81
		66.58 ±8.33		0.10	Increase	Increase	114.29		0.15	0.58
		944.74 ±23.26		1.20	Increase	Increase	1092.12		1.24	0.87
	Ab$_{C3c}$	100.05 ±3.75	73.26 ±23.40	0.13	Decrease	Increase	132.95	99.36 ±29.48	0.10	0.75
		62.94 ±2.79		0.14	Decrease	Decrease	87.35		0.15	0.72
		56.79 ±3.94		0.11	Decrease	Increase	77.79		0.12	0.73
	Ab$_{HPF}$	1563.94 ±260.34	667.88 ±788.57	2.36	Increase	Decrease	2703.13	1099.50 ±1398.35	3.75	0.58
		360.03 ±27.53		0.44	Decrease	Decrease	460.89		0.51	0.78
		79.68 ±7.30		0.18	Decrease	Decrease	134.47		0.23	0.59
CoTCPc	Ab$_{HSA}$	63.77 ±8.50	---	0.04	Decrease	Increase	86.85	---	0.04	0.73
	Ab$_{C3c}$	315.79 ±15.71	---	0.27	Increase	Increase	366.37	---	0.27	0.86
	Ab$_{HPF}$	1292.69 ±24.04	---	1.07	Increase	Increase	1625.92	---	0.99	0.80

a: Probe antibody for the detection of adsorbed HSA (Ab$_{HSA}$), complement factor C3 (Ab$_{C3c}$), and HPF(Ab$_{HPF}$)
b: Sauerbrey-determined film parameter. Standard deviation is obtained from 3 overtone responses.
c: Antibody probe mass as a proportion of total blood protein mass
d: Viscoelastic film parameters indicating film rigidity levels
e: Indicates level of film hydration

Human Serum Albumin Detection

Analysis of Ab_{HSA} probe binding to the blood protein coat deposited on the MPc films, suggests; through Sauerbrey analysis the $GePcS_{mix}$ coated surface demonstrates the highest level of bound and exposed HSA, followed by $CoPcS_{mix}$, $ZnPcS_{mix}$, CuTSPc, $AlPcS_{mix}$, and CoTCPc-modified surfaces; through Voigt analysis, $GePcS_{mix}$, again, demonstrates the highest level of HSA, followed by CuTSPc, $CoPcS_{mix}$, $ZnPcS_{mix}$, CoTCPc, and $AlPcS_{mix}$-modified surfaces (Table 3.8). However, analysis of the probe antibody, as a proportion of the total blood protein bound (Ab_m/BP_m), suggests high levels of HSA were deposited on the $GePcS_{mix}$-modified surface, followed by $CoPcS_{mix}$, CuTSPc, $AlPcS_{mix}$ and CoTCPc-modified surfaces (Table 3.8). The categorisation of $ZnPcS_{mix}$-modified surfaces was influenced by the low reproducibility of the probe antibody binding results, however, two out of the three replicants indicate similar results, suggesting $ZnPcS_{mix}$ surfaces would demonstrate higher levels of HSA in comparison to $AlPcS_{mix}$, but lower levels in comparison to CuTSPc (Table 3.8). The levels of Ab_{HSA} (Ab_m/BP_m) adsorbed to the MPc-modified surface did not exceed that of the positive control (i.e. Ab_{HSA}-modified surface) levels (Chapter 2; Table 2.6).

According to Figure 3.9, similar Ab_m/BP_m responses were recorded for the $CoPcS_{mix}$ and CuTSPc-modified surfaces. Both the above mentioned films were concluded to be composed of a monolayer of planar orientated MPc molecules, therefore exposing the hydrophobic ring structure to a large extent. According to the preliminary planar surface studies (Chapter 2; Section 2.3.2.3) higher levels of Ab_{HSA} (Ab_m/BP_m) were recorded on hydrophobic gold in comparison to negatively charged MUA. However, the immobilised MPc films demonstrated differences in the film interface (Table 3.3; ave. *f* % CV). This leads one to consider that surface charge carries a greater influence over HSA binding in comparison to surface topography and chemical composition.

The CoTCPc film immobilised for the detection of HSA was concluded to be a monolayer composed of edge-on orientated molecules. Lower levels of Ab_{HSA} binding (Ab_m/BP_m) were recorded in comparison to that of the planar orientated $CoPcS_{mix}$ surface. An explanation for this occurrence may be the decrease in surface hydrophobicity of the CoTCPc surface, as CoTCPc immobilisation analysis suggested the edge-on conformation was adopted. This

edge-on conformation is predicted to result in a higher negative surface charge in comparison to the aromatic planar conformation. This increase in negative charge corresponds with the preliminary studies (Chapter 2; Section 2.3.2.3).

Reproducibility

Although analysis of the surface modification process with $ZnPcS_{mix}$ revealed similar surface topographies of the deposited films, large variations were observed when assessing the HSA binding, via the proposed method of utilising Ab_{HSA} as a probe (Figure 3.9). Higher levels of Ab_{HSA} binding were detected on the MPc film which demonstrated the sharpest interface (ave. Δf % CV: 4.39), of which the MPc orientation analysis suggested a film composed of mixed orientated MPc molecules. Lower levels of binding were reported on films which demonstrated slightly rougher film interfaces. According to literature, HSA has a greater affinity towards negatively charged surfaces, as well as hydrophobic over hydrophilic surfaces [18, 96]. As sulphonated MPc molecules are comprised of both hydrophobic and hydrophilic portions, therefore variations in the orientation of the MPc molecules on the surface may greatly influence the surface charge characteristics [104]. Without further knowledge of the MPc film surface charge, it is uncertain if the detection of HSA binding to a target surface, utilising the proposed QCM-D method, has a low reproducibility, or in fact if it is due to the variability of the MPc surface formation.

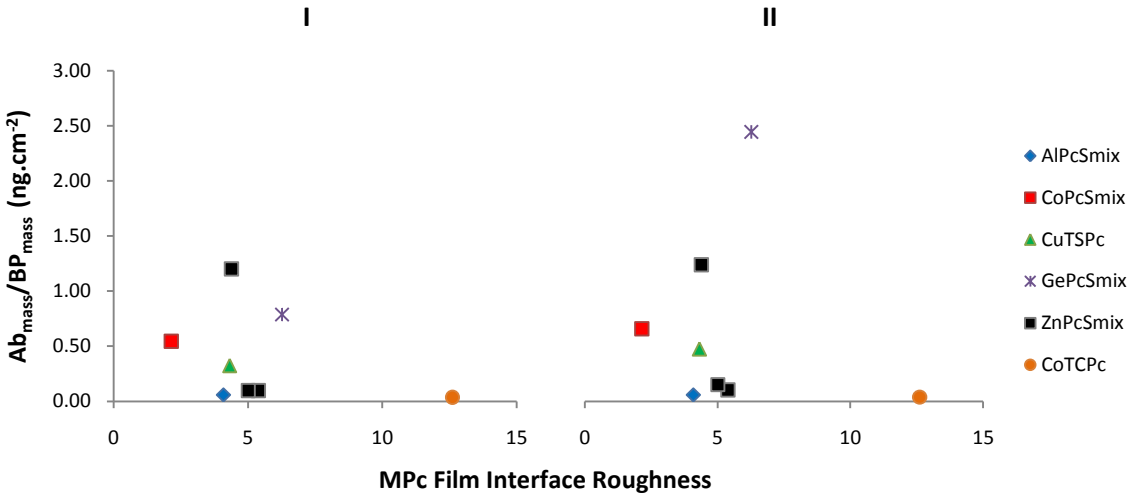

Figure 3.9. Sauerbrey- (I) and Voigt- (II) determined adsorbed anti-human albumin mass, as a proportion of total blood protein mass, versus immobilised MPc film interface property. The MPc film interface property illustrated is the average *f* percentage coefficient of variation.

Human Serum C3c Detection

According to Sauerbrey analysis of Ab_{C3c} probe binding, $GePcS_{mix}$, demonstrated the highest level of total antibody bound, followed by CoTCPc, $AlPcS_{mix}$, $CoPcS_{mix}$, $ZnPcS_{mix}$, and CuTSPc-modified surfaces. Voigt analysis, however, suggests a different trend where $GePcS_{mix}$ demonstrates the highest level of antibody binding, followed by CoTCPc, $CoPcS_{mix}$, $ZnPcS_{mix}$, $AlPcS_{mix}$, and CuTSPc. Evaluation of Ab_{C3c} binding, and therefore subsequent detection of complement C3, utilising the Ab_m/BP_m values, suggests similar trends for both the Sauerbrey and Voigt models, where $GePcS_{mix,}$ indicates the highest level of detection, followed by CoTCPc, $ZnPcS_{mix}$, $CoPcS_{mix}$, and ($AlPcS_{mix}$ or CuTSPc). Figure 3.10 illustrates the Sauerbrey- and Voigt-determined adsorbed Ab_{C3c} mass, as a proportion of total blood protein mass, versus immobilised MPc film interface property. In each case, the levels of Ab_{C3c} (Ab_m/BP_m), were within the range of the positive and negative controls (Chapter 2; Table 2.6).

The level of complement C3 detected on the $AlPcS_{mix}$-modified surfaces served as an indication of the levels acceptable in the biological system, which would not activate an immune response, as sulfonated AlPc preparations have been utilised in biomedical application [104].

In conclusion, higher levels of complement C3, in comparison to $AlPcS_{mix}$, were detected on all surfaces, with the exception of the CuTSPc-modified surfaces. The higher level of antibody binding to the CoTCPc surface was unexpected due to the low levels detected on the planar orientated $CoPcS_{mix}$, as the CoTCPc film was assumed to be orientated in the edge-on position. This orientation is expected to expose carboxyl groups to the surface, which are known to be non-activating of the complement system [9, 18, 29].

Reproducibility

Reproducibility analysis, using $ZnPcS_{mix}$-modified surfaces, revealed similar levels of antibody binding, regardless of the variations in MPc film topography (Figure 3.10). Detection of complement C3 binding using a probe antibody appears to be more reproducible

demonstrating variability below 30%. The small size of the complement C3c protein may have attributed to the higher reproducibility, as it limits the number of antibody molecules that may bind to the target protein.

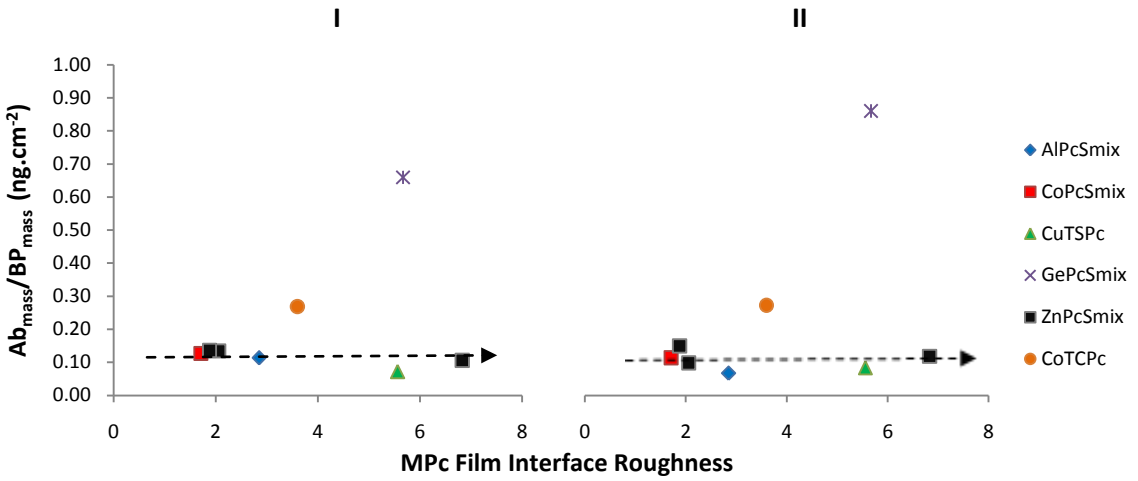

Figure 3.10. Sauerbrey (I) and Voigt (II) determined adsorbed anti-human C3c mass, as a proportion of total blood protein mass, versus immobilised MPc film interface property. The MPc film interface property illustrated is the average *f* percentage coefficient of variation.

Human Plasma Fibrinogen Detection

Sauerbrey determined Ab_{HPF} bound mass suggested the highest levels of exposed HPF molecules on surfaces coated with $AlPcS_{mix}$-coated surfaces followed by $CoPcS_{mix}$, CoTCPc, CuTSPc, $GePcS_{mix}$, and $ZnPcS_{mix}$-modified surfaces. Voigt-determined parameters revealed a similar trend, with the exception of $ZnPcS_{mix}$-modified surfaces demonstrating a higher level than $GePcS_{mix}$-coated surfaces (Table 3.8). Furthermore, analysis of Ab_{HPF} detection of surface bound HPF, using Ab_m/BP_m, indicated the highest levels of HPF were deposited on the $AlPcS_{mix}$-modified films, followed by the CuTSPc, $CoPcS_{mix}$, and either $GePcS_{mix}$, or CoTCPc-modified surfaces (Figure 3.11). In the case of HPF detection, the levels of Ab_{HPF} recorded to bind to the MPc-modified surfaces, when assessing Ab_m/BP_m, exceeded that generated by the positive control (i.e. Ab_{HPF}-modified surface). This occurrence highlights the HPF orientation as a highly influential factor when detecting bound levels using antibody probes.

Reproducibility

Detection of HPF on $ZnPcS_{mix}$-modified surfaces revealed low experimental reproducibility, as highly variable levels of target antibody were reported to bind (Figure 3.11). However, a trend was observed, where an increase in surface roughness correlated with an increase in antibody binding. Fibrinogen is reported to be a flexible, elongated (47 x 4.5 x 4.5 nm^3) protein, which demonstrates an affinity towards hydrophobic surfaces [105, 106]. The structural dimensions of the protein may explain the variations observed in Ab_{HPF} binding. The sharper surfaces may allow for side-on adsorption of the HPF molecule (planar), while the 'rougher' surfaces may inhibit this action, therefore resulting in the possibility of conformational change, leading to a V-shape orientation, where larger portions of the protein are surface exposed, in comparison to the planar orientated molecule. Although this may occur when assessing a macro-surface modified with MPc molecules, this is not a realistic representation of what may occur when the MPc molecules are solubilised as in PDT application.

However, greater levels of HPF were detected on the surface modified with $CoPcS_{mix}$ molecules in comparison to CuTSPc molecules, even though similar surface topographies were observed. This fact highlights the dependency of HPF binding on chemical composition.

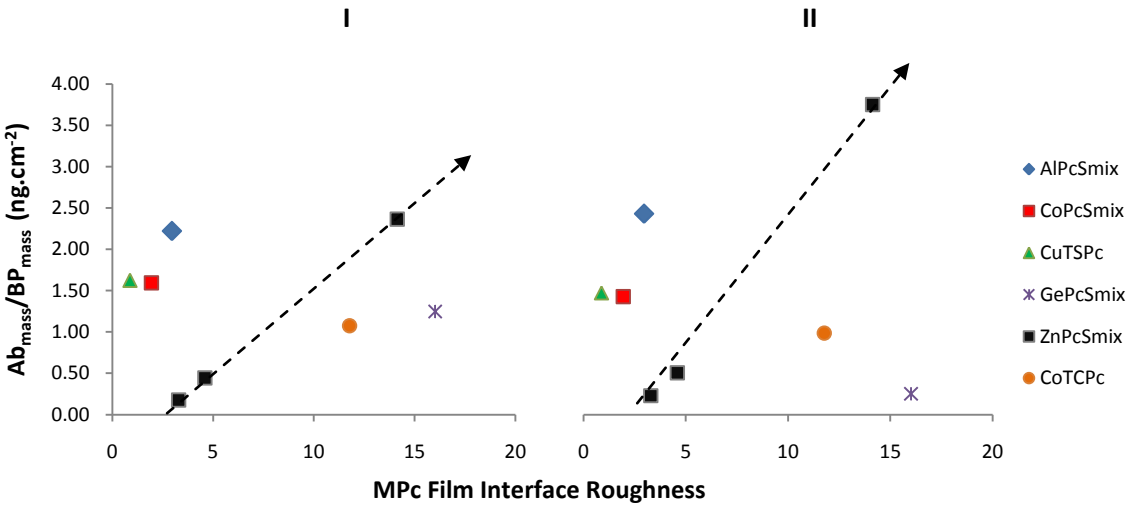

Figure 3.11. Sauerbrey (I) and Voigt (II) determined adsorbed anti-human fibrinogen mass, as a proportion of total blood protein mass, versus immobilised MPc film interface property. The MPc film interface property illustrated is the average *f* percentage coefficient of variation.

3.4. CONCLUSION

In summary, the detection of bound HSA, indicated by probe Ab_{HSA} bound mass as a proportion of the total HS adsorbed mass, demonstrated the following binding trend: $GePcS_{mix}$ > $CoPcS_{mix}$ > CuTSPc > $ZnPcS_{mix}$ > $AlPcS_{mix}$ > CoTCPc (Table 3.8). The experimentally determined results therefore suggest that $GePcS_{mix}$, $CoPcS_{mix}$, CuTSPc, and $ZnPcS_{mix}$ molecules would demonstrate a circulation half-life greater than that of the $AlPcS_{mix}$ preparation, which is currently being utilised in biomedical applications [49, 56].

The experimentally determined binding trend of complement C3c, and therefore complement C3, was recorded as follows: $GePcS_{mix}$ > CoTCPc > $ZnPcS_{mix}$ > $CoPcS_{mix}$ > (CuTSPc and/or $AlPcS_{mix}$) (Table 3.8). The higher levels of detected adsorbed complement C3 on the $GePcS_{mix}$-, CoTCPc-, $ZnPcS_{mix}$-, and $CoPcS_{mix}$-modified surfaces, in comparison to the $AlPcS_{mix}$-modified surface, suggests the possibility of the surfaces inducing complement activation.

HPF protein detection analysis, using Ab_{HPF} as a probe molecule, suggested the following binding trend when assessing MPc-modified sensor surfaces: $AlPcS_{mix}$ > CuTSPc > $CoPcS_{mix}$ > ($GePcS_{mix}$ or CoTCPc). Highly variable results were obtained for the reproducibility analysis using $ZnPcS_{mix}$-modified surfaces, however, a correlation between the surface topography (i.e. roughness) and HPF detection was identified.

It is important to note, the accuracy of the proposed experimental design in representing real life biomolecular occurrences is flawed, as deposited MPc films do not realistically represent the MPc surfaces that would be encountered when in dispersed in solution for application in PDT. However, the alternative methods utilised in assessing protein binding present their own set of drawbacks. For example, spectroscopic analysis has been reported to assess protein interactions with MPc molecules, such as HSA and $AlPcS_4$ molecules in solution [99]. This technique allows for the analysis of binding kinetics and the identification of binding sites, however, it is limited to analysis of one protein, therefore, it may not be utilised as an alternative to the proposed method of analysis. Furthermore, analysis of binding kinetics,

utilising a single protein, may be carried out using QCM-D technology [107]. Another means of blood protein adsorption analysis on target particles is that of two-dimensional gel electrophoresis (2D-PAGE) [10]. This method, however, requires extensive sample preparation, which is both time consuming and financially costly, in addition to the method demonstrating 'false-positives'.

In addition, MPc molecules, deposited in a film arrangement, have been reported to demonstrate application in biosensors, as electrocatalysts for biologically significant molecules, for example lactate and nitric oxide [55, 108]. The analysis of the biomolecular interactions that occur at the MPc film interface are therefore of great importance in sensor design, and optimisation.

In terms of experimental reproducibility, MPc immobilisation is of the greatest concern. High variability was reported, even when assessing identical MPc preparations, chiefly when immobilising MPc samples which demonstrated aggregation in the sample buffer, $PBS_{Mg/Ca}$, such as $AlPcS_{mix}$, $GePcS_{mix}$ and $ZnPcS_{mix}$. Possible means of improving immobilisation reproducibility may be through chemical modification of the MPc molecule itself, dispersal of the MPc molecules to limit aggregation, or alterations to the deposition process, such as electrochemical deposition or SAM composition modifications.

Chemical modification of the MPc molecules may be achieved through altering ring substituents to promote more controlled binding to a chosen SAM surface, therefore limiting random immobilisation. An example of such modifications may include the introduction of an amine group to a chosen number of substituent, which will be immobilised on a carboxyl terminating SAM, such as a mercapto undecanoic acid SAM. However, problems associated with this technique may arise when assessing MPc preparations with tri-, di- and mono-substitutions, as control over the position of the substituent modification is challenging. Chemical modifications, if not strictly regulated and assessed, may result in interference with protein binding analysis.

Addition of surfactants, such as sodium dodecyl sulphate (SDS) and Triton X-100, although resulting in monomerisation of the MPc aggregates, is predicted to result in protein denaturation of the SAM layer, therefore prohibiting the use protein linkers to aid immobilisation [99, 102]. Chemical modification of the MPc preparation would therefore be required to facilitate immobilisation to the gold sensor surface.

Electrochemical deposition of the MPc molecules to the sensor surface has been reported to achieve immobilisation with high reproducibility [109]. Although this deposition may be achieved utilising Electrochemical Quartz Crystal Microbalance (E-QCM) technology, extensive optimisation of the immobilisation process will be required. Alterations to the composition of the SAM, such as utilisation of various length linkers, may aid in the control of the immobilisation of the MPc molecules, however, optimisation would be required for each MPc samples, therefore extending experimental time. The aim of the proposed method of protein detection is to develop a rapid means of assessment. Introducing a sample preparation step would therefore eliminate this aspect of the experimental procedure.

Additionally, reproducibility of the level of blood protein adsorption appears to be reliant on, not only surface charge and composition, but also MPc film topography. Although this level varies, it is not an indication of alterations to the composition, and patterning, of the adsorbed protein coat.

Analysis of Ab_{HSA}, for the detection of adsorbed HSA, suggests low reproducibility of the method, however, this may not be the case, as variations in MPc surface charge may greatly influence HSA binding. Moreover, the low reproducibility may be due to conformation changes in HSA following adsorption to the MPc film. Further analysis into HSA adsorption to each surface, as an independent protein, would be required to assess conformational changes. Detection of complement component C3c was reported to be a more reproducible process, while HPF results suggested fibrinogen binding is dependent on surface topography.

In conclusion, with optimisation of the immobilisation process, and analysis of the effect of adsorption on target protein conformation, QCM-D technology may be utilised for the detection of target proteins adsorbed to MPc molecules, through target antibody binding.

CHAPTER 4:

IMPORTANCE OF NANOSTRUCTURES IN BIOMEDICAL APPLICATION: CARBON NANOTUBES

4.1. INTRODUCTION

4.1.1. Multi-Walled Carbon Nanotube Functionalisation

CNT surface functionalisation through chemical oxidation not only increases CNT dispersion (by increasing hydrophobicity), but also promotes CNT purification, via oxidation of synthesis catalysts, such as Fe, Ni, V and Y, as well as removing amorphous carbon [110]. For the purpose of this research, given the wide utilisation thereof, two methods of acid functionalisation were of immediate interest, where CNTs were functionalised through oxidation using nitric and sulphuric acid, and nitric acid alone during extended ultrasonication. Figure 4.1 schematically illustrates the acid functionalisation of CNTs through these two methods.

Nitric and sulphuric acid functionalisation of the CNTs results in the 'cutting', and exfoliating of the CNT walls, as well as functionalising the CNT sidewalls with carboxyl groups [76]. Initial functionalisation of the nanotubes occurs at end cap defect sites, which results from hexagon-heptagon pair strain. Removal of the end caps is rapid, generating open-ended tubes bearing carboxyl substituents. The 'cutting' of the CNTs is a result of the 'attacking' of the nanotubes surface by high temperature microscopic domains generated by cavity bubbles collapsing, during sonication. This 'attacking' of the nanotubes generates defect sites, which are susceptible to chemical oxidation, and therefore functionalisation, producing carboxylic acid groups [76]. The second method employed involves the mild oxidation of the CNTs in nitric acid. Unlike the nitric and sulphuric acid functionalisation, this process does not 'cut' the nanotubes, or functionalise the side walls, rather, it results in the functionalisation of the nanotube ends with the carboxyl groups, through cap digestion [75]. This second method results in longer tubes with less surface exposed carboxyl groups, in theory. The functionalisation of the CNTs with carboxyl groups generates a net negative charge on the nanoparticle and increases the CNT hydrophilic nature, which aids in particle dispersal through electrostatic repulsion [75]. Both afore mentioned acid functionalisation

techniques result in the exfoliation of the CNT walls and the removal of the metal impurities and amorphous carbon, and subsequently increasing the purity of the CNT sample [75, 76].

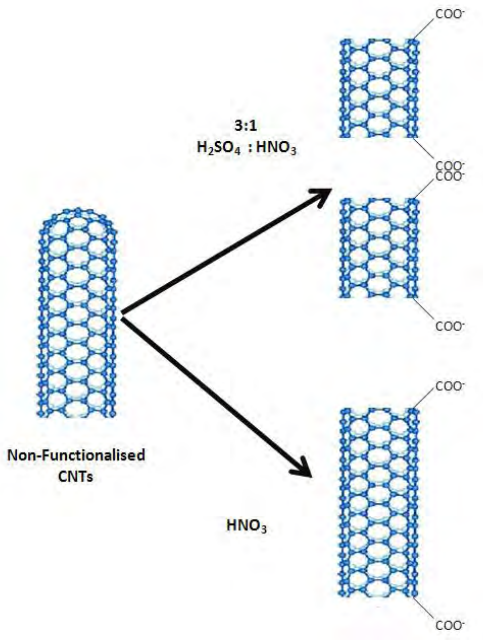

Figure 4.1. Schematic representation of the chemical oxidation functionalisation of CNTs.

4.1.2. Chapter Aims and Objectives

The aim of this section of research was to assess the applicability of the proposed method of protein detection, using QCM-D technology, for functionalised MWCNT biocompatibility analysis.

Objectives

1. Chemically functionalise MWCNTs via chemical oxidation using nitric and sulphuric acid (a:*F*MWCNTs), and nitric acid alone (b:*F*MWCNTs)
2. Characterise the *F*MWCNTs in terms of chemical functionalisation-induced morphological changes
3. Immobilise *F*MWCNT to the gold QCM-D sensor surface to produce *F*MWCNT-modified surfaces
4. Monitor and quantify blood protein adsorption to the prepared *F*MWCNT-surfaces, using QCM-D

5. Monitor and quantify probe antibody binding to the previously prepared blood protein coated surfaces, using QCM-D

4.2. INSTRUMENTATION AND METHODOLOGY

4.2.1. Instrumentation

MWCNT functionalisation involved the utilisation of centrifugation using a Beckman Coulter (Avanti J-E) centrifuge, and heat drying of the final *F*MWCNT preparations using the Prolab PL001 oven. Characterisation of the morphological changes in multi-walled carbon nanotubes, as a result of acid functionalisation, was carried out using Joel Transmission Electron Microscopy (Jem-1210; 110 kV).

4.2.2. Additional Reagents

MWCNTs utilised were purchased from Sigma-Aldrich (> 90% purity). The dimension of the stock of MWCNTs is as follows: outer diameter of 10-15 nm, inner diameter of 2-6 nm, length of 0.1-10 μm. Acid functionalisation of the MWCNTs was performed using concentrated sulphuric acid (95%; Merck), and nitric acid (55%; Merck).

The buffer utilised in the immobilisation of the acid functionalised MWCNTs, and carboxylated metallophthalocyanines, was 2-(N-morpholino)ethanesulfonic acid (Sigma-Aldrich), commonly known as MES. 50 mM MES buffer solutions, prepared using MilliQ water, were adjusted to a pH value of 4.7 using 0.2 mM KOH. MES is reported as an optimum buffer for ethyl(dimethylaminopropyl) carbodiimide (EDC) and *N*-hydroxysuccinimide (NHS) activity, due to the lack of phosphate ions.

4.2.3. Methodology

4.2.3.1. Acid Functionalisation of Multi-Walled Carbon Nanotubes

Chemical oxidation through ultrasonication in concentrated sulphuric and nitric acid was undertaken. Acid functionalisation was employed to allow for immobilisation on the crystal surface, as well as increasing the CNT purity.

The protocol carried out on MWCNTs for carboxyl functionalisation involved the dissolution of the CNTs in either a 1:3 solution of 55% nitric acid and 95% sulphuric acid (a:*F*MWCNTs), or pure 55 % nitric acid (b:*F*MWCNTs), in a concentration of 0.03 g/ml of CNTs. The solution was ultrasonicated, while covered, for periods of 2, 4, 6, 8 and 24 hrs, in the case of a:*F*MWCNTs, and 4, 8, 12, 20 hrs, in the case of b:*F*MWCNTs. Following sonication, MilliQ water was added to make up a volume of approximately 250 ml. This MWCNT solution was then centrifuged at a speed of 12 000 rpm for a period of 15 min, at 4°C. The supernatant was removed and replaced with MilliQ water. Centrifugation was repeated until a supernatant with approximately pH 7.0 was obtained. Once the final supernatant was removed, the CNT solution was heat dried at 70.0°C to obtain functionalised multi-walled carbon nanotubes (*F*MWCNTs).

4.2.3.2. Characterisation of Acid Functionalised Multi-Walled Carbon Nanotubes

Characterisation of non-functionalised and acid functionalised (a:*F*MWCNTs and b:*F*MWCNTs) to monitor structure and texture changes was carried out using Transmission Electron Microscopy (TEM). 0.1 mg/ml suspensions of each sample were prepared in ethanol. Prior to analysis, CNT solutions were ultrasonicated (S10H Elmasonic) for a period of 10 min to fully disperse the MWCNTs. The prepared *F*MWCNT ethanolic solutions were drop-dried on carbon coated copper grids, and visualised using TEM.

4.2.3.3. Surface Modification with *F*MWCNTs

The immobilisation of *F*MWCNTs was facilitated via the formation of amide bonds between the nanoparticle carboxyl group and 11-amino undecane thiol (11-AUT) SAM terminating amine groups, mediated by EDC/NHS. The production of the NHS-activated molecule has been reported to be achieved in reduced time using an MES buffer at the optimum pH of approximately 5.0, while the stability of the NHS-activated molecules ester group is substantially decreased above pH 5.0. Hence the immobilisation was performed in MES buffer at pH 4.7 [77]. Figure 4.2 schematically illustrates the linking action of EDC/NHS in the immobilisation of *F*MWCNTs to 11-AUT SAM-modified gold sensor surface.

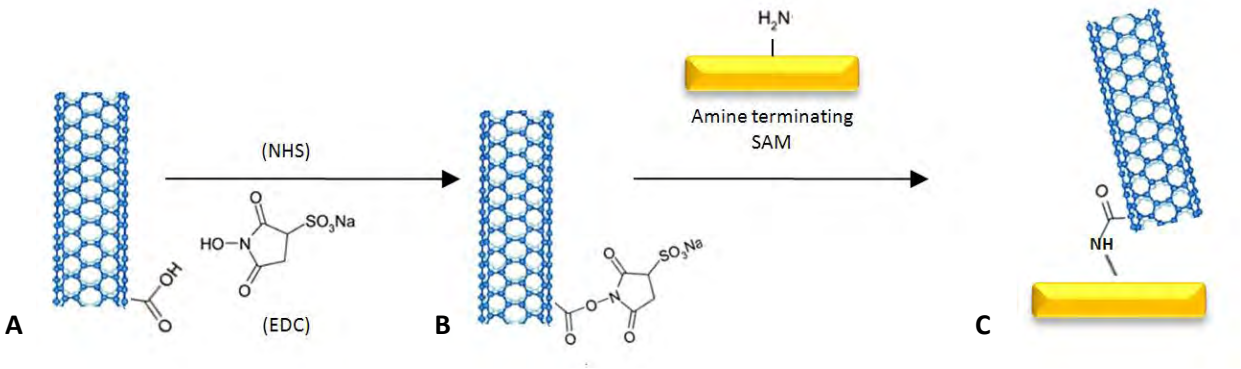

Figure 4.2. Schematic representation of the EDC/NHS activity in immobilisation of *F*MWCNTs to 11-AUT SAM-modified surface.

As illustrated in Figure 2.2, carboxyl functionalised MWCNT incubation with EDC and NHS (A), results in the formation of a highly reactive, and unstable, acylurea derivative, which forms a stable ester in the presence of NHS (B). In the presence of an amino group (i.e. 11-AUT SAM), a nucleophilic substitution reaction occurs between ester and the amino group, resulting in the formation of an amide bond, and therefore the generation of *F*MWCNT-modified surface (C) [111].

The immobilisation protocol for *F*MWCNTs onto the 11-AUT SAM was performed *ex situ*, due to concerns regarding aggregation of the *F*MWCNTs *in situ* for QCM-D. *F*MWCNTs suspensions were prepared by ultrasonicating dried *F*MWCNTs in MES buffer (pH 4.7) for a period of 30 min. 15m M EDC and 15m M NHS was then introduced to the suspension, to activate the carboxyl groups. The *F*MWCNTs-EDC/NHS solution was ultrasonicated, in the dark, for a period of 30 min prior to the introduction of 11-AUT SAM modified sensor crystals. Immobilisation was allowed to take place for approximately 12 hrs before rinsing the nano-modified surface with ethanol and water, and then drying with nitrogen gas.

4.2.3.4. QCM-D Monitoring and Quantification

For the determination of blood protein binding, and subsequent probe antibody binding, to acid functionalised MWCNTs a similar approach was utilised as to that used for protein analysis of various surfaces (Chapter 2; Section 2.2.4).

4.3. RESULTS AND DISCUSSION

Section 4.3.1 investigates the visible surface changes, and changes in particle dispersion, of MWCNTs, as a result of chemical oxidation. Section 4.3.2 assesses the interaction between the *F*MWCNT-modified surface and blood proteins, namely HS and HP, using QCM-D. Section 4.3.3 focuses on the QCM-D aided detection of HSA, complement C3c, and HPF through the antibody-antigen specific interactions, in a similar manner as outlined in Chapter 2.3.1.

4.3.1. Characterisation of Acid Functionalised Multi-Walled Carbon Nanotubes

Transmission Electron Microscopy (TEM) was utilised to monitor aggregant morphological changes of the MWCNTs as a result of acid functionalisation. This means of assessment has been well documented in literature [112-114].

Figure 4.3. illustrates TEM imaging of non-functionalised MWCNTs, which served as a comparison for the *F*MWCNT preparations. According to TEM results, non-functionalised MWCNTs indicated tightly associated agglomerates of MWCNTs, with finer tubules protruding from the mass (Figure 4.3: A). Large rod-shaped structures were also observed, which were assumed to be CNT aggregates, where the tubules are orientated parallel to one another, and possibly coated with sample contaminants, namely, metallic catalysts and amorphous carbon, as observed in the rough, nodular nature of the structure surfaces (Figure 4.3: B).

Several characteristics of the CNT structure have been reported to result in the formation of nanotube aggregates, firstly, CNTs are reported to be hydrophobic in nature, therefore resulting in nanotube aggregation through Van der Waals interactions, secondly, CNTs have displayed a tendency to wrap around the metal catalysts introduced during the synthesis process, and thirdly, the long, thin nature of the tubules permits entanglement during synthesis, generating congeries [115-118]. Acid functionalisation of the CNTs, using nitric and sulphuric acid, aimed at improving nanotube dispersion, has been well documented in literature [75, 112].

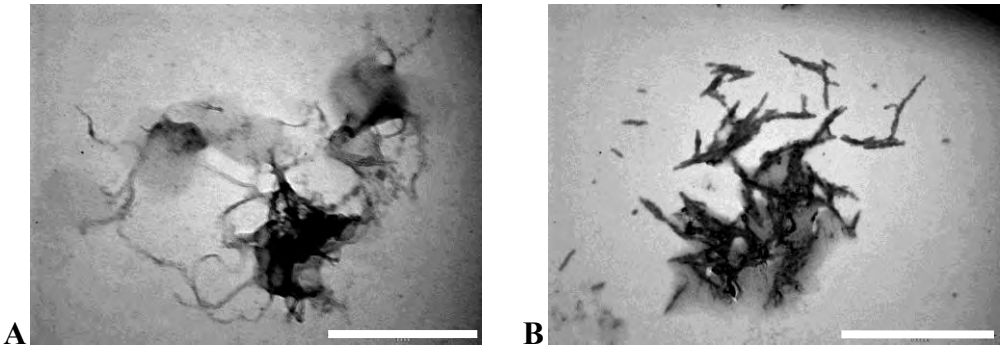

A Scale: 500 nm B Scale: 1000 nm

Figure 4.3. Transmission Electron Microscope imaging of non-functionalised MWCNTs. Scale bars are represented by the white line bottom left of each image.

Figure 4.4 illustrates the TEM images of MWCNTs chemically oxidised, using nitric and sulphuric acid, for periods of 2 hrs, 4 hrs, 6 hrs, 8 hrs, and 24 hrs (a:*F*MWCNs).

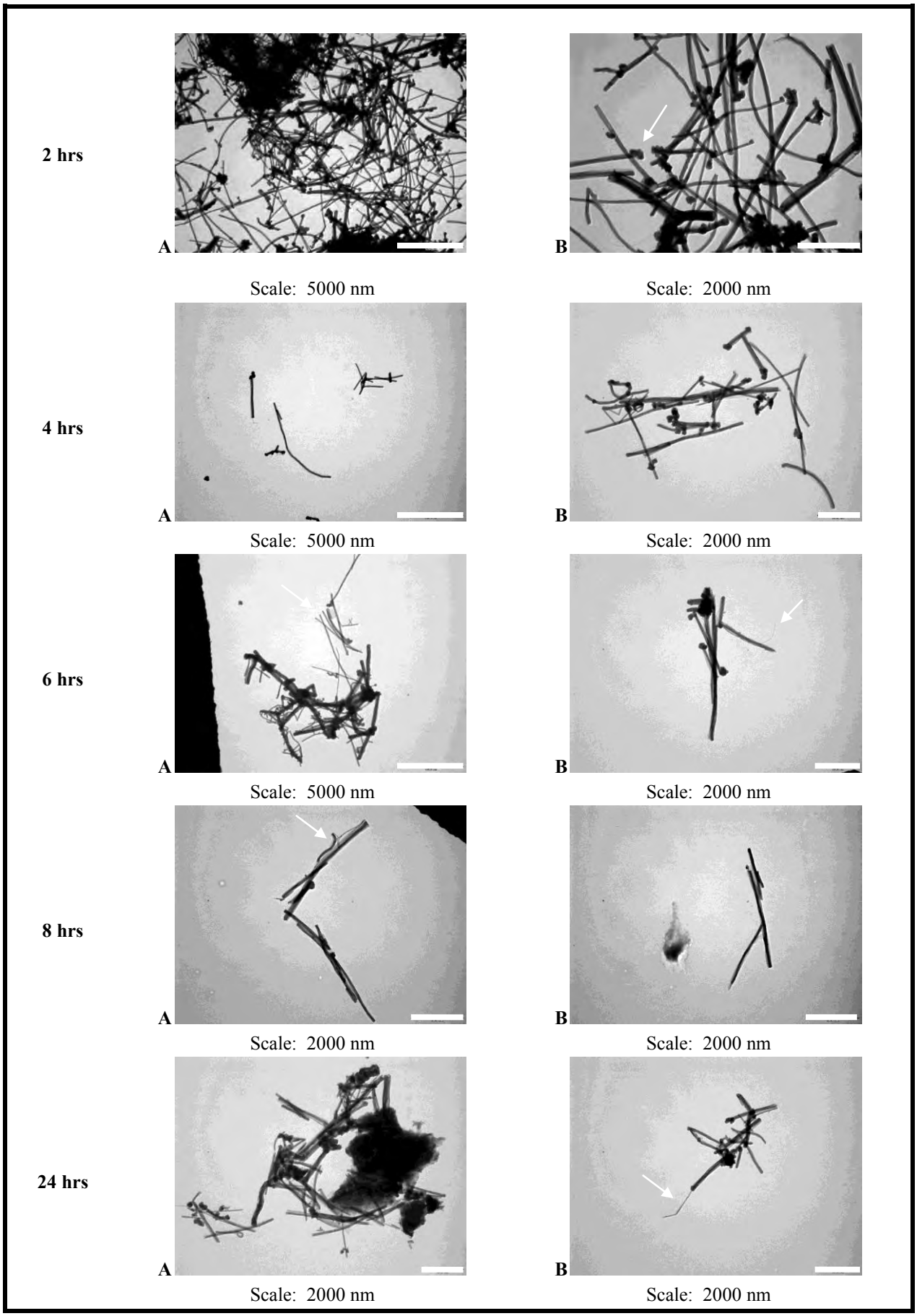

Figure 4.4. Transmission Electron Microscopy images of nitric acid and sulphuric functionalised MWCNTs (a:*F*MWCNTs). Acid treatment times ranged from 2 hrs to 24 hrs. Scale bars are represented by the white line bottom left of each image. Arrows are discussed in text.

Noticeable changes were observed in the structure of the CNTs following the 2 hr chemical oxidation (Figure 4.4; 2 hrs). Tubules appeared thicker in diameter, suggesting aggregation in a parallel orientation, and shorter in length, indicating the 'cutting' action of the nitric and sulphuric acid has occurred. In addition, nodules were observed, predominantly at the tubule ends, indicating the presence of defect sites due to the oxidation process (arrow in Figure 4.4; 2 hrs B). Following 4 hrs of oxidation, an increase in dispersal of the a:*F*MWCNT preparation was observed, along with an overall decrease in the size of the nodules, tubule diameter and length (Figure 4.4; 4 hrs B). It is important to note the high level of variability, in terms of CNT length, following chemical oxidation with nitric and sulphuric acid. This high variability highlights reproducibility as a possible problem area when assessing biological interactions with the functionalised preparations.

Six hrs of chemical oxidation resulted in *F*MWCNT samples composed of a mixture of aggregates demonstrating both thick and thin diameters (Figure 4.4; 6 hrs). The overall level of defect sites present on the tubules, observed as nodules, decreased, in comparison to the *F*MWCNT sample treated for 4 hrs, as defect sites due to the cutting action of the acid treatment to shorten the CNTs. This was observed in the lack of nodules present on the majority of the open-ended tubules (arrow in figure 4.4; 6 hrs A). Furthermore, fine tubules were observed protruding from the surface of the thicker tubules, indicating detangling of individual CNTs from the MWCNT aggregate (arrow in figure 4.4; 6 hrs B). Following 8 hrs of acid functionalisation, CNTs displayed separation of tubules from the aggregates more frequently (arrow in figure 4.4; 8 hrs A), along with a decrease in nodules present on the surface. 24 hrs of functionalisation, with nitric and sulphuric acid, resulted in the overall shortening of the tubular length (Figure 4.4; 24 hrs A), and indicated further increase in dispersion, observed as the presence of finer tubules protruding from the aggregates (arrow in figure 4.4; 24 hrs B). In addition, large aggregates of contamination were observed, assumed to be amorphous carbon that has been exfoliated from the CNT surface and degradation products of CNT oxidation.

In general, acid functionalisation of MWCNTs, utilising nitric and sulphuric acid, resulted in an increase in particle dispersal, and a decrease in observed nanotube length, which

corresponded to an increase in functionalisation time (Figure 4.4). These observations correlate with literature [112, 113, 117].

According to literature, nitric acid functionalisation of CNTs is limited to surface exfoliation and carboxyl functionalisation of the tubule ends [2]. Figure 4.5 illustrates the TEM images visualising the structural changes of MWCNTs as a result of chemical oxidation with nitric acid for the periods of 4 hrs, 8 hrs, 12 hrs and 20 hrs (b:*F*MWCNT).

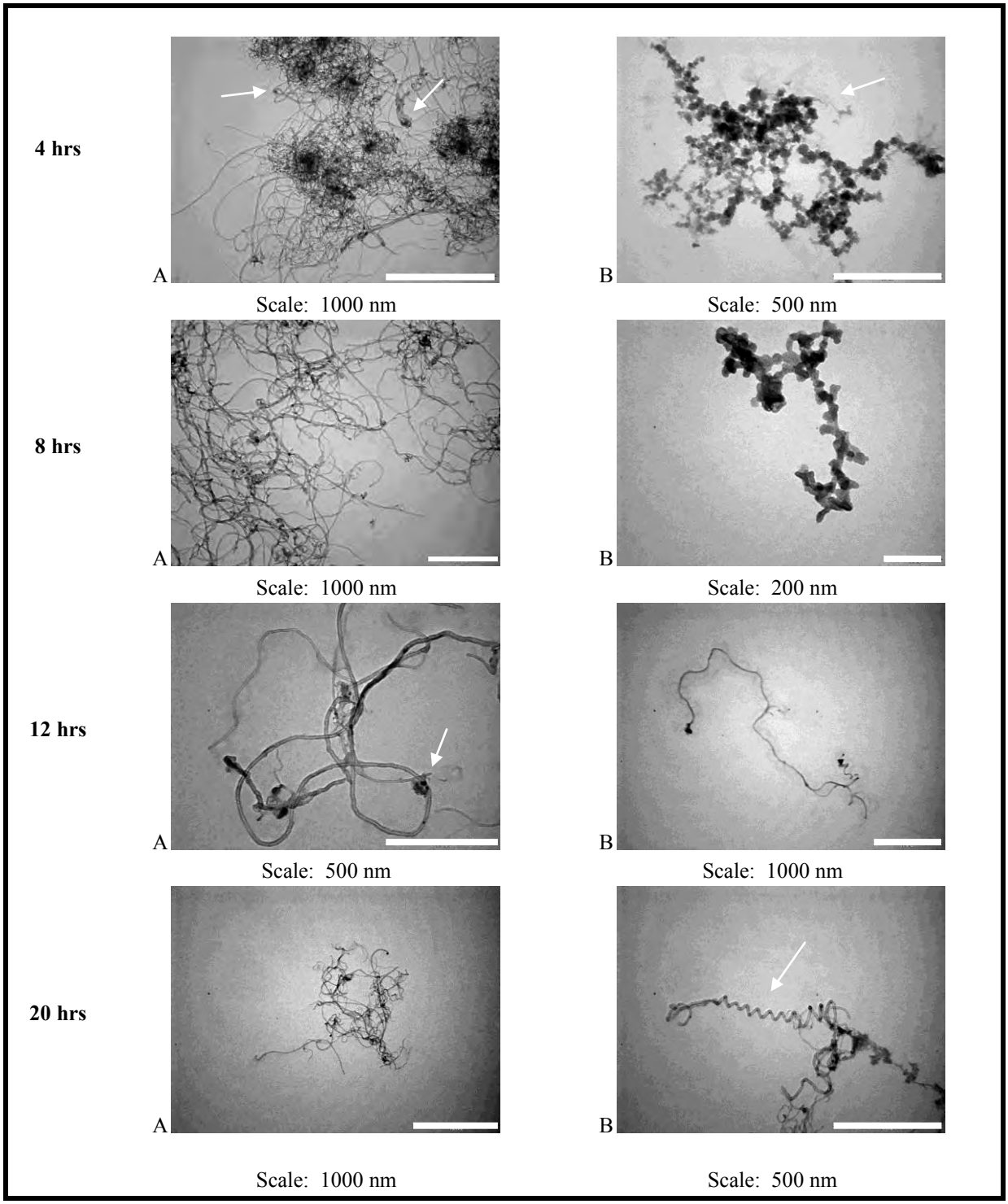

Figure 4.5. Transmission Electron Microscopy images of nitric acid functionalised MWCNTs (b:*F*MWCNTs). Nitric acid treatment times ranged from 4 hrs to 20 hrs. Scale bars are represented by the white line at bottom left of each image. Arrows are discussed in text.

The changes observed in the nanotube structure following nitric acid functionalisation (Figure 4.5), were less apparent in comparison to the changes observed during functionalisation using nitric and sulphuric acid (Figure 4.4). Following 4 hrs of chemical oxidation with nitric acid, fine tubules were present, similar to those observed in the pristine

MWCNT sample (Figure 4.3; A). Surface defects were visible on the nanotube surface, which were observed as nodules (arrows in figure 4.5; 4 hrs A). However, an increase in particle dispersion was noted, including the presence of contamination aggregates, assumed to be amorphous carbon and metallic catalysts (Figure 4.5; 4 hrs B). Fine tubules were observed to protrude from the latter aggregates. It has been documented that nanoparticle aggregates of amorphous carbon surround the CNTs when functionalising with nitric acid alone [75]. The detanglement of nanotubes may be explained by the decrease in surface contaminants, and increase in carboxylation at the site of the tubule ends [112, 113]. 8 hrs of acid functionalisation resulted in an increase in nanotube dispersions, and the generation of smaller aggregates of amorphous carbon (Figure 4.5; 8 hrs)

A noticeable increase in nanotube dispersion was observed following functionalisation for 12 hrs, where individual tubes were observed in isolation (Figure 4.5; 12 hrs). Defects sites were still visible on the surface of the nanotubes, as indicated by the arrow in Figure 4.5; 12 hrs A. Similar observations were recorded for the *F*MWCNT sample following 20 hrs of functionalisation. However, surface defects were observed in the nanotube structure, which were unique to the 20 hr preparation. The latter defects were observed as 'kinks' in the nanotube structure, resulting in a helical conform (arrows in Figure 4.5; 20 hrs B). It was therefore unexpected to visualise alterations on the tubule surface walls. A possible explanation for the presence of these defects is due to interactions between the metal catalyst and the nanotube surface, resulting in the CNTs wrapping around the impurities.

In conclusion, nitric acid functionalisation of MWCNTs was observed to increase particle dispersal, as functionalisation time increased. This increase in particle dispersal indicates the effective exfoliation of the nanotube surface, removing impurities, and/or confirming carboxyl functionalisation.

4.3.2. QCM-D Analysis of Biomolecular Interactions with *F*MWCNT-Modified Surfaces

Surface modification analysis of the 11-AUT SAM surfaces with the acid functionalised MWCNTs was not carried out using QCM-D monitoring, due to aforementioned physical limitations of the QCM-D system, and similar such techniques, e.g. SPR. Immobilised *F*MWCNT film parameters, such as film mass, thickness, viscosity and shear modulus, were therefore unattainable. Following surface modification, using the prepared *F*MWCNT, blood protein adsorption, and subsequent probe antibody binding was analyses using QCM-D.

4.3.2.1. QCM-D Monitoring and Quantification of Blood Protein Adsorption on *F*MWCNT-Modified Surfaces

The film surface characteristics of the blood protein coating, subsequently adsorbed to the *F*MWCNT-modified surface, were utilised as an indication of firstly, the effectiveness of the EDC/NHS immobilisation of *F*MWCNT on the SAM surface, and secondly to obtain a crude indication of the film surface topography, in addition to providing a means of protein detection.

Table C.1 presents the relevant frequency (*f*) and dissipation (D) responses recorded for blood protein adsorption to the *F*MWCNT-modified surfaces as a function of acid functionalisation time and treatment method (a: H_2SO_4:HNO_3; and b: HNO_3). Of interest were the *f*/D values derived from overtones 7, 9, and 11, and the average *f* and D responses. In general, *f*/D values greater than 10 were recorded, suggesting the deposition of fairly rigid films, in addition to validating the utilisation of the Sauerbrey model. Furthermore, low coefficient of variation percentages were determined, on average, from the *f* shifts, indicating the sharp nature of the blood protein coat interface. Deviations from the general trends are proposed to be the result of the highly varied nature of the *F*MWCNT immobilised film.

Sauerbrey- and Voigt-determined film parameters of the blood protein coat are summarised in Table 4.1. In each case, the adsorbed blood protein films were reported to be fairly rigid in nature, as indicated by the high film viscosity and shear moduli recorded. Furthermore,

varying degrees of film hydration were reported ($Sauerbey_{mass}/Voigt_{mass}$) between the modified surfaces, suggesting varying degrees of protein denaturation occur between the surfaces. It is important to note that the accuracy of film analysis using the viscoelastic model (i.e. Voigt model), is questionable, as the *F*MWCNT immobilised films are not in compliance with the requirements of the mathematical model. In particular, due to the length variations noted in TEM, the film is not laterally homogeneous or infinite, and not thin-film [Alternative Reference 1].

Table 4.1. Sauerbrey and Voigt Modelled Analysis of Blood Protein Adsorption on *F*MWCNT-Modified 11-Amino Undecane Thiol SAM Surfaces

*F*MWCNT [a]		Sauerbrey Model		Voigt Model				$\frac{Sauerbrey_m}{Voigt_m}$ [d]
		Areal Mass (ng/cm²) [b]	**Ave. Mass % CV**	**Viscosity (kg/m.sec) [c]**	**Shear Modulus (Pa) [c]**	**Areal Mass (ng/cm²)**	**Ave. Mass % CV**	
2 a:*f*MWCNT	HS	622.66 ±14.59	5.57	2.28E-03	8.03E+04	1168.24	25.86	0.53
	HS	673.76 ±21.91		3.88E-03	8.37E+05	807.03		0.71
	HP	1138.30 ±25.55	---	4.37E-03	4.51E+05	1461.81	---	0.86
4 a:*f*MWCNT	HS	684.15 ±22.28	20.22	2.99E-03	3.96E+05	956.87	4.84	0.88
	HS	513.00 ±22.13		2.11E-03	2.50E+05	893.60		0.89
	HP	781.59 ±25.92	---	2.57E-03	2.97E+05	1210.98	---	0.83
6 a:*f*MWCNT	HS	762.42 ±19.52	1.52	3.59E-03	1.04E+06	883.06	1.32	0.57
	HS	778.95 ±27.88		4.01E-03	1.14E+06	899.66		0.87
	HP	827.38 ±18.8	---	2.97E-03	2.02E+06	867.28	---	0.85
8 a:*f*MWCNT	HS	536.20 ±20.98	30.12	3.87E-03	1.29E+06	610.16	32.16	0.86
	HS	826.36 ±25.66		3.78E-03	9.64E+05	969.32		0.78
	HP	682.58 ±47.68	---	3.00E-03	1.09E+06	865.82	---	0.65
24 a:*f*MWCNT	HS	326.27 ±6.31	53.21	5.44E-03	1.23E+06	367.05	55.08	0.95
	HS	719.92 ±13.87		3.82E-03	1.03E+06	835.33		0.79
	HP	511.30 ±8.76	---	4.51E-03	8.55E+05	601.25	---	0.85
4 b:*f*MWCNT	HS	768.90 ±37.04	9.73	4.14E-03	6.58E+05	950.95	26.71	0.81
	HS	882.54 ±27.7		2.83E-03	1.94E+05	1393.82		0.84
	HP	1024.00 ±26.79		4.18E-03	1.13E+06	1164.17	---	0.88
8 b:*f*MWCNT	HS	784.88 ±19.3	9.10	3.89E-03	9.52E+05	932.78	25.38	0.78
	HS	892.88 ±19.33		3.05E-03	2.57E+05	1340.72		0.63
	HP	831.26 ±16.79	---	4.37E-03	7.77E+05	997.44	---	0.67
12 b:*f*MWCNT	HS	721.32 ±9.87	7.18	4.41E-03	2.41E+06	760.88	2.22	0.83
	HS	651.59 ±51.22		2.98E-03	9.81E+05	785.10		0.73
	HP	962.66 ±24.49	---	3.55E-03	5.50E+05	1251.94	---	0.59
20 b:*f*MWCNT	HS	580.17 ±28.91	9.30	3.35E-03	5.97E+05	746.21	13.84	0.83
	HS	661.80 ±26.05		3.07E-03	4.71E+05	908.14		0.77
	HP	928.39 ±304.93	---	1.86E-03	9.72E+04	1663.58	---	0.56

a: *Surface modification molecule and blood protein sample adsorbed to the test surface*
b: *Sauerbrey-determined adsorbed mass. Standard deviation is obtained from 3 overtone responses.*
c: *Viscoelastic film parameters indicating film rigidity levels*
d: *Indicates level of film hydration*

Analysis of the level of adsorbed blood protein mass, as a function of MWCNT functionalisation time is illustrated in Figure 4.6 and 4.7, for a:*F*MWCNT- and b:*F*MWCNT-modified surfaces, respectively. Blood protein adsorption to the modified surfaces provides a crude means of assessing surface hydrophobicity, as blood proteins are

reported to demonstrate a higher affinity towards such surfaces [35]. This observation was previously corroborated when assessing HS adsorption to the unmodified gold surface and SAM-modified surfaces (Chapter 2; Section 2.3.2.2), where the highest level of HS was detected to adsorb to the gold hydrophobic surface. In general, lower levels of both HS and HP were recorded to adsorb to the negatively charged SAM-modified surface (MUA SAM), in comparison to the unmodified gold surface. Therefore, acid functionalisation of MWCNTs should, in theory, decrease the level of blood protein adsorption.

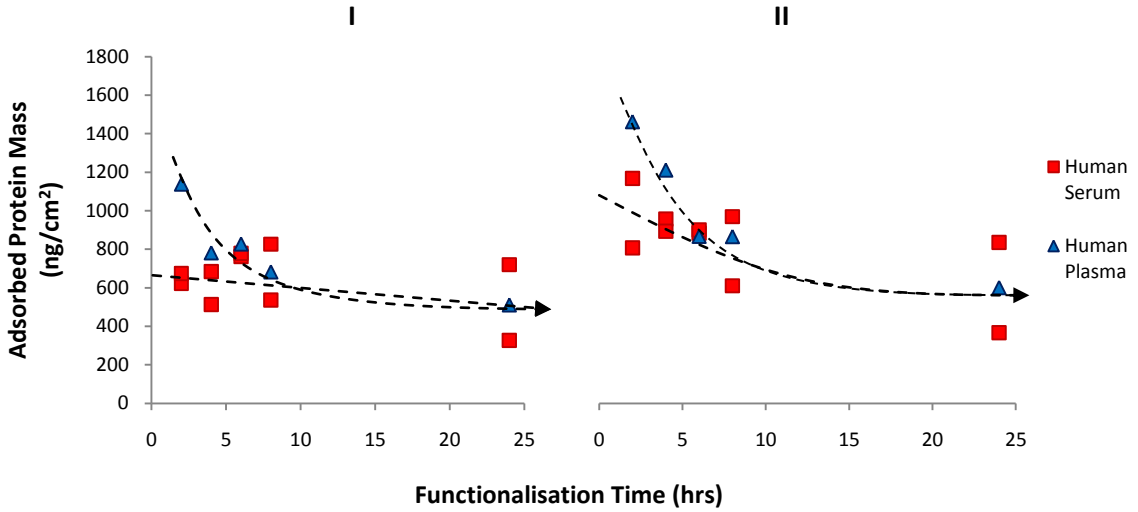

Figure 4.6. Sauerbrey- (I), and Voigt- (II) determined adsorbed human serum (Red) and human plasma (Blue) protein mass to the nitric and sulphuric acid functionalised MWCNT-modified surfaces. Dashed arrows indicate observed trends.

HS adsorption to the a:*F*MWCNT-modified surfaces indicated fairly stable level of mass addition, independent of the functionalisation time, when assessing the Sauerbrey-determined parameter, with the exception of 24 hrs a:*F*MWCNT prepared surface (Figure 4.6; I), where a lower level of adsorbed blood protein was recorded. Voigt analysis of the adsorbed mass, however, indicated a general decrease in mass correlating with an increase in functionalisation time (Figure 4.6; II). As previously mentioned, HS proteins demonstrate a greater binding affinity toward hydrophobic surfaces, in comparison to negatively charged surfaces. This decrease in bound HS mass with increasing in functionalisation time, therefore suggests the surface, and more specifically the a:*F*MWCNT sample, increases in negative charge, and/or decreases in hydrophobicity, as the functionalisation time is increased. This theory is supported by the TEM imaging results, which displayed an increase in nanotube

dispersal with an increase in functionalisation time, indicating a decrease in hydrophobicity, and impurities, and an increase in CNT carboxylation (Figure 4.4).

Sauerbrey and Voigt analysis of HP adsorption indicated a general decrease in adsorbed mass corresponding with an increase in functionalisation time (Table 4.1). HP adsorption to planar surfaces in the preliminary studies (Chapter 2; Section 2.3.2.2), suggested little variance between mass deposition on hydrophobic and negatively charged surfaces. However, film hydration analysis indicated less hydrated HP films (Table 2.5; $Sauerbrey_m/Voigt_m$) were deposited on the hydrophobic planar surfaces, in comparison to negatively charged SAM-modified surfaces. Investigation into the hydration of the HP films adsorbed to the a:*F*MWCNT-modified surfaces ($Sauerbey_{mass}/Voigt_{mass}$) indicated an apparent increase in hydration with an increase in functionalisation time (Table 4.1). This increase in film hydration with increase in functionalisation time, in conjunction with the preliminary analysis of adsorbed HP film hydration on planar surfaces, suggests a decrease in hydrophobicity and/or increase in negative charge occurs as functionalisation time increases (Table 4.1). This conclusion is in agreement with the deduction made from HS adsorption to the a:*F*MWCNT-modified surfaces.

Investigation into reproducibility of the HS adsorption process, between the two prepared samples (Table 4.1; Ave. Mass % CV), indicates low levels of Sauerbrey determined HS mass reproducibility for the 4 hr, 8 hr and 24 hr a:*F*MWCNT-modified surfaces, and low levels of Voigt determine HS mass reproducibility for the 2 hr, 8 hr and 24 hr a:*F*MWCNT-modified surfaces. The low reproducibility of the HS adsorption process is attributed to the variability of the acid functionalisation products (Figure 4.4), and therefore the subsequent variability of the *F*MWCNT- modified film.

Sauerbrey and Voigt analysis of HS adsorption to the surfaces modified with b:*F*MWCNTs indicated a general decrease in adsorbed mass with increasing CNT-functionalisation time (Figure 4.7), which correlates with a decrease in surface hydrophobicity and/or increase in the negative charge of the surface, similar to the behaviour observed for a:*F*MWCNTs. Similar levels of reproducibility were determined for the Sauberbrey adsorbed HS mass

(Table 4.1; Ave. Mass % CV), however, reproducibility decreases substantially when assessing protein adsorption using the Voigt model, with the exception of the 12 hr and 20 hr preparations. The more favourable reproducibility of HS adsorption to the 12 hr and 20 hr b:*F*MWCNT-modified surfaces, suggests reproducibility is improved with prolonged functionalisation. This increase in reproducibility with increased functionalisation may be attributed to the improved, and more uniform dispersion of the b:*F*MWCNT preparations, as well as the increase in the purity of the MWCNT preparations, as observed via TEM analysis (Figure 4.5), therefore resulting in more reproducible deposition of the CNTs on the SAM surfaces.

HP adsorption to b:*F*MWCNT-modified surfaces, however, demonstrated a general increase in adsorbed mass with an increase in functionalisation time, therefore contradicting the previously proposed assumption. According to the studies performed in Chapter 3 (Section 3.3.3.1), the adsorption of HPF, a component of HP, is greatly influenced by the underlying surface topography. It is therefore proposed that the unexpected HP adsorbed mass trend is the result of the variability in the surface topography of the b:*F*MWCNTs which can itself be partially observed via tracking of topography of attaching protein film. The assumption of the latter high variability is supported by the TEM imaging of the CNT sample, which indicated a network of tubules was present following each functionalisation time (Figure 4.5). It was therefore necessary to assess protein adsorption in terms of the generated HS or HP surface topography (Table C.1; Ave. f % CV).

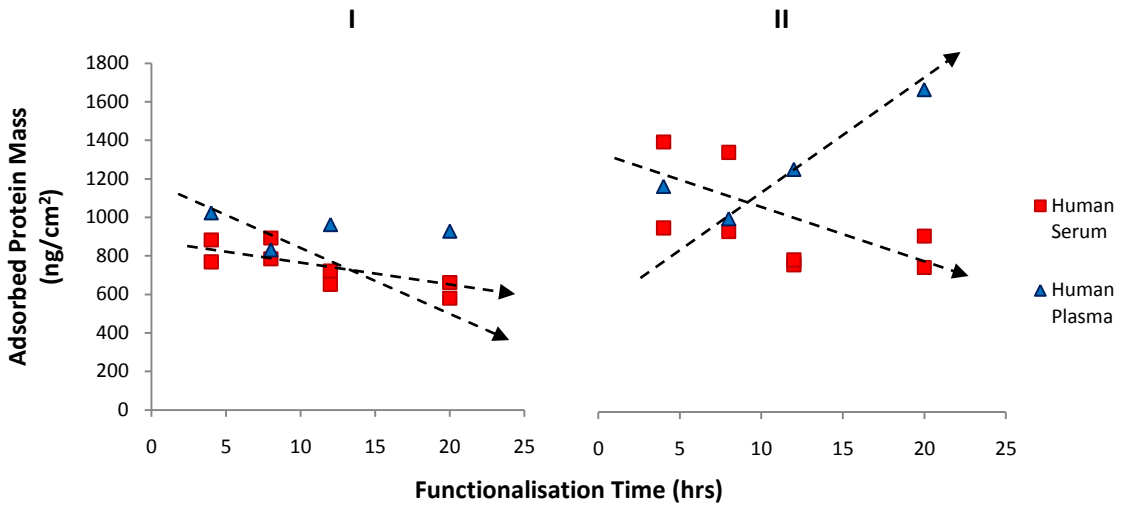

Figure 4.7. Sauerbrey- (I), and Voigt- (II) determined adsorbed human serum (Red) and human plasma (Blue) protein mass to the nitric acid functionalised MWCNT-modified surfaces. Dashed arrows indicate observed trends.

Assessment of the blood protein adsorption as a factor of the deposited protein interface sharpness is illustrated in Figure 4.8 for a:*F*MWCNT-modified surfaces.

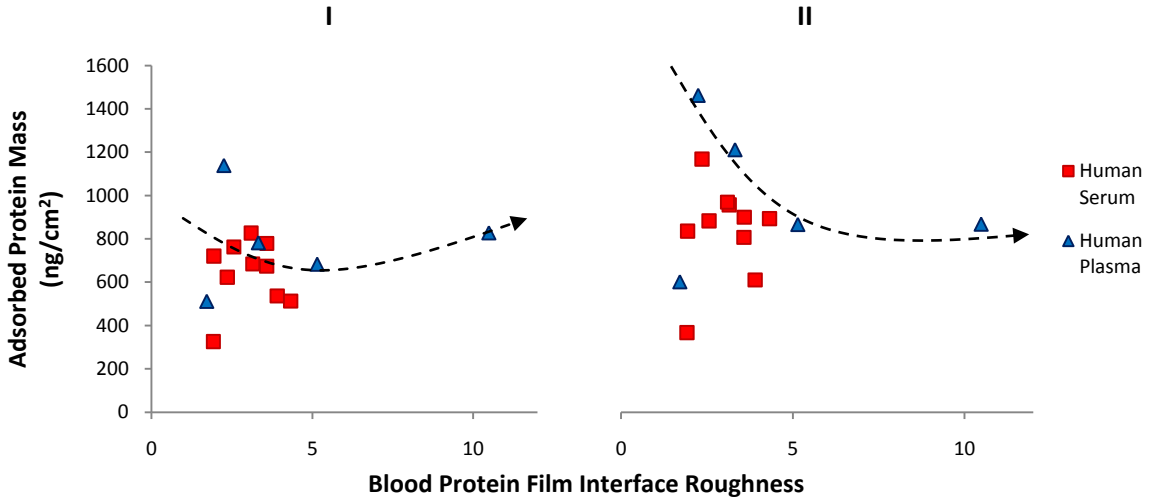

Figure 4.8. Sauerbrey- (I), and Voigt- (II) determined adsorbed human serum (Red) and human plasma (Blue) protein mass to the a:*F*MWCNT-modified surfaces as a function of the blood protein film interface. The blood protein film interface property illustrated is the average *f* percentage coefficient of variation, which is an indication of surface roughness. Dashed arrows indicate observed trends.

The level of HS adsorbed mass (Table 4.1) to the a:*F*MWCNT-modified surfaces appeared to be independent of the film interface topography generated (Table C.1; ave. *f* % CV),

observable by the absence of an apparent trend (Figure 4.8). HP adsorption demonstrated a general decrease in adsorbed mass, with an increase in surface roughness, with the exception of 8 hrs and 24 hrs a:*F*MWCNT samples (Figure 4.8). These deviation from the general trend, exhibited by 8 hrs and 24 hrs sample, may be the result of increased CNT dispersion, therefore generating surface topographies different to those of 2 hrs, 4 hrs and 6 hrs prepared surfaces (Figure 4.2). The topography-dependent adsorption of HP (Figure 4.6 and 4.8) indicates a more nuanced dependence of protein attachment to surfaces than can be tracked using merely bound masses (Figure 4.7).

Both the HS and HP adsorption to the b:*F*MWCNT-modified surface appeared to be independent of the surface topography, with the exception of the 20 hr a: *F*MWCNT sample (Table 4.1). Surface topographies generated by the immobilisation of b:*F*MWCNTs is predicted to be far more complex than that of the a:*F*MWCNTs surfaces, due to the long, thin, unique fibrous networks present in the b:*F*MWCNTs preparations assessed via TEM (Figure 4.4). The surface topography-independent adsorption of blood protein to the b:*F*MWCNTs-modified surfaces is therefore concluded to be an effective means of crudely assessing surface charge and hydrophobicity.

4.3.2.2. QCM-D Monitoring and Quantification of Probe Antibody Binding

The *f* and D shifts observed for the probe antibody binding to the prepared target surfaces, in general, indicated highly viscoelastic films were deposited, therefore suggesting the underestimation of the adsorbed Sauerbrey-determined film parameters (Table C.2). Minimal deductions could be derived from the *f* and D responses alone.

Voigt analysis of the deposition of probe antibody films indicated a general decrease in the viscoelastic film properties, namely viscosity and shear modulus, in comparison to the underlying blood protein film, and varying levels of film hydration (Table 4.2). The anticipated inability of the Voigt-based model to accurately derive the film parameters of the deposited protein layers on the *F*MWCNT-modified surfaces, due to *F*MWCNT-films via Voigt viscoelastic model, therefore inhibits in-depth analysis of the film parameters.

Table 4.2. Sauerbrey and Voigt Modelled Analysis Probe Antibody Binding to Blood Protein Coated *F*MWCNT-modified surfaces

*f*MWCNT [a]	Probe [b]	Sauerbrey Model		Voigt Model				$\frac{\text{Sauerbrey}_m}{\text{Voigt}_m}$ [f]
		Δ Mass (ng/cm^2) [c]	$\frac{\Delta Ab_m}{\Delta BP_m}$ [d]	Δ Viscosity (kg/m.sec) [e]	Δ Shear Modulus (Pa) [e]	Δ Mass (ng/cm^2)	$\frac{\Delta Ab_m}{\Delta BP_m}$	
2 a: *F*MWCNT	Ab_{HSA}	998.49 ±55.86	1.60	Decrease	Increase	719.17	0.62	1.39
	Ab_{C3c}	32.47 ±6.62	0.05	Decrease	Increase	37.72	0.05	0.11
	Ab_{HPF}	197.2 ±15.27	0.17	Decrease	Decrease	320.07	0.22	0.75
4 a: *F*MWCNT	Ab_{HSA}	146.59 ±27.2	0.21	Decrease	Decrease	1325.25	1.38	0.72
	Ab_{C3c}	32.36 ±2.41	0.06	Decrease	Increase	50.34	0.06	0.73
	Ab_{HPF}	209.91 ±18.11	0.27	Decrease	Increase	319.33	0.26	0.86
6 a: *F*MWCNT	Ab_{HSA}	188.53 ±8.71	0.25	Decrease	Decrease	250.51	0.28	0.64
	Ab_{C3c}	70.96 ±7.55	0.09	Decrease	Decrease	94.38	0.10	0.75
	Ab_{HPF}	787.03 ±82.58	0.95	Decrease	Decrease	981.75	1.13	0.73
8 a: *F*MWCNT	Ab_{HSA}	516.14 ±33.02	0.96	Decrease	Decrease	720.15	1.18	0.67
	Ab_{C3c}	97.17 ±9.29	0.12	Decrease	Decrease	132.29	0.14	0.62
	Ab_{HPF}	329.99 ±24.65	0.48	Decrease	Decrease	468.83	0.54	0.66
24 a: *F*MWCNT	Ab_{HSA}	238.52 ±12.4	0.73	Decrease	Decrease	326.91	0.89	0.80
	Ab_{C3c}	81.2 ±5.29	0.11	Decrease	Decrease	121.9	0.15	0.70
	Ab_{HPF}	153.66 ±15.56	0.30	Decrease	Decrease	270.78	0.45	0.57
4 b: *F*MWCNT	Ab_{HSA}	510.8 ±65.52	0.66	Decrease	Decrease	954.18	1.00	0.54
	Ab_{C3c}	63.91 ±5.87	0.07	Increase	Increase	42.35	0.03	0.45
	Ab_{HPF}	1153.89 ±79.32	1.13	Decrease	Increase	1309.08	0.89	0.88
8 b: *F*MWCNT	Ab_{HSA}	237.36 ±37.75	0.30	Decrease	Decrease	532.68	0.57	0.54
	Ab_{C3c}	50.53 ±9.71	0.06	Decrease	Increase	140.22	0.10	1.51
	Ab_{HPF}	184.67 ±26.2	0.22	Decrease	Decrease	443.34	0.44	0.36
12 b: *F*MWCNT	Ab_{HSA}	87.18 ±2.73	0.12	Decrease	Increase	81.32	0.11	0.42
	Ab_{C3c}	27.26 ±14.03	0.04	Decrease	Decrease	65.08	0.08	0.51
	Ab_{HPF}	311.46 ±45.07	0.32	Decrease	Decrease	742.32	0.59	0.61
20 b: *F*MWCNT	Ab_{HSA}	3472.12 ±443.75	5.98	Decrease	Decrease	6405.16	8.58	0.42
	Ab_{C3c}	12.07 ±3.96	0.02	Decrease	Increase	23.48	0.03	0.42
	Ab_{HPF}	1294.77 ±35.50	1.40	Decrease	Increase	1336.38	0.80	0.97

a: *Surface modification molecule*
b: *Probe antibody for the detection of adsorbed HSA (Ab_{HSA}), complement factor C3 (Ab_{C3c}), and HPF(Ab_{HPF})*
c: *Sauerbrey-determined film parameter. Standard deviation is obtained from 3 overtone responses.*
d: *Antibody probe mass as a proportion of total blood protein mass*
e: *Viscoelastic film parameters indicating film rigidity levels*
f: *Indicates level of film hydration*

The total Sauerbrey- and Voigt-determined Ab_{HSA} binding to the a:*F*MWCNT- and b:*F*MWCNT- modified surface are illustrated in Figure 4.9; A and B, respectively. A general decrease in Sauerbrey–determined adsorbed mass, from 2 hr, to 8 hr and 24 hr samples, with an increase in functionalisation time (Figure 4.9; A) was observed, while an increase in probe antibody binding was observed from 4 hr to 8 hr samples. The Voigt-determined adsorbed mass indicated a slight difference in trend, where adsorbed Ab_{HSA} mass decreased from 4 hr, to 8 hr and 24 hr samples, and from 2 hr to 6 hr samples (Figure 4.9; A). This lack of a continuous trend may be either the result of the complex nature of the functionalised MWCNT samples, or the nature of the deposited film. Analysis of Ab_{HSA} binding to the b:*F*MWCNT-modified surfaces indicated a general decrease in both the Sauerbrey- and Voigt-determined adsorbed mass, corresponding to an increase in time, with the exception of the 20 hr sample (Figure 4.9; B). In the case of a:*F*MWCNT-modified surfaces, this decrease

in HSA detection suggests a decrease in HSA binding on increasingly negative surfaces, while the decrease in HSA detection on b:*F*MWCNTs, with increase in functionalisation time, suggests a decrease in HSA binding on increasing exposure of the hydrophobic MWCNT sidewalls, due to increase in CNT dispersion.

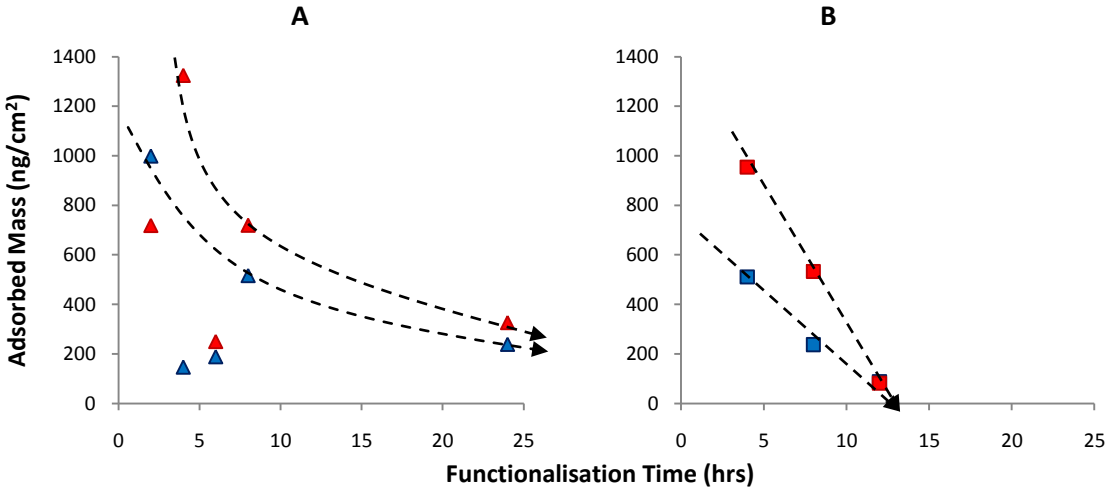

Figure 4.9. Sauerbrey- (Red) and Voigt- (Blue) determined adsorbed anti-human albumin mass to the human serum coated a: *F*MWCNT (A) and b:*F*MWCNT (B) modified surfaces. The 20 hr b:*F*MWCNT preparation was omitted from the figure B. Dashed arrows indicate observed trends.

Due to the complex nature of the *F*MWCNTs, and their subsequent variable immobilisation and blood protein adsorption patterns, it was necessary to assess the antibody adsorption as a proportion of the total adsorbed blood protein, therefore eliminating the level of exposed CNT surface area as an influencing factor in the deposition of blood proteins. This was achieved via assessing the Antibody$_{mass}$/Blood Protein$_{mass}$ (Ab_m/BP_m) value as a function of the functionalisation time (Table 4.2). Figure 4.10 illustrates the Ab_m/BP_m versus functionalisation time for Ab_{HSA} binding. This means of assessment generated similar trends to that observed when assessing total antibody binding. However, a more accurate comparison to the Ab_{HSA} binding results obtained from the analysis of planar surfaces (Chapter 2; Section 2.3.2.3) may be made.

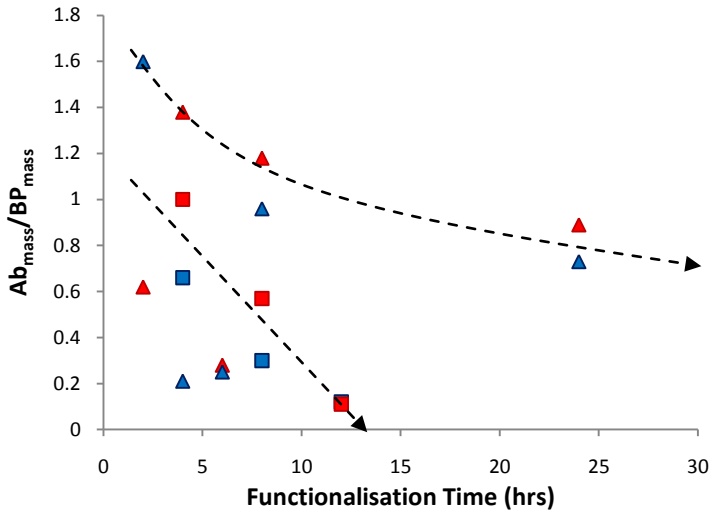

Figure 4.10. Sauerbrey- (Blue) and Voigt- (Red) Determined Anti-Human Albumin Adsorbed Mass to a: *F*MWCNT- (▲) and b: *F*MWCNT- (■) modified surfaces as a Proportion of the Total Human Serum Adsorbed Mass. 20 hrs b: *F*MWCNT was omitted from the figure. Dashed arrows indicate observed trends.

Figure 4.10 illustrates a general decrease in Ab_m/BP_m values, when assessing Ab_{HSA} binding to a:*F*MWCNT-modified surfaces, from the 4 hr to 8 hr, and 24 hr, and from the 2 hr to 6 hrs samples, and Ab_{HSA} binding to a:*F*MWCNT-modified surfaces, from 4 hrs to 8 hrs, and 12 hrs. This means of assessment indicated similar results to that of the total adsorbed probe antibody mass results, and therefore identical conclusions were drawn, where levels of HSA decreased with increasing negative charge (Figure 4.9; A) and hydrophobicity (Figure 4.9; B).

The detected level of HSA absorption, via analysis of Ab_m/BP_m, on *F*MWCNT-modified surfaces, did not exceed that of the positive control (Chapter 2; Section 2.3.2.3), with the exception of the 20 hr b:*F*MWCNTs. The deviation of the 20 hr b:*F*MWCNT preparation from the general trend may be attributed to the high levels of exfoliated amorphous carbon present in solution, following nitric acid functionalisation for an extended period of time. This amorphous carbon may be closely associated with the immobilised *F*MWCNTs, and/or may interact directly with the SAM surface, therefore influencing HS protein adsorption, and subsequent probe antibody binding.

Analysis of the Sauerbrey- and Voigt-determined adsorbed Ab_m/BP_m values, for detection of complement factor C3c, on the a:*F*MWCNTs- and b:*F*MWCNT-modified surfaces are illustrated in Figure 4.11.

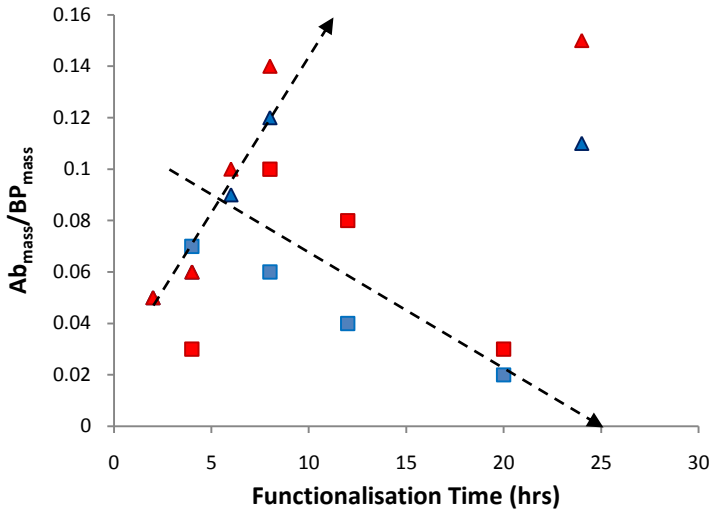

Figure 4.11. Sauerbrey- (Blue) and Voigt- (Red) Determined Anti-Human C3c Adsorbed Mass to a: *F*MWCNT- (▲) and b: *F*MWCNT- (■) modified surfaces as a Proportion of the Total Human Serum Adsorbed Mass.

A general increase in Ab_{C3c} binding, with an increase in functionalisation time, when assessing a:*F*MWCNT-modified surfaces, with the exception of the 24 hr sample (Figure 4.11) was observed. Ab_{C3c} binding to the protein coated b:*F*MWCNT-modified surfaces, on the other hand, demonstrated a general decrease in the antibody adsorbed mass corresponding to an increase in functionalisation time, with the exception of the 4 hr sample.

This increase in Ab_{C3c} binding, and therefore complement C3 detection, when examining a:*F*MWCNT-modified surfaces, with increasing functionalisation time, suggests complement C3 deposition increases with increasing surface negativity, and/or purity, and/or the possible decrease in surface hydrophobicity. However, according to complement factor C3 detection studies on planar surfaces, and literature, a decrease in Ab_m/BP_m value indicates an increase in negative charge on the surface (Chapter 2; Table 2.6), which therefore contradicts the aforementioned increase [40]. One possible explanation for this unexpected occurrence is dependent on the nature of the deposited MWCNT film, in terms of both the surface charge and orientation of the MWCNTs particles. It was proposed that the formation of the

MWCNT aggregates is due to the hydrophobic nature of the nanotube wall and presence of metallic impurities [117]. TEM imaging of the a: *F*MWCNT samples indicated the CNTs were present in the form of rigid rod-shaped aggregates, demonstrating reasonably large tube diameters, which were reduced in size with an increase in functionalisation time (Figure 4.2). In the case of planar deposition of the a:*F*MWCNTs aggregates on the SAM surface, the level of exposed hydrophobic surface is expected to increase with particle dispersion, and therefore with functionalisation time. This increase in surface hydrophobicity corresponds with the experimentally determined increase in Ab_{C3c} adsorption as functionalisation time increases.

The experimentally determined bound Ab_{C3c}, and therefore adsorbed complement C3 levels, deposited on the b:*F*MWCNT surfaces, indicate a decrease in bound complement C3 levels with increase in MWCNT functionalisation time, and therefore increase in negative charge, purity, and/or increase in hydrophobicity (in the case of b:*F*MWCNT-modified surfaces). These results correspond with literature, and preliminary studies of planar surfaces, (Chapter 2; Table 2.6). The levels of Ab_{C3c} bound on the *F*MWCNT-modified surfaces, in terms of Ab_m/BP_m, fall within the range of the positive and negative controls (Chapter 2; Section 2.3.2.3).

The Sauerbrey- and Voigt-determined Ab_m/BP_m value for the deposition of Ab_{HPF} on the *F*MWCNT-modified surfaces are illustrated in Figure 4.12.

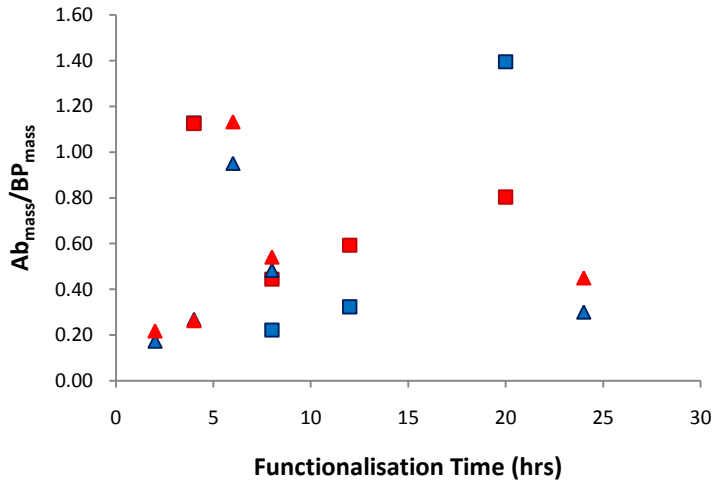

Figure 4.12. Sauerbrey- (Blue) and Voigt- (Red) Determined Anti-Human Fibrinogen Adsorbed Mass to a:*F*MWCNT- (▲) and b:*F*MWCNT- (■) modified surfaces as a Proportion of the Total Human Serum Adsorbed Mass.

A general increase in binding, corresponding with an increase in functionalisation time, for both the *F*MWCNT samples, with the exception of 6 hr and 24 hr a: *F*MWCNT and 4 hr b:*F*MWCNT surfaces were observed. Detected adsorbed HPF levels, in terms of Ab_m/BP_m, did not exceed that of the positive control surface (Chapter 2; Section 2.3.2.3). As indicated in Table 4.4, hydrophobic surfaces (i.e. gold) demonstrate the highest level of Ab_{HPF}/HP binding in comparison to hydrophilic SAM surfaces [35, 36]. The experimentally determined levels of adsorbed HPF are therefore contradictory to the predicted response to decreasing hydrophobicity with increase in functionalisation times.

Surface topography has been indicated as an influential factor influencing the orientation of the fibrinogen molecules on the surface, and therefore the level of detected fibrinogen (Chapter 3; Section 3.3.3.2). The high level of variability in both the a:*F*MWCNT- and b:*F*MWCNT-modified surfaces is therefore a limiting factor in the analysis of HPF interactions with *F*MWCNTs, utilising the proposed method of detection. An additional factor proposed to influence the binding of HPF, and therefore the subsequent Ab_{HPF} , in terms of protein orientation, is that of surface charge density. Figure 4.13 schematically illustrates the proposed HPF orientation on surfaces demonstrates low surface charge density (A), and high surface charge density (B). Initial adsorption of HPF is reported to occur between the HPF αC-domain and the substrate, followed by reorientation of the protein, allowing substrate interaction with the D-domains [28]. In the case of HPF adsorption to surfaces demonstrating low charge density (i.e. low acid functionalised MWCNTs), the planar orientation of the protein is predicted to occur (Figure 4.13; A). However, adsorption of HPF to highly charged surfaces (i.e. highly acid functionalised MWCNTs), the protein is predicted to adopt a V-shaped orientation, where larger portions of the protein are surface exposed, in comparison to the planar orientated molecule (Figure 4.13; B). This higher level of HPF exposure, predicted to occur on surface modified with highly functionalised MWCNT preparations, may explain the increase in Ab_{HPF} bound levels. Although the increase in detected HPF levels is due to the charge characteristics of the *F*MWCNTs, the response is not indicative of the 'real-life' situation, where the CNT preparations are suspended in solution (i.e. blood).

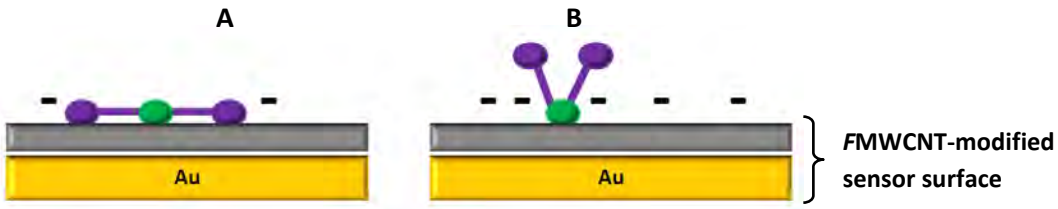

Figure 4.13. Schematic illustration of surface topography on human plasma fibrinogen binding. A, and B illustrates the proposed HPF adsorption to surfaces demonstrating low, and high negative charge density, respectively.

4.4. CONCLUSION

The assessment of HS and HP adsorption to the a:*F*MWCNT-modified surfaces allowed for the crude analysis of the surface hydrophobicity and negative charge. However, the surface topography-dependence was evident when assessing b:*F*MWCNTs. This dependence on surface topography emphasises further analysis of the *F*MWCNT surface is required. This may be achieved by performing preliminary studies on the *F*MWCNT preparations aimed at assessing degree of functionalisation, using Raman Spectroscopy, or via simple acid-base titration techniques [76]. Analysis of the deposition patterns of the *F*MWCNT on the SAM surface, to assess surface topography and aggregation, may be addressed using Atomic Force Microscopy (AFM) and Scanning Electron Microscopy (SEM) [119].

In general, the levels of detected HSA deposited to the *F*MWCNT-modified surfaces corresponded with the predicted outcomes, based on the theoretical-based predictions of the acid functionalisation of MWCNTs. Due to the experimentally determined HSA adsorption results corresponding with the theoretical predictions, the detection of HSA on *F*MWCNT-modified surfaces, using the proposed QCM-D technique, was therefore concluded to be successful in crudely assessing HSA adsorption to nanoparticles. A decrease in Ab_{HSA} binding, and therefore HSA adsorbed, was observed with an increase functionalisation time on both the a:*F*MWCNT- and b:*F*MWCNT-modified surfaces. HSA adsorption is reported to increase the circulation half-life of therapeutic particles, once introduced to the circulatory system [18]. The decrease in adsorbed HSA, as a result of acid functionalisation, is therefore undesirable. The proposed HSA detection method, using QCM-D to monitor subsequent antibody binding, may serve as a useful guide to the extent of

functionalisation (low amounts) which could extend circulation times, as well as aid in the design and development of more biocompatible MWCNT preparations.

As observed with Ab_{HSA} binding, a decrease in Ab_{C3c} binding, corresponding to an increase in functionalisation time, was reported on the surfaces modified with b:*F*MWCNTs, while an increase in Ab_{C3c} was observed on the a: *F*MWCNT-modified surfaces. This decrease in the detection of adsorbed complement factor C3c, on b:*F*MWCNT-modified surfaces, corresponds with literature, which reports carboxyl-bearing surfaces as non-complement activating [40]. Although the increase in Ab_{C3c} observed, with increasing functionalisation time, on a:*F*MWCNT-modified surfaces was unexpected, the occurrence may be explained by the increase in CNT dispersion. The positive correlation between Ab_{C3c} binding, and subsequent detection of the complement activating potential of the *F*MWCNT-films, with the theoretical prediction, suggests the success of the proposed detection method.

The monitoring and quantification of Ab_{HPF} binding to the *F*MWCNT-modified surfaces, for the detection of adsorbed HPF, demonstrated a considerable dependence on the surface topography and charge density. This significant dependence of the immobilisation of the target particles, and the subsequent film surface parameters, suggests the proposed method of HPF detection is not applicable for MWCNT biocompatibility analysis.

CHAPTER 5

METALLOPHTHALOCYANINE-INDUCED CYTOTOXICITY IN MCF-7 CELL LINE

5.1. INTRODUCTION

5.1.1. Metallophthalocyanine Application in Photodynamic Therapy

Metallophthalocyanine complexes have demonstrated biomedical application in the photodynamic treatment of various cancers, namely, lung, stomach, bladder, skin and oesophageal cancer [48]. Therapeutic efficiency of MPc molecules as photosensitising agents is owed to their ability to generate reactive oxygen species upon irradiation with visible light and their proposed selective localisation within tumours [49, 120]. The physical properties of MPc molecules, their application in PDT, and the mechanism of PDT are outlined extensively in chapter 4.

According to literature, cellular uptake and biodistribution of the Pc therapeutic is governed by the physical properties of the molecules, namely the side chain, composition and position, and the nature of the molecules core, i.e. the metal ion [95]. MPc molecules which utilised paramagnetic, or open shell metal ions, such as Cu^{2+}, and Co^{2+} ions, are reported to result in the generation of short triplet lifetimes, therefore rendering the molecule photoinactive. However, MPc molecules with diamagnetic, or closed shell metal ions, such as Al^{3+} and Zn^{2+}, generate high triplet yields, favourable for PDT [121].

Although aggregation poses a problem with MPc PDT efficiency, due to dissipative loss of the electronic energy, this is reported to be hindered via the addition of serum proteins, namely serum albumin [49, 95]. Following intravenous administration, hydrophilic MPc molecules are reported to adsorb serum proteins, in particular serum albumin, which aids in the distribution of the therapeutic within the blood system. Serum albumin, a dominant protein that plays a significant role in drug delivery, binds readily to sulphonated MPc molecules through electrostatic interactions [95, 122]. The administration of hydrophobic MPc

molecules, on the other hand, results in strong binding of lipoproteins, which aids in the selective transport of the therapeutic to malignant tissue [123].

5.1.2. Cytotoxicity of Metallophthalocyanine Molecules

Cytotoxicity of MPc molecules, following irradiation with visible light, has been well documented in literature, however, toxicity studies aimed at particle toxicity, omitting irradiation, to my knowledge, has not yet been a research focus [47, 95, 124-126].

Sulphonated AlPc preparations are currently being utilised as a photosensitising agent for the photodynamic treatment of various cancers [60, 61, 95, 99]. Their toxicity following irradiation exposure, cellular uptake, and biodistribution has been well documented in mammalian cell lines, in particular that of $AlPcS_4$ molecules [47]. Water-soluble $AlPcS_4$ molecules are reported to be free of both systemic and local toxicity, when irradiation is omitted [47, 126]. The degree of sulphonation has been highlighted as playing a significant role in cellular uptake, as an increase in lipophilicity (i.e. decrease in sulphonation) corresponds with an increase in cellular uptake [126]. $AlPcS_4$ molecules are reported to demonstrate poor penetration in cancer cells, and rather accumulate around the tumour in the connective tissue, while $AlPcS_2$ molecules demonstrate efficient penetration, due to their amphiphilic nature when ring substituents are adjacently situated [95, 124].

5.1.3. Chapter Aims and Objectives

Aims

The following studies address MPc-induced cytotoxicity, in the presence of natural light, within the mammalian breast cancer cell line, MCF-7. The central aim was to test the cytotoxicity of the MPc preparations and identify any correlation between the composition of the adsorbed blood protein coat, assessed in chapter 4, with the biological response.

Objectives

1. Identification of MPc Interference with Cytotoxicity Analysis
    a. Spectrophotometric analysis of MPc preparations
    b. Spectrophotometric analysis of MTT and WST-1 cell proliferation assays
2. Validation of the WST-1 cell proliferation assay
3. Assessment of the cytotoxicity, in natural light, of the MPc preparations
4. Analysis of the correlation between serum/plasma protein binding, assessed in chapter 4, and MPc-induced cytotoxicity

5.2. INSTRUMENTATION AND METHODOLOGY

5.2.1. Instrumentation and Additional Reagents

Absorbance of the WST-1 and MTT formazan was measured using a spectrophotometric microplate reader, Powerwave XS (Bio-Tek Instruments, Inc.) at the test wavelength of 460 nm and the reference wavelength of 600 nm. Absorbance spectral scans were performed between 200 nm and 999 nm for the detection of MPc absorbance interference.

MCF-7 human mammary epithelial cells were obtained from the American Type Culture Collection (ATCC). The cells were cultured in a Dulbecco's Modified Eagle Medium (DMEM) obtained from ATCC, medium supplemented with 5% foetal calf serum, 100 U/ml penicillin, 10μg/ml streptomycin, and 25 ng/ml amphotericin B. MPc preparations were initially dispersed in dimethyl sulfoxide (Fluka Chemicals). The cell proliferation reagent, WST-1, and cell proliferation kit, MTT, were obtained from Roche, L-ascorbic acid was purchased from Sigma.

5.2.2. Methodology

5.2.2.1. MPc Preparation

MPc samples were dispersed, via ultrasonication, in DMSO, at a concentration of 1 mg/ml. Dilutions were prepared, ranging between 0 – 10 μg/ml, from the DMSO-stock solution using

DMEM culture media. Ultrasonication was performed following each dilution to ensure complete dispersal of the MPc molecules.

5.2.2.2. Identification of MPc Interference with Cytotoxicity Analysis

5.2.2.2.1. Spectrophotometric Analysis of MPc Preparations

Absorbance spectrophotometric analysis of MPc dilutions prepared in $PBS_{Mg/Ca}$ buffer and $PBS_{Mg/Ca}$-DMEM was carried out to assess the absorbance detection range of the MPc preparations for the identification of possible MPc interference with cytotoxicity analysis.

5.2.2.2.2. Spectrophotometric Analysis of MTT and WST-1 Cell Proliferation Assays

Spectrophotometric analysis of the tetrazoluim salts employed in the MTT (3-[4,5-dimethylthiazol-2-yl]-2,5-diphenyl tetrazolium bromide) and WST-1 (4-[3-(-iodophenyl)-2-(4-nitrophenyl)2H-5-tetrazolio]-1,3-benzene disulfonated) cell proliferation assays were carried out, including analysis of the respective formazan cleavage products. Cell-free reduction of the tetrazolium salts was achieved through the incubation of the tetrazolium salts with L-ascorbic acid, for a period of 1 hr. Ascorbic acid-induced reduction of both the MTT and WST-1 tetrazolium salts has been reported in literature [128, 129]. Prior to the absorbance measurements of the MTT formazan product, the Solubilisation solution, containing 10 % SDS in 0.01 mM HCl, was added and incubated for a period of 1 hr, followed by shaking for 1 min.

5.2.2.3. MCF-7 Culture Preparation

All cell cultures were grown in 75 cm^3 culture flasks and maintained at 37°C under a 9% CO_2 atmosphere. For sample preparation, cells were allowed to grow to near confluence, at which time cells were washed with PBS buffer (pH 7.4). Washed cells were detached from the flasks by treating with trypsin, followed by centrifugation in DMEM growth media. The cell populations were determined via Trypan blue staining, followed by a cell count using a hemocytometer.

5.2.2.4. WST-1 Cell Proliferation Assay

5.2.2.4.1. Validation of WST-1 Cell Proliferation Assay

For the control experiment, cells were seeded at concentrations ranging from 0 - 6 $\times 10^4$ cells/ml into a 96-well microplate plate to a final volume of 100 µl/well, followed by an incubation at 37°C and 9% CO_2, for a period of 48 hrs. WST-1 Cell Proliferation Reagent was introduced (10 µl/well) and the samples were incubated for a further 6 hrs. Absorbance of the samples was measured at 460 nm (reference λ = 600 nm), following shaking for 1 min.

Analysis of interference of the MPc sample preparation with the WST-1 assay efficiency was assessed through performing WST-1 cell proliferation assays of cell-free samples containing MPc concentrations ranging from 0 – 10 µg/ml. Prepared MPc samples were added to the microplate wells, to give a final volume of 100 µl/well. WST-1 reagent was introduced and incubated for a further 6 hrs. Absorbance of the samples was measured at 460 nm (reference λ = 600 nm), following shaking for 1 min.

5.2.2.4.2. Cytotoxicity Analysis of MPc Preparations

For the study of MPc-induced cytotoxicity, cells were seeded into 96-well microplates at a concentration of 6 $\times 10^3$ cells/well, to a final volume of 50 µl/well. Prepared sample plates were incubated at 37°C and 9% CO_2, for a period of 48 hrs. Following the incubation prepared MPc samples were added, to give a final volume of 100 µl/well. The samples were incubated for a period of 48 hrs under the prior conditions. The wells were emptied and flooded with DMEM culture media, which was subsequently cleared, to remove residual MPc molecules. WST-1 reagent was added, in a 1:11 dilution with DMEM to result in a final volume of 110 µl/well, and incubated for a further 6 hrs. Absorbance of the samples was measured at 460 nm (reference λ = 600 nm), following shaking for 1 min. % MCF-7 survival was calculated with respect to the absorbance intensity of the MPc-free cell sample, which was designated 100 %. The concentration of the MPc molecules which resulted in half the maximal response (IC_{50}) was calculated from the trendline linear equation ($y = mx + c$), where y was designated the value of 50, and x was determined.

5.3. RESULTS AND DISCUSSION

Section 5.3.1. investigates MPc interference that may be encountered when assessing cytotoxicity using colourimetric-based assays, namely WST-1 and MTT cell proliferation assays. Section 5.3.2. addresses the WST-1 cell proliferation assay validation. Section 5.3.3. reports on the MPc-induced cytotoxicity recorded using the WST-1 cell proliferation assay, and section 5.4.4. examines the correlation between human serum albumin and complement factor C3 binding levels, detected using QCM-D, and the results obtained from the cytotoxicity analysis.

5.3.1. Identification of MPc Interference with Cytotoxicity Analysis

5.3.1.1. Spectrophotometric Analysis of MPc Preparations

Absorbance spectral scans were performed on the MPc preparations, dispersed in $PBS_{Mg/Ca}$-DMEM, to determine the absorbance ranges of the MPc molecules. Figure 5.1 illustrates the absorbance spectra recorded for the target MPc preparations, namely, $AlPcS_{mix}$, $CoPcS_{mix}$, CuTSPc, $GePcS_{mix}$, $ZnPcS_{mix}$, and CoTCPc. The spectrophotometric analysis identified B-band and Q-band absorbance peaks ranging from approximately 240 nm - 440nm, and 500 nm - 800 nm, respectively [95, 124]. The presence of absorbance peaks identifies the wavelength range in which MP-interference will occur when using an absorbance-based detection assay. However, the $CoPcS_{mix}$, CuTSPc, and CoTCPc preparations indicated minor absorbance, of approximately 0.100, within the wavelength range of 440 nm – 500 nm. This occurrence suggests MPc-interference is unavoidable when utilising an absorbance-based assay to assess MPc-induced cytotoxicity of $CoPcS_{mix}$, CuTSPc, and CoTCPc. It was therefore concluded that an optimum assay, which would experience the lowest level of MPc interference, would demonstrate a detection range between 440 nm and 500 nm.

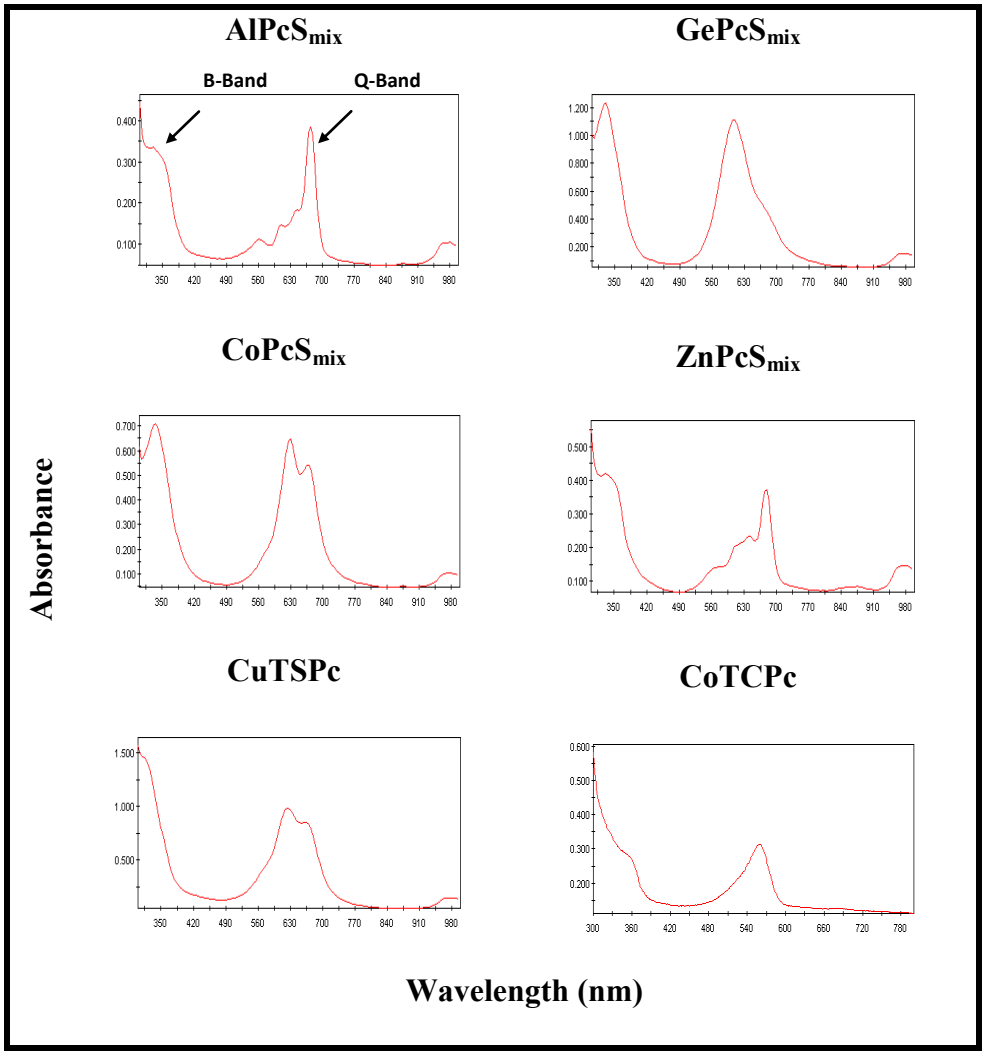

Figure 5.1. Absorbance spectral scans of MPc preparations prepared in PBS$_{Mg/Ca}$-DMEM. Spectrophotometric analysis performed to determine the absorbance detection ranges of the MPc preparations.

5.3.1.2. Spectrophotometric Analysis of MTT and WST-1 Cell Proliferation Assays

Spectrophotometric analysis of both the WST-1 and MTT tetrazolium salts, and their respective formazan cleavage products, was performed to aid in the selection of an optimum cell proliferation assay, in terms of MPc absorbance interference, for the examination of MPc-induced cytotoxicity. Figure 5.2 illustrates the absorbance spectra of the relevant compounds solubilised in DMEM. With respect to the tetrazolium salts, both the WST-1 and MTT reagents demonstrated low intensity peaks at approximately 560 nm. In addition, the WST-1 cleavage product spectral scan indicated an absorbance peaks at 438 nm, which demonstrated a peak range between 350 nm and 600 nm, while the MTT product indicated an absorbance peak at 567 nm, ranging between 400 nm and 650 nm. These absorbance ranges

correspond with literature which reports the optimum detection of the formazan product is achieved between 420 nm and 480 nm when using the WST-1 reagent, and between 550 nm and 600 nm when using the MTT reagent.

According to the required specifications of a colourimetric assay intended for MPc use, outlined in section 5.3.1.1, an optimum assay would demonstrate an absorbance detection range between 440 nm and 500 nm. The use of the MTT cell proliferation assay was therefore concluded as an unreliable means of analysing sulphonated MPc cytotoxicity, as the detection wavelength of the formazan product occurs within the Q-band range of the MPc spectral scans (500 nm – 800 nm). This was an unexpected occurrence as the application of the MTT assay, for the analysis of sulphonated MPc-induced cytotoxicity, has been well documented in literature [129-131]. Use of the WST-1 cell proliferation assay for the analysis of MPc-induced cytotoxicity was favoured for the application in these studies.

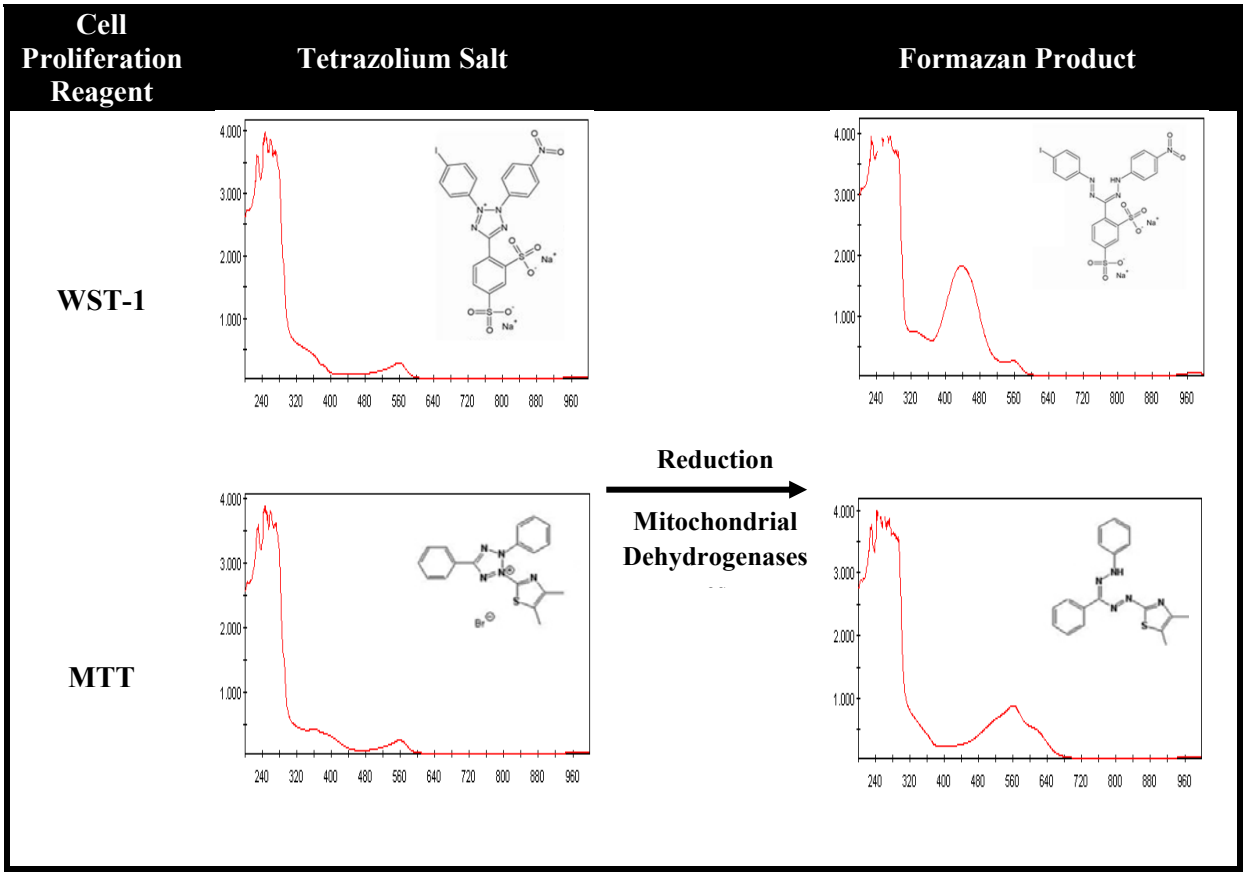

Figure 5.2. Absorbance spectrophotometric analysis of the tetrazolium salts, and the respective cleavage products, employed in the WST-1 and MTT cell proliferation assays.

5.3.2. Validation of WST-1 Cell Proliferation Assay

MCF-7 Cell Proliferation Analysis

Analysis of MCF-7 cell proliferation was performed to validate the WST-1 cell proliferation assay. As illustrated in figure 5.3, an increase in the absorbance intensity, at 460 nm, with an increase in cell population was observed. The tetrazolium salt (WST-1) is cleaved to produce water-soluble formazan, via mitochondrial dehydrogenase activity, therefore allowing the spectrophotometric detection of metabolically active cells through the measuring of the latter product. An increase in the formazan product, and therefore absorbance intensity at 460 nm, is an indication of an increase in the number of viable cells/well [49]. The experimentally determined correlation between the absorbance intensity and the cell concentration corresponds with the theoretical prediction.

MCF-7 cells were chosen due to their availability, great range of pathophysiological changes, and high sensitivity [132]. The utilisation of a cancer cell line was favoured in this study as PDT is directed towards cancer treatment, as well as the fact that MPc molecules are reported to retain preferentially within malignant tumours [61].

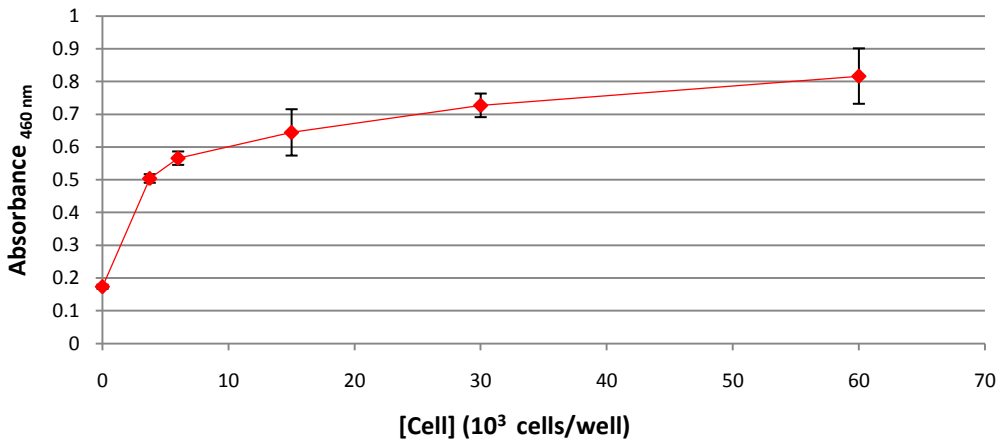

Figure 5.3. MCF-7 cell proliferation studies using Cell Proliferation Reagent WST-1. Absorbance intensity, at 460 nm, measuring the level of WST-1 formazan cleavage product, and therefore cell viability, assessing increasing concentrations of MCF-7 cells. The absorbance intensity was measured for the cell population range from $0 – 6 \times 10^3$ cells/well. Error bars represent standard deviation (n = 3).

Analysis of Sample Preparation Influence

Investigation into the influence of the MPc preparations, dispersed in DMSO/DMEM, was achieved through performing the WST-1 cell proliferation assay in the absence of MCF-7 cells. Figure 5.4. indicates the absorbance intensities recorded at 460 nm for these procedures. Absorbance analysis reported fairly stable absorbance intensities for the $AlPcS_{mix}$, $GePcS_{mix}$, and $ZnPcS_{mix}$ preparations over the selected concentration range, while slight concentration-dependent shifts in absorbance intensity were recorded for $CoPcS_{mix}$, CuTSPc, and CoTCPc preparations. In addition, the absorbance spectra of the MPc preparations in $PBS_{Mg/Ca}$-DMEM (Figure 5.1) suggested absorbance interference, at 460 nm, when assessing $CoPcS_{mix}$, CuTSPc, and CoTCPc preparations. This occurrence suggests the concentration-dependent shifts, observed in figure 5.4., are the result of the presence of the MPc molecules within the sample, rather than an interaction between the WST-1 tetrazolium salt. However, these MPc-induced shifts in absorbance intensity are expected to have little influence over the MPc MCF-7 cytotoxicity analysis, as the MPc-free cellular induced formazan absorbance intensity is reported as approximately 0.57, when assessing 6×10^3 cells/well (Figure 5.1). In addition, a dose-dependent change in the absorbance of WST-1, with increasing MPc concentration was not observed. MPc-induced interference was therefore concluded to be negligible.

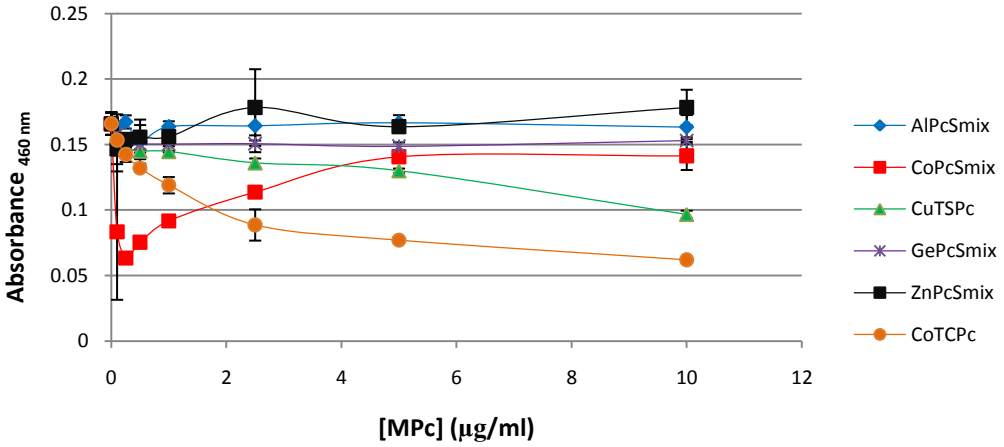

Figure 5.4. Analysis of MPc interference with WST-1 cell proliferation assay efficiency. The absorbance intensity at 460 nm was recorded following incubation of the MPc preparation with the WST-1 reagent. Error bars represent standard deviation (n = 3).

Assessment of the effect of DMSO addition to the cell culture samples revealed the solvent demonstrated minor cytotoxicity over cell induced absorbance intensity at 460 nm, when assessing the lower concentrations, however, little, or no interference was reported at concentrations higher than 0.5 µl/ml (v/v) (Figure 5.5.). DMSO usage in cell culture analysis has been well documented, and has been reported to be highly suitable for use with MTT assays [133, 134]. The usage of both DMSO and serum proteins has demonstrated an improvement in the detection of MTT formazan generated by cell cultures. However, DMSO grade, and storage conditions, namely exposure to air, has been suggested to negatively influence absorbance, and therefore detection of the MTT formazan dye [134]. The latter may be an explanation for the deviating absorbance of the WST-1 formazan product when MCF-7 cells are supplemented with DMSO dilutions. The absorbance trend of the DMSO supplemented cells, in terms of percentage MCF-7 viability, was utilised as a comparison when assessing the cytotoxicity of each MPc preparation.

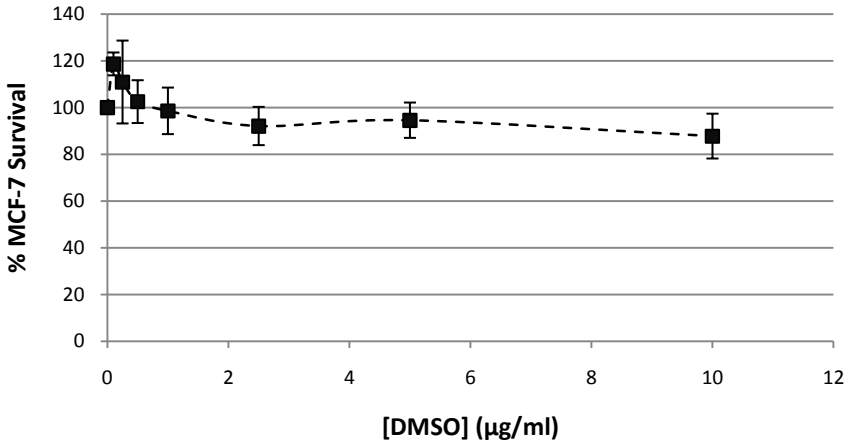

Figure 5.5. Analysis of the effect of DMSO on cell viability as measured by WST-1 cell proliferation assay efficiency. The absorbance intensity at 460 nm was recorded following incubation of the DMSO supplemented cell preparation with the WST-1 reagent. Error bars represent standard deviation (n = 3).

5.3.3. MPc-Induced MCF-7 Cytotoxicity

$AlPcS_{mix}$-Induced Cytotoxicity

Analysis of $AlPcS_{mix}$-induced cytotoxicity in MCF-7 cells revealed fluctuations in percentage survival following administration of low MPc concentrations (Figure 5.6). Both the presence of the organic solvent, DMSO, and serum protein supplemented DMEM culture media, are

reported to increase monomerisation of the MPc molecules in solution [49, 95, 136]. According to the QCM-D analysis of $AlPcS_{mix}$-modified SAM surfaces, high levels of human serum (HS) protein adsorption, 1034.12 ng.cm^{-2} – 1233.86 ng.cm^{-2}, were detected to deposit at this surface (Chapter 4; Section 4.3.3). This high degree of serum protein adsorption, together with the low levels of MPc concentration, and therefore high protein to MPc ratio, may provide an explanation for the varying percentage survival at low MPc concentrations, as the higher protein to MPc ratio is expected to decrease MPc aggregation. An increase in MPc monomerisation may influence cellular toxicity, firstly via increasing the photoactivity of the MPc molecules, and/or secondly, via increasing the proportion of the MPc preparation available for cellular uptake [135, 136]. This reasoning was applied to the remainder of the MPc cytotoxicity analyses to explain percentage survival fluctuations at low MPc concentrations. Slight decreases in the percentage MCF-7 survival were recorded at MPc concentrations of 2.5 µg/ml (85.95 ±9.70 %) and 5 µg/ml (91.52 ±12.57 %), however, the trend observed over the MPc concentration range, 0 – 10 µg/ml, appears to be similar to that observed when assessing DMSO supplemented cells, therefore suggesting the $AlPcS_{mix}$ preparation was not cytotoxicy, or at least cytostatic. This corresponds with literature as sulphonated AlPc preparations are reported as non-toxic under conditions eliminating irradiation, and are currently being utilised for their biomedical application in the photodynamic treatment of various cancers [104]. A means of examining the influence of ambient light within the current study would be to assess cytotoxicity under conditions eliminating light completely.

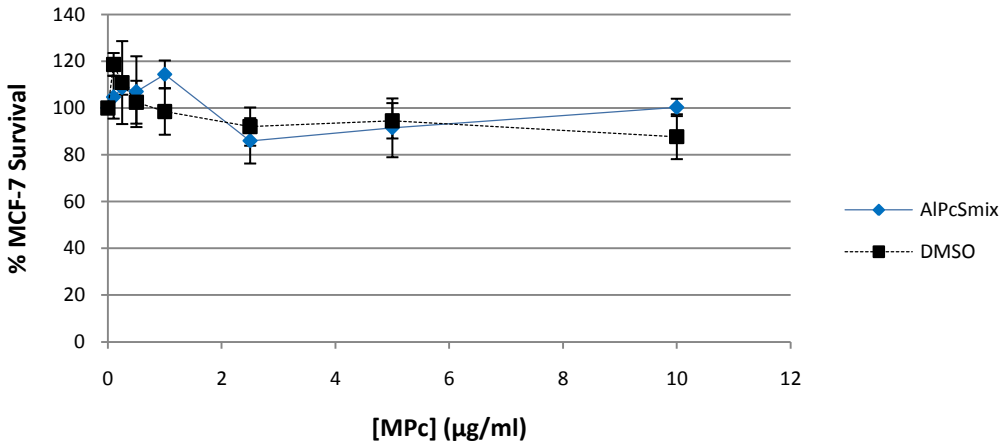

Figure 5.6. $AlPcS_{mix}$-induced cytotoxicity in MCF-7 cell line. MPc preparations were prepared in DMSO and DMEM culture media. The MCF-7 cell population utilised was 6×10^{-3} cells/well. Absorbance intensity was measured at 460 nm. The error bars represent standard deviation (n = 3).

Insufficient studies have been reported in literature utilising the remainder of the MPc molecules assessed in this study, in terms of the exact chemical structure (i.e. metal core coupled with ring substitutions) to make comparison with the cytotoxicity results obtained in the current study. The following studies are therefore novel, in terms of both the MPc molecules assessed and the cell line utilised.

Modified and Unmodified CoPc-Induced Cytotoxicity

As observed with low concentrations of $AlPcS_{mix}$, fluctuations in percentage survival were recorded for all three samples, namely, CoPc, $CoPcS_{mix}$ and CoTCPc (Figure 5.7). QCM-D analysis of $CoPcS_{mix}$ and CoTCPc-modified SAM surfaces reported HS protein adsorption of approximately 875.82 $ng.cm^{-2}$ – 1010.97 $ng.cm^{-2}$, and 136.04 $ng.cm^{-2}$ – 1649.55 $ng.cm^{-2}$, on each surface, respectively. As previously discussed the high level of HS adsorption is predicted to result in MPc monomerisation, therefore affecting cellular uptake and increasing the MPc photoactivity. The CoPc samples demonstrated an increase in percentage MCF-7 survival in comparison to $CoPcS_{mix}$ and CoTCPc samples, between the concentration range of 1 μg/ml and 10 μg/ml. Furthermore, similar percentage survival trends were observed, over the selected MPc concentration range, for the modified and unmodified CoPc preparations. Although the modified CoPc molecules demonstrated a slightly more cytotoxic effect in comparison to the unmodified CoPc molecules, the percentage survival trends observed were similar to that observed when assessing the influence of DMSO, therefore suggesting the molecules were cytostatic. The variations in the cytotoxicity reported for the three CoPc preparations, although slight, highlight the potential effect of ring substitution on toxicity.

For this study, it was proposed that the addition of negatively charged ring substitutions to the MPc molecules results in an increase in the cytotoxicity. This increase in cytotoxicity highlights a concern regarding the biomedical application of MPc molecules. For intravenous administration of an MPc therapeutic, the particles are required to be hydrophilic in nature [50]. MPc hydrophilicity, and therefore solubility, is dependent on ring subsititution.

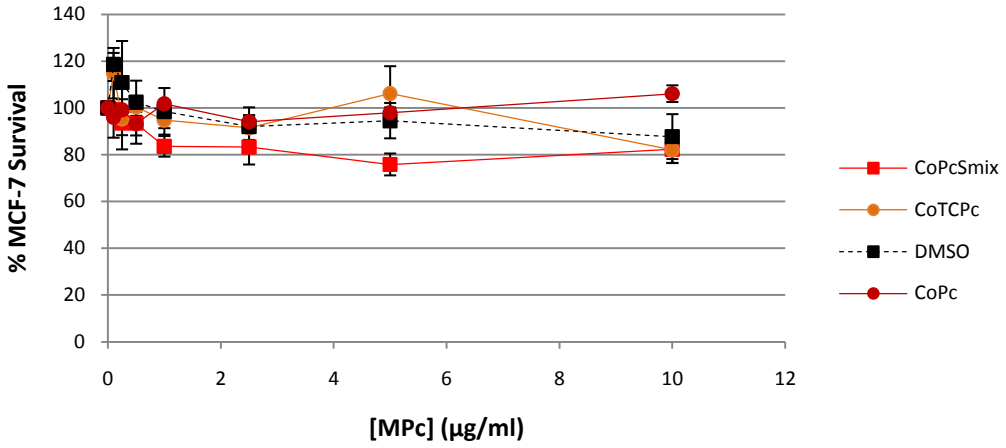

Figure 5.7. Cytotoxicity of modified and unmodified CoPc's in MCF-7 cell line. MPc preparations were prepared in DMSO and DMEM culture media. The MCF-7 cell population utilised was 6×10^{-3} cells/well. Absorbance intensity was measured at 460 nm. The error bars represent standard deviation (n = 3).

MPc molecules composed with Co^{2+} metal ions as the central core have been demonstrated to produce short triplet lifetimes, therefore highlighting their inefficiency as a PS agent in the photodynamic treatment of cancer [5]. The inclusion of the non-substituted CoPc in the toxicity studies was performed to assess the influence of the ring substitutions on MCF-7 cytotoxicity.

CuTSPc-Induced Cytotoxicity

Cytotoxicity analysis of the CuTSPc preparations indicated minor decreases in MCF-7 cell viability occurred at low MPc concentration (Figure 5.8). Analysis of HS adsorption to CuTSPc-modified SAM surfaces, via QCM-D analysis, indicated protein adsorption ranging between 867.90 $ng.cm^{-2}$ and 1093.89 $ng.cm^{-2}$. It was therefore concluded that the variations in cell viability, as a result of low concentrations of CuTSPc, may be due to an increase in monomerisation of the molecules within the DMSO supplemented DMEM growth media, as previously stated. The general trend of the percentage MCF-7 survival curve indicated a slight increase in cell viability corresponding to an increase in CuTSPc concentration, similar to that of the trend recorded for DMSO supplemented cells. It was therefore concluded that

the CuTSPc preparation was non-toxic up to the concentration of 10 µg/ml. As stated with CoPc molecules, CuPc molecules generate short triplet lifetimes, and are therefore not favoured for application in PDT [121].

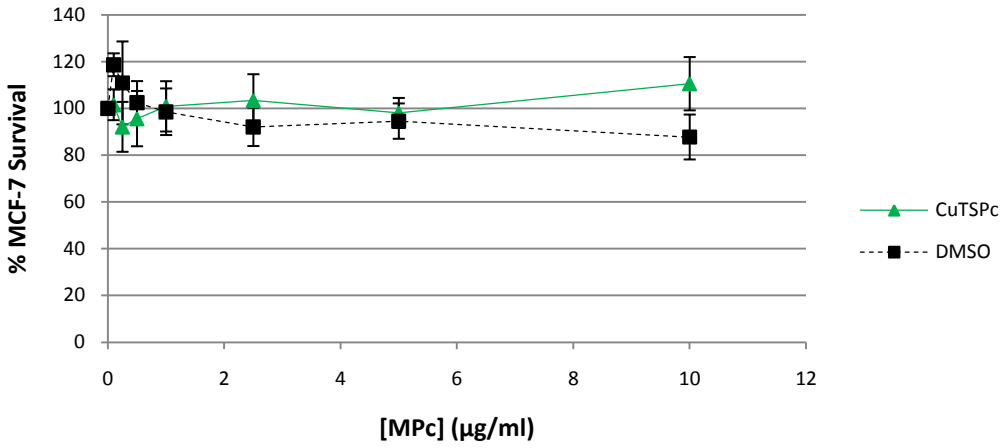

Figure 5.8. CuTSPc-induced cytotoxicity in MCF-7 cell line. MPc preparations were prepared in DMSO and DMEM culture media. The MCF-7 cell population utilised was 6×10^{-3} cells/well. Absorbance intensity was measured at 460 nm. The error bars represent standard deviation (n = 3).

$GePcS_{mix}$-Induced Cytotoxicity

According to the WST-1 cytotoxicity analysis, $GePcS_{mix}$ samples demonstrate no cytotoxicity, up to a concentration of 10 µg/ml (Figure 5.9). However, an increase in MPc concentration corresponded with a general decrease in cell viability, demonstrating a similar trend to the DMSO response, therefore suggesting $GePcS_{mix}$ as being non-toxic, or cytostatic. QCM-D analysis of HS protein binding to $GePcS_{mix}$-modified SAM surfaces reported high levels of protein binding, approximately 933.99 $ng.cm^{-2}$ – 113.59 $ng.cm^{-2}$. These high levels of HS protein coating suggest monomerisation may have attributed to the deviations if percentage MCF-7 cell survival at low MPc concentrations. $GePcS_{mix}$ preparations have been reported to demonstrate photophysical and photochemical behaviour superior to that of other $MPcS_{mix}$ samples, including that of $AlPcS_{mix}$ [137]. The cytostatic nature of the $GePcS_{mix}$, in natural light, is an excellent feature of the molecule, which would promote its use in biomedical applications, as unintentional photoactivation of the molecule would be avoided, therefore decreasing the photosensitivity side-effect [58].

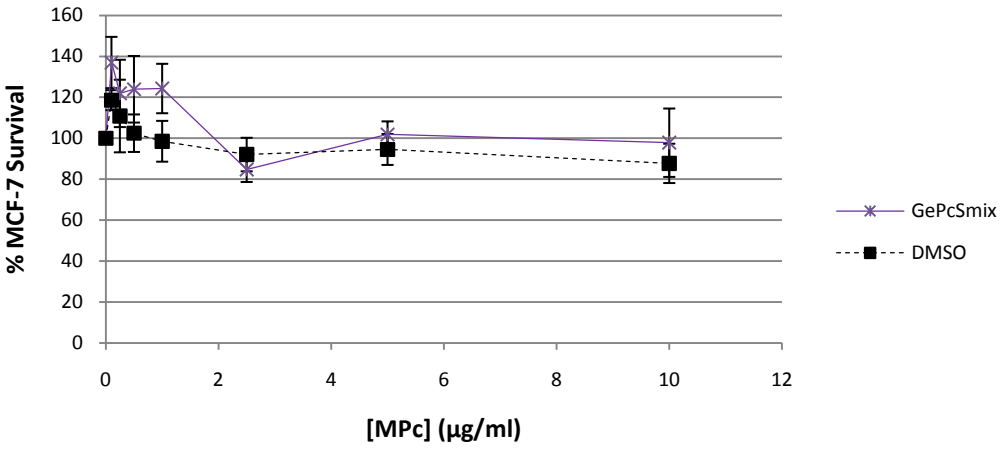

Figure 5.9. $GePcS_{mix}$-induced cytotoxicity in MCF-7 cell line. MPc preparations were prepared in DMSO and DMEM culture media. The MCF-7 cell population utilised was 6×10^{-3} cells/well. Absorbance intensity was measured at 460 nm. IC_{50} was recorded to be 6.6 µg/ml. The error bars represent standard deviation (n = 3).

$ZnPcS_{mix}$-Induced Cytotoxicity

According to WST-1 assay results (Figure 5.10), $ZnPcS_{mix}$ demonstrated a concentration-dependent decrease in the percentage MCF-7 cell survival, therefore suggesting the MPc preparation as being cytotoxic. The IC_{50} of the viability curve was determined to be 6.58 µg/ml. The effective dose concentration of encapsulated ZnPc molecules, for the *in vivo* application in PDT, in human test subjects, has been reported to be as low as 35 µg/kg [28]. Assuming the average weight of an individual is 70 kg, and on average there is 4.7 L of blood within the body, the average dose concentration administered would be approximately 0.52 µg/ml. This is well below the *in vitro* IC_{50} recorded for $ZnPcS_{mix}$ cytotoxicity. While sulfonated ZnPc preparations have been assessed, in terms of their application as PS agent in the photodynamic treatment of cancer, little is reported on their influence on cellular cultures, in particular, cytotoxicity [61, 121].

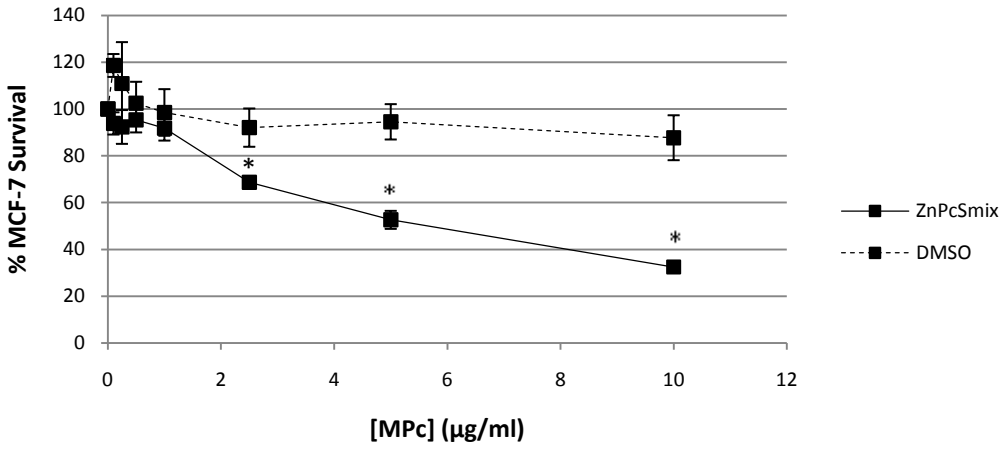

Figure 5.10. $ZnPcS_{mix}$-induced cytotoxicity in MCF-7 cell line. MPc preparations were prepared in DMSO and DMEM culture media. The MCF-7 cell population utilised was 6×10^{-3} cells/well. Absorbance intensity was measured at 460 nm. The error bars represent standard deviation (n = 3). Comparison with unpaired student t-test of % MCF-7 survival with DMSO versus MPc ($p = 0.01$).

5.3.4. Comparison Between MPc Protein Binding Analysis and Cytotoxicity Studies

MPc-induced cytotoxicity results generated from the WST-1 cell viability assay were assessed against the protein analysis results obtained utilising QCM-D technology (Chapter 4). A comparison with the fibrinogen studies was unachievable due to the culture media being supplemented with serum, which is prepared from plasma through the removal of fibrin and other clotting factors [138].

A comparison between the detected antibodies bound to the HS coat adsorbed to MPc-modified surfaces, namely Ab_{C3c} and Ab_{HSA}, and the cell viability of MCF-7 cells following incubation with 10 µg/ml of MPc preparations, indicated no apparent link between the composition of the adsorbed protein coat and cellular toxicity (Figure 5.11 and 5.12). This lack of correlation suggests one of three things, firstly, the influence of the adsorbed protein composition on biocompatibility is far more complex to be predicted through the adsorption of just two proteins. Secondly, photoactivation of the MPc molecules, by natural light, may have played a role in the generation of cytotoxicity, and thirdly, the cytotoxicity analysis using cell proliferation assays may not be an accurate representation of the MPc-induced biological effects. Analysis of the effects of MPc photoactivation, in the presence of

ambient light, may be achieved through performing the WST-1 cytotoxicity assays under conditions where light is removed completely. In the event of cytotoxicity still being observed, MPc photoactivation-induced cytotoxic effects may be eliminated as a possible cause of toxicity. Analysis of the influence of the protein coat complexity, and the accuracy of the WST-1 cytotoxicity investigations may be achieved utilising *in vivo* analysis.

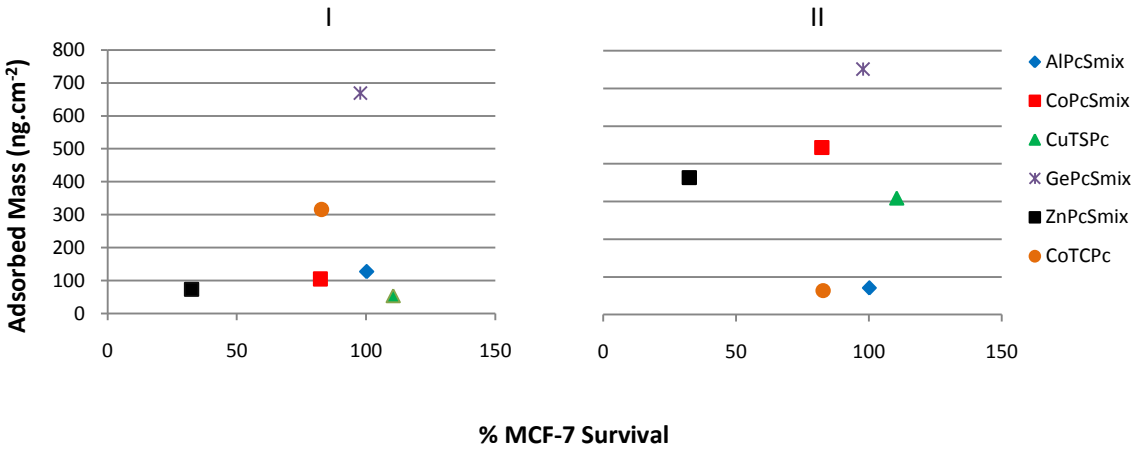

Figure 5.11. Comparison between Sauerbrey-determined adsorbed antibody mass and the percentage cell survival of MCF-7 cells following the administration of MPc preparations. Adsorbed anti-human C3c and anti-human albumin are represented by I and II, respectively. The MPc concentration administered was 10 µg/ml.

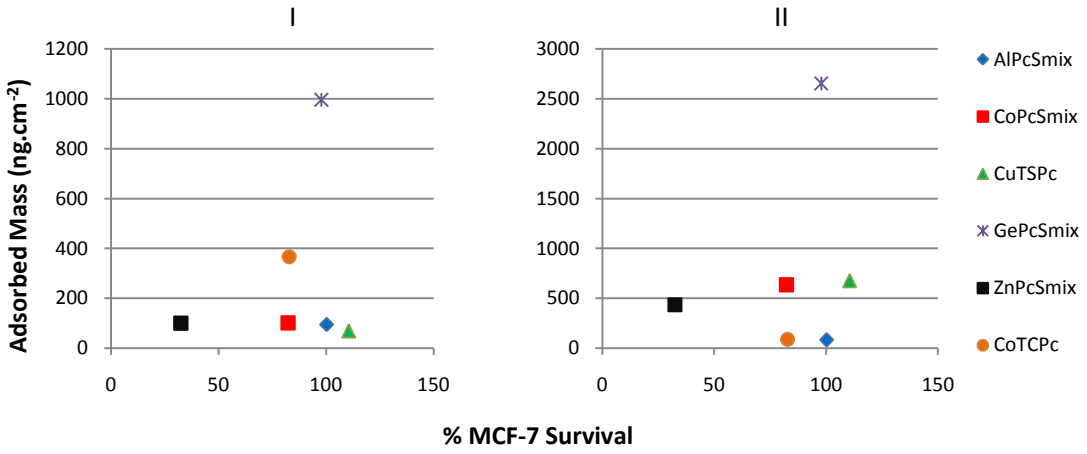

Figure 5.12. Comparison between Voigt-determined adsorbed antibody mass and the percentage cell survival of MCF-7 cells following the administration of MPc preparations. Adsorbed anti-human C3c and anti-human albumin are represented by I and II, respectively. The MPc concentration administered was 10 µg/ml.

5.4. CONCLUSION

Cytotoxicity analysis of MPc preparations, using the Cell Proliferation Reagent WST-1, indicated high levels of cytotoxicity generated by the $ZnPcS_{mix}$ preparations, where an IC_{50} of 6.58 μg/ml was calculated. A large MPc concentration-dependent decrease in cell viability was observed when assessing 10 μg/ml of $ZnPcS_{mix}$ preparations (-65.40 %), followed by minor cytotoxicity levels for $GePcS_{mix}$ (-28.60 %), CoTCPc (-28.58 %), $CoPcS_{mix}$ (17.13 %), and no detection of cytotoxicity for $AlPcS_{mix}$ (-4.18 %). Incubation with CuTSPc preparations, however, resulted in an increase in cell viability (+ 8.86 %), suggesting minor MPc-induced growth. The cytostatic nature recorded for $AlPcS_{mix}$ preparations corresponds with literature, as $AlPcS_n$ preparations have been utilised in biomedical applications [47].

Although cytotoxicity was recorded for $ZnPcS_{mix}$, and minor cytotoxicity for $GePcS_{mix}$, $CoPcS_{mix}$ and CoTCPc, it was unclear whether toxicity was a result of the presence of the MPc molecules, or in fact, activation of the molecules, by natural light, to generate toxic reactive oxygen species. Further studies would have to be performed, aimed at assessing cytotoxicity, while eliminating natural light. Another means of assessing photoactivation of the MPc preparations in natural light involves the assessment of the generation of reactive oxygen species. These studies may be carried out using photometric detection methods aimed at investigating the superoxide anion and singlet oxygen concentrations [139].

Analysis directed at examining the link between adsorbed serum proteins and cytotoxicity were inconclusive, therefore raising further questions regarding biocompatibility of MPc molecules. It is well understood that the composition of the protein coat adsorbed to therapeutic particles, in terms of protein identity, adsorption pattern, and amount, govern the biological responses generated, namely biodistribution and biocompatibility. A means of assessing the influence of the serum protein coat on the cytotoxicity assay analysis includes performing the cytotoxicity analysis on MPc preparations in serum free DMEM, or varying concentrations of the serum supplemented DMEM. However, further knowledge of the protein kinetics, affinities, as well as the stoichiometry of both adsorbed and free protein appears to be essential when developing a method aimed at biocompatibility prediction through protein adsorption analysis [92].

CHAPTER 6:

OVERALL CONCLUSIONS

The aim of the current study was to design a rapid means of assessment, using QCM-D technology, for target particle biocompatibility, in terms of identifying key influential proteins present in the blood protein corona adsorbed to the biomaterial surface. The target proteins of interest included, human serum albumin (HSA), complement factor C3c, and human plasma fibrinogen (HPF). HSA, a dysopsonin, adsorption to biomedical surfaces has been of particular interest, with regards to biocompatibility analysis in reported studies, as its adsorption governs the circulation half-life of the proposed therapeutic within the biological system [18]. In addition, HSA adsorption has been reported to limit further blood protein binding, including opsonin proteins such as complement C3 and fibrinogen, therefore hindering the activation of the complement and coagulation cascades [38]. High levels of adsorbed HSA on biomedical surfaces is therefore favourable, in terms of haematocompatibility.

Complement factor C3, and therefore complement C3c, adsorption on biomedical surfaces, however, is an unfavourable occurrence, as it is indicative of complement activation. This activation of the complement system suggests the uptake of the therapeutic by the mononuclear phagocyte system (MPS), resulting in interference with the biodistribution and efficiency of the therapeutic, in addition to the potential to generate negative side effects, such as hypersensitivity and anaphylaxis [9]. Similarly, high levels of HPF adsorption indicates coagulation cascade activation, and therefore the potential of the biomedical surface to induce the formation of blood clots and subsequent occlusion of the blood vessels [42-44]. Adsorption of both complement C3, and HPF, is therefore unfavourable when designing a therapeutic intended for intravenous administration.

The assessment of the above mentioned favourable and unfavourable blood protein adsorption patterns on surfaces intended for biomedical application, was proposed to serve as a crude but rapid means of biocompatibility analysis.

Preliminary analysis of probe antibody detection of target proteins, on generic biomedical surfaces, indicated higher levels of HSA on hydrophilic SAM surfaces (Cyst And 11-AUT), in comparison to the unmodified SiO_2 and gold (Chapter 2; Section 2.3.3.2). Similarly, HPF analysis indicated higher adsorbed protein levels on Cyst and 11-AUT SAM-modified surfaces, in comparison to the unmodified SiO_2. Complement C3 indicated a binding trend which favoured more hydrophobic surfaces, over hydrophilic ones. It was concluded, from the preliminary protein detection analysis, that HSA adsorption is influenced by surface charge, while HPF adsorption demonstrates a dependence on surface topography. Reproducibility analysis, of probe antibody binding, suggested detection of complement C3 as the most reproducible (Sauerbrey: 9.15 % CV; Voigt: 5.05 % CV) of the three analyses, possibly attributed to by the small size of the target protein. The lower reproducibility of HSA and HPF detection was proposed to be the result of target protein conformational change, and variability of adsorbed protein orientation, due to surface topography, respectively (Table 2.6). The experimentally determined binding trends observed aided in the analysis of the binding trends observed when assessing target particle modified surfaces, namely MPc-modified (Chapter 3) and *F*MWCNT-modified (Chapter 4) SAM surfaces.

Protein detection analysis on prepared MPc-modified, and *F*MWCNT-modified, surfaces indicated HSA adsorption is greatly influenced by the surface charge, resulting in low reproducibility due to target protein conformational change. Furthermore, surface topography-dependence of HPF was evident. In general, complement C3 detection, using Ab_{C3c}, proved to be the most reliable of the three analyses, as conformational change was limited, and topography-dependence was negligible. However, with further analysis of the target surface, in terms of topography, obtainable using AFM and scanning electron microscopy (SEM), and surface charge, obtainable through simple titration analysis, the variability of the protein detection trend may be accounted for, and therefore experimental accuracy may be further assessed. An alternative means of approaching the concern of reproducibility and accuracy involves optimisation of the surface modification process. This may proceed via controlled immobilisation, in terms of target particle patterning on the underlying SAM surface, obtainable using variable length linkers (i.e. SAM molecules).

Protein corona identification results, although variable in some cases (i.e. HSA and HPF) due to variability in surface charge and topography, correlated with literature-based predictions, and preliminary studies (Chapter 2). It was therefore concluded that the proposed protein detection method, using QCM-D technology for the monitoring and quantification of probe antibody binding, was successful in crudely assessing the protein corona adsorbed on target particle-modified surfaces and represents a potentially promising tool for such studies. However, further optimisation of the surface modification is required, and/or analysis of the modified surface characteristics, in terms of charge and topography, to improve accuracy and reproducibility of the proposed means of protein detection. With optimisation, the proposed QCM-D based may prove applicable in drug design studies, in addition to providing essential information regarding the complex relationship between blood protein adsorption and biocompatibility.

Areas of interest, for future studies, include combining QCM-D technology with alternative protein detection methods, such as SPR. The coupling of QCM-D and SPR techniques has been reported to be successful in literature, where SPR analysis served as validation for QCM-D application [20-22]. The utilisation of QCM-D, in conjunction with surface topography based analyses, such as AFM and SEM, has also been reported [96, 111].

Alternative QCM-D-based studies, we propose, include; analysis of target protein adsorption to the modified surfaces, to assess subsequent target protein conformation change and binding kinetics; and competitive binding analysis, using a combination of the three target proteins. Analysis of fibrinogen adsorption, and subsequent fibrin clot formation, may also prove helpful when assessing biocompatibility. The latter study has been reported using polymer-coated surfaces, where the clot formation was analysed via monitoring film density shifts in time-based studies [29].

APPENDIX

Table A.1. QCM-D Frequency and Dissipation Shifts Monitoring the Adsorption of Blood Proteins to the Target Surfaces

Surface [a]	Blood Protein	Δf_7 ΔD_7	Δf_9 ΔD_9	Δf_{11} ΔD_{11}	Ave. Δf [b]	Ave. Δf % CV	Ave. ΔD [b]
Ab_{HSA} (new crystal)	HS	14.56	13.31	9.16	-43.14 ±1.37	3.18	3.64 ±0.96
		13.54	12.62	12.28	-25.40 ±0.64	2.52	1.98 ±0.05
		10.86	11.14	9.99	-33.79 ±0.94	2.78	3.17 ±0.10
Ab_{HSA} (used crystal)		10.12	9.79	9.23	-30.67 ±1.3	4.24	3.16 ±0.04
		16.90	15.92	14.59	-23.86 ±0.36	1.51	1.51 ±0.09
		10.42	9.91	9.49	-39.9 0±1.42	3.56	4.02 ±0.05
Ab_{IgG}	HS	9.73	13.36	10.16	-34.26 ±1.57	4.58	3.15 ±0.50
	iHS	7.16	8.33	6.48	-15.72 ±0.99	6.30	2.17 ±0.26
Ab_{HPF}	HP	12.59	12.50	10.76	-58.40 ±1.27	2.17	4.91 ±0.33
Surface [a]	**Blood Protein**	f_7 D_7	f_9 D_9	f_{11} D_{11}	**Ave. f [b]**	**Ave. f % CV**	**Ave. D [b]**
Gold	HS	16.74	16.36	16.29	-64.68 ±1.15	1.78	3.93 ±0.03
		35.33	10.56	10.12	-70.34 ±6.30	8.96	3.69 ±5.07
		23.61	22.89	22.66	-66.58 ±0.98	1.47	2.89 ±0.02
		20.27	17.70	16.82	-66.62 ±1.54	2.31	3.67 ±0.27
		20.27	17.66	16.86	-66.61 ±1.56	2.34	3.66 ±0.27
		13.61	13.68	13.04	-71.66 ±1.44	2.01	5.33 ±0.03
	HP	15.32	14.20	13.47	-55.81 ±0.98	1.76	3.90 ±0.18
		9.00	8.08	7.20	-22.63 ±0.83	3.67	2.81 ±0.21
		16.10	14.44	14.87	-56.03 ±2.26	4.03	3.71 ±0.17
Silicon Dioxide	HS	26.18	26.58	25.32	-62.90 ±0.79	1.26	2.42 ±0.05
		19.85	20.98	19.27	-62.42 ±1.11	1.78	3.12 ±0.12
		18.56	18.41	17.34	-54.34 ±0.95	1.75	3.00 ±0.07
	HP	17.44	17.47	16.61	-52.28 ±1.18	2.26	3.05 ±0.05
11-AUT SAM	HS	15.32	14.88	14.60	-54.62 ±1.41	2.58	3.66 ±0.01
		15.92	15.67	15.30	-64.26 ±1.55	2.41	4.11 ±0.02
		12.68	12.70	12.99	-52.63 ±1.44	2.74	4.12 ±0.17
	HP	13.63	12.85	12.58	-48.44 ±1.05	2.17	3.72 ±0.08
Cyst. SAM	HS	18.43	18.91	17.37	-44.97 ±1.30	2.89	2.47 ±0.07
		18.24	22.79	26.87	-40.74 ±0.28	0.69	1.85 ±0.36
		17.66	16.84	15.94	-45.26 ±0.67	1.48	2.70 ±0.10
	HP	27.44	26.78	24.19	-50.99 ±0.53	1.04	1.96 ±0.12
MUA SAM	HS	18.25	17.14	25.55	-33.16 ±0.73	2.20	1.69 ±0.36
		21.44	22.00	20.77	-40.30 ±0.61	1.51	1.88 ±0.04
		13.67	13.90	13.71	-38.25 ±0.77	2.01	2.78 ±0.07
	HP	12.38	11.96	11.92	-29.10 ±0.63	2.16	2.41 ±0.02

a: *Surface modification molecules utilised in the fabrication of the control surfaces*
b: *Average values determined using responses obtained from overtones 7 -11*

Table A.2. QCM-D Frequency and Dissipation Shifts Monitoring Probe Antibody Binding to Blood Protein Coated Target Surfaces

Surface [a]	Probe	Δf_7 ΔD_7	Δf_9 ΔD_9	Δf_{11} ΔD_{11}	Ave. Δf [b]	Ave. Δf % CV	Ave. ΔD [b]
Ab_{HSA} (new crystal)	$A_{b(A)}$	8.57	7.66	6.95	-146.01 ±5.67	3.88	18.97 ±1.22
		9.66	8.89	8.40	-147.21 ±4.96	3.37	16.42 ±0.6
		18.28	16.95	14.73	-127.73 ±2.62	2.05	7.72 ±0.71
Ab_{HSA} (used crystal)		19.77	17.01	14.81	-121.35 ±1.58	1.30	7.15 ±0.93
		15.14	13.83	12.66	-120.86 ±2.19	1.81	8.75 ±0.62
		18.49	15.98	14.51	-102.38 ±1.72	1.68	6.33 ±0.66
Ab_{IgG}	$A_{b(C)}$	7.01	7.65	6.56	-37.88 ±2.60	6.86	5.36 ±0.34
	$A_{b(C-)}$	0.92	0.85	233.4	-43.26 ±73.45	169.79	-0.83 ±0.28
Ab_{HPF}	$A_{b(F)}$	65.44	52.35	101.61	-37.18 ±238.28	640.88	2.18 ±0.8
Gold	$A_{b(A)}$	4.65	4.39	4.05	-6.31 ±0.54	8.56	1.44 ±0.03
		5.14	0.41	1.86	-5.30 ±3.59	67.74	1.68 ±2.81
		4.85	4.15	3.92	-6.78 ±0.69	10.18	1.58 ±0.03
	$A_{b(C)}$	24.03	10.54	14.75	-16.27 ±1.65	10.14	1.09 ±0.38
		24.01	10.62	14.6	-16.27 ±1.56	9.59	1.09 ±0.33
		12.88	12.77	11.10	-13.82 ±0.37	2.68	1.13 ±0.08
	$A_{b(F)}$	40.89	29.37	23.81	-58.21 ±0.79	1.36	1.95 ±0.49
		28.43	21.87	17.85	-66.15 ±0.46	0.70	3.02 ±0.67
		30.40	19.21	19.91	-46.03 ±2.38	5.17	2.06 ±0.44
Silicon Dioxide	$A_{b(A)}$	3.35	3.03	2.99	-5.62 ±0.69	12.28	1.80 ±0.11
	$A_{b(C)}$	-9.59	24.49	5.22	-2.31 ±0.44	19.05	0.18 ±0.234
	$A_{b(F)}$	17.91	24.19	13.19	-6.38 ±0.59	9.25	0.37 ±0.10
11-AUT SAM	$A_{b(A)}$	6.29	5.91	5.77	-11.94 ±0.83	6.95	1.99 ±0.05
	$A_{b(C)}$	9.51	8.79	8.61	-15.77 ±0.92	5.83	1.76 ±0.03
	$A_{b(F)}$	4.00	3.53	3.25	-11.44 ±1.14	9.97	3.18 ±0.04
Cyst. SAM	$A_{b(A)}$	7.78	7.52	6.59	-17.53 ±1.27	7.24	2.40 ±0.05
	$A_{b(C)}$	9.85	11.22	11.33	-7.80 ±0.20	2.56	0.73 ±0.07
	$A_{b(F)}$	22.95	35.02	59.90	-65.84 ±0.94	1.43	-1.94 ±0.86
MUA SAM	$A_{b(A)}$	2.20	1.58	1.91	-4.25 ±0.95	22.35	2.25 ±0.35
	$A_{b(C)}$	-6.80	-6.06	-5.54	-6.64±0.18	2.71	0.43 ±0.02
	$A_{b(F)}$	421.17	146.12	86.73	-2.57 ±0.11	4.28	0.01 ±0.02

a: *Surface modification molecules utilised in the fabrication of the control surfaces*
b: *Average values determined using responses obtained from overtones 7 -11*

Table B.1. QCM-D Change in Frequency and Dissipation Shifts due to Target Antibody Binding to Blood Protein Coated MPc-Modified Surfaces

MPc [a]	Probe [a]	f_7 D_7	f_9 D_9	f_{11} D_{11}	Ave. f [c]	Ave. f % CV	Ave. D
AlPcS$_{mix}$	Ab_{HSA}	13.74	10.54	12.93	-3.97 ±0.26	6.55	0.32 ±0.04
	Ab_{C3c}	-8.89	8.83	7.30	-7.11 ±0.11	1.55	0.86 ±0.10
	Ab_{HPF}	15.30	13.76	12.20	-122.13 ±3.28	2.69	8.94 ±0.77
CoPcS$_{mix}$	Ab_{HSA}	6.31	6.11	5.49	-24.77 ±1.36	5.49	4.15 ±0.13
	Ab_{C3c}	126.00	52.55	276.00	-5.87 ±0.40	6.81	0.03 ±0.08
	Ab_{HPF}	28.93	23.15	20.54	-114.94 ±1.11	0.97	4.84 ±0.77
CuTSPc	Ab_{HSA}	5.71	5.63	5.21	-17.27 ±1.47	8.51	3.13 ±0.21
	Ab_{C3c}	7.58	5.86	5.24	-3.01 ±0.40	13.29	0.49 ±0.03
	Ab_{HPF}	12.23	9.38	8.07	-58.65 ±2.48	4.23	6.07 ±1.00
GePcS$_{mix}$	Ab_{HSA}	1.85	1.67	1.60	-36.39 ±6.99	19.21	21.16 ±2.47
	Ab_{C3c}	5.87	5.27	5.02	-37.39 ±3.17	8.48	6.94 ±0.03
	Ab_{HPF}	12.74	20.82	16.16	-54.92 ±1.70	3.10	3.45 ±0.81
ZnPcS$_{mix}$	Ab_{HSA}	12.82	12.34	11.33	-4.42 ±0.41	9.28	0.36 ±0.02
		7.96	7.92	7.83	-3.46 ±0.16	4.62	0.44 ±0.02
		14.40	13.38	12.46	-52.79 ±1.30	2.46	3.94 ±0.19
	Ab_{C3c}	8.08	7.00	6.61	-5.59 ±0.21	3.76	0.78 ±0.05
		6.36	6.04	5.46	-3.52 ±0.16	4.55	0.59 ±0.02
		5.95	5.22	4.78	-3.17 ±0.22	6.94	0.60 ±0.03
	Ab_{HPF}	3.90	3.52	2.95	-87.40 ±14.55	16.65	25.19 ±0.79
		7.82	6.91	6.06	-20.12 ±1.54	7.65	2.92 ±0.15
		4.12	3.72	3.53	-4.45 ±0.41	9.21	1.17 ±0.02
CoTCPc	Ab_{HSA}	4.56	3.06	4.17	-3.56 ±0.47	13.20	0.92±0.09
	Ab_{C3c}	11.95	12.01	9.64	-17.65 ±0.88	4.99	1.59 ±0.14
	Ab_{HPF}	10.00	9.85	10.72	-72.24 ±1.35	1.87	7.10 ±0.38

a: *Surface modification molecules utilised in the fabrication of the control surfaces*
b: *Probe Antibody*
c: *Average values determined using responses obtained from overtones 7 -11*

Table C.1. QCM-D Frequency and Dissipation Responses Monitoring Blood Protein Adsorption to the *f*MWCNT-Modified 11-Amino Undecane Thiol SAM Surfaces

*f*MWCNT [a]	Blood Protein	f_7 D_7	f_9 D_9	f_{11} D_{11}	Ave. f [b]	Ave. f % CV	Ave. D
2 a:*f*MWCNT	HS	16.10	15.15	15.13	-34.80 ±0.82	2.36	2.25 ±0.04
	HS	14.45	14.02	13.99	-37.73 ±1.35	3.58	2.67 ±0.06
	HP	16.15	17.07	13.34	-63.61 ±1.43	2.25	4.14 ±0.47
4 a:*f*MWCNT	HS	10.47	10.74	10.94	-38.16 ±1.29	3.38	3.57 ±0.20
	HS	6.15	8.82	7.78	-28.67 ±1.24	4.33	3.88 ±0.87
	HP	8.66	8.66	8.88	-43.68 ±1.45	3.32	5.00 ±0.23
6 a:*f*MWCNT	HS	13.83	13.58	12.18	-42.61 ±1.09	2.56	3.24 ±0.15
	HS	15.46	11.66	13.90	-43.53 ±1.56	3.58	3.22 ±0.38
	HP	17.43	17.24	14.71	-43.98 ±4.61	10.48	2.82 ±0.21
8 a:*f*MWCNT	HS	16.53	9.51	14.89	-29.96 ±1.17	3.91	2.31 ±0.62
	HS	13.99	13.74	12.69	-46.18 ±1.43	3.10	3.43 ±0.08
	HP	12.36	11.69	10.13	-42.35 ±2.18	5.15	3.73 ±0.20
24 a:*f*MWCNT	HS	22.28	24.29	21.66	-18.23 ±0.35	1.92	0.8 0±0.04
	HS	14.59	13.84	13.47	-40.23 ±0.78	1.94	2.88 ±0.06
	HP	17.68	17.68	17.30	-28.57 ±0.49	1.72	1.63 ±0.01
4 b:*f*MWCNT	HS	15.44	9.74	13.20	-42.97 ±2.07	4.82	3.47 ±0.77
	HS	12.46	13.34	13.06	-49.32 ±1.55	3.14	3.81 ±0.21
	HP	15.73	14.54	17.32	-57.22 ±1.50	2.62	3.63 ±0.37
8 b:*f*MWCNT	HS	14.00	13.74	13.02	-43.86 ±1.08	2.46	3.23 ±0.05
	HS	13.60	12.73	13.05	-49.90 ±1.08	2.16	3.80 ±0.12
	HP	15.66	15.47	13.11	-46.45 ±0.94	2.02	3.17 ±0.26
12 b:*f*MWCNT	HS	29.07	22.17	20.08	-40.31 ±0.55	1.36	1.74 ±0.30
	HS	12.05	3.35	10.60	-36.41 ±2.86	7.85	5.57 ±3.84
	HP	11.80	11.84	12.05	-53.80 ±1.37	2.55	4.52 ±0.16
20 b:*f*MWCNT	HS	12.36	12.01	10.73	-32.42 ±1.62	5.00	2.77 ±0.08
	HS	10.55	10.70	11.06	-38.07 ±0.94	2.47	3.54 ±0.12
	HP	42.65	3.46	9.03	-52.12 ±17.62	33.81	6.04 ±5.04

a: *Surface modification molecules utilised in the fabrication of the control surfaces*
b: *Average values determined using responses obtained from overtones 7 -11*

Table C.2. QCM-D Frequency and Dissipation Responses Monitoring Probe Antibody Binding to Blood Protein Coated *F*MWCNT-Modified Surfaces

*f*MWCNT [a]	Probe [b]	f_7 D_7	f_9 D_9	f_{11} D_{11}	Ave. f [c]	Ave. f % CV	Ave. D
2 a:*f*MWCNT	Ab_{HSA}	5.66	5.41	5.24	-55.80 ±3.12	5.59	10.26 ±0.18
	Ab_{C3c}	7.87	6.01	4.80	-1.76 ±0.3	17.05	0.29 ±0.03
	Ab_{HPF}	5.83	5.74	4.25	-11.02 ±0.85	7.71	2.11 ±0.23
4 a:*f*MWCNT	Ab_{HSA}	1.50	1.45	1.38	-8.19 ±1.52	18.56	5.66 ±0.82
	Ab_{C3c}	4.15	7.28	5.88	-1.81 ±0.13	7.18	0.33 ±0.11
	Ab_{HPF}	4.47	4.21	3.93	-11.73 ±1.01	8.61	2.79 ±0.06
6 a:*f*MWCNT	Ab_{HSA}	6.91	6.56	5.89	-10.54 ±0.49	4.65	1.64 ±0.06
	Ab_{C3c}	7.41	4.50	5.82	-3.97 ±0.42	10.58	0.69 ±0.1
	Ab_{HPF}	5.00	3.87	10.7	-46.24 ±1.05	2.27	11.08 ±1.27
8 a:*f*MWCNT	Ab_{HSA}	7.24	5.08	6.56	-28.84 ±1.85	6.41	4.66 ±0.72
	Ab_{C3c}	5.54	4.76	3.98	-5.43 ±0.52	9.58	1.15 ±0.08
	Ab_{HPF}	5.73	4.93	4.28	-20.20 ±1.79	8.86	4.09 ±0.42
24 a:*f*MWCNT	Ab_{HSA}	7.22	7.23	6.55	-13.33 ±0.69	5.18	1.9 ±0.02
	Ab_{C3c}	4.63	4.38	3.94	-4.54 ±0.3	6.61	1.05 ±0.03
	Ab_{HPF}	4.18	3.84	3.51	-8.59 ±0.87	10.13	2.23 ±0.03
4 b:*f*MWCNT	Ab_{HSA}	5.41	3.55	4.28	-28.54 ±3.66	12.82	6.58 ±1.02
	Ab_{C3c}	88.74	119.02	21.58	-3.57 ±0.33	9.24	0.07 ±0.07
	Ab_{HPF}	10.83	8.18	14.56	-64.48 ±4.43	6.87	6.75 ±0.94
8 b:*f*MWCNT	Ab_{HSA}	2.79	2.60	5.05	-13.26 ±2.11	15.91	5.25 ±0.21
	Ab_{C3c}	21.61	7.08	5.96	-2.82 ±0.54	19.15	0.29 ±0.34
	Ab_{HPF}	3.26	3.18	2.45	-10.32 ±1.46	14.15	3.49 ±0.18
12 b:*f*MWCNT	Ab_{HSA}	83.31	15.38	9.64	-4.87 ±0.15	3.08	0.29 ±0.22
	Ab_{C3c}	2.43	0.26	1.19	-1.52 ±0.78	51.32	1.81 ±1.35
	Ab_{HPF}	3.53	3.18	3.35	-17.40 ±2.52	14.48	5.18 ±0.56
20 b:*f*MWCNT	Ab_{HSA}	3.60	3.06	2.67	-194.03 ±24.8	12.78	62.51 ±1.39
	Ab_{C3c}	3.24	1.93	2.17	-0.95 ±0.28	29.47	0.39 ±0.02
	Ab_{HPF}	34.27	4.36	9.78	-72.11 ±19.01	26.36	7.6 ±5.52

a: *Surface modification molecules utilised in the fabrication of the control surfaces*
b: *Probe Antibody*
c: *Average values determined using responses obtained from overtones 7 -11*

REFERENCES

1. Richter, R., Mukhopadhyah, A. and Brissonm A. (2003). Pathways of Lipid Vesicle Deposition on Solid Surfaces: A Combined QCMD-AFM Study. *Biophysical Journal*. **85**: 3035-3047
2. Caruthers, S., Wickline, S. and Lanza, G. (2007). Nanotechnological applications in medicine. *Current Opinion in Biotechnology*. **18:** 26-30
3. Dobrovolskaia, M., Aggarwal, P., Hall, J. and McNeil, S. (2008). Preclinical Studies To Understand Nanoparticle Interaction with the Immune System and Its Potential Effects on Nanoparticle Biodistribution. *Molecular Pharmaceutics*. **5:** 487-495
4. Dobrovolskaia, M. and McNeil, S. (2007). Immunological properties of engineered nanomaterials. *Nature Nanotechnology*. **2**: 469-478
5. Lassen, B. And Malmsten, M. (1996). Structure of Protein Layers during Competitive Adsorption. *Journal of Colloid and Interface Science*. **180:** 339-349
6. Owens, D.E. And Peppas, N.A. (2006). Opsonisation, biodistribution, and pharmacokinetics of polymeric nanoparticles. *International journal of pharmaceutics*. **307**: 93-102
7. Aggarwal, P., Dobrovolskaia, M., Hall, J. and McNeil, S. (2008). Preclinical Studies To Understand Nanoparticle Interaction with the Immune System and Its Potential Effects on Nanoparticle Biodistribution. *Molecular Pharmaceutics*. **5**: 487-495
8. Adriaens, A., Bultinck, P., Depal, D., De Wael, K., Temmerman, E., Vandenabeele, P. and Westbroek, P. (2005). Study of the deposition and Raman and XPS characterization of a metal ion tetrasulphonated phthalocyanine layer at gold surfaces: density functional theory calculations to model the vibrational spectra. *Electrochemistry Communications*. **7**: 87-96
9. Andersson, J., Ekdahl, K., Larsson, R., Nilsson, U. And Nilsson, B. (2002). C3 Adsorbed to a Polymer Surface Can Form an Initiating Alternative Pathway Convertase. *The Journal of Immunology*. **168**: 5786-5791
10. Gref., R., Luck, M., Quellec, P., Marchand, M., Dellacherie, E., Harnisch, S., Blunk, T. and Muller, R. (2000). 'Stealth' corona-core nanoparticles surface modified by polyethylene glycol (PEG): indluences of the corona (PEG chain length and surface density) and of the core composition on phagocytic uptake and plasma protein adsorption. *Colloids and Surfaces B: Biointerfaces*. **18**: 301-313
11. Göppert, T. and Müller, R. (2005). Adsorption kinetics of plasma proteins on solid lipid nanoparticles for drug targeting. *International Journal of Pharmaceutics*. **302**: 172-186
12. Kainthan, R., Janzen, Levin, E., Devine, D. and Brooks, D. (2006). Biocompatibility Testing of Branched and Linear Polyglycidol. *Biomacromolecules*. **7(3):** 703-709
13. Rose, S., Lewis, A., Hanlon, J. and Lloyd, A. (2004). Biological responses to cationically charged phosphoycholine-based materials in vitro. *Biomaterials*. **25:** 5125-5135
14. Salvador-Morales, C., Flahaut, E., Sim, E., Sloan, J., Green, M. and Sim, R. complement activation and protein adsorption by carbon nanotubes. *Molecular Immunology*. **43:** 193-201
15. Salvador-Morales, C., Zhang, L., Langer, R. and Farokhzah, O. (2009). Immunocompatibility properties of lipid-polymer hybrid nanoparticles with heterogeneous surface functional groups. *Biomaterial*. **30:** 2231-2240
16. Gessner, A., Lieske, A., Paulke, B. and Muller, R. (2004). Influence of surface charge density on protein adsorption on polymeric nanoparticles: analysis by two-dimensional electrophoresis. *European Journal of Pharmaceutics and Biopharmaceutics*. **54:** 165-170
17. Dobrovolskaia, M,., Patri, A., Zheng, J., Clogston, J., Ayub, N., Aggarwal, P., Neun, B., Hall, J. and McNeil, E. (2009). Interaction of colloidal gold nanoparticles with human blood: effects on particle size and analysis of plasma protein binding profiles. *Nanomedicine: Nanotechnology, Biology, and Medicine*. **5:** 106-117
18. Andersson, J. (2003). Complement Activation Triggered by Biomaterial Surfaces. Mechanisms and Regulation. Acta Universitatis Upsaliensis. *Comprehensive Summaries of Uppsala Dissertations from Faculty of Medicine*. **1253:** 45
19. Chang, K and Lee, Y. (2005). Application of a flow type quartz crystal mircrobalance immunosensor for real time determination of cattle bovine ephemeral fever virus in liquids. *Talanta*. **65**: 1335-1342.
20. Spangler, B., Wilkinson, E., Murphy, J. and Tyler B. (2001). Comparison of the Spreeta® surface plasmon resonance sensor and a quartz crystal microbalance for detection of *Escherichia coli* heat-labile enterotoxin. *Analytica Chimica Acta*. **444**: 149-161
21. Sellborn, A., Andersson, M., Chevallier, J. and Besenbacher, F. (2002). Methods for research on immune complement activation on modified sensor surfaces. *Colloids and Surfaces B*. **27**: 295-301
22. Limson, J., Odunuga, O., Green, H., Höök, F. and Blatch, G. (2004). The use of a quartz crystal microbalance with dissipation for the measurement of protein-protein interactions: a qualitative and quantitative analysis of the interactions between molecular chaperones. *South African Journal of Science*. **100:** 678-682

23. Höök, F., Kasemo, B., Nylander, T., Fant, C., Scott, K. and Elwing, H. (2001). Variations in coupled water, viscoelastic properties and film thickness of a Mefp-1 protein film during adsorption and cross-linking: a QCM-D, ellipsometry and SPR study. *Analytical Chemistry.* **73:** 5796-5804
24. Fält, S., Wågberg, L., Vesterlind, E. (2003). Swelling of Model Films of Cellulose Having Different Charge Densities and Comparison to the Swelling Behavior of Corresponding Fibers. *Langmuir*. **19:** 7895-7903
25. Lord, S., Modin, C., Foss, M., Duch, M., Simmons, A., Pedersen F., Milthorpe, B., and Besenbacher, F. (2006) Monitoring cell adhesion on tantalum and oxidized polystyrene using a quartz crystal microbalance with dissipation. *Biomaterials*.**27:** 4529- 4537
26. Kabin, J., Tolstedt, S., Sáez, A., Grant, C. and Carbonell, R. (1998), Removal of Organic Films From Rotating Disks Using Aqueous Solutions of Nonionic Surfactants: Effect of Surfactant Molecular Structure. *Journal of Colloid and Interface Science*. **206:** 102–111.
27. Berglin, M., Andersson, M., Sellborn, A. and Elwing, H. (2004). The effect of substrate molecular mobility on surface induced immune complement activation and blood plasma coagulation. *Biomaterials*. **25:** 4581-4590
28. Hermmersam, A., Foss, M., Chevallier, J. and Besenbacher, F. (2005). Adsorption of fibrinogen on tantalum oxide, titanium oxide and gold studied by QCM-D technique. *Colloids and Surfaces B: Biointerfaces*. **43:** 208-215
29. Andersson, M., Andersson, J., Sellborn, A., Berglin, M., Nilsson, B. and Elwing, H. (2005). Quartz crystal microbalance-with dissipation monitoring (QCM-D) for real time measurements of blood coagulation density and immune complement activation on artificial surfaces. *Biosensors and Bioelectronics.* **21:** 79-86
30. Johannsman, D. (2008). Viscoelastic, mechanical, and dielectric measurements on complex samples
31. Höök, F. and Rudh, M. (2005). Quartz crystal microbalances (QCM) in biomacromolecular recognition. *Bio Tech International*. **17:** 8-13
32. Höök, F. and Kasemo, B. (2001). Variations in Coupled Water, Viscoelastic Properties, and Film Thickness of a Mefp-1 Protein Film during Adsorption and Cross-linking: A Quartz Crystal Microbalance with Dissipation Monitoring, Ellipsometry, and Surface Plasmon Resonance Study. *Analytical Chemistry*. **73:** 5796-5804
33. Vogt, B. Lin, E., Wu, W. and White, C. (2004). Effects of Film Thickness on the Validity of the Sauerbrey Equation for Hydrated Polyelectrolyte Films. *Journal of Physical Chemistry B*. **108:** 12685-12690
34. Voinova, M., Rodahl, M., Jonson, M. and Kasemo, B. (1999). Viscoelastic Acoustic Response of layered Polymer Films at Fluid-Solid Interfaces: Continuum Mechanics Approach *Physica Scripta*. ***59:*** 391-396
35. Dietschweiler, C. Protein adsorption at solid surfaces. Department of Environmental Sciences, Institute of Biogeochemistry and Pollutant Dynamics (IBP), Swiss Federal Institute of Technology (ETH), Zűrich.
36. Cederval, T., Lynch, I., Lindman, S., Berggård, T., Nilsson, H., Dawson, K. And Linse, S. (2007). *Proceedings of the National Academy of Sciences*. **104:** 2050-2055
37. Wang, D., Chen, B., Ji, J. and Feng, L. (2002). Selective Adsorption of Serum Albumin on Biomedical Polyurethanes Modified by Poly(ethylene oxide) Coupling-Polymer with Cibacron Blue (F3G-A) Endgroups. *Bioconjugate Chemistry*. **13:** 792-803
38. Wasdo, S., Barber, D., Denslow, N., Powers, K., Palazuelos, M., Stevens, S., Moudgil, B. and Roberts, S. (2008). Differential binding of serum proteins to nanoparticles. *International Journal of Nanotechnology*. **5:** 92-115
39. Das, S., Banerjee, R. and Bellare, J. (2005). Asprin Loaded Albumin Nanoparticles by Coacervation: Implications in Drug Delivery. *Trends in Biomaterials & Artificial Organs*. **18:** 203-212
40. Coico, R., Sunshine, G. and Benjamini, E. (2003). Immunology: A Short Course 5th edition. John Wiley & Son, Inc. USA.
41. Gorbet, M and Sefton, M. (2004). Biomaterial-associated thrombosis: roles of coagulation factors, complement, platelets and leukocytes. *Biomaterials*. **25:** 5681-5703
42. Hulander, M., Hong, J., Andersson, M., Gerven, F., Ohrlander, M., Tengvall, P. and Elwing, H. (2009). Blood Interactions with Nobel Metals: Coagulation and Immune Complement Activation. *ACS Applied Materials & Interfaces*. **1:** 1053-1062
43. Tunc, S., Maitz, M., Steiner, G., Vázquez, L., Pham, M. and Salzer, R. (2005). In situ conformational analysis of fibrinogen adsorbed on Si surfaces. *Colloids and Surfaces B: Biointerfaces*. **42:** 219-225.
44. Guicai, L., Xiaoli, S., Ping, Y., Ansha, Z. And Nan, H. (2008). Investigation of fibrinogen adsorption on solid surface by quartz crystal microbalance with dissipation (QCM-D) and ELISA. *Solid State Ionics*. **179:** 932-935

45. Wertz, C. and Santore, M. (1999). Adsorption and Relaxation Kinetics of Albumin and Fibrinogen on Hydrophobic Surfaces: Single-Species and Competitive Behaviour. *Langmuir*. **15:** 8884-8894
46. Gessner, A., Lieske, A., Paulke, B. and Müller, R. (2002). Influence of surface charge density on protein adsorption on polymeric nanoparticles: analysis by two-dimensional electrophoresis. *European Journal of Pharmaceutics and Biopharmaceutics*. **54:** 165-170
47. Kolárová, H., Bajgar, R., Tománková, K., Krestýn, E., Doleźal, L. and Hálek, J. (2007). *In vitro* Study of Reactive Oxygen Species Production during Photodynamic Therapy in Ultrasound-Pretreated Cancer Cells. *Physiolical Research*. **56:** 27-32
48. Pazos, M. and Nader, H. (2007). Effect of photodynamic therapy on the extracellular matrix and associated components. *Brazilian Journal of Medical and Biological Research*. **40:** 1025-1035.
49. Nyokong, T. (2008). Electrocatalytic and photosensitising behaviour of metallo-phthalocyanine complexes. *Journal of Porphyrins and Phthalocyanines*. **12:** 1005-1021
50. Ochsne, M. (1997). Photophysical and photobiological processes in the photodynamic therapy of tumors. *Journal of Photochemistry and Photobiology B: Biology*. **39:** 1-18
51. Agboola, B. (2007). Catalytic activities of Metallophthalocyanines towards Detection and Transformation of Pollutants. Rhodes University
52. Kolárová, H., Kubínek, R., Lenobel, R., Bancirová, M., Strnad, M., Jírová, D. and Lasovský, J. In vitro Photodynamic therapy with phthalocyanines on the MCF-7 cancer cells. Second International Conference of Photochemistry and Photobiology. 1999. http://www.photobiology.com/photobiology99/contrib/kolarova/index.htm
53. Pashkovskaya, A., Sokolenko, E., Sokolov, V., Kotova, E. and Antonenko, Y. (*2007)*. Photodynamic activity and binding of sulfonated metallophthalocyanines to phospholipid membranes: Contribution of metal-phosphate coordination. *Biochimica et. Biophysica Acta*. **1768:** 2459-2465
54. Martin, P., Gouterman, M., Pepich, B., Renzoni, G. and Schindele, D. (1991). Effects of Ligands, Solvent, and Variable Sulfonation on Dimer Formation of Aluminum and Zinc Pthalocyaninesulfonates. *Inorganic Chemistry*. **30:** 3305-3309.
55. Nyokong, T. and Vilakazi, S. (2002). Phthalocyanines and related complexes as electrocatalysts for the detection of nitric oxide. *Talanta*. **61:** 27-35
56. Bedioui, F., Griveau, S., Nyokong, T., Appleby, J., Caro, C., Gulppi, M., Ochoa, G. and Zagal, J. (2007). Tuning the redox properties of metalloporphyrin- and metallophthalocyanine-based molecular electrodes for the highest electrocatalytic activity in the oxidation of thiols. *Physical Chemistry, Chemical Physics.* **9**: 3383-3396
57. Fogel, R., Mashazi, P., Nyokong, T. and Limson, J. (2007). Critical assessment of the Quartz Crystal Microbalance with Dissipation as an analytical tool for biosensor development and fundamental studies: Metallophthalocyanine-glucose oxidase biocomposite sensor. *Biosensors and Bioelectronics.* **23:** 95-101
58. Liu, M., Tai, C., Sain, M., Hu, A. and Chou, F. (2003). Photodynamic applications of phthalocyanines. *Journal of Photochemistry and Photobiology A: Chemistry*. **165:** 131-136
59. Wael, K., Wastbroek, P. and Temmerman, E. (2004). Study of the deposition of cobalt(II)tetrasulfophthalocyanine layer at gold surface in alkaline solutions. *Journal of Electroanalytical Chemistry*. **567:** 167-173
60. Camp, P., Jones, A., Neely, R. and Speir, N. (2002). Aggregation of Copper (II) Tetrasulfonated Phthalocyanine in Aqueous Salt Solutions. *Journal of Physical Chemistry A*. **106:** 10725-10732.
61. Chatterjee, S. and Srivastava, T. (2000). Spectral investigations of the interaction of some porphyrins with bovine serum albumin. *Journal of Porphyrins and Phthalocyanines*. **4:** 147-157
62. Fraczek, A., Manaszek, E., Paluszkeiwicz, C. and Blazewicz, M. (2008). Comparative in vivo biocompatibility study of single- and multi-walled carbon nanotubes. *Acta Biomaterialia*. **4:** 1593-1602.
63. Foldvari, M. and Bagonluri, M. (2008). Carbon nanotubes as functional excipients for nanomedicine: II. Drug delivery and biocompatibility issues. *Nanomedicine: Nanotechnology, Biology, and Medicine*. **4:** 183-200
64. Cheng, C., Müller, K., Koziol, K., Skepper, J., Midgley, P., Welland, M. and Porter, A. (2009). Toxicity and imaging of multi-walled carbon nanotubes in human macrophage cells. *Biomaterials*. **30:** 4152-4160
65. Hamad, I., Hunter, A., Rutt, K., Liu, Z., Dai, H. And Moghimi, M. (2008). Complement activation by PEGylated single-walled carbon nanotubes is independent of C1q and alternative pathway turnover. *Molecular Immunology*. **45:** 3797-3803
66. Jos, A., Pichardo, S., Peurto, M., Sánches, E, Grilo, A. and Cameán, A. (2009). Cytotoxicity of carboxylic acid functionalized single wall carbon nanotubes on the human intestinal cell line Caco-2. *Toxicology in Vitro*. **23:** 1491-1496

67. Pulskamp, K., Diabaté, S. and Krug, H. (2007). Carbon nanotubes show no sign of acute toxicity but induce intracellular reactive oxygen species in dependence on contaminants. *Toxicology Letters*. **168:** 58-74
68. Kaiser, J., Wick, P., Manser, P., Spohn, P. and Bruinink, A. (2008). Single walled carbon nanotubes (SWCNT) affect cell physiology and cell architecture. *Journal of Material Science: Material Medicine*. **19:** 1523-1527
69. Shvedova, A., Kisin, E., Porter, D., Schulte, P., Kagan, V., Fadeel, B. And Castranova, V. (2009). Mechanisms of pulmonary toxicity and medical applications of carbon nanotubes: Two faces of Janus?. *Pharmacology & Therapeutics*. **121:** 192-204
70. Zhang, T., Xu, M., He, L., Xi, K., Gu, M. and Jiang, Z. (2008). Synthesis and characterization of and cytotoxicity of phyosphoryl choline-grafted waters-soluble carbon nanotubes. *Carbon*. **46:** 1782-17
71. Brown, D., Kinloch, I., Bangert, U., Windle, A., Walter, D., Walker, G., Scotchford, C., Donaldson, K. and Stone, V. (2007). An in vitro study of the potential of carbon nanotubes and nanofibres to induce inflammation mediators and frustrated phagocytosis. *Carbon*. **45:** 1743-1756
72. Bottini, M., Bruckner, S., Nika, K., Bottini, N., Bellucci, S., Magrini, A., Bergamaschi, A. and Mustelin, T. (2006). Multi-walled carbon nanotubes induce T lymphocyte apoptosis. *Toxicology Letter*. **160:** 121-126
73. Ding, L., Stilwell, J., Zhang, T., Elboudwarej, O., Huijian, J., Selegur, J., Cooke, P., Gray, J. and Chen, F. (2005). Molecular characterization of the cytotoxic mechanism of multiwalled carbon nanotubes and nano-onions on human skin fribroblasts. *Nano Letter*. **5:** 2448-2464
74. Datsyuk, V., Malyva, M., Papagelis, K., Parthenios, J., Tasis, D., Siokou, A., Kallitsis, I. and Galiotis, C. (2008). Chemical oxidation of multiwalled carbon nanotubes. *Carbon*. **46:** 833-840
75. Marshall, M., Popa-Nita, S. and Shapter, J. (2006). Measurement of functionalised carbon nanotube carboxylic acid groups using a simple chemical process. *Carbon*. **44:** 1137-1141
76. Kakade, B. and Pillai, K. (2008). An efficient route towards the covalent functionalisation of single walled carbon nanotubes. *ACS Applied Surface Science*. **254:** 4936-4943
77. Green, R., Frazier, R., Shakesheff, K., Davies, M., Roberts, C. and Tendler, S. (2000). Surface plasmon resonance analysis of dynamic biological interactions with biomaterials. *Biomaterials*. **21:** 1823-1835
78. Jung, H., Kim, J., Kim, Y., Tae, G., Kim, Y. And Johannsmann, D. (2009). QCM and AFM Analysis of Anticoagulant Activities of Sulfonated Polymers against Fibrin Formation. *Langmuir*. **25:** 7032-7041
79. Benesch, J., Mano, J. and Reis, R. (2010). Analysing protein competition on self-assembled mono-layers studied with quartz crystal microbalance. *Acta Biomaterialia*. **6:** 3499-3505
80. Höök, F., Vörös, J., Rodahl, M., Kurrat, R., Böni, P., Ramsden, J., Textor, M., Spencer, N., Tengvall, P., Gold, J. and Kasemo, B. (2002). A comparative study of protein adsorption on titanium oxide surfaces using in situ ellipsometry, optical waveguide lightmode spectroscopy, and quartz crystal microbalance/dissipation. *Colloids and Surfaces B: Biointerfaces*. **24:** 155-170
81. Hemmersam, A., Foss, M., Chevallier, J. and Besenbacher, F. (2005). Adsorption of fibrinogen on tantalum oxide, titanium oxide and gold studied by QCM-D technique. *Colloids and Surfaces B: Biointerfaces*. **43:** 208-215
82. Toda, M. and Iwata, H. (2010). Effects of Hydrophobicity and Electrostatic Charge on Complement Activation by Amino Groups. *ACS Applied Materials & Interfaces*. **2:** 1107-1113.
83. Chen, D., and Li, J. (2006). Interfacial design and functionalisation on metal electrodes through self-assembled monolayers. *Surface Science Reports*. **61:** 445-463
84. Porter, M., Bright, T., Allara, D. and Chidsey, C. (1987). Spontaneously Organized Molecular Assemblies. 4. Structural characterization of *n*-Alkyl Thiol Monolayers on Gold by Optical Ellipsometry, Infrared Spectroscopy, and Electrochemisry. *Journal of American Chemical Society*. **109:** 3559-3568
85. Molina, S. (2006). Surface Functionalization of a Cantilever Sensor. Thesis in Chemistry. Texas Tech. University.
86. Kankare, J., Laajalehto, K., Laiho, T., Leiro, J., Lukkari, J. and Meretoja, M. (2005). Chemisorption of alkyl thiols and S-alkyl thiosulfates on Pt(111) and polycrystalline platinum surfaces. *Surface Science*. **584:** 83-89
87. Bowen, J., Manickam, M., Evans, S., Critchley, K., Kendall, K. and Preece. (2008) The pH-dependent adhesion of nanoparticles to self-assembled monolayers on gold. *Thin Solid Films*. **516:** 2987-2999
88. Ito, S., Matsubayashi, K., Miwa, N., Mori, T., Sawaguchi, T. and Takada, H. (2006). Preclinical studies on safety of fullerene upon acute oral administration and evaluation from no mutagenesis. *Toxicology*. **225:** 48-54

89. You, H., Disley, D., Cullen, D. and Lowe, C. (1993). Physical adsorption of immunoglobulin G on gold studied by scanning tunnelling microscopy. *International Journal of Biological Macromolecules*. **16:** 87-91
90. Stobiecka, M., Hepel, M. and Radecki, J. (2005). Transient conformation changes of albumin adsorbed on gold piezoelectrodes. *Electrochemica Acta*. **50:** 4873-4887
91. Barbose, J., Barbosa, M. and Águas, A. (2004). Inflammatory responses and cell adhesion to self – assembled monolayers of alkanethiolates on gold. *Biomaterials*. **25:** 2557-2563
92. Aggarwal, P., Hall, J., McLeland, B., Dobrovolskaia, M. and McNeil, S. (2009). Nanoparticle interaction with plasma proteins as it relates to particle biodistribution, biocompatibility and therapeutic efficacy. *Advanced Drug Delivery Reviews*. **61:** 428-437
93. Mayer, G. Microbiology and Immunology On-line. Immunology. Complement. University of South Carolina School of Medicine. http://pathmicro.med.sc.edu/ghaffar/complement.htm
94. Adkins, J., Varnum, S., Auberry, K., Moore, R., Angell, N., Smith, R., Springer, D. and Pounds, J. (2002). Towards a Human Blood Serum Proteome. *Molecular & Cellular Proteomics*. **1:** 947-955
95. Filyasova, A., Kudelina, I. and Feofanov, A. (2001). A spectroscopic study of the interaction of tetrasulfonated aluminium phthalocyanine with human serum albumin. *Journal of Molecular Structure*. **565-566:** 173-176
96. Figueira, V. and Jones, J. (2008). Viscoelastic study of the adsorption of bovine serum albumin on gold and its dependence on pH. *Journal of Colloidal and Interface Science*. **325:** 107-113
97. Shim, M., Wong Shi Kam, N., Chen, R., Li, Y. and Dai, H. (2002). Functionalization of Carbon Nanotubes for Biocompatibility and Biomolecular Recognition. *NanoLetters*. **2:** 285-288
98. Barbisa, J., Barbosa, M. and Aguas, A. (2004). Inflammatory responses and cell adhesion to self-assembled monolayers of alkanethiolates on gold. *Biomaterials*. **25:** 2558-2563
99. Rodriguez, M., Fernández, D., Awruch, J. Braslavsky, S. and Dicelio, L. (2006). Effect of aggregation of a cationic phthalocyanine in micelles and in the presence of human serum albumin. *Journal of Porphyrins and Phthalocyanines*. **10:** 33-42
100. Nyokong, T. (2007). Effects of substituents on the photochemical and photophysical properties of main group metal phthalocyanines. *Coordination Chemistry Review*. **251:** 1707-1722**.**
101. Ogunisipe, A. and Nyokong, T. (2005). Photophysical and photochemical studies of sulphonated non-transitionmetal phthalocyanines in aqueous and non-aqueous media. *Journal of Photochemistry and Photobiology A: Chemistry*. **173:** 211-220
102. Bertoncello, P. and Peruffo, M. (2008). An investigation on the self-aggregation properties of sulfonated copper (II) phthalocyanine (CuTsPc) thin films. *Colloids and Surfaces A: Physiochemical Engineering Aspects.* **321:** 106-112
103. Rosengren, A., Pavlovic, E., Oscarsson, S., Krajewski, A., Ravaglioli, A. and Piancastelli, A. (2002). Plasma protein adsorption pattern on characterized ceramic biomaterials. *Biomaterials*. **23:** 1237-1247
104. Stylii, S., Hill, J., Sawyer, W. and Kaye, A. (1995). Aluminium phthalocyanine mediated photodynamic therapy in experimental malignant glioma. *Journal of Clinical Neuroscience*. **2:** 146-151
105. Toscano, A. and Santore, M. (2006). Fibrinogen Adsorption on Three Silica-Based Surfaces: Conformation and Kinetics. *Langmuir*. **22**: 2588-2597
106. Nilsson, B., Nilsson, E., Mollnes, T. and Lambris, J. (2007). The role of complement in biomaterial-induced inflammation. *Molecular Immunology*. **44**: 82-91
107. Marx, K. (2003). Quartz Crystal Microbalance: A Useful Tool for Studying Thin Polymer Films and Complex Biomolecular Systems at the Solution-Surface Interface. *Biomacromolecules*. **4:** 1099-1120
108. Wang, K., Xu, J. and Chen, H. (2006). Biocomposite of cobalt phthalocyanine and lactate oxide for lactate biosensing with MnO_2 nanoparticles as an eliminator of ascorbic acid interference. *Sensors and Actuators B: Chemical*. **107:** 768-772
109. Peeters, K. (2007). Tetrasulphonated phthalocyanine thin films deposited on gold electrodes: a study using voltammetry and synchrotron micro X-ray fluorescence. Universiteit Gent. Faculty of Science. Department of Analytical Chemistry.
110. Singh, K., Pandey, R., Wang, X., Lake, R., Ozkhan, C., Wang, K. And Ozkan, M. (2006). Covalent functionalisation of single walled carbon nanotubes with peptide nucleic acid: Nanocomponents for molecular level electronics. *Carbon*. **44**: 1730-1739
111. Veetil, J. and Ye, K. (2007). Development of Immunosensors Using Carbon Nanotubes. *Biotechnology Progress*. **23:** 517-531
112. Osoria, A., Silveira, I., Bueno, V. and Bergmann, C. (2008). H_2SO_4/HNO_3/HCl-Functionalization and its effect on dispersion of carbon nanotubes in aqueous media. *Applied Surface Science*. **255:** 2485-2489

113. Hu, C., Su, J. and Wen, T. (2007). Modification of multi-walled carbon nanotubes for electric double-layer capacitors: Tube opening and surface functionalisation. *Journal of Physics and Chemistry of Solids*. **68:** 2353-2362
114. Piret, J., Detriche, S., Vigneron, R., vankoningsloo, S., Rolin, S., Mejia Mendoza, J., Masereel, B., Lucas, S., Delhalle, J., Luizi, F., Saout, C. and Toussaint, O. (2010). Dispersion of multi-walled carbon nanotubes in biocompatible dispersants. *Journal of Nanoparticle Research*. **12:** 75-82
115. Obradović, M., Vuković, G., Stevanović, S., Panic, V., Uskoković, P., Kowal, A. and Goijović, S. (2009). A comparative study of the electrochemical properties of carbon nanotubes and carbon black. *Journal of Electroanalytical Chemistry*. **634:** 22-30
116. Wang, Y. , Wu, J. and Wei, F. (2003). A treatment method to give separated multi-walled carbon nanotubes with high purity, high crystallization and large aspect ratio. *Carbon*. **41:** 2939-2948.
117. Sahoo, N., Rana, S., Cho, J., Li, L. and Chan, H. (2010). Polymer nanocomposites based on functionalized carbon nanotubes. *Progress in Polymer Science*. **35:** 837-867
118. Schierz, A. and Zanker, H. (2009). Aqueous suspensions of carbon nanotubes: Surface oxidation, colloidal stability and uranium sorption. *Environmental Pollution*. **157:** 1088-1094
119. Tune, D., Flavel, B., Quinton, J., Ellis, A. and Shapter, J. (2010). Single walled carbon nanotube network electrodes for dye solar cells. *Solar Energy Materials & Solar Cells*. **94:** 1665-1672
120. Milanovich, N., Reinot, T., Hayes, J. and Small, G. (1998). Aluminum Phthalocyanine Tetrasulfonate in MCF-10, Human Breast Epithelial Cells: A Hole Burning Story. *Biophysical Journal*. **74:** 2680-2688
121. Atilla, D., Saydan, N., Durmus, M., Gürek, A., Khan, T., Rück, A., Walt, H., Nyokong, T. and Ahsen, V. (2007). Synthesis and photodynamic potential of tetra- and octa-triethyleneoxysulfonyl substituted zinc phthalocyanines. *Journal of Photochemistry and Photobiology A: Chemistry*. **186:** 298-307
122. Ogunsipe, A., Nyokong, T. and Durmus, M. (2007). Photophysical, photochemical and bovine serum albumin binding studies on water-soluble gallium (II) phthalocyanine derivatives. *Journal of Porphyrins and Phthalocyanines*. **11:** 635-644
123. Kunz, L., Connelly, J., Woodhams, J. and MacRobert, A. (2007). Photodynamic modification of disulfonated aluminium phthalocyanine fluorescence in a macrophage cell line. *Photochemical & Photobiological Sciences*. **6:** 940-948
124. Haywood-Small, S., Vernon, D., Griffiths, J., Schofield, J. and Brown, S. (2006). Phthalocyanine-mediated photodynamic therapy induces cell death and a G_0/G_1 cell cycle arrest in cervical cancer cells. *Biochemical and Biophysical Research Communications*. **339:** 569-576
125. Glassberg, E., Lewandowski, L., Lask, G. and Uitto, J. (1990). Laser-Induced Photodynamic Therapy with Aluminum Phthalocyanine Tetrasulfonate as the Photosensitizer: Differential Phototoxicity in Normal and Malignant Human Cell In Vitro. *Selective Photodynamic Toxicity*. **94:** 604-610
126. Korbelik, M. (1993). Distribution of disulfonated and tetrasulfonated aluminum phthalocyanine between malignant and host cell populations of murine fibrosarcoma. *Journal of Photochemistry and Photobiology B: Biology*. **20:** 173-181
127. Schoemaker, M., Cohen, I. and Campbell, M. (2004). Reduction of MTT by aqueous herbal extracts in the absence of cells. *Journal of Ethnopharmachology*. **93:** 381 – 384
128. Berridge, M., Tan, A., McCoy, K. and Wang, R. (1996). The Biochemical and Cellular Basis of Cell Proliferation Assays That Use Tetrazolium Salts. *Biochemica*. **4:** 14-19
129. Labanauskiene, J., Gehl, J. and Didziapetriene, J. (2007). Evaluation of cytotoxic effect of photodynamic therapy in comparison with electroporation in vitro. *Bioelectrochemistry*. **70:** 78-82
130. Lee, E., Cho, H., Lee, C., Lee, D., Chung, K. and Paik, S. (2004). Phthalocyanine Tetrasulfonates Affect the Amyloid Formation and Cytotoxicity of α-Synuclein. *Biochemistry*. **43:** 3704-3715
131. Cauchon, N., Tian, H., Langlois, R., Madeleine, C., Martin, S., Ali, H., Hunting, D. and van Lier, J. (2005). Structure-Photodynamic Activity Relationships of Substituted Zinc Trisulfophthalocyanines. *Bioconjugate Chemistry*. **16:** 80-89
132. Matthews, E. And Cui, Z. (1990). Photodynamic action of sulphonated aluminium phthalocyanine (SALPC) on AR4-2J cells, a carcinoma cell line of rate exocrine pancreas. *British Journal of Cancer*. **61:** 659-701
133. Vittar, N., Prucca, C., Strassert, C., Awruch, J, Rivarola, V. (2008). Cellular inactivation and antitumor efficacy of new zinc phthalocyanine with potential use in photodynamic therapy. The international Journal of Biochemistry & Cell Biology. **40:** 2192-2205
134. Jin, C., Zhu, B., Wang, X. and Lu, Q. (2008). Cytotoxicity of Titanium Dioxide Nanoparticles in Mouse Fibroblast Cells. *Chemical Research in Toxicology*. **21:** 1871-1877
135. Alley, M., Scudiero, D., Monks, A., Hursey, M., Czerwinski, M., fine, D., Abbott, B., Mayo, J., Schoemaker, R. and Boyd, M. (1988). Feasibility of Drug Screening with Panels of Human Tumor Cell Lines Using a Microculture Tetrazolium Assay. *Cancer Research*. **45:** 589-601

136. Edrei, R., Gottfried, V., van Lier, J. and Kimel, S. (1998). Sulfonated phthalocyanines: photophysical properties, *in vitro* cell uptake and structure-activity relationships. *Journal of Porphyrins and Phthalocyanines*. **2:** 191-199
137. Seotsanyana-Mokhosi, I., Kresfelder, T., Abrahamse, H. And Nyokong, T. (2006). The effect of Ge, Si and Sn phthalocyanine photosensitizers on cell proliferation and viability of human oesophageal carcinoma cells. *Journal of Photochemistry and Photobiology B: Biology*. **23:** 55-62
138. Reddi, E., Cernuschi, S., Biolo, R. and Jori, G. (1990). Liposome-or LDL-administered Zn(II)-phthalocyanine as Photodynamic Agent for Tumours III. Effect of Cholesterol on Pharmacokinetic and Phototherapeutic Properties. *Lasers in Medical Science*. **5:** 339-343
139. Atlante, A. and Passarella, S. (1999). Detection of reactive oxygen species in primary cultures of cerebellar granule cells. *Brain Research Protocols*. **4:** 266-270

Internet References

1. Q-Sense ® Official webpage
   Webpage: www.qsense.org

2. ThermExcel
   Webpage: www.thermexcel.com/english/index.htm

Alternative References

1. Q-Tools Modelling Program
   3.0.7.230